Deposit & Copying of Dissertation Declaration

UNIVERSITY OF CAMBRIDGE

Board of Graduate Studies

Please note that you will also need to bind a copy of this Declaration into your final, hardbound copy of thesis - this has to be the very first page of the hardbound thesis.

1 Surname (Family Name)	Forenames(s)	Title
Filus	Michał Tadeusz	Dr

2 Title of Dissertation as approved by the Degree Committee

Transport and Distribution of the short-lived halocarbons in the Tropical Tropopause Layer: in the Pacific Ocean: role of convection.

In accordance with the University Regulations in *Statutes and Ordinances* for the PhD, MSc and MLitt Degrees, I agree to deposit one print copy of my dissertation entitled above and one print copy of the summary with the Secretary of the Board of Graduate Studies who shall deposit the dissertation and summary in the University Library under the following terms and conditions:

1. Dissertation Author Declaration

I am the author of this dissertation and hereby give the University the right to make my dissertation available in print form as described in 2. below.

My dissertation is my original work and a product of my own research endeavours and includes nothing which is the outcome of work done in collaboration with others except as declared in the Preface and specified in the text. I hereby assert my moral right to be identified as the author of the dissertation.

The deposit and dissemination of my dissertation by the University does not constitute a breach of any other agreement, publishing or otherwise, including any confidentiality or publication restriction provisions in sponsorship or collaboration agreements governing my research or work at the University or elsewhere.

2. Access to Dissertation

I understand that one print copy of my dissertation will be deposited in the University Library for archival and preservation purposes, and that, unless upon my application restricted access to my dissertation for a specified period of time has been granted by the Board of Graduate Studies prior to this deposit, the dissertation will be made available by the University Library for consultation by readers in accordance with University Library Regulations and copies of my dissertation may be provided to readers in accordance with applicable legislation.

3 Signature	Date
Filus Michał	04/12/2017

Corresponding Regulation

Before being admitted to a degree, a student shall deposit with the Secretary of the Board one copy of his or her hard-bound dissertation and one copy of the summary (bearing student's name and thesis title), both the dissertation and the summary in a form approved by the Board. The Secretary shall deposit the copy of the dissertation together with the copy of the summary in the University Library where, subject to restricted access to the dissertation for a specified period of time having been granted by the Board of Graduate Studies, they shall be made available for consultation by readers in accordance with University Library Regulations and copies of the dissertation provided to readers in accordance with applicable legislation.

This dissertation is submitted for the degree of Doctor of Philosophy

Transport and Distribution of the Short-lived Halocarbons in the Tropical Tropopause Layer in the Pacific Ocean: the Role of Convection

Michał Tadeusz Filus

Clare Hall College

February 2017

Centre for Atmospheric Science

Department of Chemistry

University of Cambridge

Supervisor:

Prof. Neil Harris

Examiners:

Dr. A.T. Archibald

Prof. A.R. MacKenzie

Author Declaration

This dissertation is the result of my own work and includes nothing which is the outcome of work done in collaboration except where specifically indicated in the text. This dissertation has not been submitted, in whole or in part, for any other degree, diploma or other qualification at any other university. It does not exceed 60,000 words (prescribed word limit set by the Degree Committee for the Faculty of Physics and Chemistry).

Michal Filus

February 2017

Acknowledgements

The time I have spent completing my PhD in Cambridge was truly one of a kind. I have thrown myself into the world of the atmospheric science, the world where the numerical modelling and measurements intertwine, the world where the caveats and uncertainties dominate, the world where the unchartered opportunities still exist and where the challenging process of solving the unknowns creates the new far more intriguing ones. I have been on a four-year journey which has given me so much valuable experience, strengthened my skills in research and critical thinking, and opened my mind to the science communication and the science for policy areas.

I would like to thank my family: my parents and my brother for their unconditional love and everlasting support from the abroad. Equally, I would like to acknowledge my supervisor, Professor Neil Harris, without whose advice, guidance and support I would not have achieved this. Thank you for giving me an opportunity to be a member of the successful CAST campaign, the first atmospheric research campaign I have ever done, and for the past four years of the constant belief and motivation in turning me into an independent scientist and researcher.

I would like to thank the colleagues from the Centre of Atmospheric Science, in particular Dr Matt Ashfold, Dr Michelle Cain and Dr Sarah Connors – for their patience and help in explaining anything NAME model or IDL related, and others for their help and keeping the warm and positive working environment. My thanks also go to Dr Alistair Manning, Dr Elena Meneguz and Dr David Thomson from the Atmospheric Dispersion and Air Quality Group, the UK Meteorological Office for their help and extensive collaboration on the NAME model.

Finally, I would like to thank NERC for providing me with the PhD studentship and letting me have and fully enjoy what turned out to be the best PhD atmospheric science experience.

Abstract

This PhD thesis investigates the transport and distribution of short-lived halogenated organic substances in the tropical tropopause layer (TTL) in the Pacific Ocean. Short-lived halocarbons are one of the major groups of the ozone depleting substances as they provide a source for the active halogens which decrease ozone in the atmosphere. The TTL serves as the primary gateway of tropospheric air to enter the stratosphere. The air which enters the stratosphere is distributed all over the globe. Thus, the research on which tropospheric air masses go into the TTL, its structure and composition and the transport within is crucial.

This thesis uses the UK Meteorological Office Lagrangian particle dispersion model NAME to (i) support the flight planning activities and achieve the multi aircraft coordination in CAST, CONTRAST, ATTREX 2014 campaigns, and (ii) quantify the amount and distribution of short-lived halocarbons in the TTL, and explain differences in these vertical distributions and transport characteristics. The halocarbons of interest are methyl iodide (CH_3I), bromoform ($CHBr_3$) and dibromomethane (CH_2Br_2).

A new NAME procedure was developed and operated successfully to provide routine simulations and near real-time products suitable for guiding the CAST, CONTRAST and ATTREX aircraft in order to achieve their mission scientific objectives, and to make coordinated measurements.

NAME was used post-campaign to analyse distribution of short-lived halocarbons in the TTL, identify their source regions and transport timescales. A new approach is proposed to investigate the TTL composition in terms of the boundary layer air influence, and subsequently quantify CH_3I, $CHBr_3$ and CH_2Br_2 by estimating their boundary layer and background contribution. The sums of these modelled estimates are in good agreement with the ATTREX 2014 and 2013 CH_3I, $CHBr_3$ and CH_2Br_2 observations. The quantification of the contribution of short-lived bromocarbons to the active bromine in the TTL was achieved, and the results lie within the range of the recent literature studies.

The final focus of this thesis is on how well NAME represents the particle displacement via convection. Convection is the major transport pathway for the short-lived halocarbons to reach the TTL. The role of convection in transporting CH_3I, $CHBr_3$ and CH_2Br_2 to the TTL is assessed using the new convection scheme in NAME. A validation of the performance of this scheme is provided, showing that it yields improved and more realistic representation of the particle displacement via convection.

Contents

A4.7.7 Contribution of short-lived brominated organic substances to the active bromine loading in the TTL, 12 day NAME runs

Abbreviations

AAFB	Andersen Air Force Base
AMMA	African Monsoon Multidisciplinary Analysis
ATTREX	Airborne Tropical Tropopause Experiment
AVE	Aura Validation Experiment
(A)WAS	Advanced Whole Air Sampler
BAe-146	British Aerospace 146
BDC	Brewer-Dobson Circulation
CARIBIC	Civil Aircraft for the Regular Investigation of the atmosphere Based on an Instrument Container
CAST	Co-ordinated Airborne Studies in the Tropics
CONTRAST	Convective Transport of Active Species in the Tropics
CR-AVE	Costa Rica Aura Validation Experiment
CPT	Cold Point Tropopause
CTM	Chemistry Transport Model
DFRC	Dryden Flight Research Centre
ENSO	El Niño Southern Oscillation
FAAM	Facility for Airborne Atmospheric Measurements
GCM	General Circulation Model
GC-MS	Gas Chromatography – Mass Spectrometry
GH	Global Hawk

GTE	Global Tropospheric Experiment
GV	Gulfstream V
HIAPER	High-performance Instrumented Airborne Platform for Environmental Research
HIPPO	HIAPER Pole to Pole Observations
ITCZ	Intertropical Convergence Zone
LZRH	Level of Zero net Radiative Heating
MEI	Multivariate ENSO Index
MJO	Madden-Julian Oscillation
MODIS	Moderate Resolution Imaging Spectroradiometer
NOAA	National Oceanic and Atmospheric Administration
NAME	Numerical Atmospheric-dispersion Model Environment
NASA	National Aeronautics and Space Administration
NCAR	National Centre for Atmospheric Research
NERC	Natural Environment Research Council
NEWCONV	NAME runs with new convection scheme
NOCONV	NAME runs with no convections scheme
NSF	National Science Foundation
NWP	Numerical Weather Prediction
ODS	Ozone Depleting Substances
OLR	Outgoing Longwave Radiation
PEM	Pacific Explanatory Mission
PRE-AVE	Pre-Aura Validation Experiment
RA	Release Altitude
RF	Research Flight
RMS	Root Mean Square

SCOUT-O3	Stratospheric-Climate links with emphasis On the Upper Troposphere and lower stratosphere - Ozone
SEAC^{4}RS	Studies of Emissions, Atmospheric Composition, Clouds and Climate Coupling by Regional Surveys
SHIVA	Stratospheric Ozone: Halogen Impacts in a Varying Atmosphere
SPCZ	South Pacific Convergence Zone
SST	Sea Surface Temperature
STRAT	Stratospheric Tracers of Atmospheric Transport
TC4	Tropical Composition, Cloud and Climate Coupling
TOGA	Trace Organic Gas Analyser
TORERO	Tropical Ocean Troposphere Exchange of Reactive Halogen Species and Oxygenated Volatile Organic Compounds
TTL	Tropical Tropopause Layer
UHF-LOS	Ultra High Frequency – Line of Sight
UKCA	United Kingdom Chemistry and Aerosols
UM	Unified Model
UTC	Coordinated Universal Time
VOCs	Volatile Organic Compounds
VSL	Very Short-Lived
WMO	World Meteorological Organisation

1. Introduction

This chapter provides an overview of the scientific basis behind this thesis. The primary focus of this chapter is to describe the atmospheric dynamics in the Pacific region (Section 1.1), explain the role of the tropical tropopause layer (TTL) in the transport of tropospheric air to the stratosphere (Section 1.2), and discuss the current understanding of the role and transport of the short-lived halogenated organic substances in the tropical troposphere and TTL (Section 1.3). The structure of the atmosphere is provided first. Then, the atmospheric circulation in the Pacific region is described, including its zonal and meridional components. The formation of deep convective systems is mentioned then. This is followed by descriptions of the Madden-Julian Oscillation (MJO) and El Niño Southern Oscillation (ENSO) phenomena which cause the intraseasonal and interannual variability in the atmospheric circulation within the Pacific region. The structure of the TTL and its role in the transport of tropospheric air masses to the stratosphere is highlighted. Short-lived halogenated organic substances are characterised next, including their emission sources, speciation, distribution and transport within the tropical troposphere and the TTL. Two approaches of how atmospheric transport events are modelled are put forward. Finally, the structure of this thesis is presented, giving an overview of each chapter and listing the scientific questions which this thesis investigates.

1.1 Atmospheric dynamics

This section gives an overview of the main features of the atmospheric dynamics in the tropical Pacific region. The structure of the atmosphere is outlined first, followed by a description of the dominant components of the circulation system in the tropical Pacific region: the Hadley cell, the Walker and Brewer-Dobson circulations. The way in which deep convection develops is put forward next. The phenomena of Madden-Julian Oscillation (MJO) and El Niño Southern Oscillation which drive the intraseasonal and interannual variability in the Pacific atmospheric circulation are explained last.

1.1.1 Structure of the atmosphere

The atmosphere is characterised by distinct vertical regions based upon the meteorological and chemical parameters, such as the temperature or the ozone mixing ratio [*Jacob, 1999*; *Ahrens, 2012*]. Figure 1.1 shows the global mean vertical profiles of temperature and ozone mixing ratio, with the differentiation of the atmospheric layers: troposphere, stratosphere, mesosphere and thermosphere. Over 95% of the air masses reside within the first two atmosphere layers; thus most dynamics and chemistry, relevant to the biosphere, occurs there [*Ahrens, 2012*].

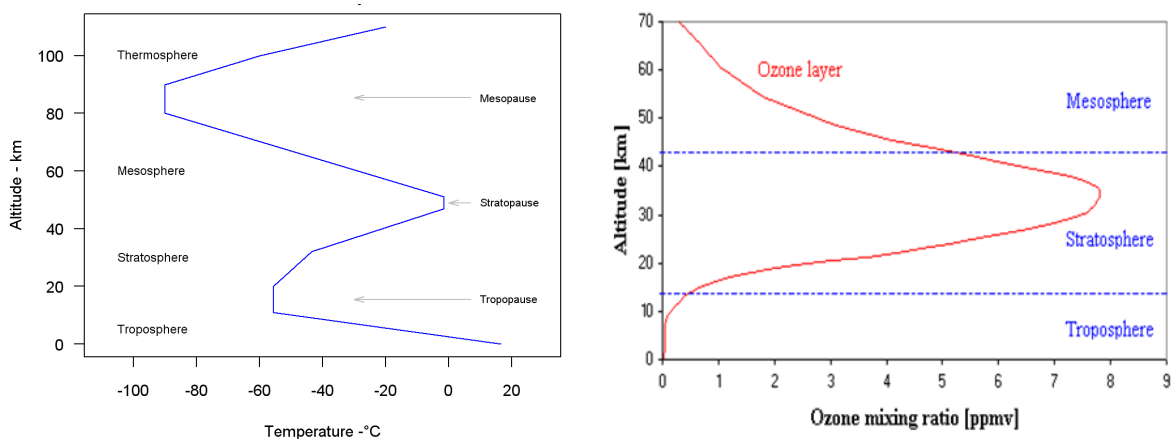

Figure 1.1 Global mean vertical profiles of temperature (left) and ozone mixing ratios (right) [*US Standard Atmosphere, 1976*].

The troposphere ranges from 0 to 10 km in the polar regions, and up to 20 km in the tropics. It is capped by the tropopause which separates the troposphere from stratosphere, i.e., two major weather-generating layers with considerably differing dynamic, chemical and radiative regimes [*Ivanova et al., 2013*]. The tropopause is of the key importance for the exchange between the troposphere and stratosphere, with its position determined in different ways (with all of them empirical to some extent). One approximation of the tropopause based on the difference in thermal regimes of the troposphere and stratosphere is a definition of the cold-point tropopause (CPT) - being a level where temperature reaches the minimum [*Highwood and Hoskins, 1998*]. The tropopause can be determined thermally in different way as a level where the environmental lapse rate decreases to 2 ^{o}C/km or less for at least 2 km altitude. The tropopause can also be defined chemically (based on the difference in the chemical composition of the troposphere and stratosphere) through identifying a cutoff from a combination of high ozone and extremely low water vapour and carbon monoxide in the stratosphere [*Danielsen, 1982*], and low ozone, high water vapour, and high and more variable carbon monoxide in the troposphere [*Levine et al., 2007*]. A dynamical tropopause can be defined by a level where the sharp gradient in the Ertel potential vorticity between the two air masses is present [*Highwood and Hoskins, 1998*; *Ivanova et al., 2013*]. The atmospheric dynamics over the tropical Pacific region, relevant to this study, is reviewed in detail.

1.1.2 Characterisation of the atmosphere over the Pacific region

A non-uniform heating of the Earth produces distinct patterns of rising and descending air masses, winds, and storms in well-defined cells around the globe (Figure 1.2). In the tropics, two major tropospheric circulation systems are present: the Hadley cell and the Walker circulation. The Brewer-Dobson circulation is the main stratospheric circulation system [*Holton, 2012*].

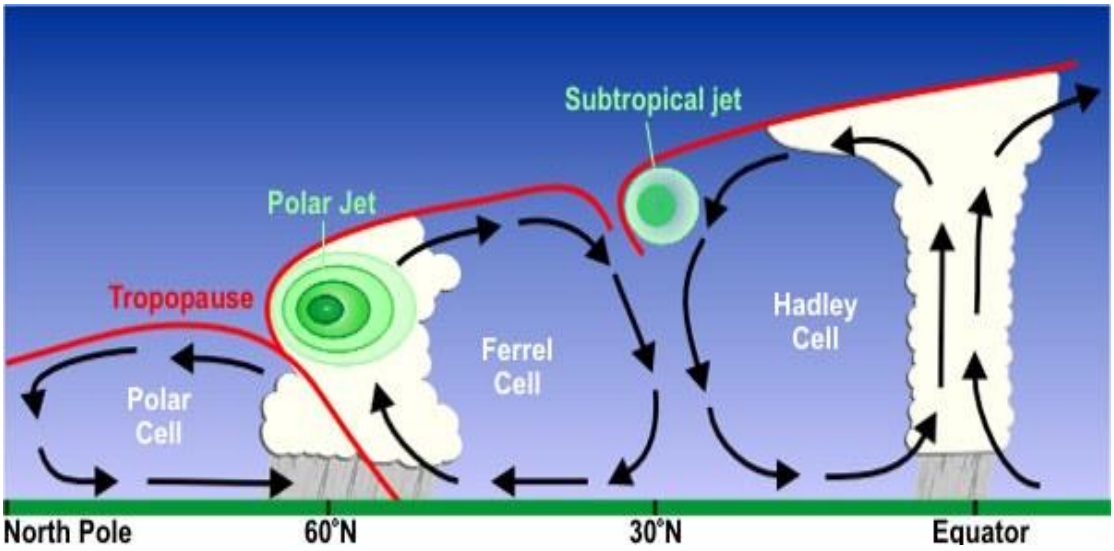

Figure 1.2 The North Hemisphere cross-section showing the tropospheric circulation [*NOAA, http://www.srh.noaa.gov/jetstream/global/jet.html*].

The Hadley cell and the Walker circulation govern the atmospheric transport of the air from the boundary layer and low troposphere to the upper troposphere and the stratosphere, where the air enters the Brewer-Dobson circulation and is transported poleward. These circulation patterns facilitate the mixing of the air of varied compositions at different altitude levels at different time scales (*IPCC, 2001*; Table 1.1). The troposphere is dynamically more unstable than the stratosphere, resulting in the shorter transport times for the physical mixing processes.

Table 1.1 Typical transport times in the atmosphere [*IPCC, 2001*].

Process	Characteristic transport time
Boundary Layer – Free Troposphere Mixing	Hours – Days
Transport via Deep Convection	Hours - Days
Zonal (Latitudinal) Transport	Days – Weeks
Meridional (Longitudinal) Transport	Months
Inter-Hemisphere Mixing	1-2 years
Troposphere – Stratosphere Exchange	1-2 years

1.1.2.1 The Hadley Cell

The Hadley cell is a meridional component of the tropospheric circulation (Figure 1.3, *Schwing et al., 2010*), spanning between the Equator and 30^{o}N on northern, and 30^{o}S on southern hemisphere, respectively. Due to the highest solar insolation occurring over the Equator, the moisture-rich boundary layer air becomes warm, expands and rises to the upper troposphere. This air can reach the tropopause via a rapid vertical uplift. The lofted air releases the latent heat, becomes colder and denser, loses its buoyancy and diverges. The diverged air moves poleward towards so-called horse latitudes (30^{o}N and 30^{o}S), being constantly cooled by radiation. The belts of the high pressure subtropical highs form there (over the Tropics of Cancer and Capricorn bands). The gradual subsidence of the air occurs over the horse latitudes. Some of the subsided air reaches the surface, and moves back with the trade winds to the equatorial low pressure surface regions [*Ahrens, 2012*]. The northeast and southeast trade winds converge along these equatorial regions called the Inter-Tropical Convergence Zone (ITCZ). It is the zone where the air rises again and continues its Hadley circulation flow. In the West Pacific, there is also a second branch of convergence extending southeastward, called the South Pacific Convergence Zone (SPCZ). ITCZ and SPCZ are characterised by rising cells of deep convection, formation of vast convective clouds and the heavy rainfall [*Wallace et al., 2006*].

1.1.2.2 The Walker Circulation

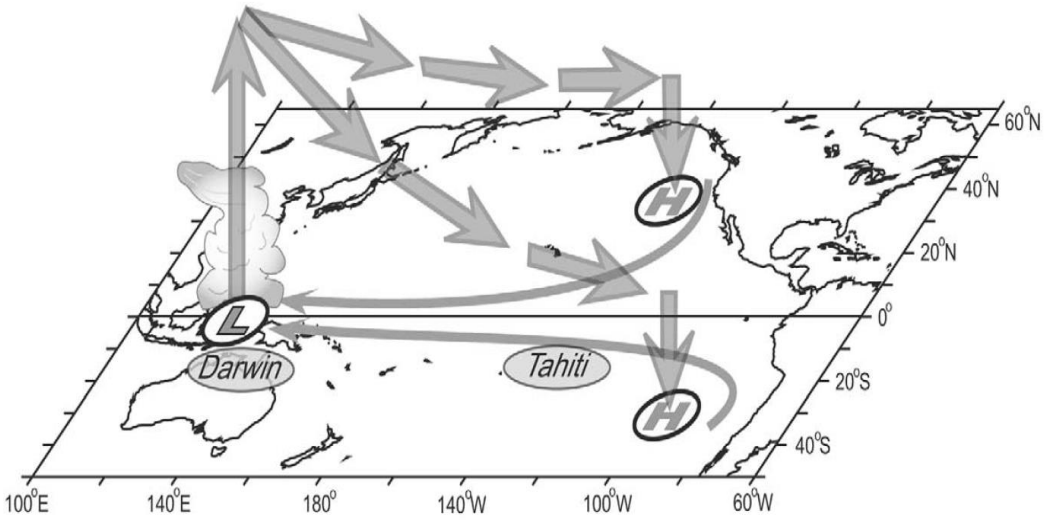

Figure 1.3 A schematic illustration of the Hadley cell (meridional arrows) and the Walker circulation (zonal arrows) in the Pacific region. The major pathways of the air circulation, the momentum and energy shift between the tropics and extra-tropics. Deep convection, poleward and meridional air flow, easterly trade winds are represented by vertical solid line arrows, eastward facing horizontal three arrows (top) and westward facing horizontal single solid line arrows, respectively. High and low sea surface pressure is labelled by H and L circles [*Schwing et al., 2010*].

The Walker circulation is a zonal component of the tropical Pacific tropospheric circulation (Figure 1.3). It is driven by a non-uniform distribution of land and sea across the tropics, along with the resulting asymmetries in atmospheric heating and the high-low pressure system build-up [*Salby, 2012*]. The warm and moist air over the Maritime Continent and the West Pacific rises to the upper troposphere, where it diverges and follows the meridional eastward flow. This air descends over the East Pacific where it brings the arid climate [*Salby, 2012*]. *Hosking et al., 2012,* reported that the Walker circulation plays an important role in the seasonality of the fast vertical transport from the low to the upper troposphere and the lower stratosphere.

1.1.2.3 The Brewer-Dobson Circulation

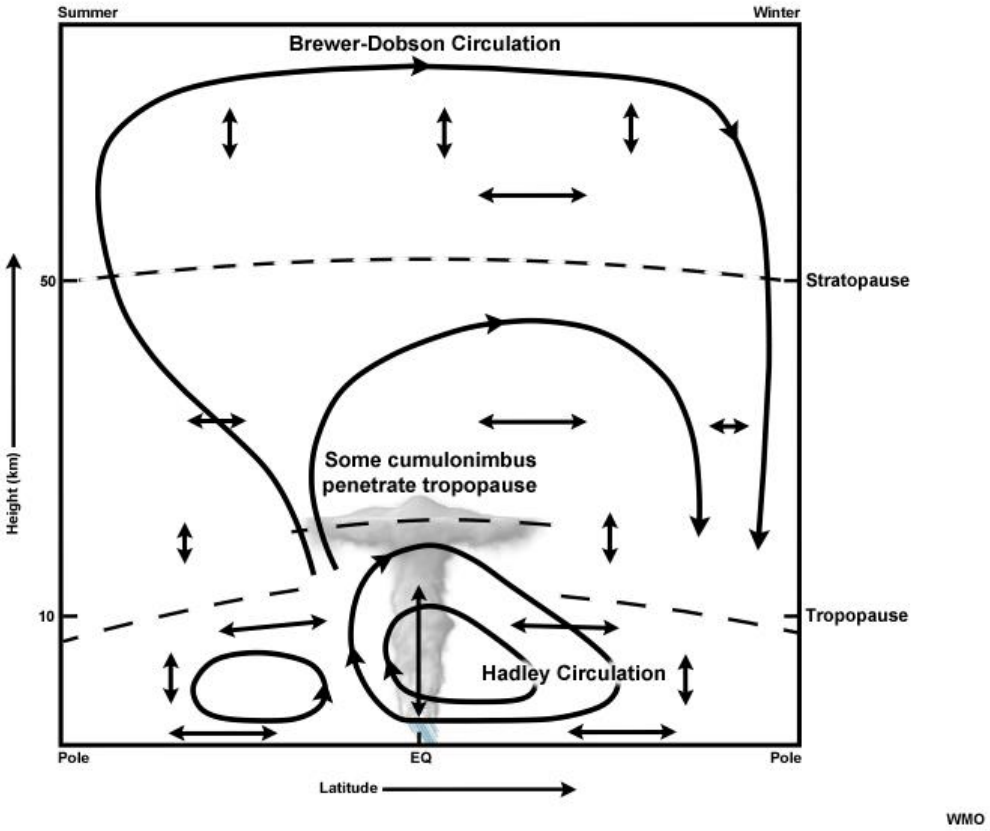

Figure 1.4 Brewer-Dobson circulation in the stratosphere (summer and winter poles, on the left-hand and right-hand side, respectively) [*Laing et al., 2011*].

Lofted tropospheric air enters the lower stratosphere through the tropopause. This air is subject to the Brewer-Dobson circulation (BDC, Figure 1.4). The BDC transfers the air poleward and sinks at high latitudes, being subject to radiative cooling, on monthly-yearly timescales [*Brewer, 1949; Newell, 1961; Holton, 1989; Roscoe, 2006; Bunzel et al., 2013*]. The position of the tropical tropopause, the frequency and magnitude of the convective systems, the presence of the phenomena driving the variability in the Pacific atmospheric circulation (MJO and ENSO), and the strength of the BDC all influence stratosphere-troposphere exchange [*Holton et al., 1995; Pommereau J-P., 2010*].

1.1.3 Deep convection

Deep convection is one of the main features of the atmospheric circulation in the Pacific region. It is also an important transport pathway for the low-level air masses to the upper troposphere, affecting the distribution of the chemical species.

Convective clouds are formed in the vertical motion that results from the instability of the atmosphere. This instability can be caused by a combination of the heating at the bottom of an air layer, the cooling at the top of an air layer, or lifting or saturation of a potentially unstable layer [*Emanuel et al., 1994*; *Convective Clouds, Atmospheric Dynamics Lecture, Wageningen University*]. A moist parcel of air, once subject to warming and unstable conditions within the boundary layer and low troposphere, expands and starts to rise. The ascending motion of the parcel decreases when the air cools due to the adiabatic expansion (the pressure dropping with height). However, the latent heat release makes the air lighter than the environment, causes the temperature to drop more slowly, extends the parcel's buoyancy and propagates the further increase in altitude. Positive buoyancy forces accelerate the parcel to its maximum velocity at the equilibrium level. There the parcel overshoots until negative buoyancy decelerates it [*Danielsen E., 1982*]. Once the air parcel loses its buoyancy, it spreads horizontally [*Ahrens, 2012*].

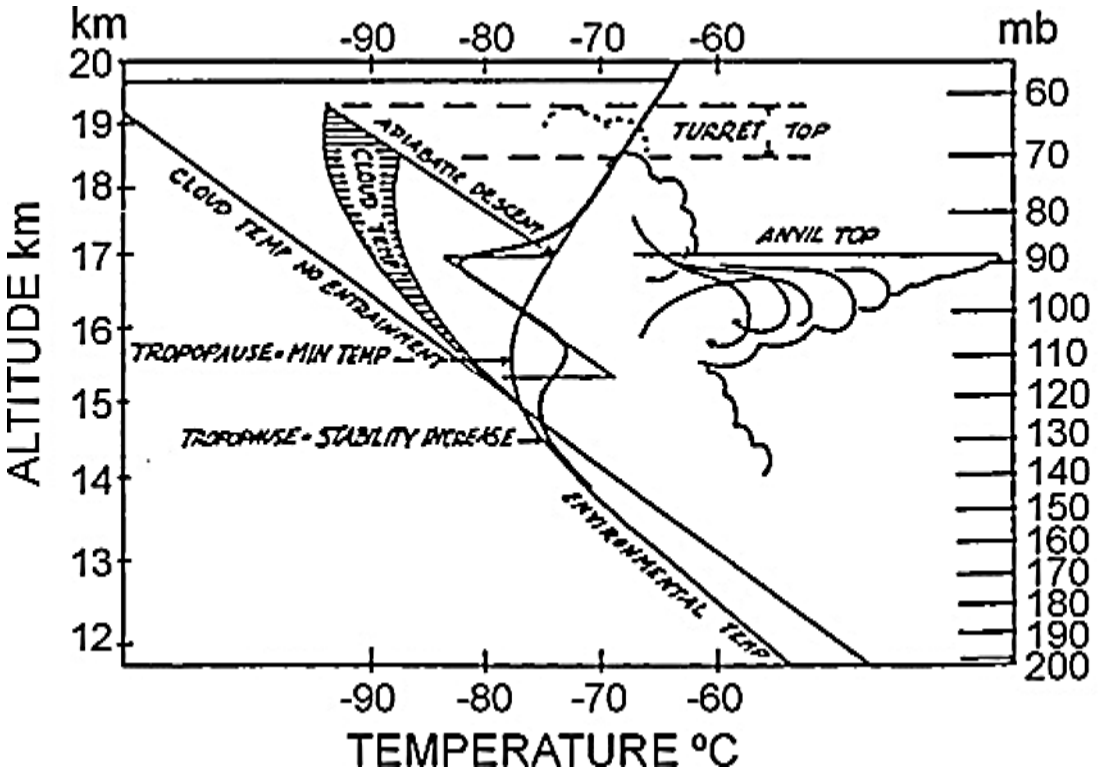

Figure 1.5 Schematic of energetic updraft of adiabatically cooled air by convective overshooting proposed by *Danielsen et al., 1982* [*Pommereau, 2010*].

The fast overshooting of adiabatically (occurring without gain or loss of heat) cooled air is proposed by *Danielsen, et al., 1982*. These events of fast overshooting are associated with deep continental convective system that is the injection of tropospheric air well above the tropopause, followed by mixing with stratospheric air. These events are recognised but are assumed to be rare and therefore their contribution is insignificant at the global scale [*Pommereau, 2010*].

Deep convection in the tropics usually reaches up to about 10-12 km (main region of the convective outflow), but the strongest convection can reach above these levels, and overshooting may even penetrate the tropopause. The updrafts in deep convective clouds can raise boundary layer air into the upper troposphere in a matter of minutes, with the outflow occurring primarily from the cloud tops. Deep convective systems are the main drivers in transport of chemical substances in the tropical troposphere: peroxides, methyl iodide, short-lived bromocarbons, dimethyl sulphide, ozone [*Chatfield et al., 1984; Cohan et al., 1999, Ziemke et al., 2015*].

1.1.4 Variability in the atmospheric circulation in the tropical Pacific

The atmospheric circulation of the Pacific region is affected by the occurrence of two major phenomena: MJO and ENSO. They drive the intraseasonal and interannual variability in the troposphere-to-stratosphere transport, respectively, by relocating the large-scale convection systems within the Pacific [*Su et al., 2013*].

1.1.4.1 Intraseasonal variability: Madden-Julian Oscillation

The MJO is the most prominent mode of intraseasonal variability in the Pacific tropical atmosphere. It is a tropical disturbance that propagates eastward along the Equator from the Indian Ocean towards the Central Pacific, with a cycle of 30-70 days (Figure 1.6). It consists of large-scale coupled atmospheric circulation and deep convection patterns [*Zhang et al., 2005*].

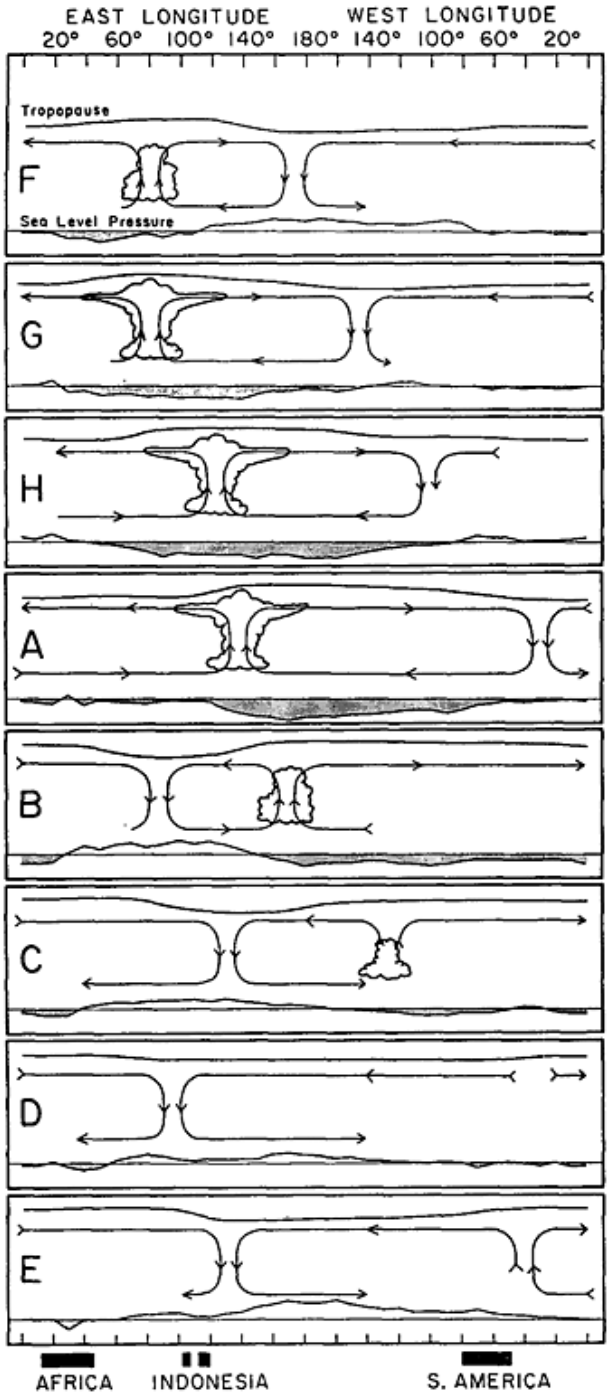

Figure 1.6 Schematic diagram of the fundamental large-scale features of the Madden-Julian Oscillation (MJO) through its life cycle (top to bottom). Cloud symbols represent the convective centre, arrows indicate the zonal circulation and the curves above and below the circulation represent perturbations in the upper tropospheric and sea level pressure. The panels are spaced roughly 5 days apart [*Madden et al., 1972*].

Figure 1.6 illustrates the evolution of MJO. In tropical Indian Ocean, the MJO signal is initiated by the emergence of large-scale convection system which propagates eastward. The signal matures over the East Indian Ocean, weakens over the Maritime Continent, strengthens again in the West Pacific, and finally dissipates near the 180^{o} longitude [*Waliser et al., 2009; Liu et al., 2014*]. The MJO is quite variable, with periods of moderate to strong activity followed by periods of little or no activity. The strong, convectively active phase of the MJO is characterised by the enhanced surface fluxes, the anomalies in the westerly winds and the heavier precipitation [*Zhang et al., 2005*]. In the tropics, MJO regulates wet and dry conditions, modulates the tropical cyclone and monsoon activities [*Camargo et al., 2009*], and influences the evolution of the ENSO cycles [*DeMott et al., 2015*]. By modulating the tropical cyclone activity in the Pacific, the MJO has a direct impact on the distribution and magnitude of large-scale convective systems over the Pacific (Figure 1.7) [*Laing et al., 2011*].

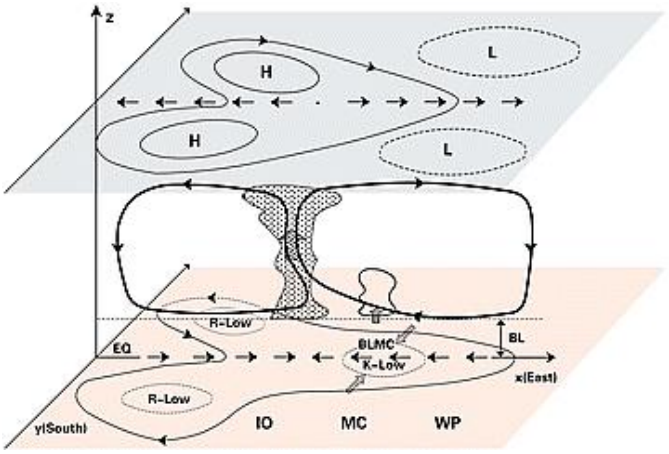

Figure 1.7 Schematic diagram illustrating three-dimensional structure of the MJO mode. BLMC represents boundary layer moisture convergence, IO – Indian Ocean, MC – Maritime Continent, WP – West Pacific, H and L – high and low pressure systems. *R-Low* and *K-Low* represent the lower pressure anomalies associated with moist equatorial Kelvin and Rossby waves, respectively. Arrows indicate the wind directions. In the equatorial vertical plane, free tropospheric wave circulation is highlighted. Wave-induced convergence is in phase with the major convection, whereas frictional moisture convergence in the *K-low* region is ahead of major convection due primarily to meridional wind convergence [*Lau et al., 2011; Wang et al., 2016*].

Over the past two decades, considerable study of the MJO has led to a better comprehension of its large scale structure, and broad influences on the tropical and extratropical weather and climate. Yet the accurate simulation and prediction of MJO, and its impact on the variability in the long-range transport of the air masses remains a challenge [*Ling et al., 2016*]. The past field campaigns and modelling experiments have suggested that the MJO driven tropical ocean-atmosphere interactions may sustain or amplify the patterns of the enhanced and suppressed convection over the Pacific.

1.1.4.2 Interannual variability: El Niño Southern Oscillation

The ENSO is a large scale coupled ocean-atmosphere perturbation to the tropical circulation that occurs with a frequency of 3-5 years. This perturbation is triggered by the shift in the oceanic thermocline, the relocation of the upwelling and downwelling regions, and the emerging anomalies in the sea surface temperatures (Figure 1.8) [*Wang et al., 2012*]. ENSO has two phases: warm (El Niño), and cold (La Niña, Figure 1.7.B-C) [*Ziemke et al., 2015*].

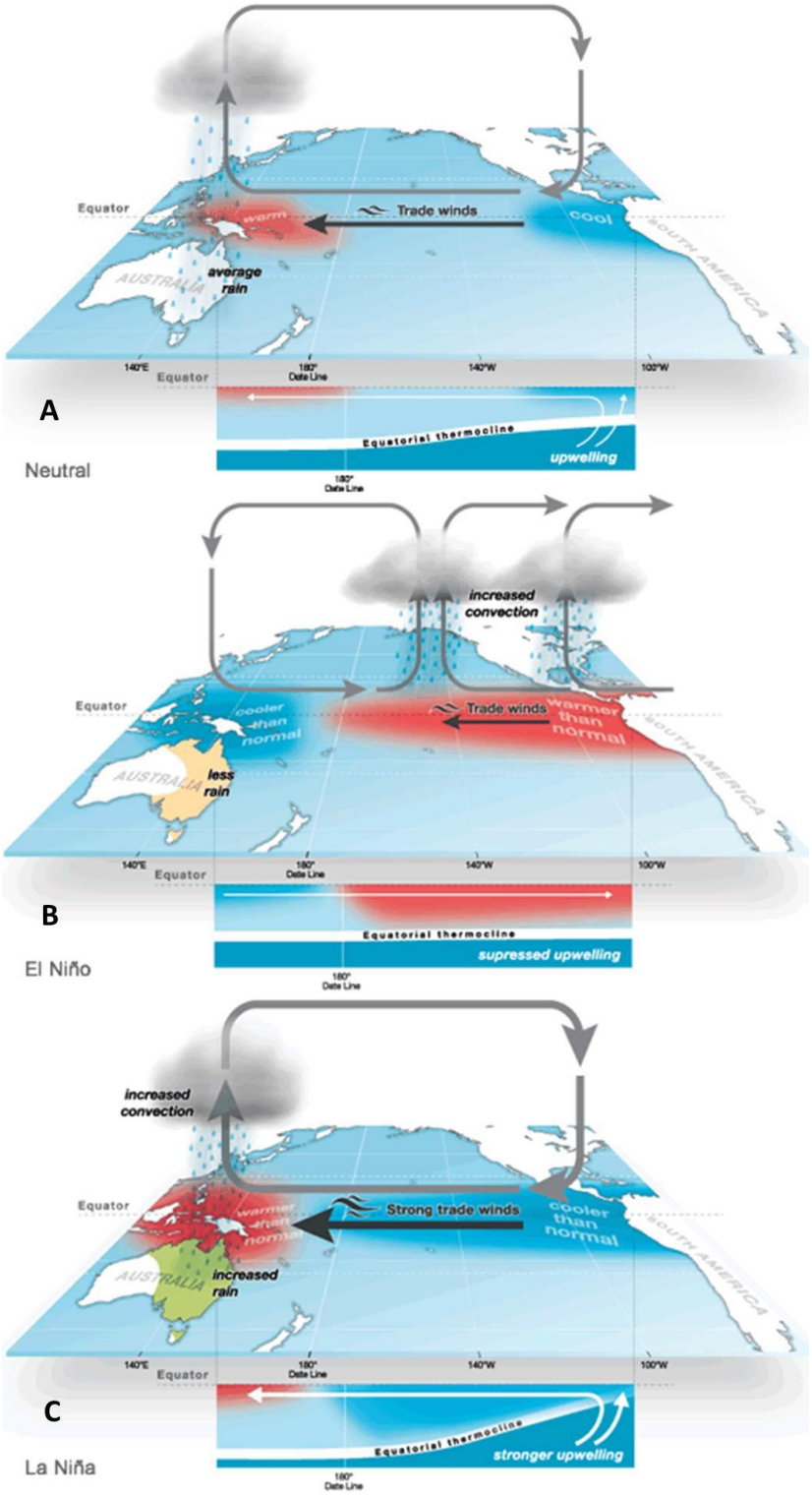

Figure 1.8 Depiction of the ENSO neutral (A), El Niño (B) and La Niña (C) conditions [*Bureau of Meteorology, Australian Government; http://www.bom.gov.au/climate/about/australian-climate-influences.shtml?bookmark=enso, last updated: 2 April 2008*].

El Niño occurs when the warmest sea surface temperatures (SSTs) and the large scale convection, normally found in the West Pacific, shift eastward into the East or Central Pacific (Figure 1.9). This produces a large change in the surface pressures, creating a longitudinal dipole. This dipole then shifts the low pressure from the West Pacific to the East Pacific, along with evaporation and latent heat transfer within the atmosphere [*Nassar et al., 2009*]. The large-scale convection systems move over the Central and East Pacific, resulting in the significant weakening or the reversal of the Walker circulation.

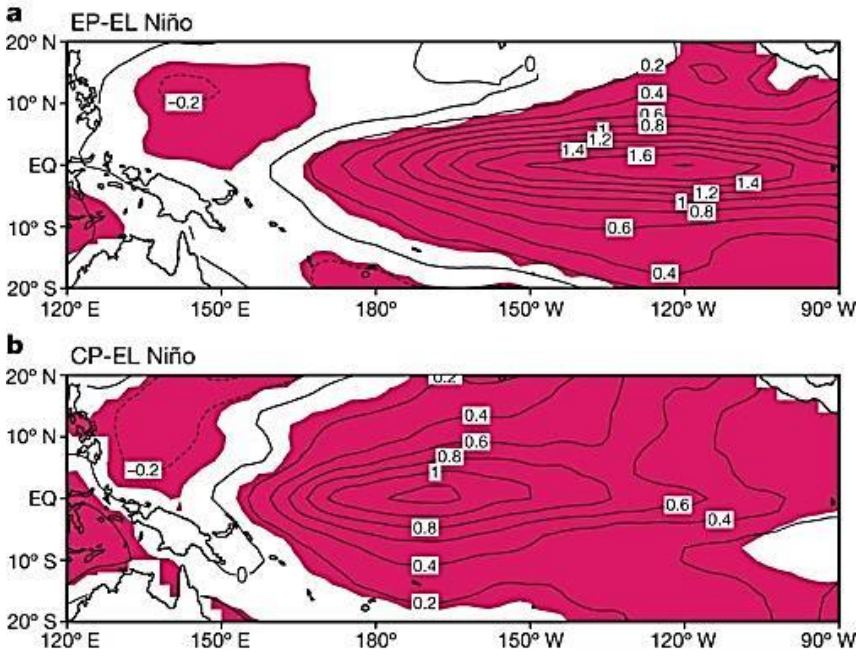

Figure 1.9 Deviations of the mean SSTs for the two types of El Niño from the 1854–2006 climatology: (a) East Pacific, and (b) Central Pacific. The contour interval is 0.2 °C and shading denotes a statistical confidence at 95% confidence level based on a Student's t-test [*Yeh et al., 2009*].

La Niña is the opposite phase of El Niño, with the SSTs anomalously warm over the Indian Ocean and the West Pacific, and anomalously cold over the Central and East Pacific. This leads to the abnormally low pressure system build-up over the West Pacific and results in the enhanced convective activity, increased precipitation, and elevated vertical transport of the low-level air to the upper troposphere in the West Pacific region (Figure 1.10).

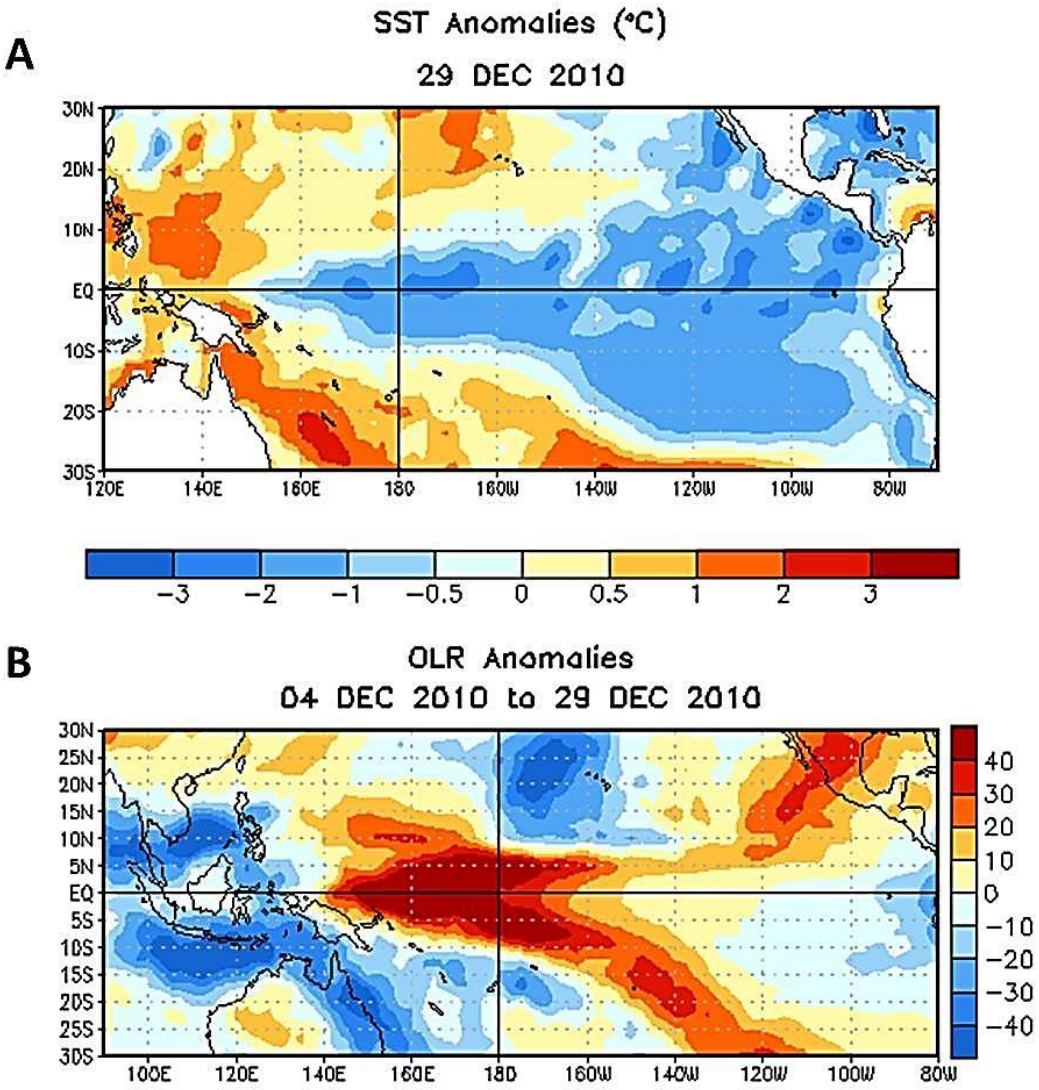

Figure 1.10 Anomalies in the SSTs (A) and the outgoing longwave radiation (OLR, indicative of the presence of large scale convective clouds, B) for moderate La Niña, 12/2010 [*El Niño Southern Oscillation, ENSO, Diagnostic Discussion, Climate Prediction Centre, NCEP, NWS*].

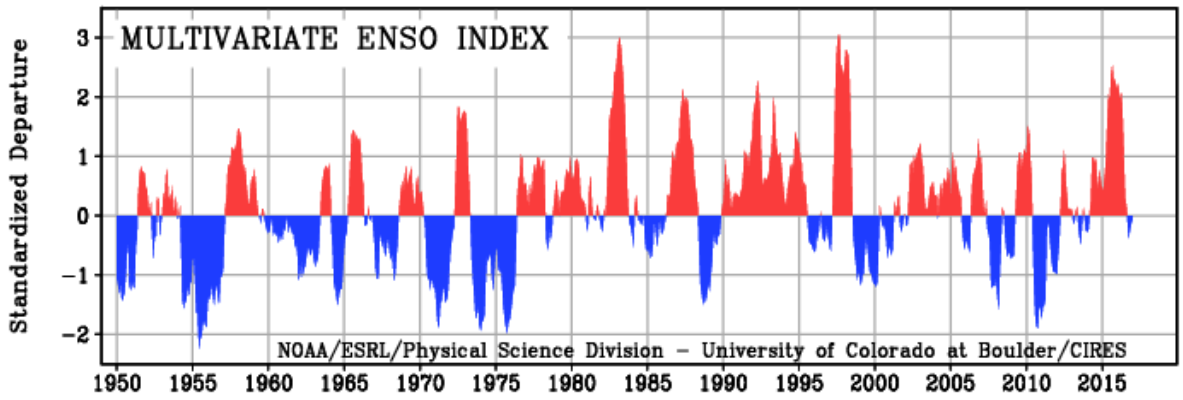

Figure 1.11 The ENSO evolution indicated by the multivariate ENSO index (MEI). MEI is based on the six main observed variables over the tropical Pacific: sea level pressure, zonal and meridional components of the surface wind, SSTs, surface air temperature, and total cloudiness fraction of the sky. The positive MEI (red) represents the El Niño years, the negative MEI (blue) represent the La Niña years [*MEI, Earth System Research Laboratory, National Oceanic and Atmospheric Administration*].

Figure 1.11 illustrates the evolution of the ENSO signal, indicated by the NOAA multivariate ENSO index (MEI). In El Niño years, the suppressed convection in the West Pacific leads to less efficient vertical transport of the low-level air to the upper troposphere [*Zeng et al., 2005*]. This vertical transport is enhanced in the East Pacific [*Zhang et al., 1993*].

The MJO may affect the development and intensity of the ENSO events. Its activity tends to be high when ENSO neutral conditions occur, and absent during the moderate-to-strong El Niño and La Niña events [*Zhang et al., 2013; Gottschalck et al., 2014*]. This connection between the MJO and ENSO is complicated and ambiguous. *Feng et al., 2015,* report that during the East Pacific El Niño which produces the lasting dry conditions in the Maritime Continent and the West Pacific, the MJO activity is weak. On the contrary, during the Central Pacific El Niño, the MJO is enhanced and suppressed in its different phases [*Gottschalck et al., 2014; Feng et al., 2015*]

The strong impact of ENSO on the interannual variability and distribution of chemicals is evident. The observed anomalies in the tropospheric column ozone and the upper

troposphere water vapour in the equatorial Pacific strongly correlate with the ENSO signal [*Zeng et al., 2005, Levine et al., 2008*]. ENSO also influences the interannual modulation of the global stratosphere-to-troposphere exchange, affecting the photochemistry and chemical composition in the tropics. *Voulgarakis et al, 2011*, observed that the El Niño can increase the amounts of stratospheric ozone entering the troposphere through the enhanced stratospheric-tropospheric exchange which may lead to the modified chemistry and elevated levels of the very short-lived substances. A strong correlation between stratosphere-troposphere exchange and ENSO is evident, with the modelled maximum and minimum of the annual total stratosphere-troposphere exchange following the El Niño years and La Niña years, respectively [*Zeng et al., 2005*].

1.2 The Tropical Tropopause Layer

This section describes the structure of the tropical tropopause layer (TTL). The importance of TTL in the troposphere-to-stratosphere transport of the air masses and chemicals is explained then.

1.2.1 Structure of the Tropical Tropopause Layer

The TTL is the transition region of the tropical atmosphere between the main convective outflow at 12-13 km and the base of the stratosphere at 17-18 km (Figure 1.12) [*Fueglistaler et al., 2009*]. The CPT indicates the temperature minimum in the TTL and is climatologically located at approximately 380 K potential temperature [*Holton et al., 1995*]. The level of zero net radiative heating (LZRH) located at 15 km, serves as an abstract fine boundary between the lower tropospheric-like TTL and the upper stratospheric-like TTL [*Gettelman et al., 2004*]. The lower TTL regime is driven by convection, whereas the upper TTL air masses are subject to the radiative heating. The chemical processes change gradually from those typical of the troposphere to those typical of the stratosphere.

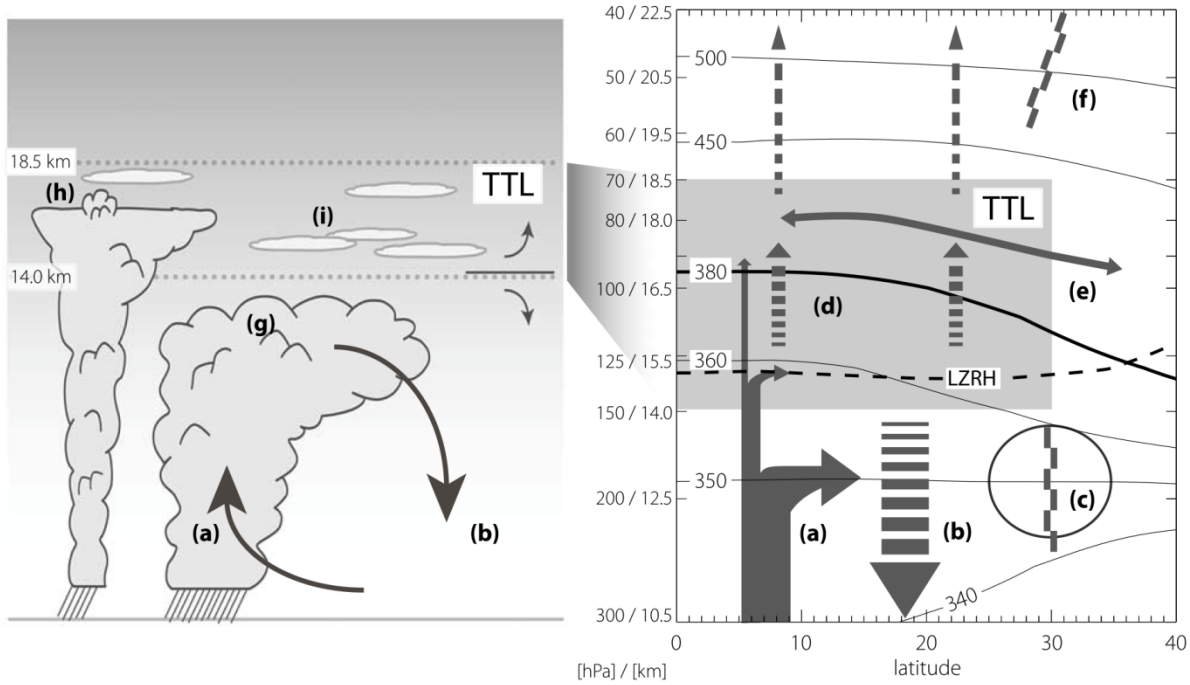

Figure 1.12 A schematic of cloud processes and transport (left) and of zonal mean circulation (right). *Arrows:* circulation, *black dashed lines*: clear-sky level of zero net radiative heating (LZRH), *black solid lines*: isentropes [K], (a) deep convection: main outflow around 200 hPa, rapid decay of outflow with height in TTL, (b) radiative cooling, (c) subtropical jets, (d) radiative heating, (e) rapid meridional transport of tracers and mixing, (f) the edge of tropics/subtropics, (g) deep convective cloud, (h) convective core overshooting its level of neutral buoyancy, (i) cirrus clouds [*Fueglistaler et al., 2009*].

1.2.2 Importance of the TTL in the troposphere-to-stratosphere transport

The upward transport in the lower TTL is dependent on convection and is thus largely tropospherically controlled. Above the LZRH, the net radiation is positive, and the air therefore rises without the aid of latent heat release. The rising is associated with the BDC mechanism, and therefore the upper TTL is more stratospherically controlled [*Gettelman et al., 2004; Fueglistaler et al., 2009; Randel et al., 2013*]

The TTL is particularly important because it is the primary gateway to the stratosphere [*Fueglistaler et al., 2009*]. The vast majority of the tropospheric air that enters the stratosphere originates from deep convection in the tropical West Pacific that detrains in the lower TTL [*Bergman et al., 2012; Randel et al., 2013*].

Levine et al., 2007, and *Hosking et al., 2012*, reported that the most efficient vertical and zonal transport of the air is modelled over the Maritime Continent in the winter, resulting from the formation of the ascending branch of the Walker circulation and developed strong deep convection. These allow for the fast transport of air into the stratosphere. The differences in the strength and vertical extent of tropical convection are important for the efficiency of the transport into the TTL.

1.3 Short-lived halogenated organic substances in the Pacific region

This section gives an overview of the short-lived halogenated organic substances, their chemistry, distribution and transport in the tropical Pacific troposphere and stratosphere. Much interest has been given to this group of substances as once they are present in the TTL they provide a source of the active halogens which reduce the ozone budget in the TTL and the lower stratosphere. The focus of this thesis is on investigating methyl iodide (CH_3I), bromoform ($CHBr_3$) and dibromomethane (CH_2Br_2). Their characteristics are described first. Then, the transport and composition in the TTL is explained, followed by highlighting their role and impact in the lower stratosphere.

1.3.1 Short-lived halogenated organic substances: Chemistry and Speciation

The halogenated organic substances comprise the major group of ozone depleting substances (ODSs) as they contain the active halogen atoms: chlorine, bromine or iodine. These species deplete stratospheric ozone and are differentiated into long-lived and short-lived, depending on their atmospheric lifetimes. The atmospheric lifetime is the mean time that a species resides in the atmosphere before it is removed by a chemical reaction, photolysis or deposition. The long-lived halogenated species include the man-made chlorofluorocarbons and halons. These made a notorious contribution to the Antarctic ozone hole in the 1980s, and since the Montreal Protocol in 1987, the long-lived halogenated species have been legally controlled, progressively replaced by the less environmentally harmful alternatives, and phased out.

Short-lived halogenated substances are trace gases with non-uniform tropospheric abundances whose atmospheric lifetimes are comparable to or shorter than tropospheric

transport timescales (less than 6 months). They provide a source of the active halogens which in reaction with ozone result in the ozone loss via catalytic cycles. The ozone depletion is facilitated by the interhalogen reactions [*Solomon et al., 1994; Sherwen et al., 2015*]. The equations below are the fundamental Chapman mechanism reactions defining the chemical formation and sinks of ozone in the stratosphere. The introduction of an active halogen atom (X = Cl, Br, I) leads to catalytic net ozone loss. The last set of reactions includes interhalogen reactions where two same or different active halogen atoms combine and further deplete ozone.

$$O_2 + h\nu \rightarrow O(^3P) + O(^3P) \quad (\lambda < 240\ nm)$$
$$O(^3P) + O_2 + M \rightarrow O_3 + M$$
$$O_3 + h\nu \rightarrow O_2 + O(^1D) \quad (\lambda < 320\ nm)$$
$$[O(^1D) + M \rightarrow O(^3P) + M]$$
$$O_3 + O(^3P) \rightarrow 2\ O_2$$

$$X + O_3 \rightarrow XO + O_2$$
$$XO + O(^3P) \rightarrow X + O_2$$
$$\textit{Net:} \quad O_3 + O(^3P) \rightarrow 2\ O_2$$

$$XO + YO \rightarrow X + Y + O_2$$
$$X/Y + 2\ O_3 \rightarrow XO/YO + 2\ O_2$$
$$\textit{Net:} \quad 2\ O_3 \rightarrow 3\ O_2$$

1.3.1.1 Iodinated short-lived organic substances: Methyl Iodide

Iodinated short-lived organic substances have weak and photochemically active iodine carbon bonds, and so they are characterised by very short lifetimes, rapid photolysis and the release of the active iodine atoms. This limits their abundance in the upper troposphere and precludes significant transport of these substances to the stratosphere, given their lifetimes being shorter than the transport times [*Solomon et al., 1994*]. However, convective clouds can transport iodocarbons very rapidly to the upper troposphere and TTL, particularly in the tropics within few hours to days [*Pickering et al., 1992; Solomon et al., 1994; Cohan et al., 1999*].

Methyl iodide (CH_3I) is the most abundant iodocarbon present in the tropical Pacific troposphere. It is emitted predominantly from the oceans (>80%), as a result of the photochemical reactions of iodine atoms and methyl radicals, and the biological production from: phytoplankton [*Oram et al., 1994*], kelp [*Lovelock et al., 1975*], macroalgae [*Chameides et al., 1980, Carpenter et al., 2012; Saiz-Lopez et al., 2014*]. The impact of other CH_3I emissions from terrestrial sources, including the biomass burning, rice production, wood rotting fungi, soil microorganisms or plant roots, is negligible [*Bell et al., 2002; California Environmental Protection Agency, 2009*; *Stemmler et al., 2014*]. The emissions of CH_3I are not well constrained (Table 1.3). Its atmospheric lifetime is 4 days in the tropical boundary layer [*Carpenter et al., 2014*]. *Saiz-Lopez et al., 2014* showed that CH_3I is the main contributor to the total organic iodine in the marine boundary layer (82%), and the free troposphere (96%), out of CH_2ICl, CH_2I_2 and CH_2IBr. It is also the predominant iodinated organic species in the free troposphere and the only iodocarbon which reaches the lower TTL by efficient convection [*Montzka et al., 2011; Tegtmeier et al., 2013 and 2014; Saiz-Lopez et al., 2014*]. CH_3I becomes the sole source of iodine in the lower TTL. The distribution of CH_3I in the upper troposphere and the TTL varies geographically as its presence there is subject to high surface emissions and the enhanced activity of the convective systems [*Tegtmeier et al., 2014*].

The photolysis of CH_3I represents 10, 60 and 83% of the total iodine sources from the iodocarbons within the marine boundary layer, free and upper troposphere, respectively [*Saiz-Lopez et al., 2014*]. Reactive iodine, once released via the iodocarbon photolysis, is indicated to be the second strongest ozone depleting family throughout the upper troposphere [*Solomon et al., 1994*, *Vogt et al., 1999; Saiz-Lopez et al., 2014*]. Thus, emissions of CH_3I, combined with the convective activity, contribute to the iodine budget in the upper troposphere and the TTL which affects the oxidising capacity there.

A combination of a relatively uniform boundary layer concentration, a well-defined lifetime and low limits of detection of 0.01 ppt makes CH_3I an attractive tracer for deep marine convection and the age of air in the upper troposphere [*Cohan et al., 1999*].

1.3.1.2 Brominated short-lived organic substances: Bromoform and Dibromomethane

The main short-lived brominated organic substances are bromoform ($CHBr_3$) and dibromomethane (CH_2Br_2). They are longer-lived than CH_3I, with atmospheric lifetimes of 15 and 94 days [*Carpenter et al., 2014*].

Bromocarbons are predominantly produced by oceans, biogenically via algae and lofted to the troposphere by deep convection in the atmosphere (Figure 1.13). $CHBr_3$ decomposes in the troposphere while convective outflow provides a steady supply of bromine to the global troposphere. Longer-lived bromocarbons, including CH_2Br_2, may slowly ascend across the tropopause. Both release active bromine which, turned into bromine oxides (BrO), facilitates the catalytic ozone loss [*Salawitch, 2006*].

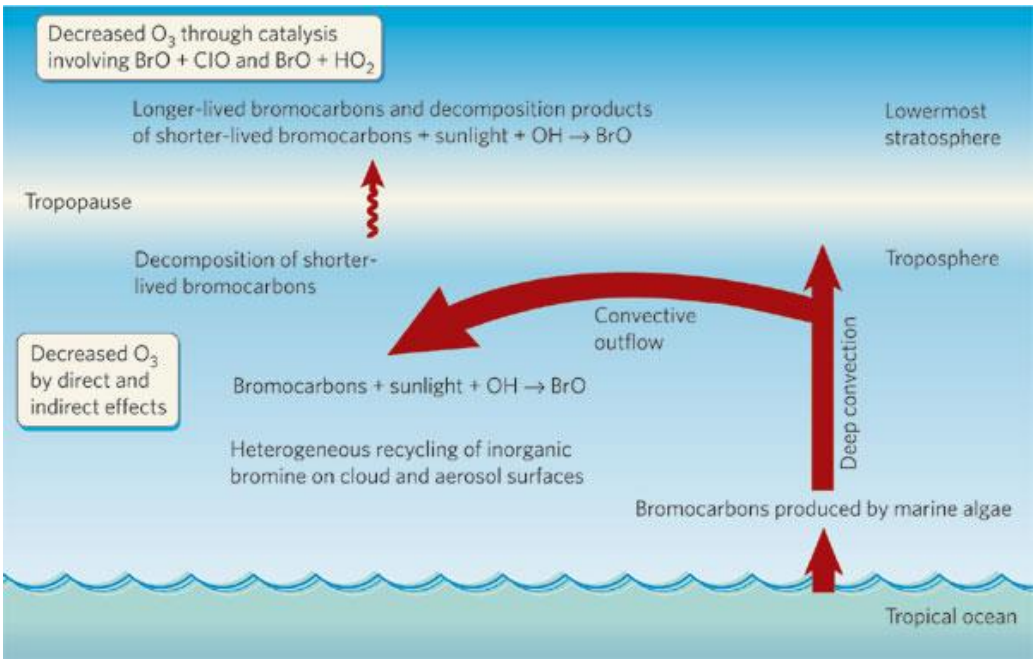

Figure 1.13 Brominated organic species life cycle: ocean - atmosphere pathway [*Salawitch, 2006*].

Vertical profiles for $CHBr_3$ and CH_2Br_2 concentrations over the Central-South and West Pacific are presented in Figure 1.14, as modelled by the UKCA-UM.

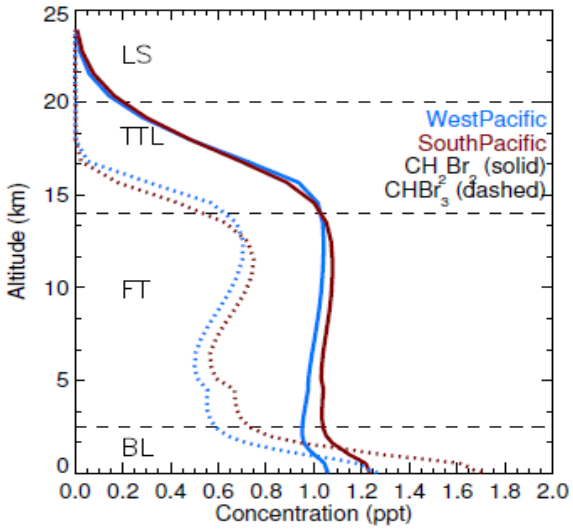

Figure 1.14 Vertical $CHBr_3$ and CH_2Br_2 concentration profiles over the Pacific, based on the UKCA-UM analysis of the 10-year means of DJF season. South Pacific (160°E-160°W, 20°S-10°N) and West Pacific (130-160°E, 10°S-30°N). BL, FT, TTL, LS – boundary layer, free troposphere, tropical tropopause layer and lower stratosphere) [*Personal communication with Xin Yang, Centre for Atmospheric Science, Cambridge, 2013*].

$CHBr_3$ and CH_2Br_2 have similar vertical profiles, with higher CH_2Br_2 in the TTL due to longer atmospheric lifetime. Highest mixing ratios are found in the boundary layer, where most emissions occur. Strong deep convection results in relocating high $CHBr_3$ and CH_2Br_2 around the maximum outflow altitudes of 10-13 km. Both decrease gradually in the TTL.

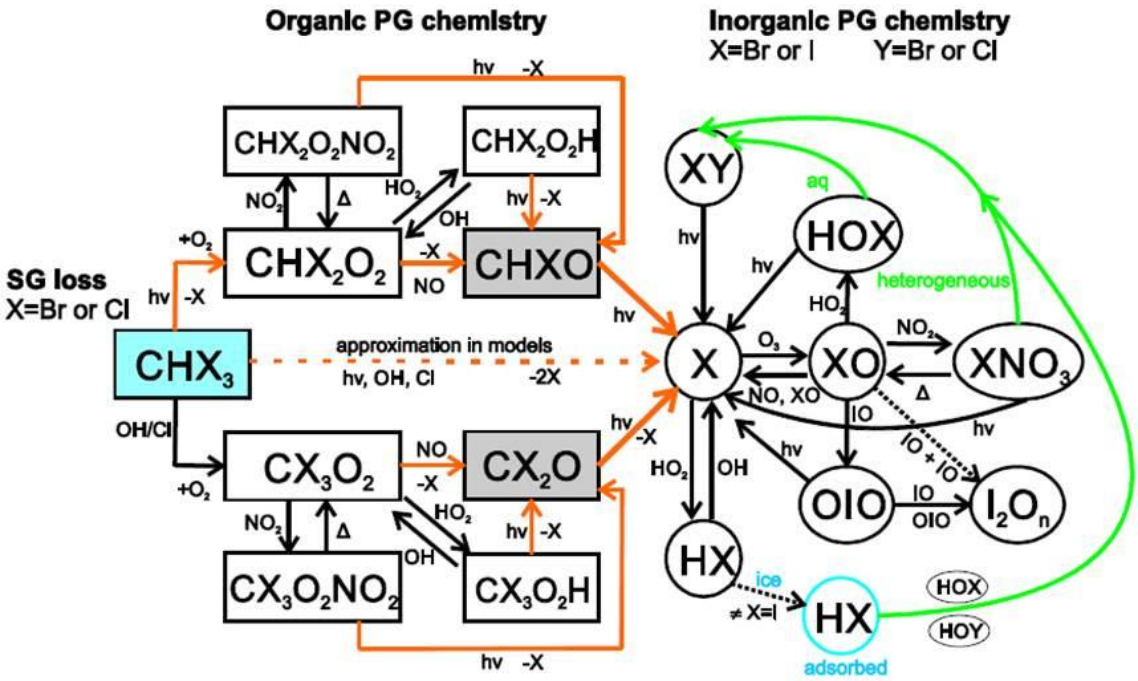

Figure 1.15 Scheme of the principal chemical reactions in the degradation of a typical tri-halogen short-lived organic substance, X - Cl, Br, I. The most stable organic intermediates are shaded gray. Orange arrows denote reactions that liberate halogen atoms, and green ones show primary gas-phase and heterogeneous reactions that cycle inorganic halogen species between active and reservoir forms [*Carpenter et al., 2014*].

Figure 1.15 shows the reactions involved in the degradation of the tri-halogen short-lived organic substances. For most of the short-lived halogenated substances, the major sinks are the radical oxidation and the photolysis. $CHBr_3$ is removed predominantly by photolysis as it contains multiple bromine atoms and has shorter lifetime. The OH oxidation is a more important sink for CH_2Br_2.

1.3.2 Importance of the short-lived halogenated organic substances in the stratosphere

Identifying transport pathways and the distribution of the short-lived halocarbons in the TTL is important, as they release the active halogen atoms, which then enter the stratosphere and cause the stratospheric ozone depletion. The rapid convective lifting into the TTL followed by the slow ascent and quasi-isentropic transport into the lower stratosphere is thought to be the main route by which these short-lived substances can substantially influence the

stratosphere [*Dessens et al., 2009; Ashfold et al., 2012*]. *Russo et al., 2015* found that the transport of short-lived species into the TTL and on to the stratosphere depends on the location of the emissions and on the location of the major vertical ascent occurring in convection. A maximum flux into the TTL would occur when the region of emission and convection exactly coincides [*Russo et al., 2015*].

The significant levels of total reactive iodine can be injected into the stratosphere via tropical convective outflow [*Carpenter et al., 2014*]. The modelled iodine-mediated ozone loss in the tropical lower stratosphere is comparable to, or even surpasses, the rate of ozone loss caused by the sum of the bromine from the short-lived bromocarbons and the stratospheric chlorine, up to about 25 km. This is a result of a two-fold effect of regeneration of iodine atoms via efficient ozone depleting catalytic cycles and the interhalogen cross-reactions [*Saiz-Lopez et al., 2016*].

The stratospheric mixing ratio of active bromine is above 20 ppt, with the largest sources being from methyl bromide (CH_3Br), and a number of anthropogenic halogens (industrial uses). The short-lived bromocarbons recently have been identified as the missing source for the stratospheric active bromine [*Pfeilsticker et al., 2000; Salawitch, 2006; Feng et al., 2007; Dessens et al., 2009*]. The current estimates of the contribution of the short-lived bromocarbons to the active bromine in the stratosphere range from 3 – 8 ppt [*Carpenter et al., 2014; Navarro et al., 2015; Butler et al., 2017*]. Much of this uncertainty is linked to contribution of $CHBr_3$ which has both the shortest lifetime and the largest emissions of the commonly observed bromocarbons.

The uncertainty in the emission inventories, the lifetimes, transport from the boundary layer to the TTL and within, the convection parameterisation, the scarcity of measurements, the large scale measurement limitations posed by the lifetimes of the short-lived halogenated organic substances contribute to the uncertainties in modelling the halogen loading in the TTL, derived from the short-lived halocarbons, and their impact on the stratosphere [*Quack et al., 2003; Schofield et al., 2011; Hossaini et al., 2013; Liang et al., 2014; Russo et al., 2015*].

Modelling studies suggest that due to future climate change, the stratosphere will get colder and the troposphere will get warmer. This would lead to a destabilisation of the mean atmospheric temperature profile, meaning the increased thermal instability. This, in turn, will increase the intensity and strength of tropical convection [*Hossaini et al., 2013*]. Thus, a significant increase in stratospheric bromine by 1-2 ppt, being about 5-10% of the total bromine abundance originating from the short-lived bromocarbons could occur. CH_2Br_2 would make the largest contribution (>90%) to the calculated changes in bromine abundance in the stratosphere between 2000 and 2100, due to its longer lifetime and the large source strength. The second largest contribution would come from $CHBr_3$, with the largest increase in the tropical upper troposphere [*Dessens et al., 2009*]. If in the future scenarios, the atmosphere gets warmer and thus more strongly convective, the increased BrO from short-lived bromocarbons might result in lower ozone levels in the troposphere and stratosphere [*Salawitch, 2006*].

1.3.3 CH_3I, $CHBr_3$ and CH_2Br_2 emissions and distribution in the TTL

Table 1.2 gives a summary of the CH_3I, $CHBr_3$ and CH_2Br_2 concentrations in the marine boundary layer and the TTL [*Carpenter et al., 2014*]. Table 1.3 presents the summary of the emissions of CH_3I, $CHBr_3$ and CH_2Br_2, constructed using various methodologies. These are not well constrained and vary significantly, depending on the geographical locations. Emissions from the oceans are the major sources, and the relative importance of coastal and open ocean sources is not well quantified, with the uncertainty linked to the lack of information on the distribution and relative strength of the dominant macro- and micro-algal sources [*Ordonez et al., 2012; Ziska et al., 2013; Stemmler et al., 2015*].

Table 1.2 Summary of observations of CH_3I, $CHBr_3$ and CH_2Br_2 in the marine boundary layer (MBL) and the TTL. The MBL values are medians, the TTL are means, the values in brackets show the range, units: ppt [*Carpenter et al., 2014*]. *Abundances in the MBL are calculated from the compilation of Ziska et al., 2013 for $CHBr_3$, CH_2Br_2, and CH_3I (20°N to 20°S). Data in and above the upper troposphere have been compiled from observations during the PEM-Tropics A and B, TC4, Pre-AVE, and CR-AVE aircraft campaigns [Schauffler et al., 1999], from the SHIVA, HIPPO, and ATTREX aircraft campaigns [Tegtmeier et al., 2013], and from balloon observations [Laube et al., 2008, Brinckmann et al., 2012]. The stated observed range represents the smallest mean minus 1 standard deviation and the largest mean plus 1 standard deviation.*

Substance	Marine Boundary Layer (MBL) 0-2 km	Lower TTL 12-14 km	LZRH 14.5-15.5 km	Upper TTL 15.5-16.5 km	Tropical Tropopause 16.5-17.5 km
CH_3I	0.80 (0.3-2.1)	0.16 (0.00-0.38)	0.04 (0.00-0.10)	0.00 (0.00-0.01)	0.01 (0.00-0.06)
$CHBr_3$	1.20 (0.4-4.0)	0.56 (0.20-1.10)	0.22 (0.00-0.63)	0.14 (0.01-0.29)	0.08 (0.00-0.31)
CH_2Br_2	0.90 (0.6-1.7)	0.89 (0.60-1.20)	0.74 (0.59-0.99)	0.66 (0.43-0.83)	0.52 (0.30-0.86)

Table 1.3 Selected fluxes of total bromine from $CHBr_3$ and CH_2Br_2, and iodine from CH_3I. Emissions are differentiated into global (G), open ocean (OO) and coastal (C) [*Carpenter et al., 2014*].

Reference	*$CHBr_3$ Flux ($Gg\ Br\ yr^{-1}$)*			*CH_2Br_2 Flux ($Gg\ Br\ yr^{-1}$)*			*CH_3I Flux ($Gg\ I\ yr^{-1}$)*		
	G	*OO*	*C*	*G*	*OO*	*C*	*G*	*OO*	*C*
Bell et al., (2002)							*272*		
Butler et al., (2007)	*800*	*150*	*650*	*280*	*50*	*230*	*550*	*270*	*280*
Carpenter et al., (2009)			*200*						
O'Brien et al., (2009)	*820*								
Liang et al., (2010)	*430*	*260*	*170*	*57*	*34*	*23*			
Jones et al., (2010)							*300*	*240*	*60*
Pyle et al., (2011)	*362*								
Ordonez et al., (2012)	*506*			*62*			*270*		
Ziska et al., (2013)	*120-200*			*62-78*			*157-184*		

1.4 Modelling of the transport events in the atmosphere

Atmospheric models are used to represent the physical processes and simulate chemical evolution and transport of substances in the atmosphere. The numerical modelling of the atmosphere takes two major approaches: Eulerian and Lagrangian. The difference between these approaches lies in how the atmospheric motion is viewed [*Stohl, 1998*].

The Eulerian approach focuses on points fixed in space through which the air flows. Regular rectangular grids are built throughout the model domain and a finite-differencing scheme is used to describe new properties of these grids, with the use of numerical equations. The accurate representation of the transport is not straightforward in this

Eulerian model framework due to the presence of negative concentrations and numerical dispersion [*Collins et al., 2002*]. Eulerian models can be developed for all scales down to large eddy simulations of convection, but are too expensive generally to be deployed over large domains for long times.

The Lagrangian perspective focuses on individual air parcels as they move through time and space. The position and the properties of these air parcels are calculated according to the meteorology fields and the parameterisation of the physical processes they are subject to [*Jones et al., 2004*]. The chemistry and transport can be uncoupled.

Lagrangian models pose smaller computational demands than Eulerian models [*Stohl, 1998*]. The Lagrangian approach involves no numerical diffusion, unavoidable in an Eulerian setup due to the use of the mixing ratio gradient to calculate the advection of a tracer. There is no stability limit on the time step in the Lagrangian setup, as well as the spatial resolution is higher where the concentration (more trajectories) is higher [*Wohltmann et al., 2009*]. However, the coherence of the identity of an air parcel (trajectory) is an especially important implicit assumption [*Seinfeld and Pandis, 2006*]

Lagrangian models are more suitable for designing the flight planning routines and analysing the flight measurements, as they operate on very low scales (provide higher horizontal resolution, as opposed to Eulerian models with large grid sizes). They are also computationally less expensive and more time available, as they can produce the requested output within hours before the flight deployment.

Three dimensional models can either be General Circulation Models (GCMs) which calculate their own wind fields and other physical parameters, or Chemistry Transport Models (CTMs) which are offline and do not solve their own dynamic transport equations. Instead, horizontal and vertical air mass fluxes are prescribed based on the output of the GCMs or using global meteorological observations.

The atmospheric models cannot consider all scales of motion. Certain processes, such as tropical deep convection, need to be parameterised in both types due to its high degree of

stochasticity, the short term initiation, the small scale area coverage and boundary layer turbulence. Thus, the more accurate parameterisation of the physical processes, the more realistic the representation of the particle transport becomes.

1.5 Thesis Outline

The main objectives of my thesis: *"Transport and Distribution of the Short-lived Halocarbons in the Tropical Tropopause Layer in the Pacific Ocean: the Role of Convection."* are to:

- **(a)** develop the capacity of the NAME model as a tool supporting the flight planning activities and achieving the multi aircraft coordination in the CAST, CONTRAST and ATTREX 2014 joint research campaigns,
- **(b)** quantify the distribution of the short-lived halogenated organic substances in the East and West Pacific TTL, and compare the modelled results against the measurements obtained from the NASA ATTREX 2013 and 2014 research campaigns,
- **(c)** assess the temporal and spatial variability in the atmospheric transport of the short-lived halogenated organic substances to the TTL. The focus is on investigating the role of convective events in moving these substances to the upper troposphere and the TTL in relatively short timescales.

The work draws heavily on the NAME applications used in the field campaigns. The model is used pre-campaign and in the campaign as a flight planning tool, and post-campaign to assess and interpret the transport and distribution of the short-lived halocarbons in the TTL.
The motivation behind this thesis is the uncertainties in the transport, abundance and fate of the short-lived halogenated organic substances, particularly bromocarbons, in the TTL [*Schofield, et al., 2011*]. These have a significant impact on the stratospheric halogen budget [*Hossaini et al., 2013*]. These uncertainties also lead to significant uncertainties in the photochemistry and composition of the lower stratospheric ozone.

Having listed the main scientific questions and the motivation behind this thesis, the structure of the thesis is now outlined.

Chapter 2 provides the methodology used in the thesis. The UK Meteorological Office Numerical Atmospheric-dispersion Modelling Environment (NAME) model is introduced as a tool for simulating atmospheric transport events. The model setup is presented along with the ways NAME represents the particle transport, turbulence and the deep convection. An example of the NAME forward and backward runs with different convection scheme setups is discussed. This is followed by a description of how very short-lived halogenated organic substances are measured during the CAST, CONTRAST, and ATTREX joint research campaign.

Chapter 3 takes an in depth look at how NAME is used to provide a flight planning tool and achieve the flight coordination in the CAST, CONTRAST and ATTREX campaigns. An overview of this joint campaign is provided. The NAME flight planning procedure is developed then, the proposed sets of NAME runs and the products are described. This procedure is tested for the ATTREX 2013, further modified and used in the CAST, CONTRAST and ATTREX 2014. This chapter shows one approach to use NAME as a Lagrangian tool for providing support in the coordinated aircraft missions.

Chapter 4 gives a detailed analysis of the measurements of the short-lived halogenated organic substances in the ATTREX 2013 and 2014 flights. The substances of interest are: methyl iodide (CH_3I), bromoform ($CHBr_3$) and dibromomethane (CH_2Br_2). This is complemented with the NAME analysis of the boundary layer air influence in the TTL. The transport of these air masses is assessed, including the analysis of the source regions.

Chapter 5 investigates the convective influence of CH_3I in the TTL. The NAME procedure is developed to quantify and explain the CH_3I distribution in the TTL. The boundary layer and background contribution estimates are differentiated. The total CH_3I modelled estimates are compared against the CH_3I measurements taken during the individual ATTREX 2014 flight, before expanding to all ATTREX 2014 and 2013 flights.

Chapter 6 tests the performance of the new convection scheme, developed and implemented in NAME in 2016. The NAME procedure to quantify the CH_3I in the TTL is applied, and the

modelled results, inferred from the NAME runs with no convection and with the new convection scheme, are compared against the CH_3I measurements taken during the four individual ATTREX 2014 flights which experienced the most convective influence. This chapter answers the question if the new convective scheme improves the representation of the particle transport via deep convection.

Chapter 7 investigates the loading and distribution of the brominated short-lived organic substances in the TTL. The same NAME procedure is used to quantify $CHBr_3$ and CH_2Br_2 in the TTL. As these are longer-lived, the background component is more important and thus needs to be further assessed. The attempt is made to estimate the contribution of the short-lived brominated organic substances to the bromine budget in the TTL.

Chapter 8 summarises the findings, provides the conclusions and offers the potential ideas for further work and development of the scientific areas embed in this thesis.

1.6 Acknowledgements

I would like to acknowledge the help of Dr Matt Ashfold, a former member of the Centre of Atmospheric Science, Cambridge University, in providing a set of IDL routine scripts which were modified and used in this thesis [*Ashfold et al., 2012*]. The UK Meteorological Office (in particular Drs Alistair Manning and Elena Meneguz) helped in designing and the routine execution of the NAME flight planning sets of runs, and in providing the beta version of the new convection scheme for the further testing and validation purposes (used in this thesis, see Chapter 6). The ATTREX AWAS measurements were made by Dr Maria Navarro and Prof Elliot Atlas, University of Miami.

2. Methodology

This chapter describes the modelling and measurement tools I used to investigate the transport and distribution of very short-lived (VSL) halogenated organic substances in the tropical Pacific. This chapter is split into four sections. Section 2.1 introduces the UK Meteorological Office NAME model, used for representing the atmospheric transport and dispersion events. All the modelling results included in this thesis are generated by NAME. In Section 2.2, a description of how NAME represents the particle transport and the turbulence is given. Section 2.3 explains the phenomenon of convection in the atmosphere and the ways it is parameterised in NAME. An example of a NAME simulation test, utilising the old and new convection scheme, is then provided. Section 2.4 gives an overview of how VSL halogenated organic substances were measured during NASA Airborne Tropical Tropopause Experiment (ATTREX), NCAR Convective Transport of Active Species in the Tropics (CONTRAST) and NERC Co-ordinated Airborne Studies in the Tropics (CAST) campaigns. Finally, a description of the Advanced Whole Air Sampler (AWAS) instrumentation and post processing steps in analysing the VSL halogenated organic substances is provided.

2.1 The NAME model: history, development and applications

The Numerical Atmospheric-dispersion Modelling Environment (NAME) is a Lagrangian particle dispersion model, developed by the UK Meteorological Office in the 1980s. Known back then as the Nuclear Accident Response ModEl, NAME aimed to (i) provide emergency responses for radioactive plume tracking in case of nuclear accidents, (ii) predict the dispersion and deposition of gases and particulates in the atmosphere, and (iii) perform air quality forecasts [*Jones et al., 2007*].

The Chernobyl disaster in 1986 stands as the first in-detailed study utilising NAME (Figure 2.1) by providing predictions of the transport of the radioactive plume and deposit estimates of radioactive material from the Chernobyl nuclear power plant explosion [*Maryon and Best, 1995*].

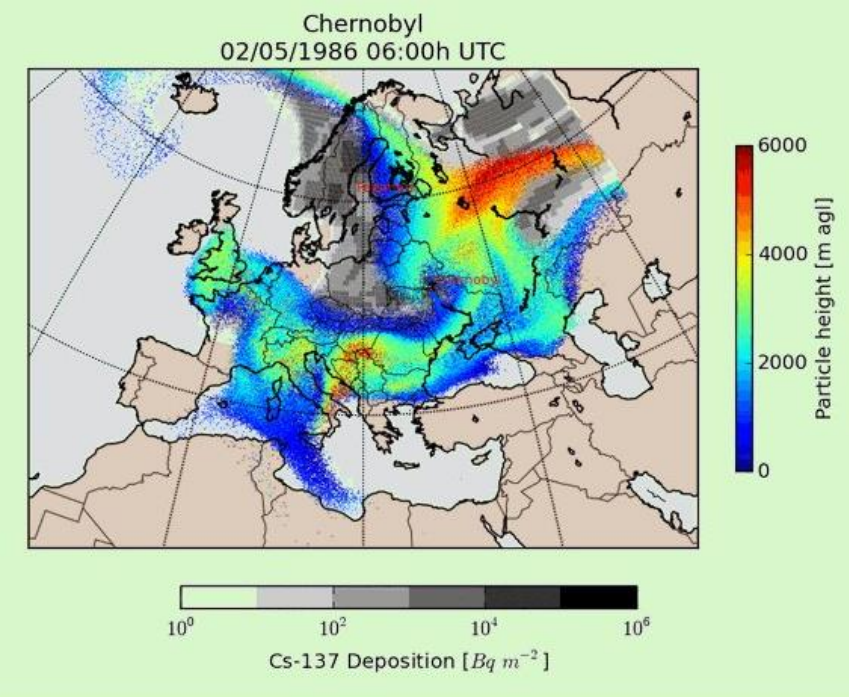

Figure 2.1 Cs-137 deposition and spread of radioactive plume after Chernobyl accident in 1986, NAME prediction map [UK Meteorological Office, Radioactive Dispersion Modelling Leaflet].

Since then, the model has undergone development to represent many types of atmospheric dispersion events [*Stohl, 1998*], ranging from volcanic ash dispersal [*Witham et al., 2011; Webster et al., 2012*], Saharan dust storm episodes [*Athanassiadou et al., 2006*] to the

analyses of fire incidents [*Leadbetter et al., 2014*]. It has recently been used to identify sources and spread of wind-borne plant and animal disease vectors e.g. *Hymenoscyphus fraxineus* fungus causing the ash dieback tree disease in the UK, or the UK outbreak of bluetongue and foot-and-mouth disease in 2001 [*Gloster et al., 2006 and 2013*]. The model's routine use in providing emergency response forecasts is globally acknowledged. In this way NAME provides support to the regulatory bodies in emission monitoring [*Ganesan et al., 2015*].

NAME simulates a dispersion event by releasing and tracking particles within a model atmosphere. This model atmosphere is driven by the meteorological fields inferred from the output from the UK Meteorological Office Numerical Weather Prediction (NWP) operational model: the Unified Model (UM). Meteorological input includes wind fields, temperature and cloudiness, and is calculated by incorporating both forecasts and archived observational data [*Cullen, 1993; Jones et al., 2007*]. This process is continuously repeated to produce a three-dimensional gridded analysis of the state of the atmosphere. Flow information (meteorological input data) is read at three-hourly intervals and multi-linearly interpolated in time and space for each Lagrangian particle and a model time step. The particles' motion has a random component to represent the effects of atmospheric turbulence.

Each modelled particle can have its own prescribed characteristics such as the molecular weight and type, the photolytic loss rate, a life-time, deposition velocity, and surface resistance. Modelled particles are released either instantaneously or constantly, and tracked in two modes: forward and backward, to represent the fate and origin of the released entities, respectively.

NAME requires the following input: (a) emission parameters: source height and location, temperature and the mass flow of particles; (b) the meteorological data driving the flow of particles: wind vectors (speed and direction), temperature, stability of the air, boundary layer height; (c) topography of the surrounding area (used for long-range applications), and (d) details of any obstruction to the flow (used for short-range applications) [*Davis, et al., 2009; Lin et al., 2012*].

2.2 Assessment of the particle transport and turbulence in NAME

The atmosphere, as a dynamic entity, is in a constant state of mixing, or turbulence. Multiple complex processes, including the movement of unstable air masses and winds experiencing friction along the Earth's surface, contribute to this turbulence, resulting in the increased stochasticity of the atmospheric system. For that reason, it is difficult to represent the turbulence in atmospheric particle dispersion models [*Stohl, 1998*].

A trajectory is the individually computed path, taken by a NAME particle after the release, driven by the modelled NAME atmosphere (defined by the meteorological and wind fields) and the parameterised turbulence component. A realistic representation of turbulence within NAME is vital to calculate the robust trajectories. Each trajectory can be calculated following Equation 2.1, which defines the position of a particle, $X_{(t+\Delta t)}$, at initial time step, t, and given simulation time step, Δt.

(2.1) $\boldsymbol{X_{t+\Delta t} = X_t + [u(X_t) + u'(X_t) + u_l'(X_t)]_{\Delta t}}$

Equation 2.1 is expanded by adding factors, affecting the position of a modelled particle: the wind velocity vector, u, the turbulent velocity vector for small scale turbulence, u', and the velocity vector for low frequency horizontal meandering, u_l' [*Ryall et al., 1998*]. A turbulent velocity vector, u′, is defined by a random walk formula which has a horizontal, u_t', and vertical, w_t', component. Equations 2.2 and 2.3 present the relationship for the horizontal, u_t', and vertical, w_t', components of a turbulent velocity vector:

$$u_{t+\Delta t}^{'} = u_t^{'}(1-\frac{\Delta t}{\tau_u}) + (\frac{2\sigma_u^2 \Delta t}{\tau_u})^{1/2} r_t$$

(2.2)

$$w_{t+\Delta t}^{'} = w_t^{'}(1-\frac{\Delta t}{\tau_w}) + (\frac{2\sigma_w^2 \Delta t}{\tau_w})^{1/2} r_t + \frac{\Delta t}{\sigma_w}\frac{\delta \sigma_w}{\delta z}(\sigma_w^2 + w_t^{'2})$$

(2.3)

These depend on velocity variances (σ_u^2 and σ_w^2), Lagrangian timescales (τ_u and τ_w) and a random Gaussian variable r_t. The first and second right-hand terms represent a memory of

previous motion and a new random perturbation, respectively. A 'drift velocity' term, preventing particles from gathering together when the standard deviation is small, is represented by the last term in Equation 2.3 [*Ryall et al., 1998*]. It includes a gradient of vertical component of turbulent velocity vector, $\delta\sigma_w/\delta z$ [*Ryall et al., 1998*].

2.3 Representation of Deep Convection Scheme in NAME

Convection is defined as the vertical uplift of air, driven by change in latent heat. It is a crucial component in atmospheric transport and mixing [*Mahlman, 1997; Collins et al., 2002*]. In moist convection, of which the intensity is very high over the tropical regions, the updraughts and downdraughts occurring inside the convective clouds play a key role in redistributing particles (inert or chemically reactive) through the troposphere, occasionally reaching the stratosphere *[Meneguz et al., 2016]*.

Convection is another component of the atmospheric dynamics which models struggle to represent well. The main limitation is that convective clouds have a small horizontal length scale (of the order of a few metres to a few kilometres) *[Emanuel, 1994; Collins et al., 2002]*. Most of the available global meteorological data, which drive the atmospheric models, do not have horizontal resolution low enough to pick up signals of individual small-scale convective events. Therefore, the convection needs to be parameterised to reproduce the vertical motions undertaken by particles due to the presence of convective clouds, which would otherwise be under-represented *[Meneguz et al., 2016]*.

In this thesis, NAME is driven by UK Met Office NWP UM assimilated 3-hourly averaged global meteorological field data with horizontal resolution of ~25 km (NAME6v4, UMG_Mk6 and UMG_Mk7, 0.352^o longitude x 0.235^o latitude grid). The latest version of NAME 6v5 uses global meteorological data (UMG_Mk9) with horizontal resolution of ~17 km (0.234^o longitude x 0.156^o latitude grid, Table 2.1). Vertical resolution of meteorology field data consists of 31 pressure levels below approximately 19 km.

Table 2.1 Horizontal resolution of global meteorological data used in NAME.

Year	Global Meteorological Data available	NAME version	Horizontal resolution [^{o}] | [km]
2008	GLOUM6	6v3	0.563 x 0.375 | ~62
2013, 2014	UMG_Mk6, UMG_Mk7	6v3, 6v4	0.352 x 0.235 | ~25
2015, 2016	UMG_Mk9	6v4, 6v5	0.234 x 0.156 | ~17

The UM meteorological field data already contain the convection parameterisation component, as the UM itself diagnoses convection via the mass-flux approach originated by *Gregory and Rowntree [1990]*. This scheme quantifies, for each grid box, the amount of mass transported in updraughts, downdraughts, entrainment of environmental air and detrainment of cloudy air [*Gregory and Rowntree, 1990*]. The horizontal resolution of the UM meteorological field data is too coarse and so the effect of particle displacement via convection events is significantly misrepresented. That is why the convection in NAME should be parameterised and used in this case. Parameterisation of convection also allows for accounting the effect of particle displacement due to convection between the grids.

The convection scheme in NAME has two goals. The first is to predict the net convective energy release in terms of known large scale variables. The second is to distribute the released energy in a realistic manner while fitting together with other parameterisation (radiation, large scale rain and boundary layer), maintaining a realistic atmospheric structure in the vertical dimension *[Meneguz et al., 2014]*.

There are three modes by which convection is represented in NAME 6v5 for tracking particles backwards and forwards: (a) convection scheme turned off: 'NO', (b) ‘OLD’ deep convection scheme activated, and (c) 'NEW' deep convection scheme activated (developed and implemented by Elena Meneguz and David Thomson, Atmospheric Dispersion & Air Quality, UK Meteorological Office, 2014-2016). The older versions of NAME have only two modes for the convection scheme: ‘NO’ and ‘OLD’, with NAME 6v4 allowing a ‘NEW’ deep convection scheme for the forward particle release only.

When the convection scheme is off, the vertical velocity is the only factor directing how fast the vertical uplift of particles is. The old convection scheme incorporates the UM diagnostics: convective cloud top and base heights, and cloud fraction. A cloud fraction represents the section of the grid box covered by a convective cloud. If the cloud depth exceeds 500 m (i.e. the cloud has 'enough' vertical extension), particles within the convective cloud fraction are randomly redistributed along the vertical direction of the cloud *[Maryon et al., 1999]*. This approach of the cloud vertical extension produces similar results to those obtained when the convection scheme is turned off *[Meneguz et al., 2014]*.

Progress in developing a more realistic representation of deep convection has been made with the launch of NAME 6v4, 2014. A new improved deep convection scheme makes better use of the diagnostic fields currently available from the UM. In contrast to the old scheme, the new scheme quantitatively estimates the amount of material transported inside the convective cloud, via a mass flux approach.

Deep convective clouds are represented in NAME as three-dimensional boxes, with base and top respectively coinciding with the UM-diagnosed convective cloud base and cloud tops (Figure 2.2). To conveniently represent the transport of air inside and outside the cloud, pressure, p, is chosen as a coordinate to represent the cloud height. An *ad hoc* one-dimensional vertical grid of equally spaced pressure levels is then built. The total number of levels, k_{max}, is first assumed to be:

(2.4) $$k_{max} = (p_{cb} - p_{ct}) / 2000$$

where p_{cb} is the cloud base and p_{ct} the cloud top, both in unit of pressure. A minimum and a maximum value for k_{max} is imposed (3 and 51, respectively) with the minimum chosen to guarantee that there is a at least one pressure level below the cloud base, one inside the cloud and one above the cloud. Once k_{max} is established, equally spaced pressure layers of depth Δp are evaluated as:

(2.5) $$\Delta p = min\left(\frac{p_{cb}-p_{ct}}{(k_{max}-1)}, \frac{p_0-p_{ct}}{(k_{max}-0.5)}\right)$$

where p_0 is the surface pressure. Depending on the result of Equation 2.5, the first pressure

level, p_1, is calculated as Equation 2.6 shows. This method always ensures that $p_1 \leq p_0$.

(2.6) $p_1 = p_{cb} + \Delta p / 2$ *or* $p_1 = p_0$

Once the vertical grid of equally spaced pressure levels is constructed, it is possible to calculate each pressure level according to the Equation 2.7.

(2.7) $p_k = p_1 - (k - 1)\Delta p \qquad k \in [1, k_{max}]$

Further, the amount of mass transported inside the cloud as a result of exchange of air between the cloud and the environment is quantified for each pressure grid box, to estimate the result of convection.

For NAME simulations in the forward mode, an empirical formula (Equation 2.8), based on the equation of conservation of mass, is used to obtain the mass fluxes of convective transport components: transport within the convective cloud (updraught), transport from the environment to the cloud (entrainment) and from the cloud to the environment (detrainment) (Figure 2.2).

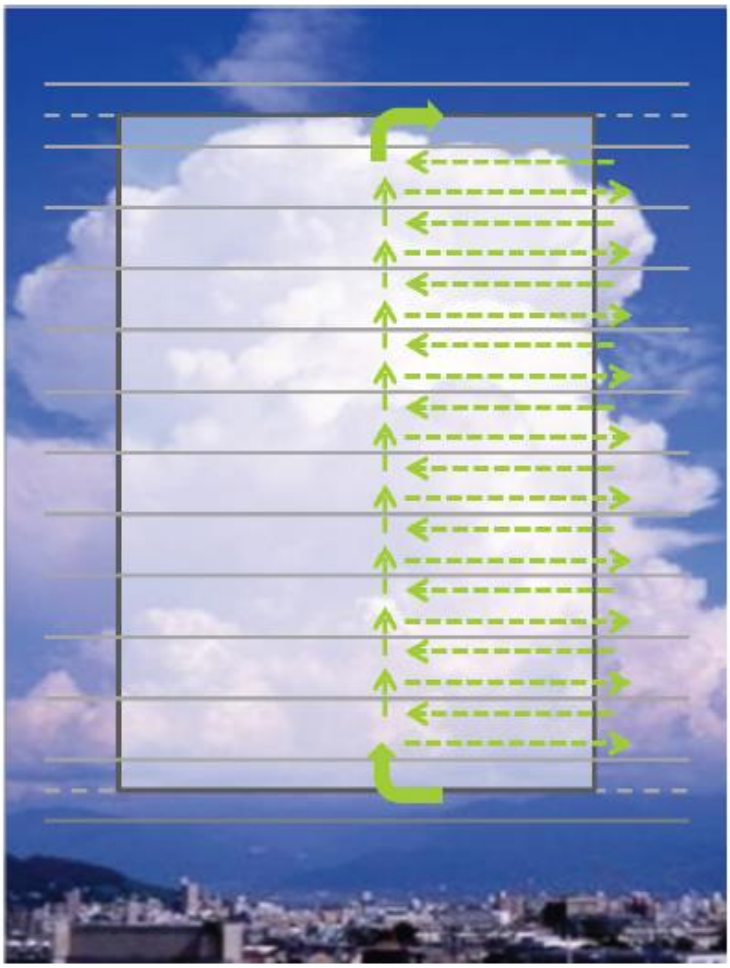

Figure 2.2 Simplified representation of a convective cloud and the exchange of air from/to the environment following the mass flux approach. Pressure levels are marked with grey solid lines, entrainment/detrainment fluxes in first and last pressure levels – green solid arrows, updraught (vertical) / detrainment /entrainment (both horizontal) fluxes in other pressure levels – green dashed lines [*Meneguz et al., 2014*].

(2.8) $M_{k+1}+D_k = M_k + E_k$

where M_k is the updraught mass flux at pressure level, k, and D_k and E_k are respectively detrainment and entrainment mass flux components (units: Pa/s) in the layer between p_k and p_{k+1}. This equation does not include downdraughts, with its absence being justified by the well-established knowledge that the downdraught mass fluxes are much smaller than the updraught ones (typically around one tenth as big). These fluxes are obtained using empirical

formulas derived from Cloud Resolving Models *[Meneguz et al., 2016]*. These fluxes are used to estimate how many particles entrain, move upward and detrain via a set of probabilities (Equation 2.9).

$$(2.9) \quad P_{ent,k} = \Delta t E_k / \Delta p, \qquad P_{up,k} = M_{k+1}/(M_k + E_k), \qquad P_{det,k} = 1 - P_{up,k}$$

For a given pressure layer, k, the probability of entrainment is calculated by taking into account the mass that entrains in a given time step over the depth of the layer. The probability of moving in an updraught, $P_{up,k}$, is evaluated by estimating the fraction of mass that moves upward with respect to the mass that enters into the cloud column. The probability of detrainment, $P_{det,k}$, is calculated in a similar way *[Meneguz et al., 2014]*.

It is possible to run NAME in the backward mode with the improved convection parameterisation. In this case, the upward vertical displacement by convection is suppressed and substituted with downward vertical displacement. The calculation of the downdraught mass, $M_{d,k}$, entrainment, $E_{d,k}$, and detrainment, $D_{d,k}$ fluxes (Equation 2.10) mirror the updraught mass, entrainment and detrainment fluxes (Equation 2.8).

$$(2.10) \quad M_{d,k} = M_k \qquad E_{d,k} = D_k \qquad D_{d,k} = E_k$$

Once the fluxes are calculated, the probabilities are estimated of how many particles entrain in a given cloud layer, *k*, move downwards and eventually detrain to the environment (Equation 2.11).

$$(2.11) \quad P_{entD,k} = \Delta t E_{D,k} / \Delta p, \quad P_{down,k} = M_{d,k}/(M_{d,k+1} + E_{d,k}), \qquad P_{detD,k} = 1 - P_{down,k}$$

Further assumptions are applied and lastly, a subsidence flux is applied to compensate for downdraught motion [*Meneguz et al., 2016*].

Implementation of the new convection scheme leads to a more realistic estimate of particle transport via convection, from lower to higher altitudes in the troposphere. This is true for simulations in forward mode; and analogous for backward runs. Furthermore, the new

scheme proves suitable for the simulation of long range dispersion events which currently relies on global meteorological fields supplied at horizontal spatial resolutions insufficient to capture the existence of convective clouds [*Meneguz et al., 2016*]. Chapter 6. *Representation of Deep Convection in NAME* provides a validation study assessing the performance of the new convection scheme using methyl iodide (CH_3I) from the AWAS observations obtained during the NASA ATTREX 2014 campaign.

2.3.1 Convection Scheme in NAME – Test Case Study

This section presents the results from a set of NAME simulations in forward and backward mode, utilising the old and new deep convection scheme. The difference in performance of these schemes is highlighted.

25,000 particles are released on 28 January 2014 from a box around the Tropical West Pacific Warm Pool (160^oE, Equator; box dimensions of 1^o x 1^o) from 0-1 / 13-14 km in the boundary layer / the lower TTL (for a forward / backward run). Particles are followed 12 days forward / backward to identify the number and timescales of trajectories reaching the upper troposphere and the tropical tropopause layer (TTL) / low troposphere and boundary layer, respectively. The NAME setup differs in the convection settings: (a) convection scheme is off, (b) old convection scheme is activated, and (c) new convection scheme is activated.

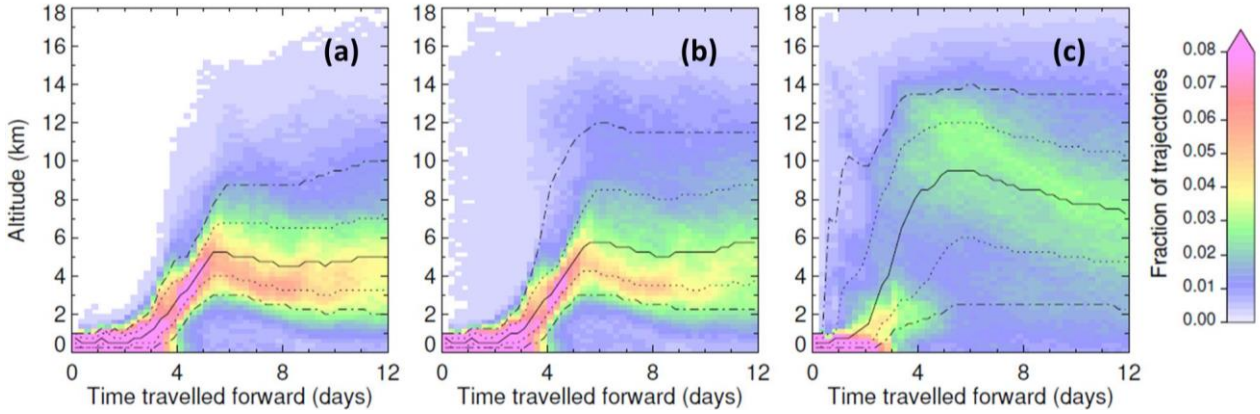

Figure 2.3 Evolution of vertical distribution of particle density in time for NAME test runs in forward mode with: (a) convection scheme off, (b) activated old convection scheme, and (c) activated new convection scheme. Lines show the percentage of trajectories below given altitude at given time step: 50% (median) – solid line, 25 and 75% - dotted lines, 10 and 90% - dot-dash lines.

Figure 2.3 illustrates the evolution of vertical distribution of particle density in time. Particles are binned into 0.25 km boxes, covering the whole troposphere and TTL, per 6-hourly output time step (a 0.25 day unit). Consequently, a time series of the vertical distribution of particles over 12 days of the NAME run duration is plotted. The flow of particles can be seen throughout the duration of the NAME run, with the presence of varied particle populations exhibiting different transport pathways.

Regarding the NAME test runs in forward mode, particles which reach above 10, 14 and 16 km are counted and turned into fractions (Table 2.3). These altitude levels correspond to levels of the upper troposphere (just above the maximum convective outflow / detrainment), a level within the lower TTL and above the approximate level of net zero radiative heating (LZRH), respectively.

Table 2.2 Fractions of trajectories [%] crossing above 10, 14 and 16 km for NAME test runs in forward mode with different convection scheme setup.

NAME runs with convection scheme setup	Fraction of trajectories [%]		
	> 10 km	> 14 km	> 16 km
NO	17	2	0
OLD	30	8	1
NEW	65	21	6

Little difference is observed between the results inferred from simulations with no convection scheme and the old convection scheme. The evolution of transport timescales and number of trajectories reaching the investigated altitude levels at given time step is similar. The runs with no / old convection scheme show higher density of particles confined around the release source and below the low troposphere, with few or no particles reaching higher altitudes (upper troposphere or TTL) within 6 days after the particle release. This is contrasted with enhanced fraction of particles (over 50%) reaching the upper troposphere within 6 days after the particle release, seen in the new convection scheme NAME run. This run also sees the significantly higher fractions of trajectories reaching the 10, 14 and 16 km altitudes.

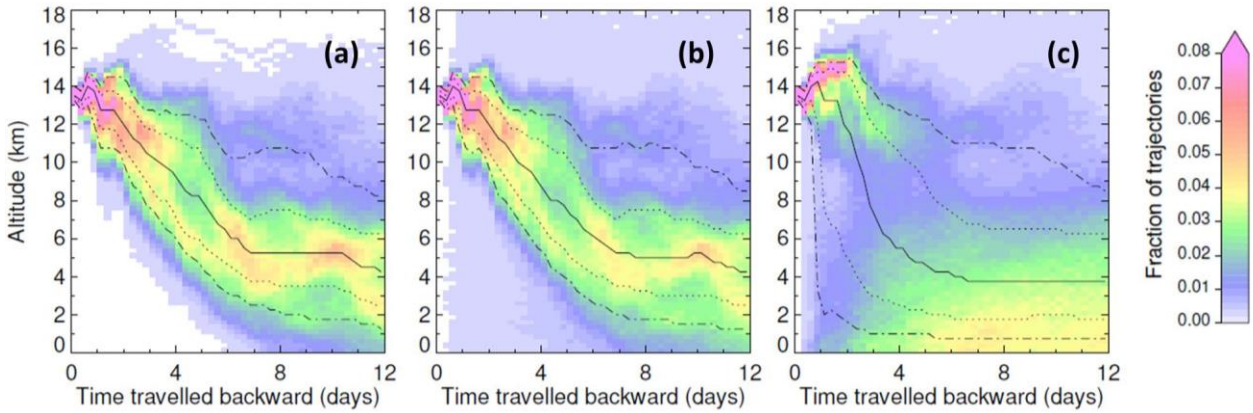

Figure 2.4 Evolution of vertical distribution of particle density in time for NAME test runs in backward mode with: (a) convection scheme off, (b) activated old convection scheme, and (c) activated new convection scheme. Lines show the percentage of trajectories below given altitude at given time step: 50% (median) – solid line, 25 and 75% - dotted lines, 10 and 90% - dot-dash lines.

Figure 2.4 illustrates the analogous evolution of vertical distribution of particle density in time, for the NAME test runs in backward mode. The fractions of trajectories reaching below 5, 3 and 1 km are calculated (Table 2.3), with altitudes corresponding to the levels of and within the low troposphere, and the approximate level of oceanic boundary layer, respectively.

Table 2.3 Fractions of trajectories [%] crossing below 5, 3 and 1 km for NAME test runs in backward mode with different convection scheme setup.

NAME runs with convective scheme setup	Fraction of trajectories [%]		
	< 5 km	< 3 km	< 1 km
NO	82	49	14
OLD	83	53	19
NEW	92	83	65

Again, little difference in fractions of trajectories below 5, 3 and 1 km is observed for the results inferred from the simulations with convection scheme switched off and the old convection scheme. Runs with no / old convective scheme show higher density of particles confined throughout 12 days, with few particles reaching below the investigated altitudes in the early stage of the NAME test runs. Conversely, for the NAME test run with a new convection scheme, a considerable fraction of trajectories reaches the low troposphere within first 6 days of the NAME run. By the final time step, 65% of the released particles reach the boundary layer.

Summing up, the new convection scheme yields higher fractions of particles reaching above / below the investigated altitudes for the forward / backward mode NAME test runs. Higher fractions of particles reach these altitudes earlier within the NAME run duration of 12 days, implying the shorter transport times. The new convective scheme produces a stronger effect of the particle displacement via convection.

2.4 Measurements of very short-lived halogenated organic substances in the CAST, CONTRAST and ATTREX joint campaign

The first campaigns which focused on measuring the VSL halogenated organic substances were the Global Tropospheric Experiment (GTE) Pacific Exploratory Missions: PEM-West-A (1991), PEM-West-B (1994) and PEM-Tropics-T (1996). These were followed by multiple airborne research campaigns (for instance: STRAT, 1996; HIBISCUS, 2001, 2003, 2004; CR-AVE, 2006; SCOUT-O3/AMMA, 2006; TC4, 2007; CARIBIC, 2009-2013; SHIVA, 2009-2013; TORERO, 2012). These campaigns provided halocarbon tracer measurements over limited regional domains and time periods in the upper troposphere and the TTL *[Jensen et al., 2009; Hamer et al., 2013]*. Measuring the TTL in the Pacific is challenging as it is hard to cover the whole tropical region spatially and vertically to achieve coordinated measurements. Limitations in the logistics and deploying specific research platforms and instruments also emerge.

The CAST, CONTRAST and ATTREX joint campaigns, held in winter 2014 in the West Pacific, characterised the chemistry, transport and distribution of the VSL halogenated organic substances in the troposphere and the TTL. Three aircraft were employed: the UK Facility for Airborne Atmospheric Measurement (FAAM) British Aerospace 146 (BAe-146, CAST); the National Science Foundation (NSF) HIAPER Gulfstream V (GV, CONTRAST); and the Northrop Grumman Global Hawk (GH, ATTREX). The three aircraft made detailed measurements of atmospheric structure and composition at different altitudes, covering the whole troposphere and the TTL *[Jensen et al., 2017; Pan et al., 2017; Harris et al., 2017]*. Together, these provide a valuable dataset to elucidate on the scientific questions on transport and distribution of VSL halocarbons in the tropical Pacific atmosphere.

All aircraft deployed the Whole Air Sampler (WAS) instrumentation to sample the VSL halocarbons (Table 2.4), with the BAe-146 and GV having on-board gas chromatography – mass spectrometry (GC-MS) system for real time analysis. The other instrument the GV used to make measurements of VSL trace substances was the in-situ coupled GC-MS and Trace Organic Gas Analyser (TOGA) *[Wang et al., 2015; Pan et al., 2017]*.

WAS instrumentation has been used routinely in previous deployments and proved that the sampling and analytical procedures employed have been capable of accessing the wide range of mixing ratios at sufficient precision to be used for tracer studies *[Schauffler et al., 1999; Park et al., 2014; Andrews et al., 2016]*.

CAST halocarbon measurements used WAS canisters and analysed in the aircraft hangar, usually within 72 hours after collection. Two litres of sample air were preconcentrated using a thermal desorption unit (Markes) and analysed with GC-MS. The measurements of a subset of halocarbons were made in flight using a thermal desorption GC-MS system. A 1-L sample of air, drawn from a window blank inlet, was pressurised, dried, alternately preconcentrated or analysed from two parallel adsorption traps of a two-channel thermal desorption system. The analyses were refocused, prior to separation by GC and detection by electron impact MS single-ion monitoring. The instrument temporal resolution, and associated sample integration period, was 5 minutes *[Andrews et al., 2013 and 2016; Harris et al., 2017]*.

CONTRAST used a combination of the Advanced WAS (AWAS) canister sampling system, TOGA and an in-situ online GC-MS. AWAS is a modified version of WAS, used in numerous research campaigns (PEM-A/B/T, 1991, 1994, 1996; STRAT, 1996; SEAC^{4}RS, 2012; *Schauffler et al., 1998, 1999*). The AWAS setup consisted of 60 canisters. Each canister was of approximately 1.1 litres. The filling time for each canister varied between 15 seconds in the boundary layer up to 50 seconds in the upper troposphere. Samples were analysed immediately after the flights, using multiple GC systems and high sensitivity MS. The limits of detection are compound-dependent and varied from ppt to sub-ppt scale, set at 0.01 ppt for $CHBr_3$, CH_2Br_2 and CH_3I. TOGA is a fast online GC-MS system and it was predominantly used for measuring volatile organic compounds (VOCs). The sampling time was every 2 minutes during the flight, with the integrated filling time of about 35 seconds [*Pan et al., 2017*].

The ATTREX payload for measuring halocarbons included the AWAS instrumentation. The sampler consisted of 90 canisters, being fully automated and controlled from the ground. The times for the AWAS samples were determined on a real-time basis depending on the flight plan. The filling time for each canister ranged from about 25 seconds at 14 km to 90 seconds

at 18 km. Canisters were immediately analysed in the field using a high performance GC-MS with a mass selective and highly sensitive electron capture detector [*Jensen et al., 2017*].

Table 2.4 Summary of measurements of VSL halogenated organic substances, CAST, CONTRAST and ATTREX (*2 stages: 2013 and 2014) campaigns [*Harris et al., 2017; Pan et al., 2017; Jensen et al., 2017*].

VSL Substance	Campaign	Method / Instrument	Average sampling fill time [s]	Limit of detection [ppt]	Average (Total) Number of Measurements
CH_3I $CHBr_3$ CH_2Br_2	NERC CAST	GC-MS WAS	30 s	0.01	30 per flight (458)
	NCAR CONTRAST	GC-MS AWAS	15-90 s	0.01	45 per flight (670)
	NASA ATTREX				80 per flight (1058*)

Halocarbons from each campaign were calibrated using the NOAA gas standard, to provide integration and inter-comparison of the measurements. The agreement between the WAS datasets for the three aircraft is good considering that these measurements were taken (i) on different times, days and locations; (ii) from multiple sampling platforms, and (iii) using different sampling techniques. The CAST WAS data showed a consistent offset for the investigated VSL halocarbons, potentially due to the high humidity operating in the tropical boundary layer. An applied correction improves the agreement between the observations for the three measurement datasets [*Andrews et al., 2016*].

2.5 Summary

This chapter provides an overview of the modelling tools and measurement instrumentation used in this thesis. The NAME model was introduced, followed by a description of how it represents the particle transport, the turbulence and the deep convection. A new convection parameterisation was then explained, with an example of its performance provided. The new convection scheme improves the representation of the particle displacement via convection by transporting more particles at shorter timescales. A description of how the VSL halogenated organic substances were measured during the CAST, CONTRAST and ATTREX joint campaigns was provided. The coordinated measurements of VSL halocarbons by different platforms deploying different instrumentation and utilising different analysing techniques were calibrated against the NOAA gas standard allowing for the integrity in the interpretative studies. The agreement between the observations for the three measurement datasets was good.

3. NAME Flight Planning Activities for CAST, CONTRAST and ATTREX 2014

This chapter introduces the NERC CAST, NCAR CONTRAST and NASA ATTREX joint campaign, which was held in the West Pacific in January-March 2014. Three research aircraft are deployed to measure the composition of the troposphere and tropical tropopause layer (TTL). These aircraft need to be coordinated to allow for sampling the same or similar air mass streams at different altitudes on fairly short timescales. NAME, as a Lagrangian particle dispersion and transport model, is used to achieve this coordination and help in the flight planning process. Section 3.1 gives an overview of the CAST, CONTRAST and ATTREX campaigns, including their scientific rationale. The procedure which uses NAME for the flight planning activities is described in Section 3.2. This procedure is tested for the ATTREX 2013 campaign (Section 3.3), and further modified, and applied in the CAST, CONTRAST, ATTREX 2014 campaigns (Section 3.4). The consistency of the meteorological forecast data, provided by the UK Meteorological Office and used in this procedure, is assessed in Section 3.5. Finally, conclusions on how well-suited NAME is in supporting the flight planning activities are drawn.

3.1 Overview of the CAST, CONTRAST and ATTREX Research Campaigns

Three airborne research campaigns: the UK-led National Environment Research Council Co-ordinated Airborne Studies in the Tropics (NERC CAST); the US-led National Centre for Atmospheric Research Convective Transport of Active Species in the Tropics (NCAR CONTRAST); and National Aeronautics and Space Administration Airborne Tropical Tropopause Experiment (NASA ATTREX) (Figure 3.1) were held in the West Pacific in January-March 2014. These research campaigns were designed to (i) characterise trace species distribution within the tropical troposphere and the TTL, (ii) investigate the role of deep convection in transporting trace gases into the TTL, and (iii) understand implications for water vapour, ozone, cirrus clouds and halogen budget in the tropical troposphere and lower stratosphere.

Figure 3.1 Logos for the NERC CAST, NCAR CONTRAST and NASA ATTREX research campaigns.

NERC CAST used the Facility for Airborne Atmospheric Measurements (FAAM) British Aerospace 146 (BAe-146) to survey the marine boundary layer (MBL) and low troposphere (0-8 km), to investigate halocarbon production and characterise the composition of the air in the main convective inflow. NCAR CONTRAST applied the National Science Foundation (NSF) Gulfstream V (GV) to principally sample the air at the same altitudes as the main convective outflow (8-15 km). NASA ATTREX deployed the Global Hawk (GH), a high-

altitude unmanned aerial vehicle, to measure the composition of the TTL and lower stratosphere (13-19 km). The value inherit in having the three aircraft flying together was found in the ability to measure from the surface up into the stratosphere (Figure 3.2) [*Harris et al., 2017; Pan et al., 2017; Jensen et al., 2017*].

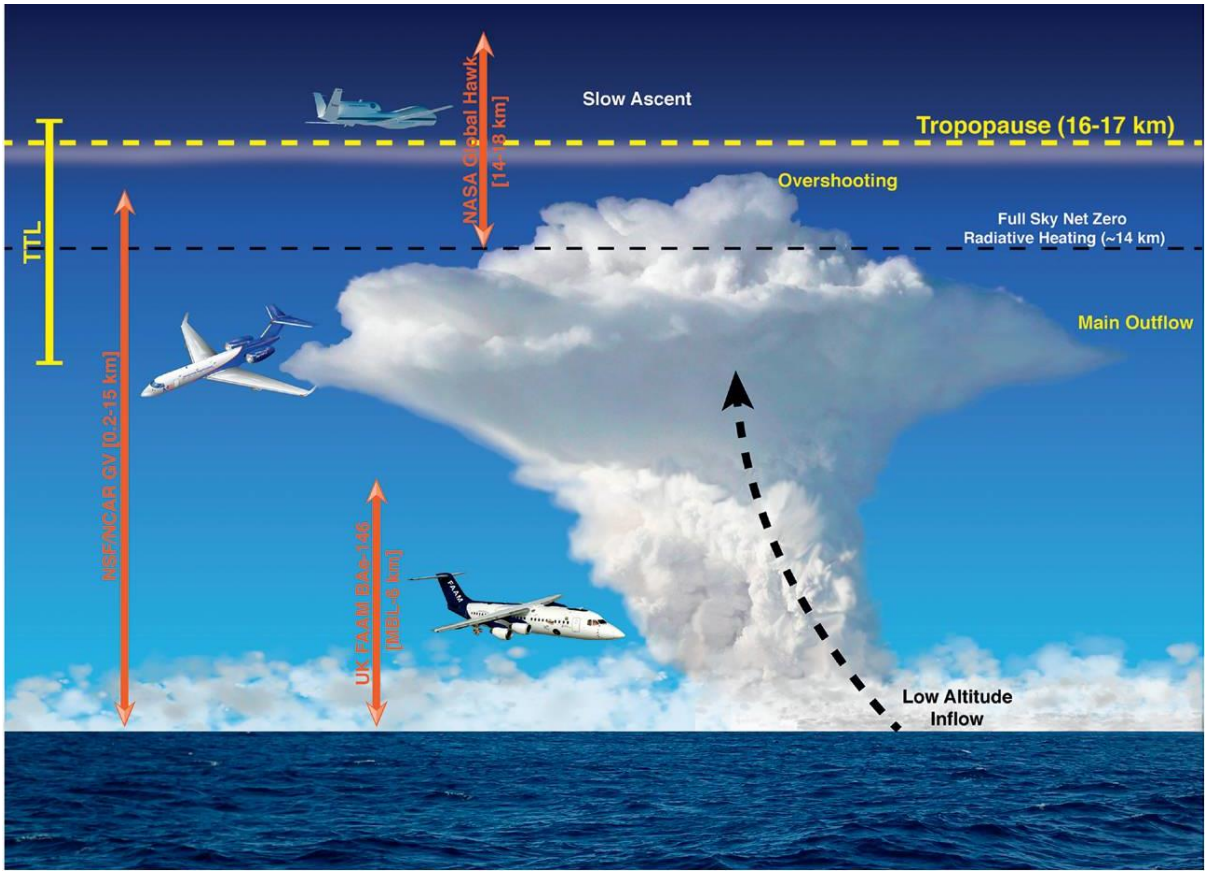

Figure 3.2 Concept of the coordinated CAST, CONTRAST and ATTREX 2014 campaigns [*Pan et al., 2017*]. Convection cloud is shown in the typical West Pacific environment, with three research aircraft at different operational altitude levels.

Despite each aircraft having its own scientific aims and objectives, appropriate to the specific aircraft's capabilities, the challenge was to achieve coordination between these three aircraft to ensure that the sampled air originates from the same or similar streams, to make consistent measurements, and to provide a comprehensive dataset for interpretative studies. Thus, the BAe-146 focused on producing measurements and probing climatology in the inflow region of the convection systems whereas the GV and GH focused on sampling the fresh convective outflow in the mid- and upper troposphere, and the TTL, respectively (Figure 3.2).

Guam, an unincorporated and organised territory of the United States located in the West Pacific (144.5^{o}E, 13.5^{o}N), was used as a research mission centre for the three campaigns. This location offered unique opportunities for short distance flights down the Equator (in case of BAe-146, Figure 3.3), and long distance flights (in case of GV and GH, Figures 3.4-5). The three research aircraft had similar payloads enabling them to measure physical properties and a broad suite of long- and short-lived chemical tracers (see Chapter 2. Methodology).

The NASA ATTREX campaign comprised four stages, occurring in 2011 until 2015. The focus here is on the second and third stage of the ATTREX campaign, in which the GH sampled the East and West Pacific TTL in January-March 2013 and 2014, respectively. Table 3.1 provides a summary of the CAST, CONTRAST and ATTREX campaigns.

Table 3.1 Summary of the CAST, CONTRAST and ATTREX campaigns.

	CAST	**CONTRAST**	**ATTREX 2013**	**ATTREX 2014**
Duration	20/1-20/2/2014	15/1-28/2/2014	05/2-03/3/2013	16/1-16/3/2014
Research Platform	British Aerospace 146	Gulfstream V	Global Hawk	
Research Flights	25	16	6	8 (2 Transit, 6 Local)
Research Flight hours [hrs]	90	128	153	146
Area Coverage	130-160^{o}E, 15^{o}N-2^{o}S	130-175^{o}E, 40^{o}N-15^{o}S	175-90^{o}W, 35^{o}N-15^{o}S	130-180^{o}E, 40^{o}N-15^{o}S
Operational Altitude [km]	0-8	1-15	13-19	13-19
Very Short Lived Substances Whole Air Sampler Measurements	695	715	388	670

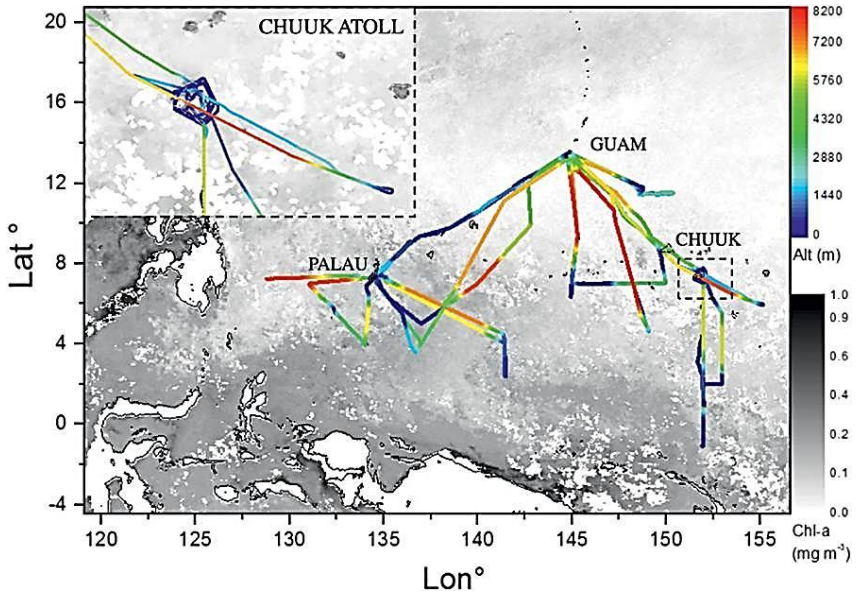

Figure 3.3 Map of the CAST BAe-146 flight tracks, 01-02/2014. The flight tracks are coloured by altitude. The background shows 01-02/2014 averaged Chlorophyll-*a* concentrations in 2014, measured by MODIS satellite [*Harris et al., 2017*].

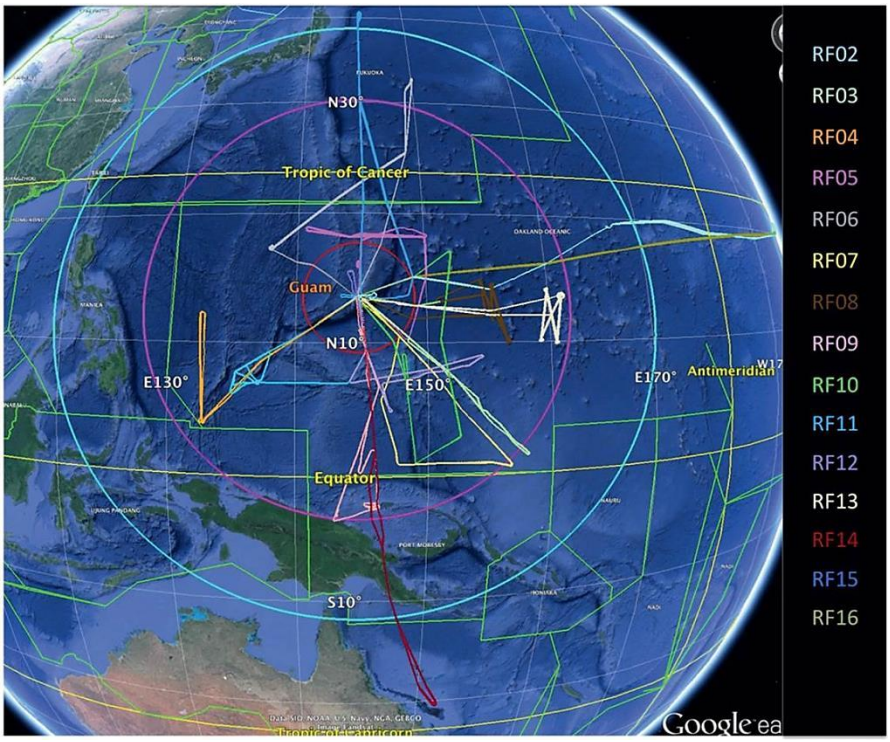

Figure 3.4 Map of the CONTRAST GV flight tracks, 01-02/2014 [*Pan et al., 2017*].

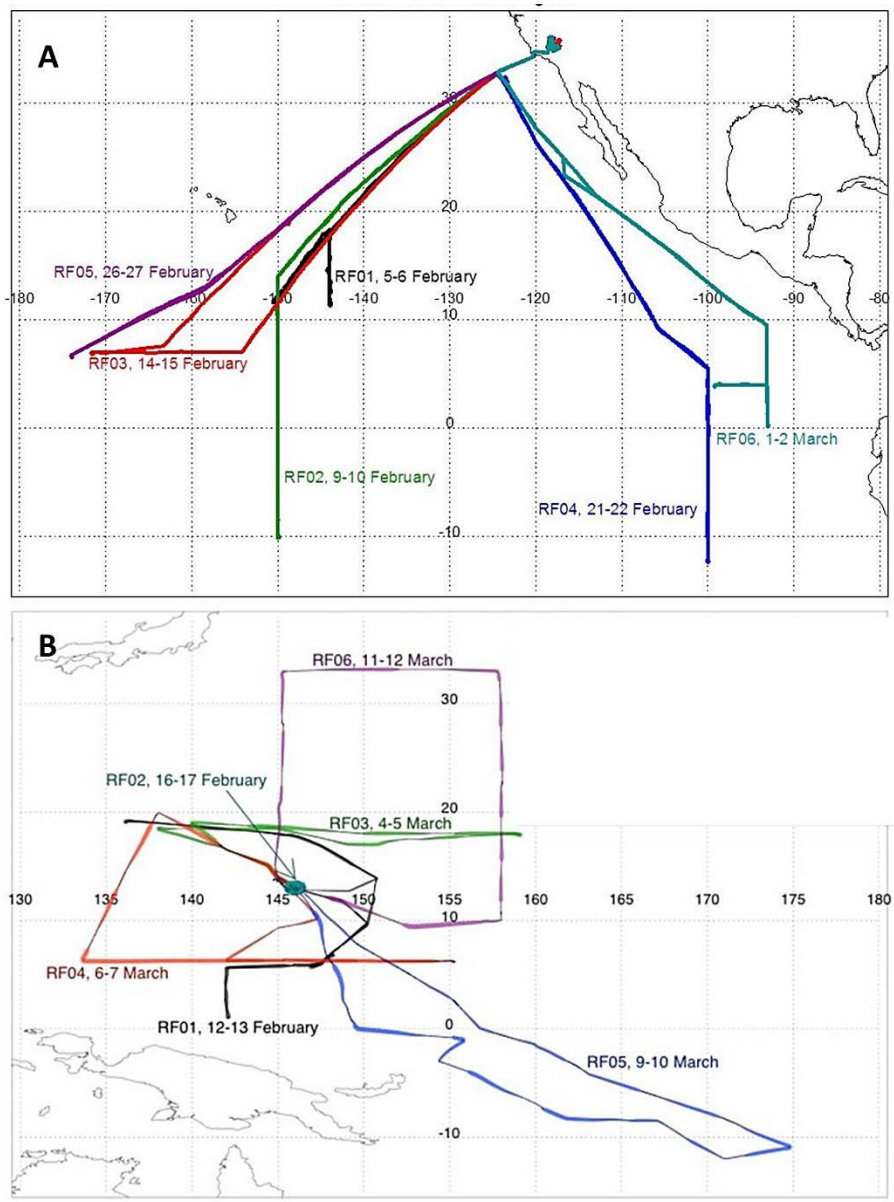

Figure 3.5 Map of the ATTREX GH flight tracks: (A) East Pacific, 01-03/ 2013, and (B) West Pacific, 01-03/2014 (transit flights are omitted) [*Jensen et al., 2017*].

There were occasions when two or three aircraft flew within less than 1 day of each other and sampled same geographic region (Figure 3.6). The coordinated flights between BAe-146 and GV were typically designed to have a segment of 'repeated track', in which the same region and altitude was sampled by two aircraft sequentially with an hourly separation to allow for instrument comparisons. Due to operational communication issues with the Global Hawk resulting in the postponement of most ATTREX 2014 flights to March 2014, the flight coordination of BAe-146 and Global Hawk was not achieved in its full capacity.

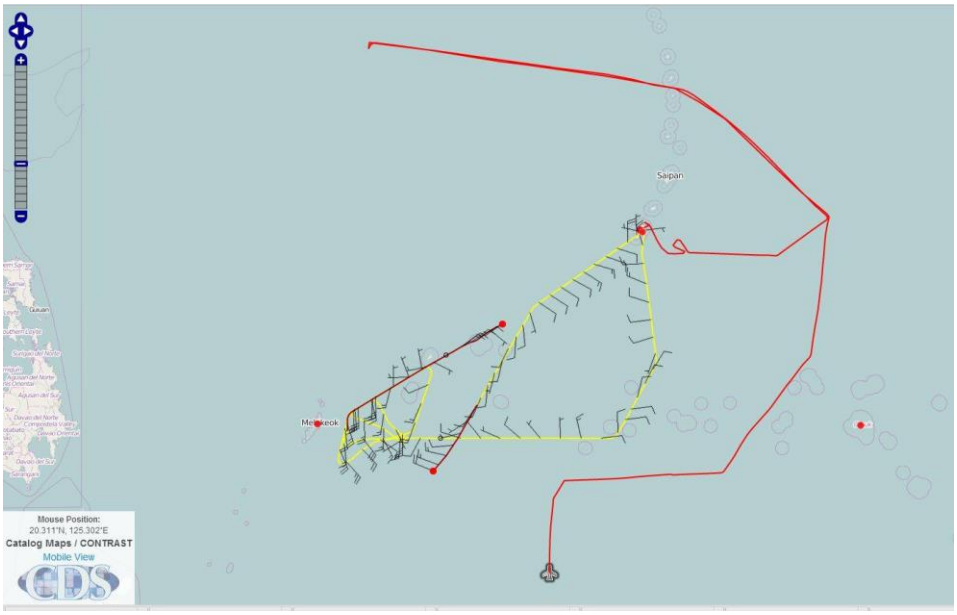

Figure 3.6 Three aircraft in the air, ATTREX GH (red solid line), CONTRAST GV (yellow solid line), CAST BAe-146 (black solid line under the red line on the left side), 12-13/02/2014.

3.2 Use of NAME in flight planning

This section introduces NAME as a tool in supporting the flight planning process in CAST, and achieving the coordination with the CONTRAST GV and ATTREX GH. A brief overview of the use of Lagrangian modelling in the flight planning applications is presented. Then, the approach which incorporates NAME products to help flight planning for CAST and achieve coordination with the CONTRAST GV and ATTREX GH is described and justified. This approach is tested for ATTREX 2013. The NAME test use for ATTREX 2013 is assessed, further modified and applied in CAST, CONTRAST and ATTREX 2014.

3.2.1 Lagrangian modelling in flight planning

Lagrangian modelling has been extensively used in field campaigns, providing accurate forecast driven simulation products which help guide the aircraft into the air masses with targeted properties [*Stohl et al., 2004*]. During most field campaigns, aircraft are sent into air masses predicted to have certain properties, and also probe the same air masses repeatedly to

investigate how the chemical composition changes with time. Trajectory models coupled with chemistry transport models can provide information on the sources and the fate of these targeted air masses in near real-time [*Stohl et al., 2004*]. The process of flight planning thus requires the implementation of a Lagrangian modelling tool to forecast the locations and transport rates of the targeted air masses in order to plan suitable flight patterns for the sampling programs [*Lin et al., 2007*].

Lagrangian models are more suitable for designing the flight planning routines and analysing the flight measurements, as they operate on very low scales (provide higher horizontal resolution, as opposed to Eulerian models with large grid sizes). They are also computationally less expensive and more time available, as they can produce the requested output within hours before the flight deployment.

3.2.2 NAME approach in supporting the flight planning activities

NAME is used as a flight planning tool in the CAST, CONTRAST and ATTREX 2014 campaigns. To meet the scientific objectives of the CAST flights, and to achieve flight coordination between the GH / GV in the TTL / upper troposphere and the BAe-146 in the low troposphere in terms of measuring the same or similar air masses at different altitude levels, the NAME output should provide information on: (i) the source origins of the TTL air over the East and West Pacific; (ii) the transport timescales – how long the air masses from the low troposphere take to reach the TTL; and (iii) the spatial and temporal variability in atmospheric transport in the East and West Pacific.

The routine produces near real-time NAME output on a daily basis to help guide the GH to sample the air masses with the evident low tropospheric air footprint, previously sampled by the BAe-146. This allows availability of the NAME products in advance of the ATTREX flight planning meetings, where these can be used along with other flight planning products, including the weather forecast and chemical tracer maps. Other factors which need to be taken into account are producing the NAME output in the most efficient and timely manner and the compatibility with the UK Meteorological Office on providing the meteorological forecasts and running NAME flight planning procedure internally.

The new procedure involves modifying three types of NAME product plots from *Ashfold et al.* [*2012*]. These are: the particle density vertical distribution over time plots, crossing location and air history maps. Figures 3.7-9 illustrate an example of each of the above products. Figure 3.7 shows the vertical distribution of particles over the NAME run duration. This represents the atmospheric transport of particles qualitatively and quantitatively. The features of vertical uplift or horizontal transport can be observed.

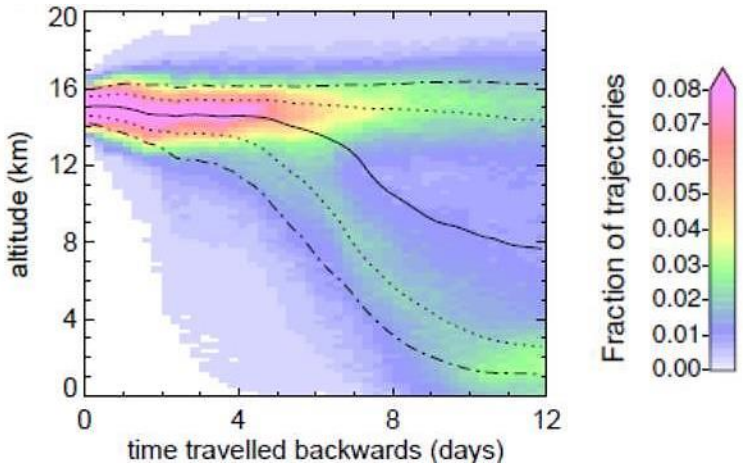

Figure 3.7 Example of a particle density vertical distribution over time plot, showing the evolution of particles released within the 14-16 km layer over 12 days for a NAME run in backward mode. Particles, released at day 0 from 14-16 km, are binned into 0.25 km squares at each 6-hourly output time step, for the duration of 12 days. Fractions are then calculated so that for each time step a colour coded boxes in each column should add up to 1. Lines show the statistical distribution of fractions of particles below a given altitude at given time step (median – solid, 25th and 75th percentile – dotted, and 10th and 90th percentile – dash-dot lines). NAME run duration: 12 days; NAME run date: 18/02/2013; NAME start date: 19/02/2013 (using a meteorological forecast: run date+1; number of particles released: 20,000; particle release location and box dimensions: 150-170^{o}W, 10^{o}S-10^{o}N, 20 x 20 x 2 deg^{2}km . Most particles stay within the altitude of release in the upper troposphere for the first 6 days after the release. >25% of the released particles move downwards after the 6th day of release.

The crossing location maps show locations of particles, released from the upper troposphere or TTL, where they first cross below the altitudes of 5 and 1 km (Figure 3.8). The 'first' is defined as the first backwards step in the calculation at which the trajectory crosses an

altitude threshold. In this case, it is either 5 or 1 km. These altitudes represent the low troposphere and the marine boundary layer, respectively. Particles are colour-coded with the times taken for these particles to reach below 5 / 1 km. The evolution of how many particles cross below 5 / 1 km over the duration of the NAME run is displayed in the adjacent histogram.

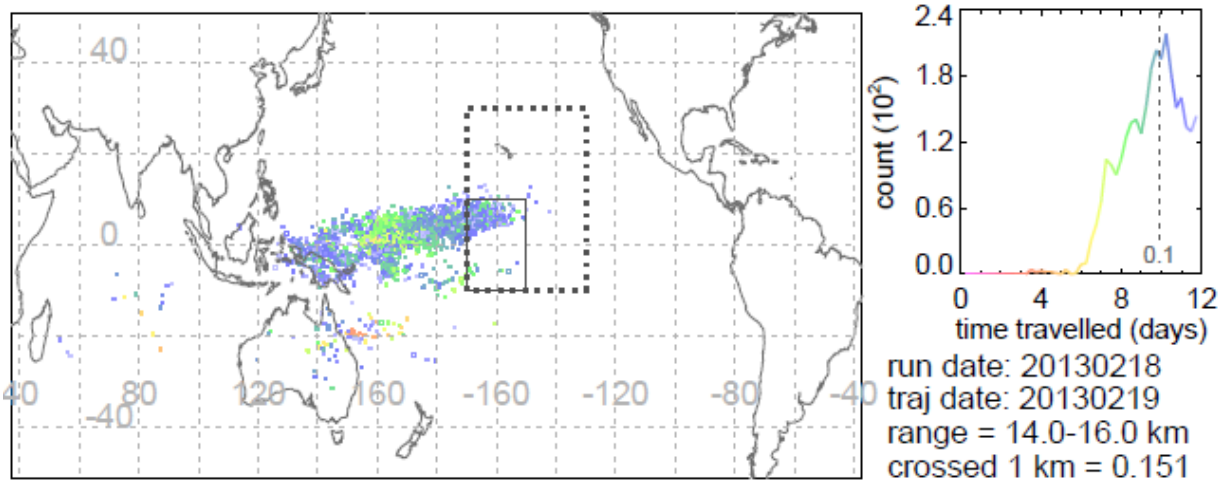

Figure 3.8 Example of the crossing location map, showing positions of trajectories which first cross below 1 km. These positions are colour-coded with transport timescales (0.25-12 day, the NAME run as in Figure 3.7) and summed in the adjacent histogram. The fraction of trajectories crossing below 1 km is given (*100 [%]). A solid line square is the box where particles were released from (at 14-16 km in the TTL), and a dotted line square represents the area of the East Pacific where NAME particles were released from during the NAME for ATTREX 2013 test (see Chapter 3.3).

Air history maps illustrate the time integrated particle mass fractions, averaged over the investigated altitude range (0-5 and 0-1 km), for the backward trajectories initialised in the upper troposphere or TTL. These show the fraction and locations of where the released air masses reside within 0-5 or 0-1 km layer (Figure 3.9).

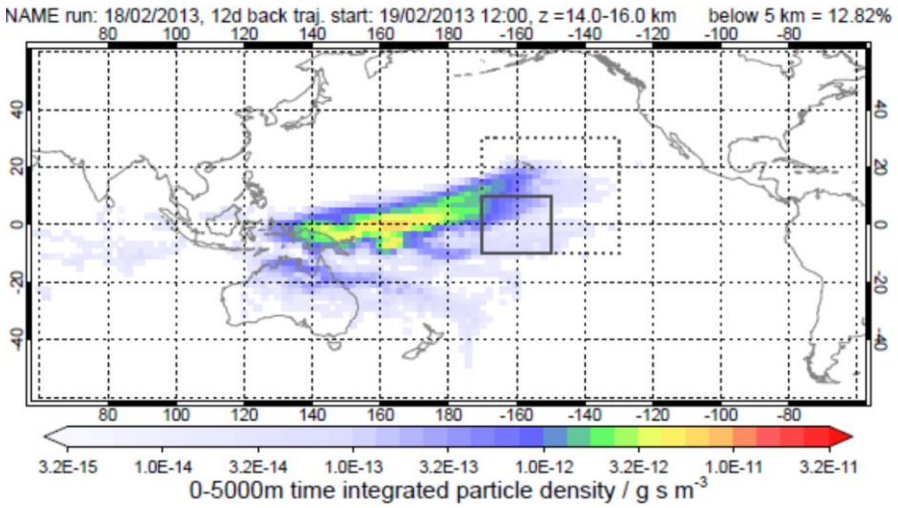

Figure 3.9 Example of the air history map, showing the 12-day integrated particle density averaged over the 0-5 km (the NAME run as in Figure 3.7).

3.3 Use of NAME flight planning procedure in ATTREX 2013

ATTREX 2013 was held in January-March, 2013 in the East Pacific. A set of NAME simulations involving the NAME output which produces the information mentioned in Section 3.2.2 was developed (Table 3.2) and tested in ATTREX 2013. The focus is on testing the efficiency of the routine production of modelled runs, and the suitability of the flight planning products, provided in near real-time. Please note all the NAME runs for flight planning procedures are with no convection scheme as the new convection scheme was not available until 2015.

Table 3.2 Summary of the routine NAME flight planning runs for ATTREX 2013.

#	Location	Area Coverage	Particle Release Altitude [km]	Number of Particle Released	Run type and duration	NAME output plots
1	East Pacific	130-170^{o}W, 10^{o}S-30^{o}N (4 20^{o} x 20^{o} boxes)	14-16 16-18	80,000	Backward mode 12 day runs starting from day +1, +2, +3, +4, +5	Crossing location maps < 1 / 5 km Particle density vertical distribution Air history maps
2	Central Pacific	160^{o}E-170^{o}W, 20^{o}S-10^{o}N	0-5	225,000	Forward mode 5 to 2 day runs starting from day 0, +1, +2, +3	Crossing location maps > 10 / 13 /16 km Particle density vertical distribution
3	West Pacific	130-160^{o}E, 5^{o}S-25^{o}N				

The first set of NAME runs aims to identify the low troposphere and boundary layer air mass influence in the East Pacific TTL, surveyed by the GH during ATTREX 2013 (Figure 3.10). Trajectories are released from the East Pacific GH flying area, split into 20 x 20 x 2 deg^{2}km boxes, representing the lower and upper TTL, 14-16 and 16-18 km, respectively, and followed 12 days backward. These use the meteorological forecasts up to 5 days forward in time. These runs also assess the consistency and credibility of the UK Meteorological Office meteorological forecasts. A number of particles was selected based on the qualitative and quantitative assessment of the test runs (by releasing 10,000, 15,000, 20,000 and 25,000 particles from a 20 x 20 x 2 deg^{2}km box).

The second and third set of NAME runs represents mock runs for an imaginary BAe-146 in Central Pacific and West Pacific, to help develop and test NAME products, give familiarity with January-March 2014 conditions, and characterise the variability in the transport of

boundary layer and low troposphere air masses to the TTL within these regions. 225,000 particles (based on the analogous quantitative assessment) are released instantaneously within the low troposphere (0-5 km) from the area covering West and Central Pacific (operational areas in CAST, CONTRAST and ATTREX 2014, Figure 3.10) and tracked 2 to 5 days forward, applying the meteorological forecasts.

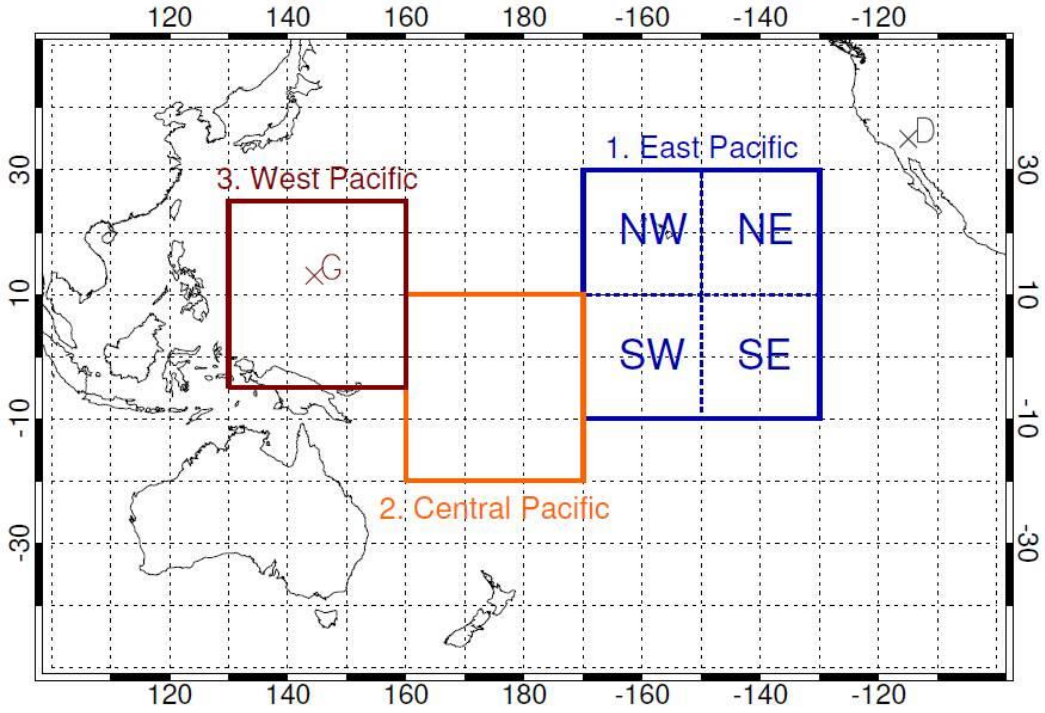

Figure 3.10 Operational area for the sets of routine NAME flight planning runs (Table 3.2): 1. East Pacific backward runs (blue), 2. Central Pacific and 3. West Pacific forward runs (yellow and red), 01-03/ 2013.

All NAME sets were run on a daily basis from the end of January till end of March. NAME (version 6.3) was used with the Unified Model assimilated 3-hourly averaged global meteorological data of horizontal resolution of ~25 km (0.352^{o} longitude and 0.235^{o} latitude; 31 vertical levels below 19 km), and the default no convection scheme option. The UK Meteorological Office ran these sets due to (i) internal access to the meteorological forecasts, (ii) the computational demand and data storage limitations in Cambridge. The computational running times for the completion of a daily batch of all the NAME sets posed a challenge in fixing the automated routine procedure (Table 3.3). These sets needed to be initialised daily at fixed time and completed so the output in the form of plots was sent to Cambridge and

available in near real-time before the ATTREX 2013 flight planning meetings (Dryden Flight Research Centre, the USA, UTC-8). The operational compatibility and time coordination had to be met. From the technical point of view, performing these NAME sets helps identify the strengths and weaknesses of the developed procedure, and provide opportunities for streamlining the procedure.

Table 3.3 Daily NAME output produced from the proposed sets of the NAME flight planning runs for ATTREX 2013.

NAME set	Total number of NAME runs with individual particle output / day	Running Time of Daily Set of NAME runs / hours	Daily Output Size / GB
1.East Pacific	40	10-11	3.5
2.Central Pacific	4	2-3	1.5
3.West Pacific	4	2-3	1.5

3.3.1 Variability in the atmospheric transport to the East Pacific TTL

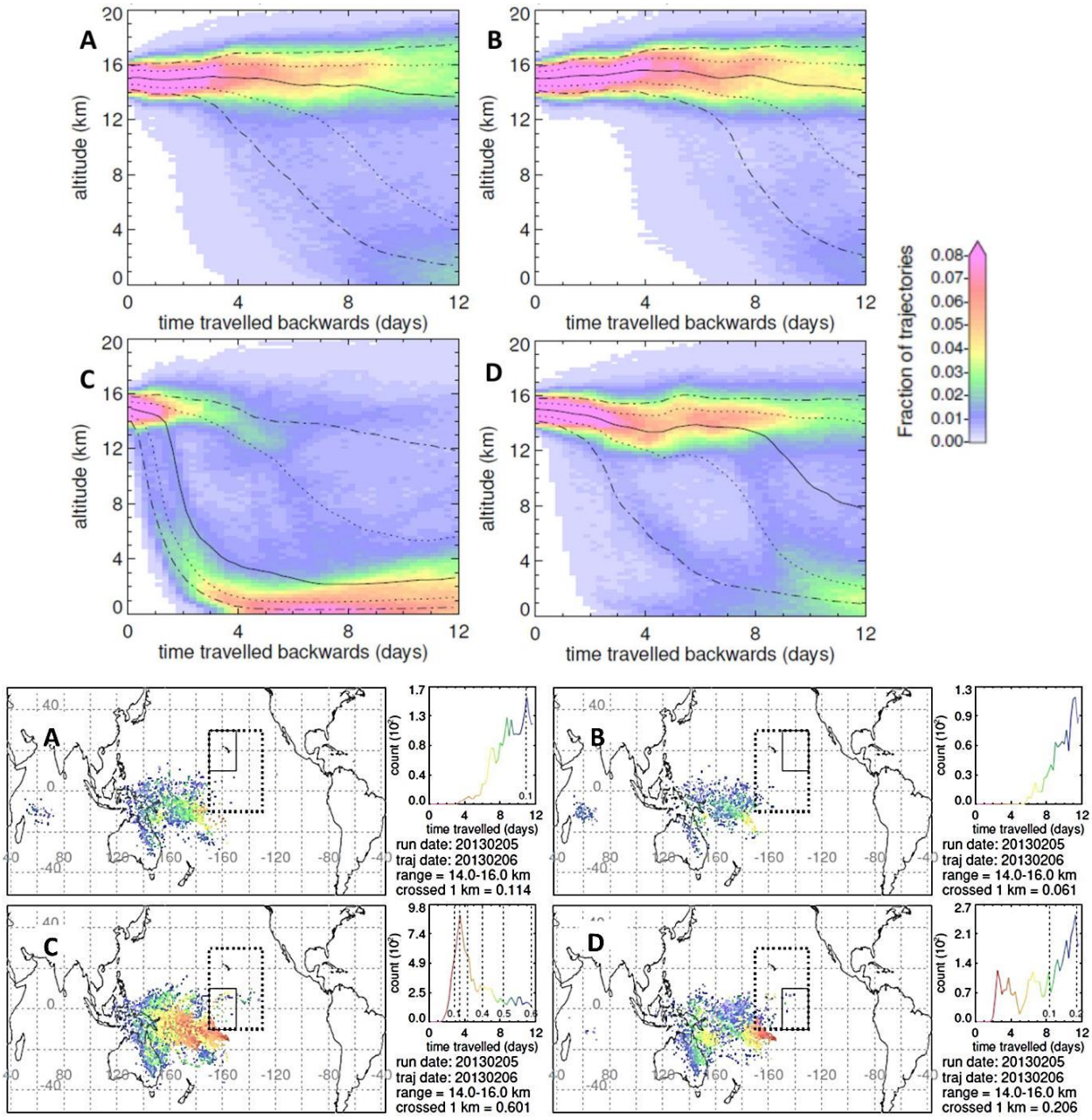

Figure 3.11 Example showing the output products: particle density vertical distribution over time plots (top) and crossing location maps for trajectories reaching 1 km (bottom) from the first set of NAME runs, East Pacific, ATTREX 2013. NAME run date: 05/02/2013 (coincident with the ATTREX 2013 Research Flight 01), NAME particle release date: 06/02/2013, meteorological forecast +1, release altitude: 14-16 km, all East Pacific NW (A), NE (B), SW (C) and SE (D) boxes (see Figure 3.10).

Figure 3.11 shows an example of daily output products from the East Pacific NAME runs. The following information can be inferred from these products: (i) how much of the TTL targeted by the Global Hawk in ATTREX 2013 Research Flight 01 is influenced by the boundary layer air masses; (ii) the movement of air masses within the tropical troposphere and TTL; (iii) the dominance of atmospheric transport pathways (vertical uplift, horizontal transport); (iv) where air masses previously released in the TTL originate in the boundary layer; and (v) the corresponding transport times from the boundary layer to the TTL.

Differences are observed between the investigated boxes (Figure 3.11), with equatorial tropical SW and SE boxes showing the highest influence of the boundary layer air masses and shorter transport timescales, compared to the NW and NE boxes located above the 10^{o}N.

The variability in atmospheric transport of particles from the low troposphere and boundary layer to the TTL (14-16 and 16-18 km) over January - March 2013 is observed between the boxes (Figure 3.12). The influence of the low troposphere and boundary layer air masses is high for the SW and SE boxes (10^{o}S-10^{o}N tropical band, indicative of high fractions of trajectories below 5 and 1 km, Figure 3.13). Two long term periods (longer than two weeks) of enhanced low level air mass footprint appear from mid-January until mid-February and from the end of February until mid-March. The SW box experiences the highest loading of the low level air masses as it is located closest to the regions these air masses predominantly originate from: the West Pacific and the South Pacific Convergence Zone, SPCZ. These low level air masses are uplifted there to the TTL and transported horizontally. This eastward horizontal transport within the TTL is mostly confined within a latitudinal range of the equatorial tropical band and does not spread above 10^{o}N. This is why the NW and NE East Pacific TTL boxes see much lower low level air mass footprint. The 16-18 km boxes experience negligible influence from the low level air masses (except for the SW box where some episodes of the enhanced influence is observed). The difference in the low level air mass loading to the 14-16 and 16-18 km boxes reflects the different composition of the lower and upper TTL, and the presence of the dynamical boundary between them.

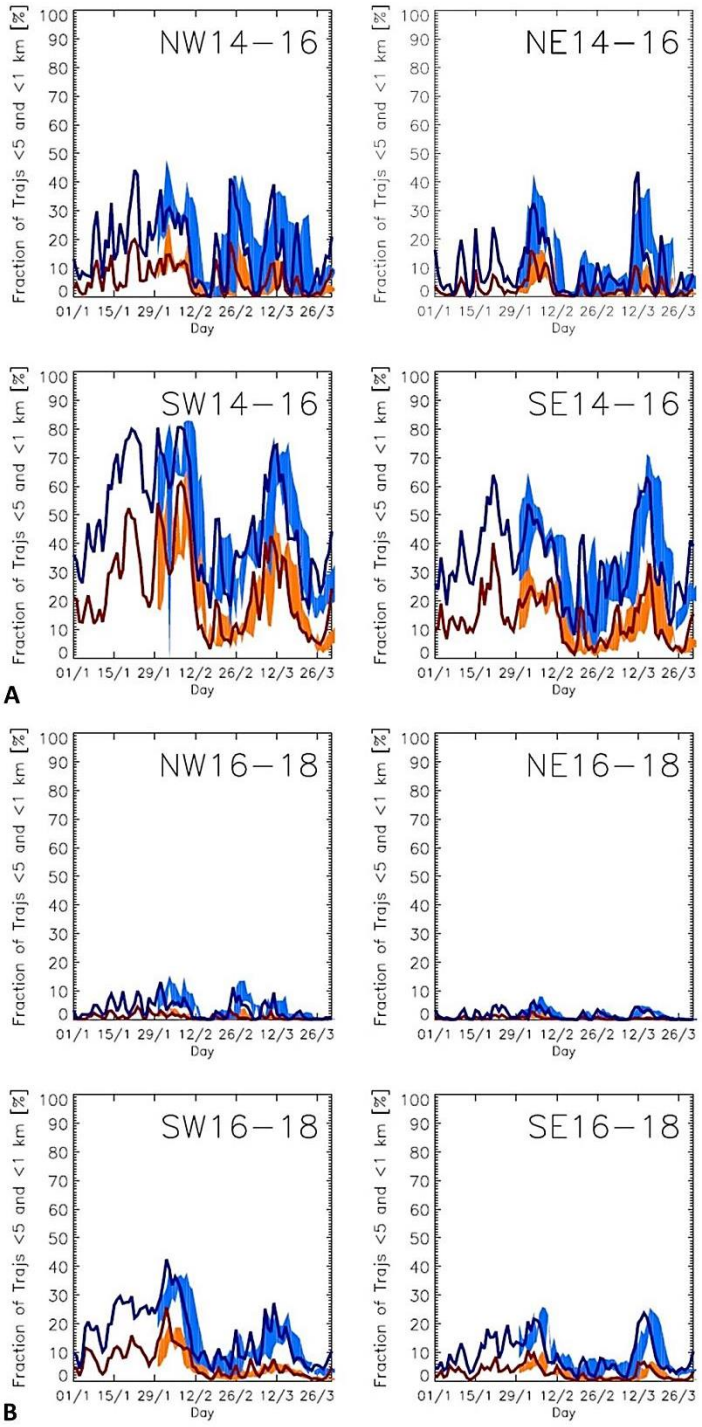

Figure 3.12 Variability in the low level air mass contribution to the NAME East Pacific TTL boxes: (A) 14-16 km, (B) 16-18 km particle release altitudes, 01-03/2013. Fractions of trajectories below 5 / 1 km for NAME runs with analyses only are represented by blue / red solid lines. The range, obtained from the NAME runs with the meteorological forecasts from +1 to +5 days, is represented by the blue / orange shading.

3.3.2 Variability in the atmospheric transport to the TTL over the West Pacific

The West and Central Pacific NAME mock runs help identify the fate of the low troposphere air masses, hypothetically being sampled by BAe-146 if it was flying in 2013, and the variability in their transport to the upper troposphere and the TTL. These mock runs, using the meteorological forecasts, were produced on a daily basis starting from 1st February until 25th March.

Figure 3.13 illustrates the evolution of the West Pacific low troposphere air mass influence to the lower and upper TTL, indicative of the fractions of trajectories crossing above 13 (Figure 3.13A) and 16 km (Figure 3.13B). The temporal variability in how much of the low troposphere air masses reach the TTL is observed. Figure 3.13 shows also the variability in distribution of where particles cross above 13 and 16 km, differentiating between the local (within the particle release box, Table 3.2) and remote regions (from within 10^{o} outside the particle release box (120^{o}–170^{o}E, 15^{o}S–35^{o}N, 50^{o}-50^{o}), to more than 20^{o} outside the box). Both the variability in magnitude and the spatial distribution of the low troposphere air mass influence to the TTL help distinguish between the episodes of high and low convective activity.

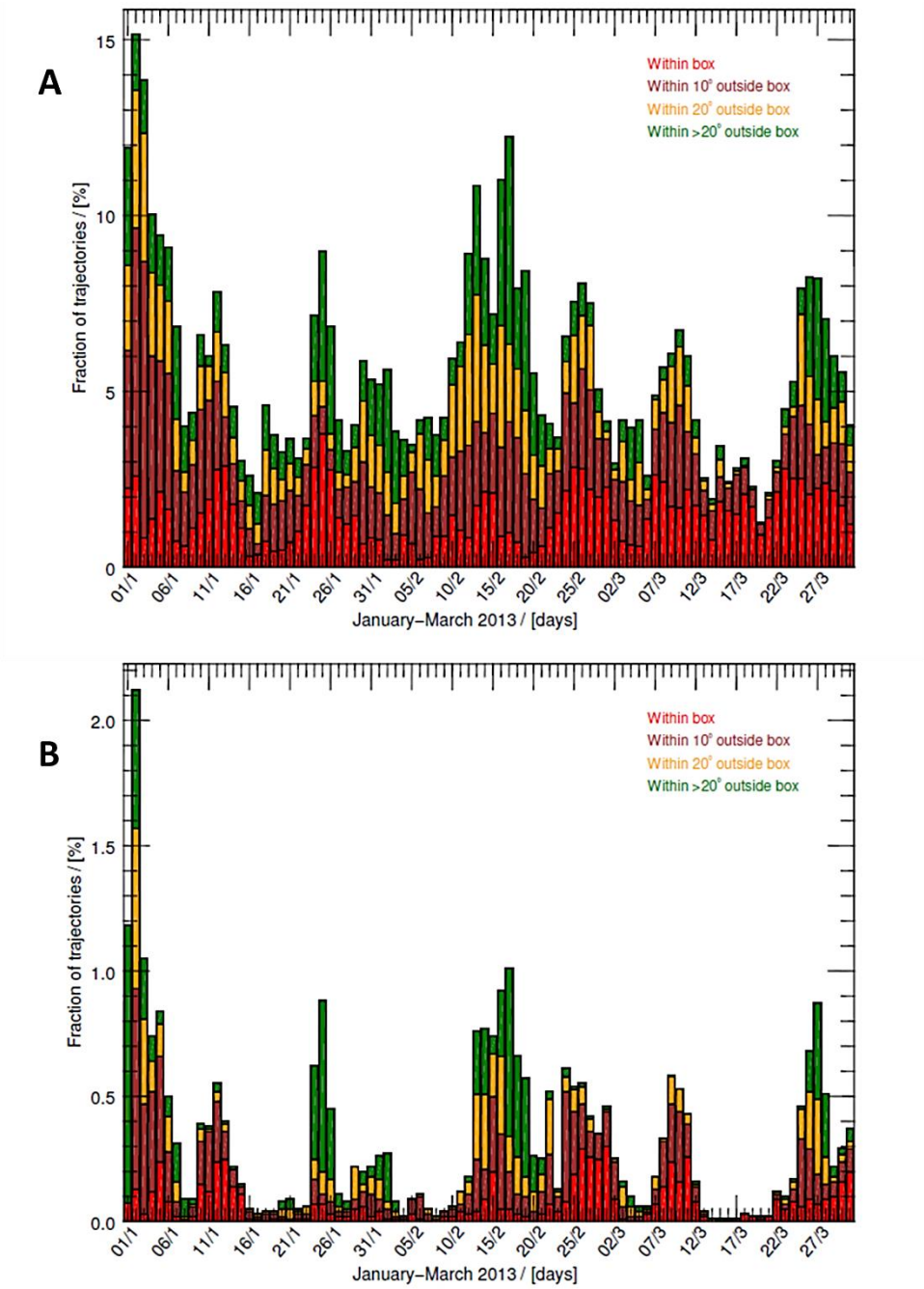

Figure 3.13 Variability in the low troposphere air mass transport to the lower and upper TTL, indicative of the fractions of trajectories reaching above 13 (A) and 16 (B) km. West Pacific NAME runs (5-day analyses only), 01-03/2013. The stacked colour-coded fractions show the distribution of locations, relative to the 130-160^{o}E, 5^{o}S-25^{o}N release box, where the particles first cross above 13 and 16 km.

Examination of individual maps (Figure 3.13) shows a cyclic pattern of most particles crossing the upper troposphere and the TTL either on the south-east or on the north-west boundary of the particle release box.

Figure 3.14 shows the fractional spatial distribution for trajectories which cross above 13 and 16 km in January-March 2013, inferred from the West Pacific NAME runs. Most of the particles released in the low troposphere spread either west- or southeast-ward, and reach the lower and upper TTL in the West and Central Pacific, and the Maritime Continent.

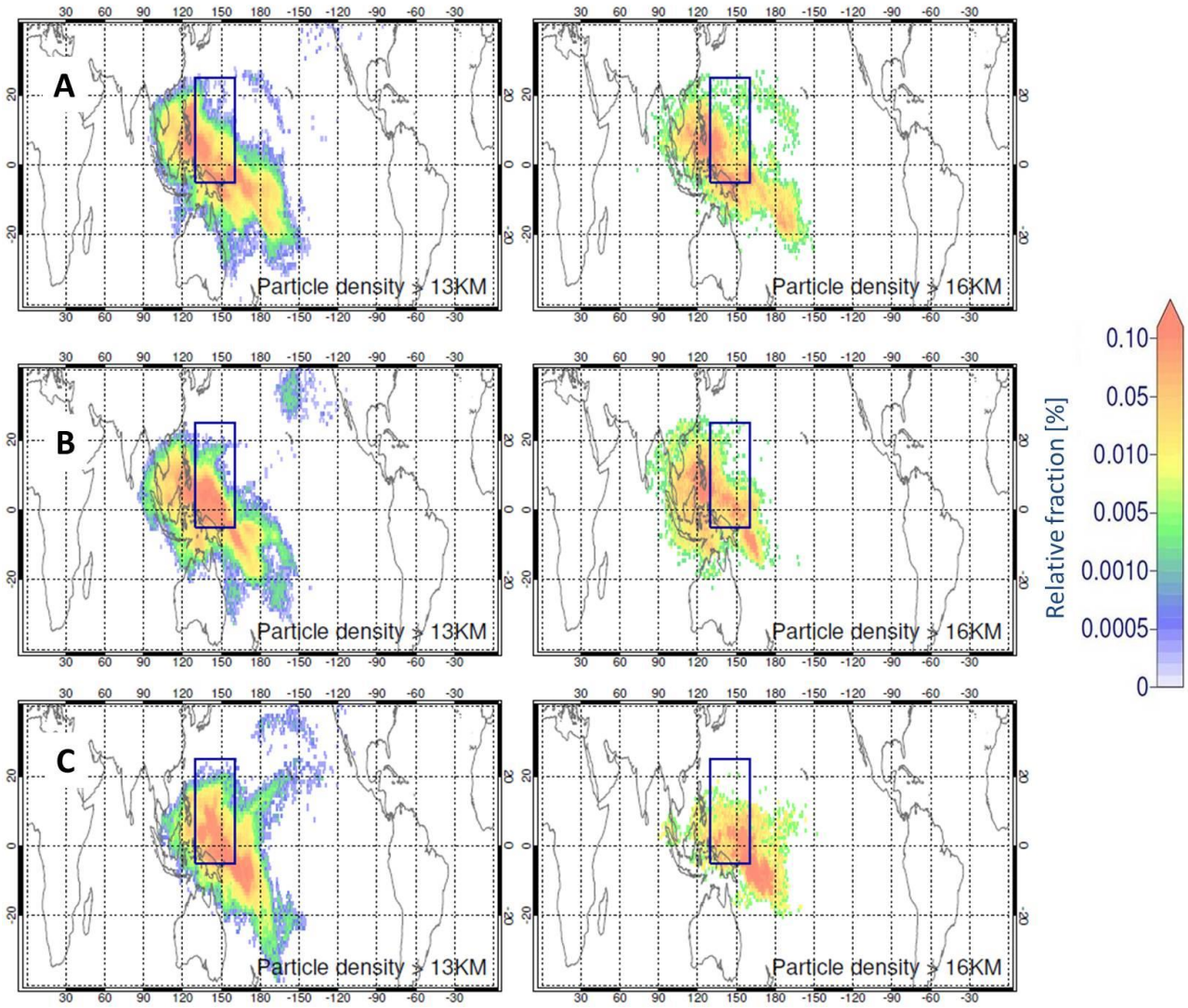

Figure 3.14 Fractional distribution of the locations where trajectories cross above 13 and 16 km, for January (A), February (B) and March (C), 2013. Trajectories are released from the West Pacific low troposphere box (blue square) and followed 5 days forward.

January-March 2013 was an ENSO neutral period. Hence, no ENSO influence is observed. The 10-day variability in high episodes of low troposphere air masses reaching the TTL is observed (Figure 3.13B). This may be related to the recurring MJO signal, being prominent over the Maritime Continent (Figure 3.14) or the shift in the main ITCZ region.

3.3.3 Summary

The NAME flight planning procedure, including the development and running of the three types of NAME sets, was solid and established products which can help in flight planning routines for the CAST, CONTRAST and ATTREX campaigns in 2014. The compatibility with the UK Meteorological Office on providing the meteorological forecasts and operating NAME was achieved. The procedure was run in a timely manner to provide NAME products near real-time, in advance of the ATTREX 2013 flight planning meetings.

The East Pacific NAME set of runs provided information on the variability of low troposphere air mass influence to the East Pacific TTL, including the source regions and transport times. The West and Central Pacific NAME sets showed the regions and how much of the low troposphere air masses reach the lower and upper TTL, within the 5 day run duration. These 2013 runs provided familiarity of conditions that may occur during the CAST, CONTRAST and ATTREX campaigns in winter 2014, given the expected neutral ENSO signal in DJF 2014 season, and the active phase of the MJO. This analysis shows the importance of cyclic low- and high- boundary layer influence to the TTL, to be considered when planning flights over several weeks.

The daily computational output of the NAME sets was large and posed a risk in the efficient operation of the NAME flight planning procedure. The options of reducing the NAME output were therefore investigated for the CAST, CONTRAST and ATTREX 2014, including the use of fewer meteorological forecasts (which produced the results of similar high consistency, Section 3.5).

3.4 NAME flight planning procedure for CAST, CONTRAST and ATTREX 2014

Building on the lessons from the performance of the NAME flight planning procedure for ATTREX 2013, the following modified sets of NAME runs are proposed for the CAST, CONTRAST and ATTREX 2014 (Table 3.4).

Table 3.4 NAME flight planning routines for CAST, CONTRAST and ATTREX 2014.

NAME sets	Particle release area (Figure 3.15)	Release altitude [km]	Number of released particles	Run type and duration	NAME output plots
1. GH	100 ^{o}E -170^{o}W, 40^{o}S-50^{o}N (9 30^{o} x 30^{o} boxes)	14-16 16-18	405,000 (9 x 45,000 / box) (instantaneous)	Backward mode 12 day runs starting from day +1, +2, +3, +5	Crossing location maps < 1 / 5 km Particle density vertical distribution All-in-1 particle maps
2. GV	120-180^{o}E, 20^{o}S-40^{o}N (9 20^{o} x 20^{o} boxes)	8-10 10-12 12-14	180,000 (9 x 20,000 / box) (instantaneous)		
3. BAe-146	135-160^{o}E, Equator-15^{o}N	0-5	7500 particles / hour / 12 days / 2 x 6 days (continuous)	Forward mode 12 days (7-day analyses and 5-day met forecasts)	Air dispersion maps (9 x 2 km vertical levels)

Technical details of the NAME runs (Table 3.4) were based on the performance of the NAME procedure for ATTREX 2013, and the sensitivity studies. These sensitivity studies were carried out before the CAST, CONTRAST and ATTREX 2014, and tested the compromise between the reliability of producing the NAME output and meeting the computational demand (Table 3.5). Dimensions of the particle release boxes were set reflecting the flying range of the GH, GV and BAe-146 (Figure 3.15, alongside with the limits of the CAST BAe-146 operational map, Figure 3.16). The use of meteorological forecasts was reduced to four days (omitting +4 day) as the others proved consistent and the data output was reduced.

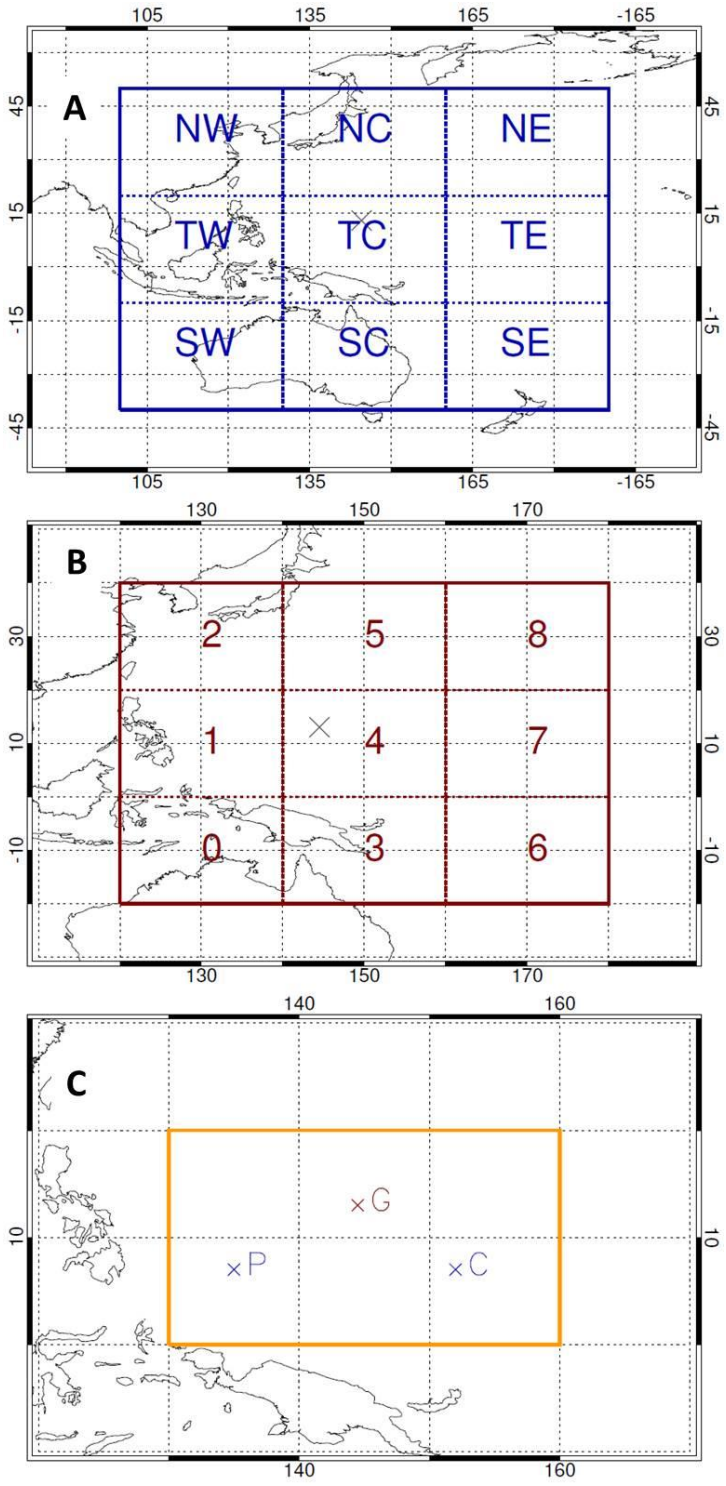

Figure 3.15 Operational areas for NAME flight planning routine runs, for the ATTREX GH (A), CONTRAST GV (B) and CAST BAe-146 (C), 01-03/2014.

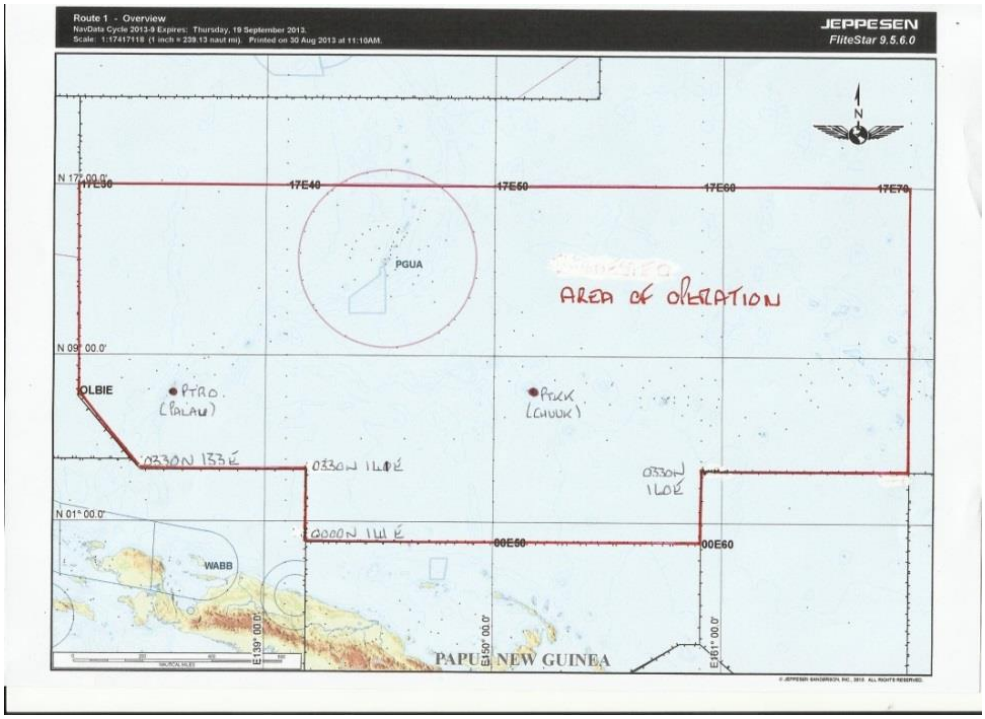

Figure 3.16 Operational flight area for BAe-146, CAST 2014.

A total daily output from the proposed NAME procedure is approximately 25 GB (Table 3.5). Thus, the storage space of >2.25 TB is required for producing the NAME output for January-March 2014 (90 days). The times required for completion of these NAME runs exceed the capability of running NAME on the Cambridge machines. Thus, all these NAME runs were executed in the UK Meteorological Office, with the parallel setup, allowing enough time for the plotting procedure and the rsync transfer (1.5 GB/hours) of the plotting products to the storage space on Cambridge machines, and the subsequent automated upload to the CONTRAST database of all the flight planning products. The NAME products were available in advance of the CAST, CONTRAST and ATTREX flight planning meetings (Figure 3.17).

Table 3.5 Sensitivity tests supporting the NAME flight planning routine procedure for the CAST, CONTRAST and ATTREX 2014 (Numbers in bold were selected).

NAME set	Number of particles released per 1 box (all boxes)	Running Time of the NAME run (daily set) / hours	Daily Output Size (gzipped) / GB
1.GH	20,000 (180,000)	1.00 (8.00)	6.0
	25,000 (225,000)	1.20 (9.60)	7.8
	30,000 (270,000)	1.25 (10.00)	9.6
	35,000 (315,000)	1.50 (12.00)	10.8
	40,000 (360,000)	1.70 (13.60)	12.0
	45,000 (405,000)	**1.75 (14.00)**	**14.4**
2. GV	15,000 (135,000)	1.00 (12.00)	6.7
	20,000 (180,000)	**1.10 (13.20)**	**9.0**
	25,000 (225,000)	1.25 (15.00)	11.0
3.BAe-146	5000 / hour	0.80	< 0.01
	7500 / hour	**1.00**	**< 0.01**

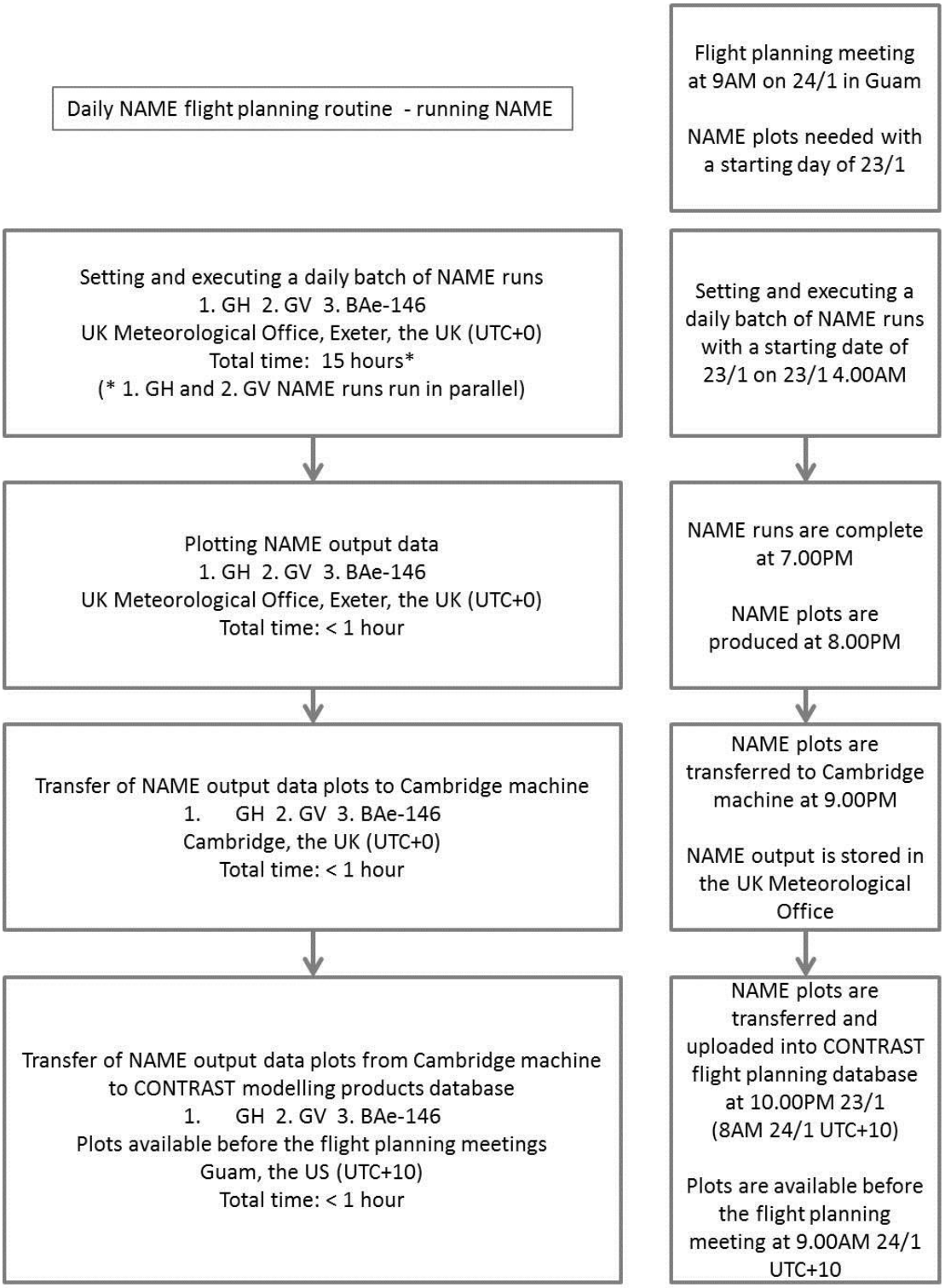

Figure 3.17 A summary flowchart showing an automated process of running NAME on a daily basis for producing NAME plots for flight planning routines used in CAST, CONTRAST and ATTREX 2014 campaigns (an example is shown on the right-hand side).

3.4.1 NAME flight planning runs for CAST, CONTRAST and ATTREX 2014

The GH and GV runs (Table 3.4, NAME sets 1 and 2) are designed as the backward simulations link the air masses travelling from the low troposphere to the upper troposphere and the TTL, and show their magnitude and transport times. This helps guide the GH and the GV in the areas where the air masses, previously sampled in the low troposphere by BAe-146, may move upwards to the sampling levels of these two aircraft.

Figure 3.18 illustrates an example of trajectory-based forecast products used for multi-aircraft flight planning. This is for 12-13 February 2014 when all three aircraft were in the same region. The three panels show the location of air parcels which had been below 1 km altitude in the preceding 12 days at 16-18, 14-16, and 12-14 km (Figure 3.18A-C, respectively). Each point is the end point of each parcel of air that had crossed below 1 km. Thus, strong, predicted low-level influence is indicated by a high percentage in each box (shown by the number), and at a given level by the denser clouds. This product was taken into account during the flight planning meetings (as an additional factor in making decisions on which air the GH and GV will sample) and was routinely checked against the flight plans for the GH and the GV to ensure that a wide range of low-level influence was sampled. In general, most flight plans met these criteria as a result of the proximity of the aircraft to the main convective region [*Harris et al., 2017*].

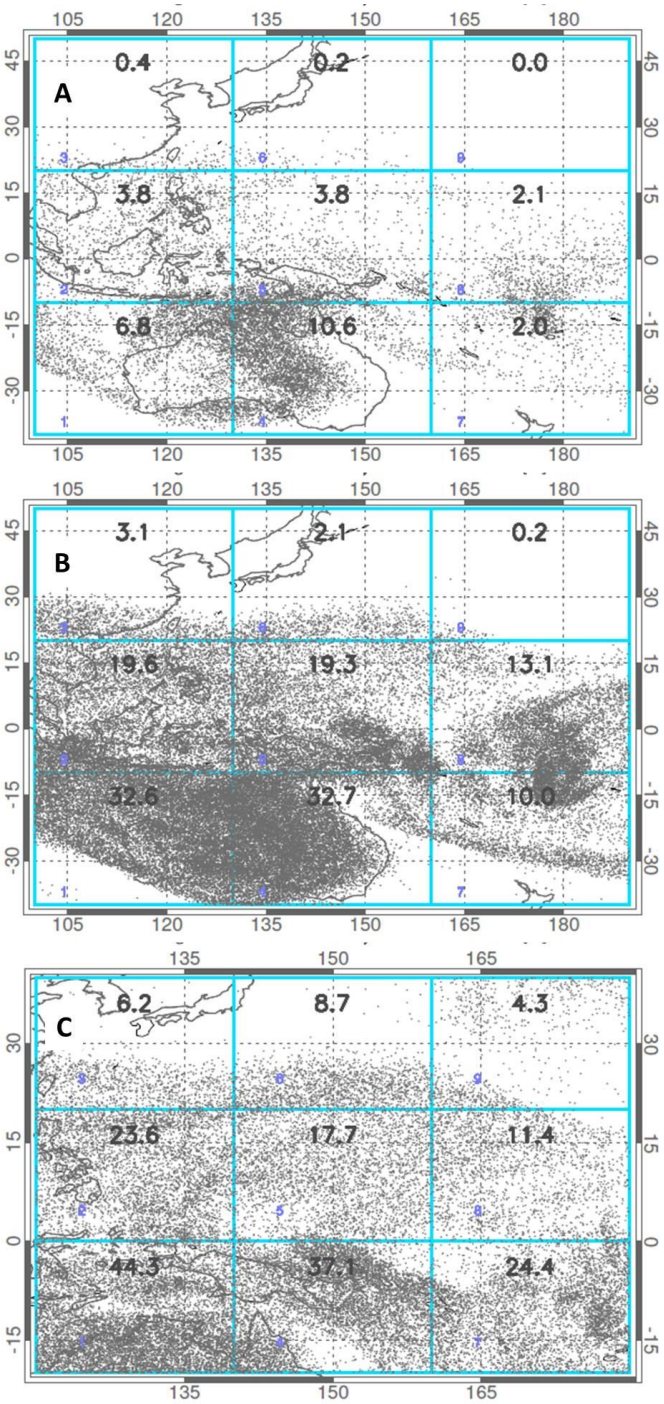

Figure 3.18 Example of the trajectory-based forecast product used for multi-aircraft flight planning, NAME run date: 12/02/2014, NAME particle release date 13/02/2014 (use of day+1 meteorological forecast). Grey dotted area represents the starting points for trajectories which crossed below 1 km within 12 days of the NAME run, and the number in bold shows the fraction of trajectories which crossed below 1 km for each GH 16-18 and 14-16 km (A, B) and GV 12-14 km (C) box.

The third set of NAME runs provided information on the vertical distribution of the trajectories, being released hourly within 6 days from the BAe-146 flying area, and tracked forward for the next 6 days. An example of the air dispersion map (Figure 3.19) shows the particle density integrated over 12 days (the run duration), for each 2 km altitude level, covering the troposphere and the TTL. These air dispersion maps show the fate of the low-level air masses and their influence in the troposphere and the TTL.

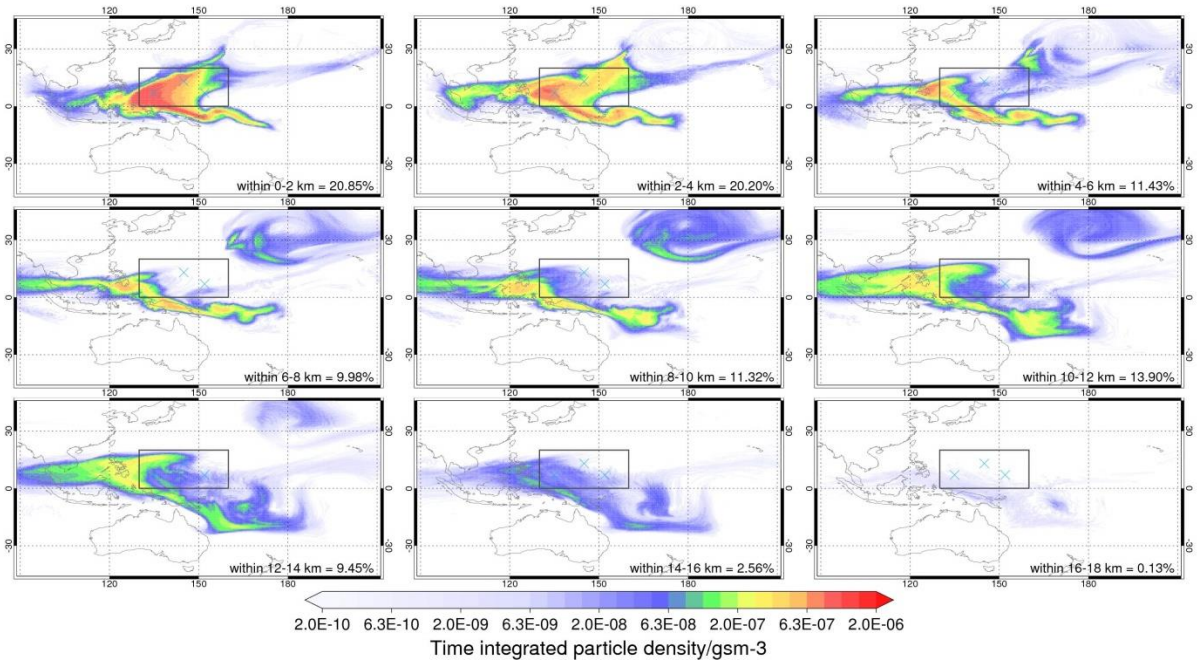

Figure 3.19 Examples of air dispersion maps, showing vertical profiles (9 x 2 km altitude bins, 0-18 km) of locations where the air masses reside within the 12 days of the NAME run. Particles are being released continuously (7500 particles /hr /6 days) from 0-5 km altitude and the 135-160^{o}E, Equator-15^{o}N box (Table 3.4).

3.4.2 Variability in the atmospheric transport to the West Pacific TTL

Variability in the atmospheric transport of the low level air masses to the TTL is observed in the West Pacific over January-March 2014. This variability is assessed for three of the boxes from the first set of NAME runs (Table 3.4), which cover the tropical band of 10^{o}S-20^{o}N: TW, TC and TE (Figure 3.15A). These boxes experience the biggest low level air mass influence, indicative of the high fractions of trajectories below 5 and 1 km (Figure 3.20).

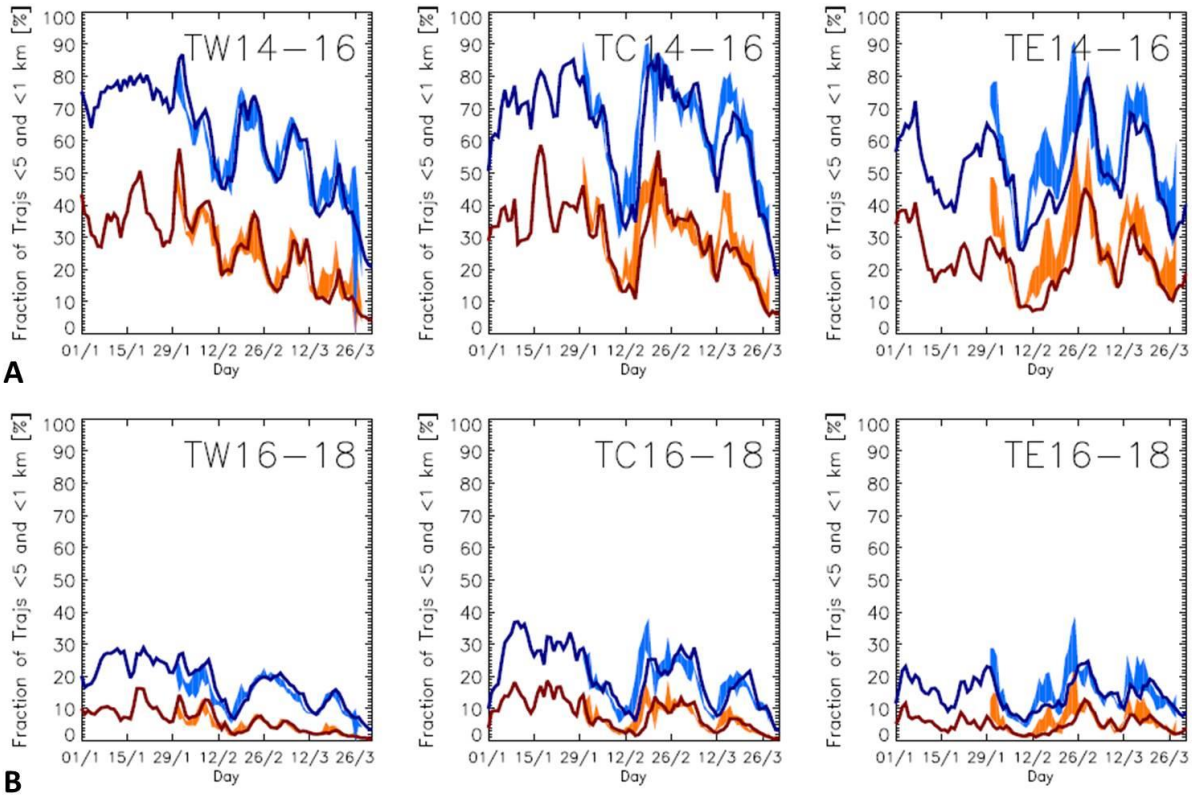

Figure 3.20 Evolution of the low level air mass influence to the lower (14-16 km) and upper (16-18 km) TTL, 01-03/2014, West Pacific GH NAME runs. Fractions of trajectories below 5 / 1 km are represented by blue / orange solid lines (NAME runs with analyses only); the shadings represent the range obtained from the values from the NAME runs which use the meteorological forecasts (+1, +2,+3 and +5).

Two major periods of elevated low level air mass influence are present mid-January and the end of February/first week of March. This is consistent with the coincident strong MJO signal and the shifts in the ITCZ. A decrease in fractions of trajectories below 1 and 5 km, observed in the end of January, comes from the dissipated MJO signal over the West Pacific region.

3.5 Meteorological data forecast consistency studies

Meteorological forecasts were used in the NAME flight planning procedure. Table 3.6 shows the verification of the forecasts, obtained from the UK Meteorological Office. The forecast consistency is probed statistically with the root mean square error metric, against the analyses and observations. The accuracy of forecast products is greater than 95% for T+24h and greater than 90% for T+120h.

Table 3.6 Verification of forecast products by the UK Met Office (statistic measure - root mean square of vector wind, RMSVW, forecast accuracy, day +1 , +3, +5), 2014 [*Personal communication with the UK Meteorological Office, 2015*]

Statistic	Parameter	Area	Verified against	T+24h	T+72h	T+120h
RMSVW error (m/s)	W 850	Tropics	Analyses	1.73	2.74	3.44
RMSVW error (m/s)	W 250	Tropics	Analyses	3.22	5.66	7.37
RMSVW error (m/s)	W 850	Tropics	Observations	3.51	4.16	4.73
RMSVW error (m/s)	W 250	Tropics	Observations	5.00	6.77	8.17

Utilising meteorological forecasts in producing NAME flight planning routine is a novel part of this study. These routines provide the output which is used to investigate the consistency of the meteorological forecasts. Figures 3.21-3.22 illustrate the comparison between the fractions of trajectories below 5 km, inferred from the NAME runs with the meteorological field analyses only (DAY0), and the NAME runs which use the meteorological forecasts from +1 to +5. The R^2 , coefficient of determination, of over 80%, are given above each plot as the metric of the forecast consistency.

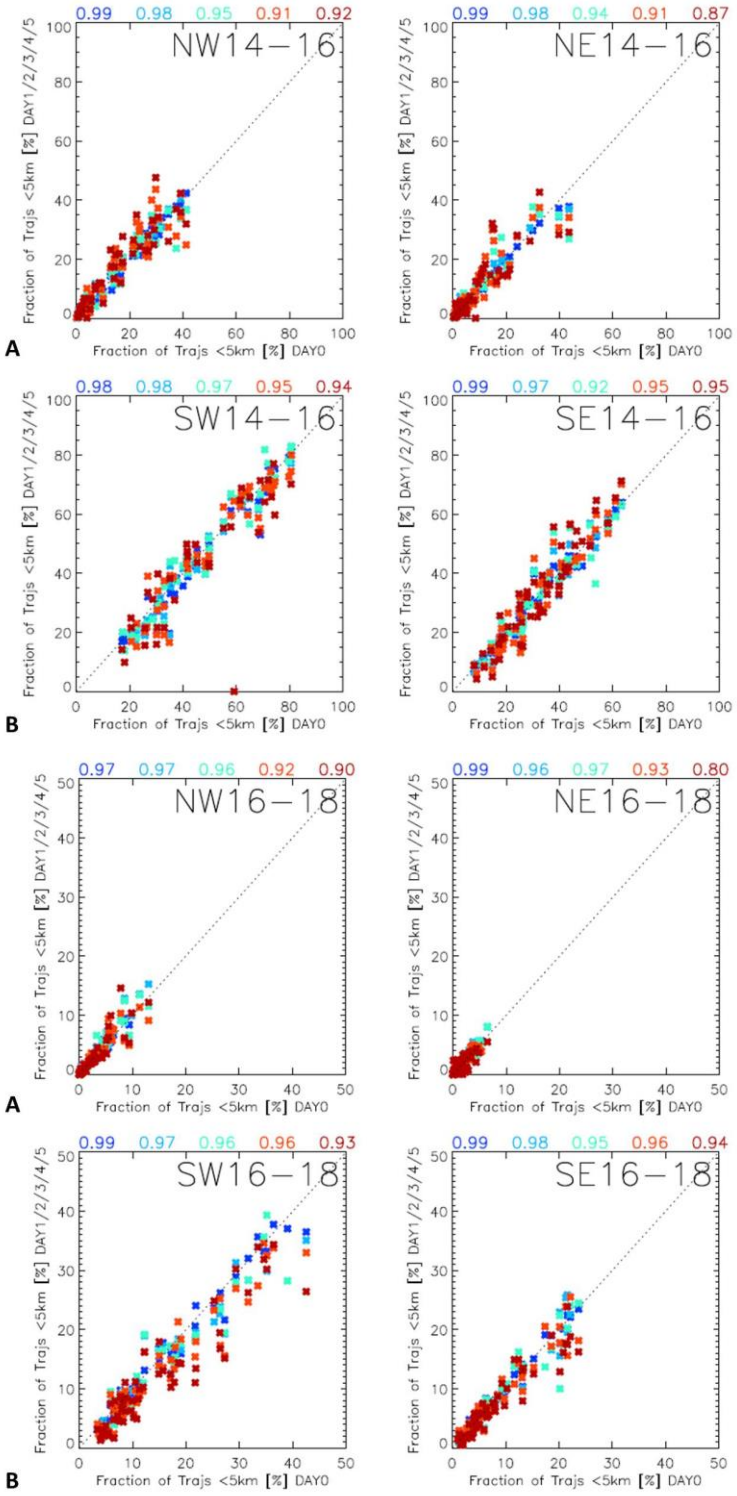

Figure 3.21 Fractions of trajectories below 5 km, inferred from the NAME runs with the meteorological data analyses only (DAY0), and the NAME runs which use the meteorological forecasts (+1 to +5, dark blue to dark red). R^2 coefficient of determination values are above each plot, 01-03/ 2013 (as in Figure 3.12).

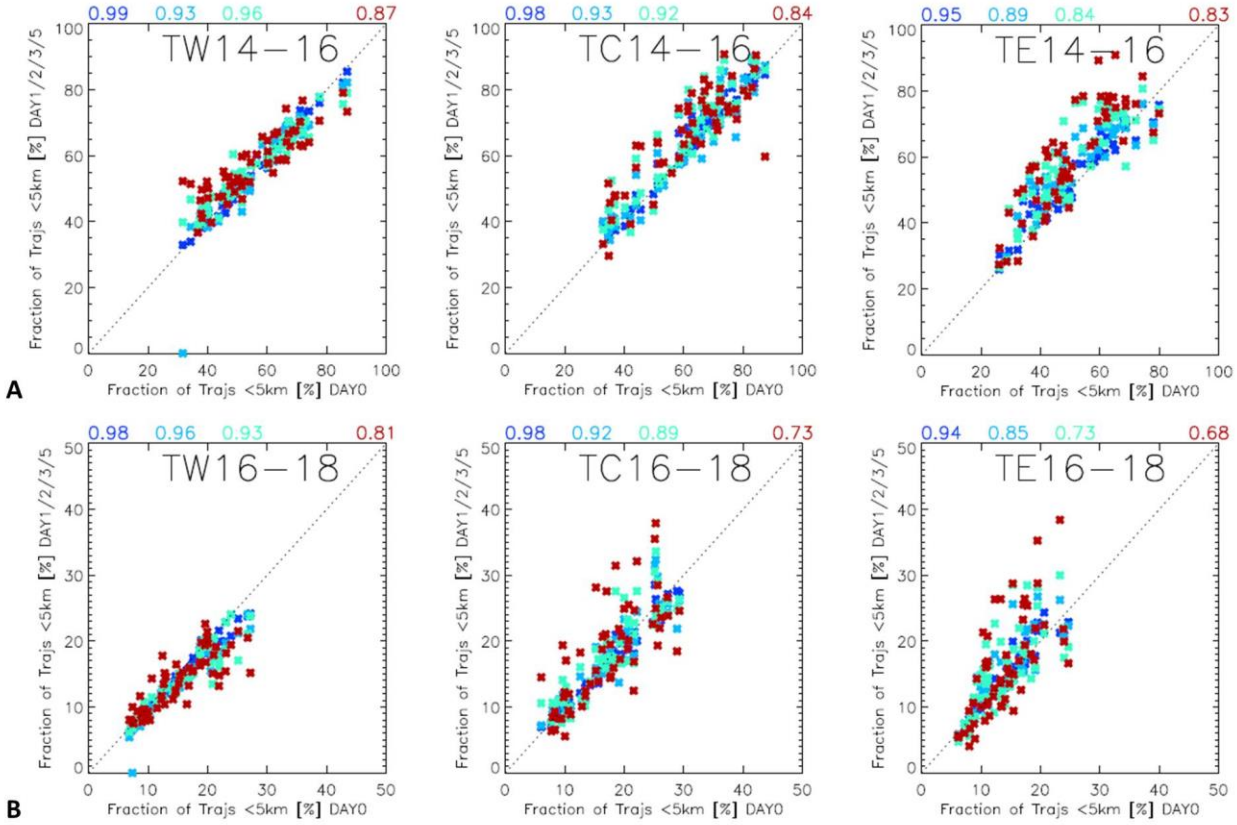

Figure 3.22 Fractions of trajectories below 5 km, inferred from the NAME runs with the meteorological data analyses only (DAY0), and the NAME runs which use the meteorological forecasts (+1, +2, +3 and +5, dark blue to dark red). The R^2 coefficient of determination values are above the each plot, 01-03/2013 (as in Figure 3.20).

The coefficients of determination from all the East Pacific GH 2013 and West Pacific GH 2014 boxes are collated, and presented cumulatively in Figure 3.23. These show the consistency of meteorological forecasts to be the greatest for Day+1, decreasing towards Day+5.

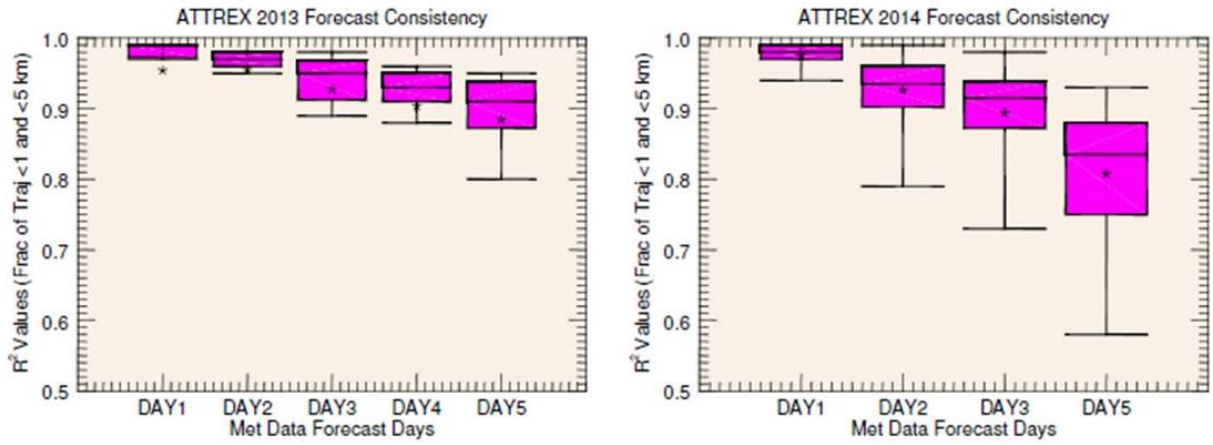

Figure 3.23 Assessment of the meteorological forecast consistency based on the NAME runs for ATTREX 2013 (East Pacific GH) and ATTREX 2014 (West Pacific GH). Box and whisker plots show the range, lower and upper quartiles and median of the R^2 coefficients of determination (consistency metrics). Means are marked as star symbols.

The mean R^2 values are over 80% for both years. The consistency for Day+3 and Day+5 is worse for the West Pacific GH 2014 boxes. This may result from the statistically larger pool of the particles released (45,000 per a 30 x 30 x 2 deg^2km box, compared to 20,000 per a 20 x 20 x 2 deg^2km box) or the use of meteorological data fields over the investigated areas. The West Pacific in 2014 is more dynamically active and convectively influenced than the East Pacific in 2013, which leads to the possibility of greater divergence in 2014.

.

3.6 Summary

This chapter gives an overview of the CAST, CONTRAST and ATTREX 2014 airborne research campaigns, including their scientific objectives. The NAME procedure which supports the flight planning activities is developed and tested for the ATTREX 2013 campaign. This procedure is further modified and adapted to meet the objectives of the CAST, CONTRAST and ATTREX 2014 research flights. It also helps achieve the flight coordination between the three aircraft surveying the West Pacific at different altitude levels. The coordination relies on measuring the same or similar air streams to allow for the interpretative studies of the chemical tracer dataset covering the whole troposphere and the TTL.

The NAME flight planning procedure, deployed in ATTREX 2013 as a test before the 2014 joint campaign, produced output in near real-time in advance of the ATTREX 2013 flight planning meetings. This output provided information on the low level air mass influence to the sampled TTL. It also helped assess the variability in the transport of these low-level air masses to the TTL, including the magnitude of this transport (indicative of fractions of trajectories below 5 and 1 km), the source regions and the transport times. Tight time management and compatibility with UK Meteorological Office operations are the key elements which resulted in the efficient performance of this NAME flight planning procedure. This relates to the use of meteorological forecasts, operating NAME and transferring the plotting products in a timely manner.

The NAME flight planning routine was modified for the CAST, CONTRAST and ATTREX 2014 joint campaign. A new set of trajectory-based forecast products was developed and used for multi-aircraft flight planning and coordination. The only limitation was the large NAME data output and the operational NAME running times.

The use of the UK Meteorological Office meteorological forecasts was crucial in the NAME flight planning routines. They show high consistency in both ATTREX 2013 and 2014 years, giving evidence for producing reliable and accurate NAME flight planning products.

This is a new approach for the NAME model to be used to support the flight planning activities in the coordinated airborne research campaign. The NAME flight planning procedures were tailored to meet the relevant scientific objectives of the CAST, CONTRAST and ATTREX campaigns. This procedure however offers the flexibility and thus it is technically straightforward to be adapted for the use in future Lagrangian airborne research campaigns, deploying different measurement platforms: aircraft, balloons, sondes, drones.

4. Assessment of the NASA ATTREX 2013 and 2014 Research Flights using NAME

In this chapter, the NAME procedure for analysing the measurements of the very short-lived (VSL) halogenated organic substances made during the NASA ATTREX 2013 and 2014 flights is developed. Section 4.1 describes the rationale and supporting sensitivity studies used to define the set-up of this NAME procedure. In Section 4.2, an overview of the ATTREX 2013 and 2014 Research Flights is given, including the vertical distribution of methyl iodide (CH_3I), bromoform ($CHBr_3$) and dibromomethane (CH_2Br_2) in the East Pacific and West Pacific TTL, inferred from two NASA ATTREX stages in 2013 and 2014, respectively. This is complemented with the assessment of the NAME modelled boundary layer influence on the sampled air, and regions which contribute the boundary layer air to this sampled air. Finally, the conclusions on the emerging relationship between the distribution of the short-lived halogenated organic substances and the NAME modelled boundary layer air mass influence in the TTL are drawn.

4.1 NAME use in the post-campaign analysis: rationale and sensitivity tests

NAME is used as a Lagrangian trajectory model to characterise TTL air masses sampled by the Global Hawk during ATTREX campaigns by identifying (i) locations where these air masses originated from, and (ii) times taken for them to reach the sampled TTL (transport timescales). This procedure relies on releasing modelled particles along each ATTREX flight path at AWAS sampling locations (source) and tracking them backwards in time to locations where they first encounter the low troposphere and the boundary layer (receptor areas).

While designing this NAME procedure set-up, the following variables are considered:

- Size of boxes NAME particles are released from
- Duration of the NAME simulation
- Number of particles released

Not only do the above need to realistically match the AWAS sampling strategy, but also be set so that the robustness of statistical analysis, and the compromise between the efficient performance of NAME and the computational demand are achieved.

The dimensions of boxes the NAME particles are released from need to match the AWAS sampling time and cover the distance which GH takes during each AWAS measurement. The sampling time for AWAS measurements ranges from 15 to 90 seconds (height-dependent). The estimated distance the GH covers in 60 seconds, given its maximum air speed of 340 knots (391 miles per hour), is 6.5 miles (10.5 km). This corresponds to the value of < 0.1 degree latitude and longitude.

The vertical resolution of global meteorological data NAME uses is not uniform. The met data is split into 59 levels, up to 30 km, with the following distribution of altitude resolution (Δz):

Table 4.1 Vertical resolution of the global meteorological data used in NAME.

Altitude Level (z) [m]	Vertical resolution (Δz) [m]
0-1000	< 100
1000-3000	< 200
3000-10,000	< 400-500
10,000-14,000	< 600
14,000-19,000	< 700-800
19,000-30,000	< 1000

The vertical dimension of box areas is chosen to be 0.3 km to cover the distance GH travels on the ascent and to avoid losing too much vertical resolution.

Trajectories are calculated 12 days backwards in time. This is chosen to capture the relatively fast transport from the surface to the upper troposphere and TTL by convective transport [*Levine et. al., 2008*]. In addition, the atmospheric lifetime of CH_3I, one of the very short-lived halogenated organic substances investigated in this thesis, is 4 days and the boundary layer mixing ratio is 0.8 ppt [*Carpenter et al., 2014*], so that these trajectories include about 3 e-folding times for CH_3I in which time its concentration decays to about 0.04 ppt (0.04 ppt is a mean value of CH_3I within a level of zero clear-sky radiative heating (LZRH) at 14.5-15.5 km [*Carpenter et al., 2014*], Equations 4.1-4.3). This makes the presence of CH_3I a good indicator of recent convection influence. A limit of detection for CH_3I AWAS instrument is 0.01 ppt.

(4.1) $$[\boldsymbol{CH_3I}]_{\boldsymbol{LZRH}} = [\boldsymbol{CH_3I}]_{\boldsymbol{BL}} \times \boldsymbol{exp}^{\left(-\frac{t}{\tau}\right)}$$

(4.2) $$\boldsymbol{t = \tau \times \ln\left(\frac{[CH_3I]_{BL}}{[CH_3I]_{LZRH}}\right)}$$

(4.3) $$\boldsymbol{t = 4 \times \ln\left(\frac{0.8}{0.04}\right) = 11.98 \approx 12\ days}$$

The number of particles released from each box is established by performing sensitivity tests. The criteria are: yielding robust statistical analysis and running NAME in the most computationally efficient way. Thus, the model output shall have the lowest file size and take the shortest computational time while maintaining the robustness of the statistics. The tests comprised releasing 500, 1,500, 5,000, 15,000, 50,000 and 100,000 particles from two NAME defined boxes (points) with dimensions of 0.1 x 0.1 x 0.3 deg^2km along the flight track of one of the ATTREX 2013 flights, Research Flight 03. Particles are tracked 12 days back in time. These test runs, with the same setup but different number of particles released, were repeated 50 times. For each NAME run, those particles which first cross below 1 and 5 km are summed and interpreted as indicative of the air mass influence from the boundary layer and the low troposphere, respectively. Subsequently, means and standard deviations (Table 4.2) are compared, and shown with medians and lower and upper percentiles (Figure 4.1).

Table 4.2 Distribution of the 5 and 1 km fractions of trajectories for NAME sensitivity test runs (means and standard deviations in brackets).

		Number of particles					
Test run	**Crossing altitude**	**500**	**1,500**	**5,000**	**15,000**	**50,000**	**100,000**
SRC110905	**Fraction < 5 km / [%]**	3.03 (0.90)	3.01 (0.47)	2.98 (0.22)	3.00 (0.14)	3.00 (0.07)	3.00 (0.06)
	Fraction < 1 km / [%]	0.17 (0.17)	0.11 (0.09)	0.11 (0.04)	0.12 (0.02)	0.11 (0.01)	0.11 (0.01)
SRC121705	**Fraction < 5 km / [%]**	2.14 (0.60)	2.22 (0.36)	2.11 (0.17)	2.16 (0.14)	2.14 (0.06)	2.14 (0.05)
	Fraction < 1 km / [%]	0.27 (0.23)	0.26 (0.18)	0.26 (0.08)	0.26 (0.04)	0.27 (0.02)	0.26 (0.02)

Table 4.3 Computational demand assessment for NAME sensitivity test runs.

	Number of particles					
Computational Demand Variables	**500**	**1,500**	**5,000**	**15,000**	**50,000**	**100,000**
Individual Particle Output File Size / [MB]	13	39	129	385	1,300	2,600
Time for completing a run / [minutes]	20	22	26	33	57	91

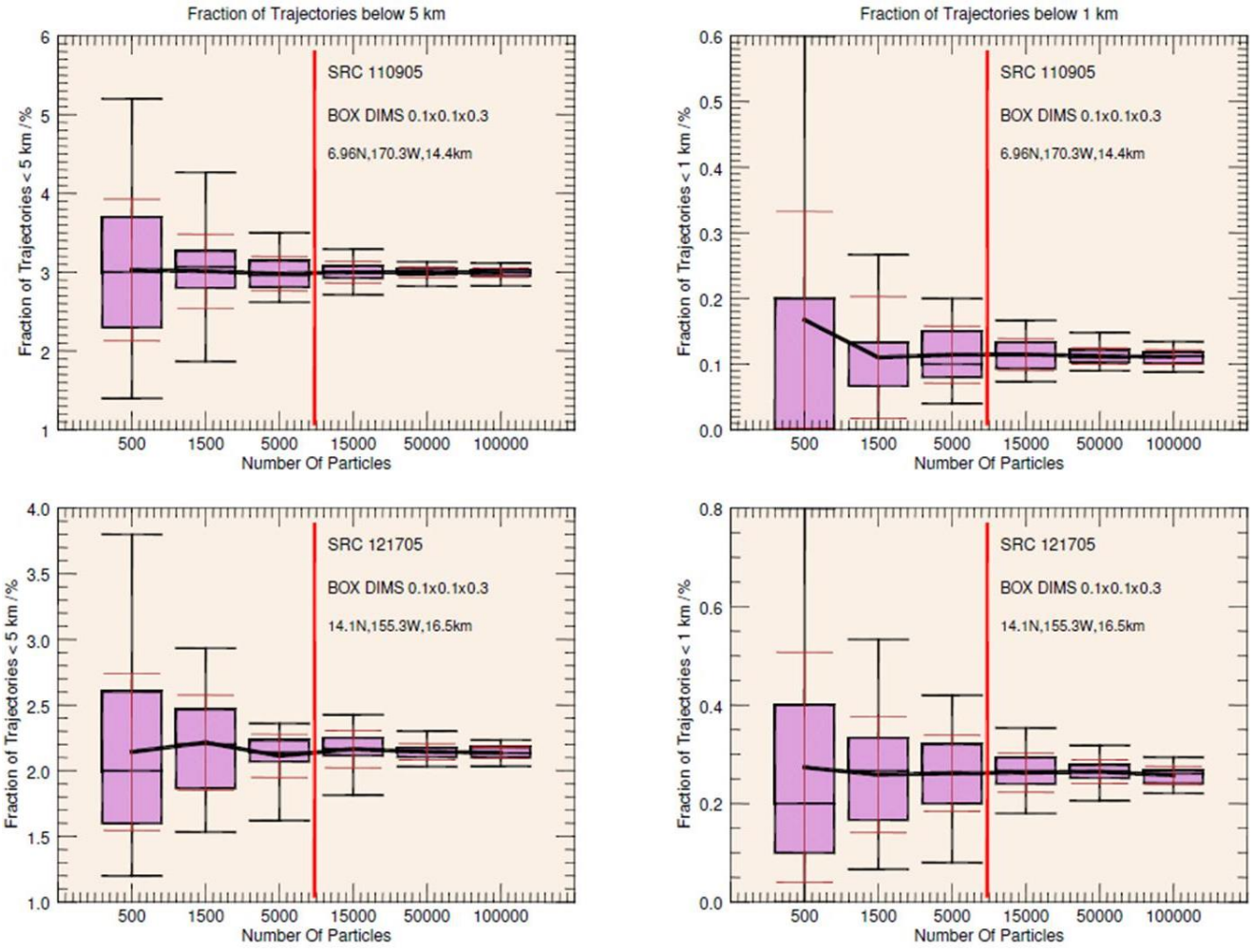

Figure 4.1 Variation in the 5 (left) and 1 (right) km fraction of trajectories for two NAME sensitivity test runs: SRC110905 (top) and SRC121705 (bottom). The means - black solid line, standard deviations - red capped lines; box and whisker lines show the range, lower and upper quartiles and median.

The means reach a plateau when the number of particles is greater than 10,000 (Fig. 4.1, to the right of vertical solid red line). The standard deviation decreases similarly, with the lowest variation observed for the highest number of the released particles. Although the most robust statistics are provided for the 100,000 particle run, this run takes the longest and produces the biggest output file size. Consequently, 15,000 is chosen as the number of particles which provides the best compromise between achieving the robustness of statistical analysis and being capable of producing the NAME output for all the AWAS measurements in a computationally efficient manner.

4.2 ATTREX 2013 and 2014 Research Flights: Overview

This section gives an overview of the vertical distribution of CH_3I, $CHBr_3$ and CH_2Br_2 in the TTL, based on the AWAS measurements taken during ATTREX 2013 and 2014. Summaries for individual flights are provided, including scientific objectives, meteorological conditions and the presence of high and low CH_3I, $CHBr_3$ and CH_2Br_2 episodes. These are complemented with an assessment of the NAME calculated fractions of trajectories below 1 km, indicative of the boundary layer air mass influence to the TTL, and the distribution of regions where this boundary layer air originated from.

4.2.1 ATTREX 2013 Research Flights

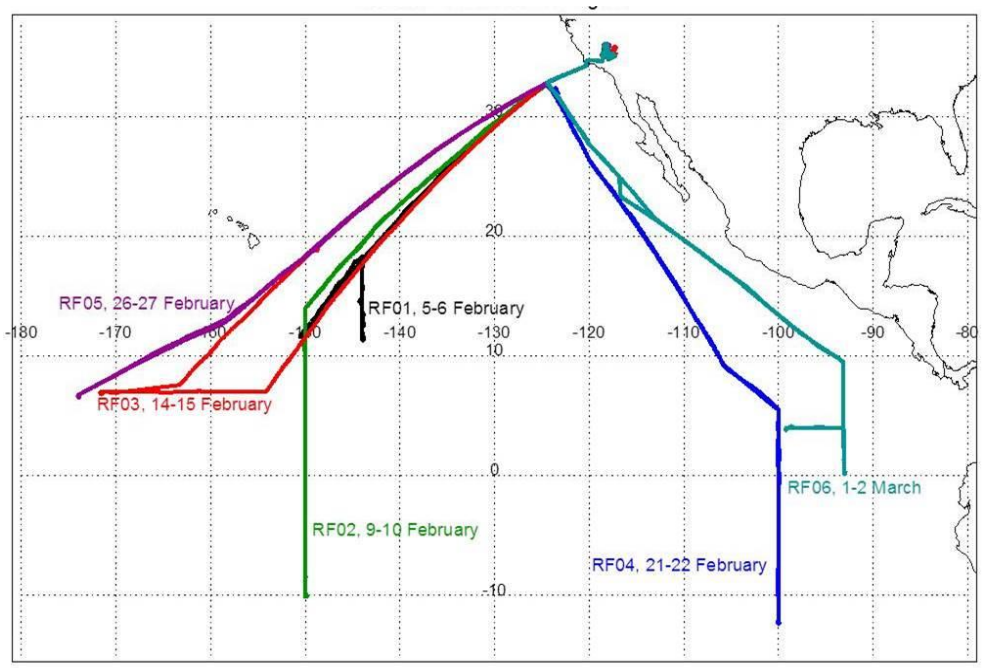

Figure 4.2 ATTREX 2013 Research Flights.

6 Research Flights (RFs) surveyed the East Pacific TTL in February-March 2013 (Figure 4.2). 4 RFs went westward from the Dryden Flight Research Centre (DFRC) sampling the area south of Hawaii and reaching the 180^{o} longitude. Minimal influence of convective activity was observed. Most of the boundary layer air, contributing to the sampled air, originated in the West Pacific and the Maritime Continent, was then uplifted to the TTL and transported horizontally within the TTL. 2 RFs took an eastward direction to sample the TTL near the Central and South American coast. Few convective episodes were observed. The sampled air has predominantly the boundary layer air mass signature from the West Pacific and Maritime Continent, with negligible influence from the localised areas and the South American tropical band.

Research Flight 01 2013-02-05/06

The Global Hawk surveyed TTL southeast of Hawaii. The AWAS pump failed so that most measurements were made above 20^{o}N, showing consistently low concentrations for CH_3I, $CHBr_3$ and CH_2Br_2 (Figure 4.3-5). One episode of high CH_3I, coincident with high $CHBr_3$ and CH_2Br_2, was observed on the profile ascent, coincident with elevated NAME modelled 1

km fractions (Figure 4.6). This air mass originated from the confined area in the Central Pacific and the South Pacific Convergence Zone (SPCZ, Figure 4.7). Horizontal transport within the TTL dominated.

Research Flight 02 2013-02-09/10

The AWAS instrument did not work and no CH_3I, $CHBr_3$, CH_2Br_2 measurements were made.

Research Flight 03 2013-02-14/15

The flight provided numerous vertical profiles through the TTL in the Central Pacific downwind of cold air and convection west of the flight track. The Global Hawk headed south of Hawaii and then due west at 7^oN to about 171^oW. CH_3I and short-lived bromocarbons show higher values in the lower TTL, decreasing with altitude (Figure 4.3-5). Minimal influence from the boundary layer air mass is observed (Figure 4.6), originating from localised (SPCZ) to more remote (the Maritime Continent) areas (Figure 4.7), with predominant horizontal transport across the TTL.

Research Flight 04 2013-02-21/22

The flight surveyed the TTL in the East Pacific. The Global Hawk flew southeast from the Dryden Flight Research Centre along the East Pacific Mexican coast, reaching 10^oS. 24 vertical profiles show variability in CH_3I, $CHBr_3$ and CH_2Br_2, which is also observed for the fraction of trajectories from below 1 km (Figures 4.3-5 and 4.6). The highest mixing ratios of the short-lived bromocarbons are observed in ATTREX 2013. Consistently high $CHBr_3$ and CH_2Br_2 values are reported at 14-15 km, decreasing with altitude. The first signal of convective uplift occurs near the Equator. Other sources of boundary layer air masses are remote: Intertropical Convergence Zone (ITCZ), SPCZ, the Maritime Continent, northern Australia and an equatorial band over the South America (Figure 4.7). These air masses are convectively picked up and horizontally transported across the TTL.

Research Flight 05 2013-02-26/27

The Global Hawk flew southwest of Hawaii, making multiple TTL profiles and reaching 180^o longitude. Episodes of high CH_3I are observed, with higher values observed also for $CHBr_3$ and CH_2Br_2 at lower TTL (Figure 4.3). Two long episodes of relatively high boundary layer

air mass influence are noted (Figure 4.6). The main source origins of the boundary layer air for the first and third quarter flight profiles are spread over the ITCZ, northern Australia and the Maritime Continent (the Arafura Sea) (Figure 4.7). On reaching the 180^{o} (second quarter of the flight), the spread of the source origins diminishes, moving northwest from SPCZ to a confined area centred over the western Pacific Tropical Warm Pool (120-160^{o}E, 0-20^{o}N). Horizontal transport across the TTL dominates.

Research Flight 06 2013-03-01/02

The Global Hawk flew southeast on a similar path to RF04. Similar CH_3I, $CHBr_3$ and CH_2Br_2 observations were recorded as for RF04 (Figure 4.3-5). Episodes of localised, recent convective uplift emerge off the east coast of Ecuador/Peru (Figure 4.6-7). Maritime Continent and the SPCZ are the major remote areas of the boundary layer air origin to the sampled East Pacific TTL.

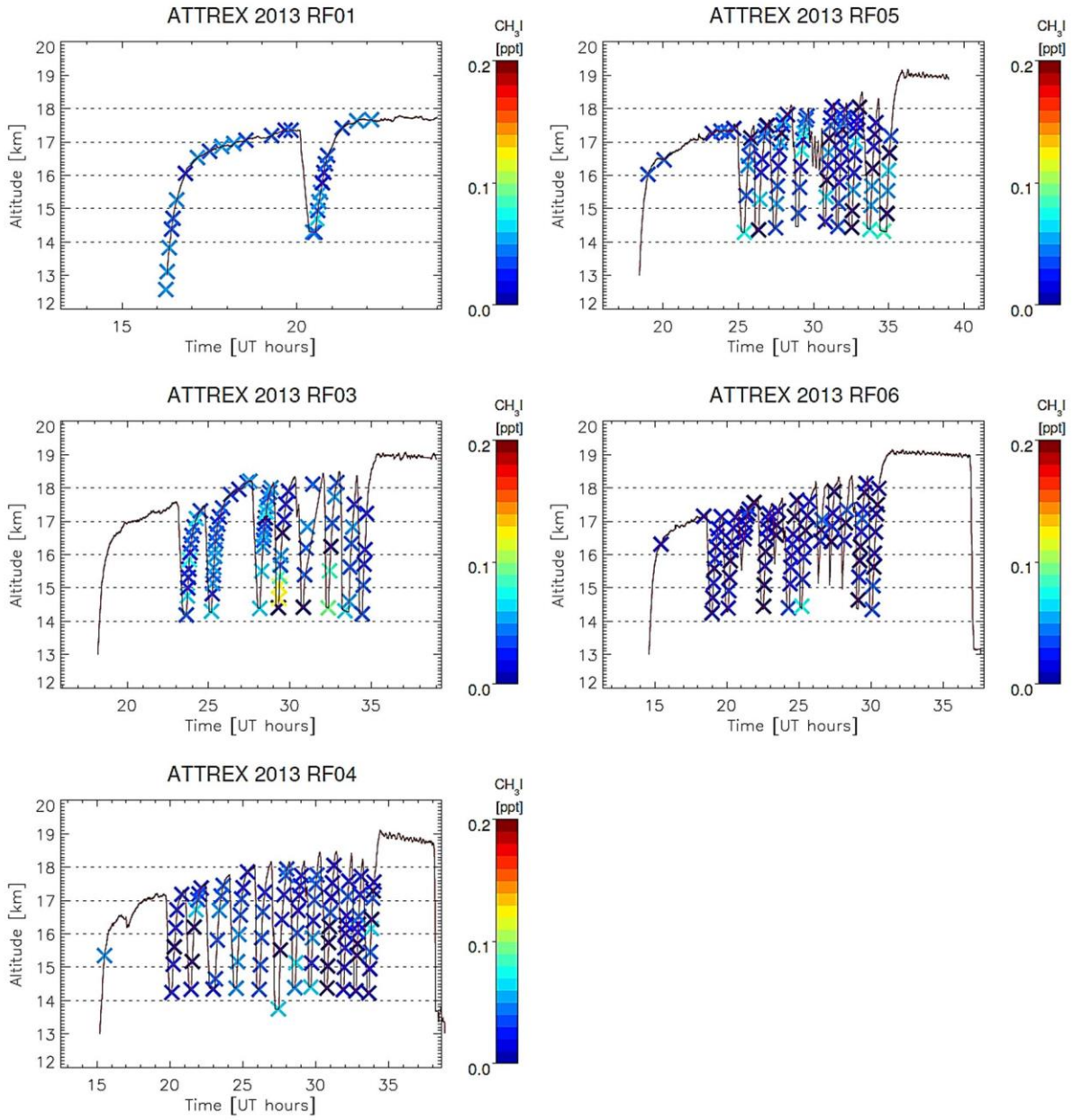

Figure 4.3 Vertical distribution of AWAS CH_3I in the TTL, ATTREX 2013.

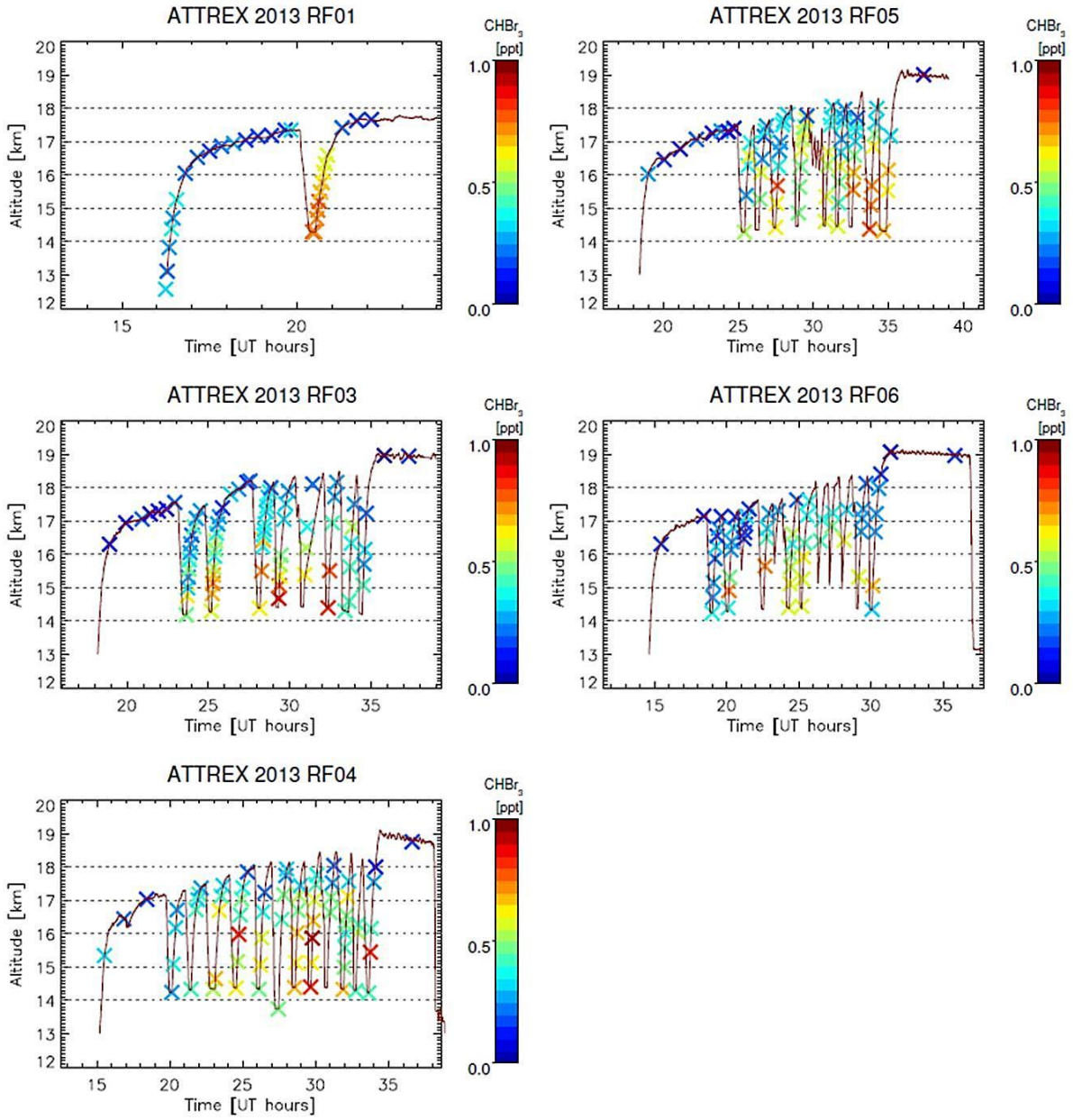

Figure 4.4 Vertical distribution of AWAS $CHBr_3$ in the TTL, ATTREX 2013.

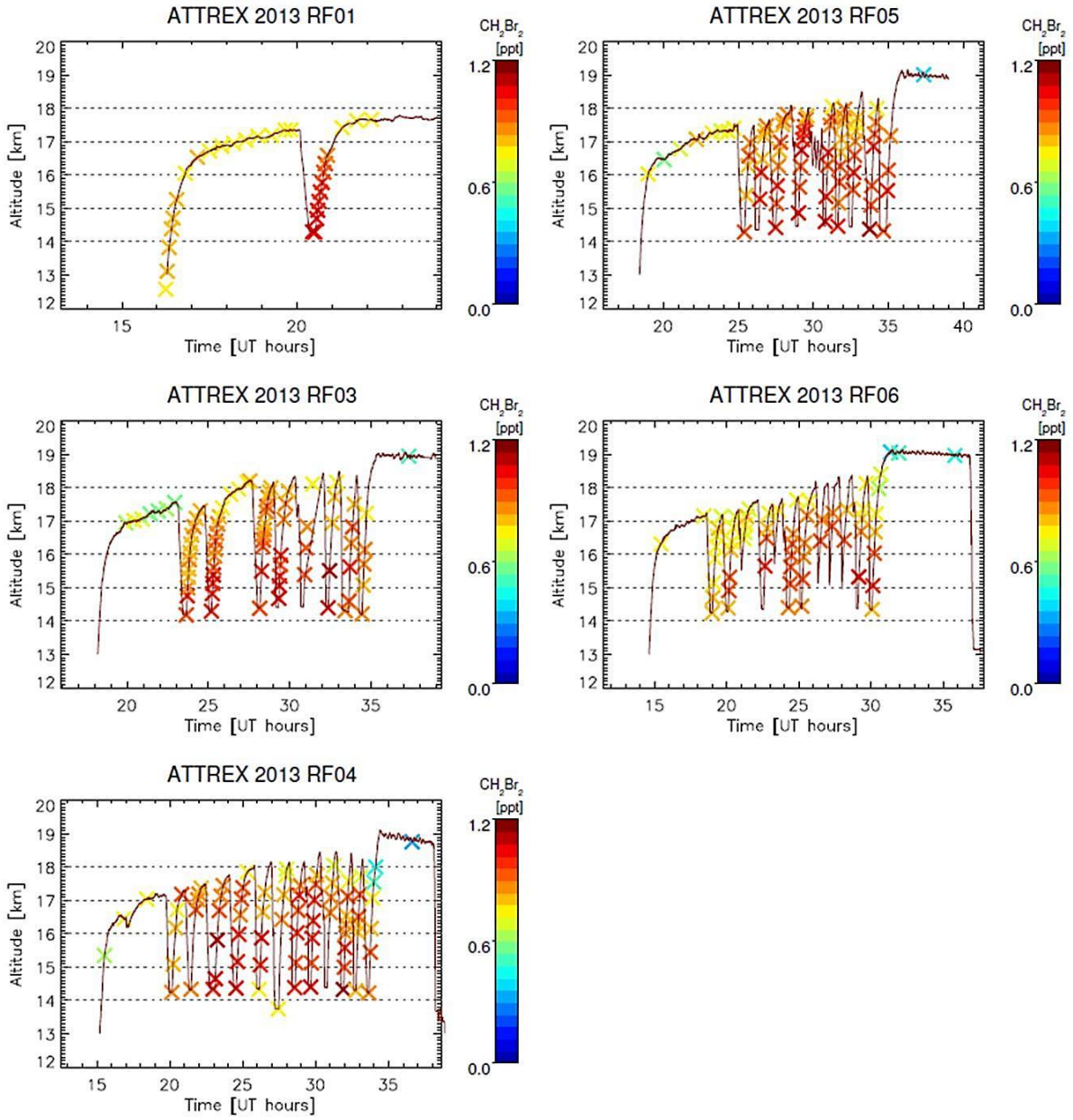

Figure 4.5 Vertical distribution of AWAS CH_2Br_2 in the TTL, ATTREX 2013.

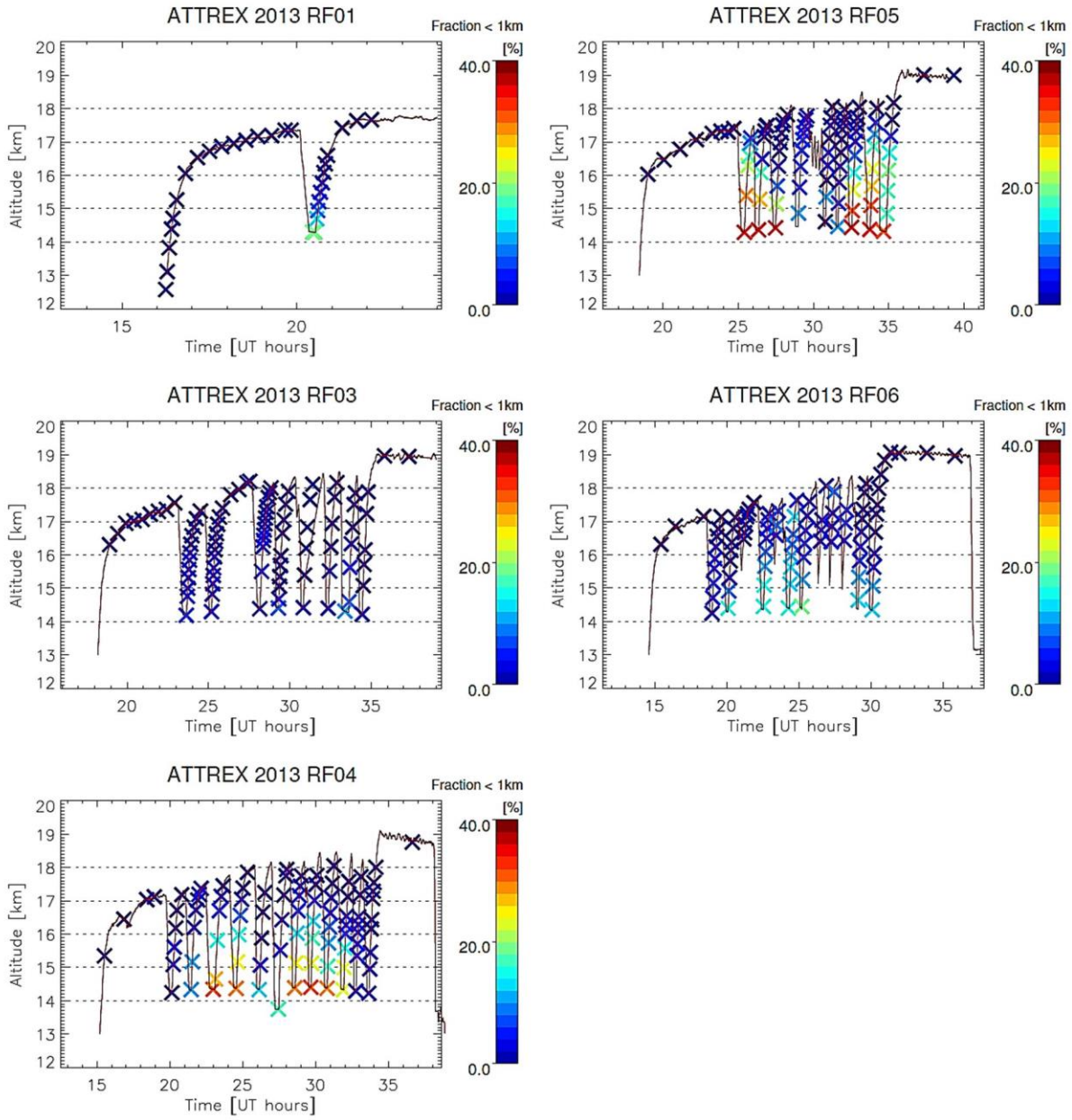

Figure 4.6 Vertical distribution of the NAME fractions of trajectories crossing below 1 km in the TTL, ATTREX 2013.

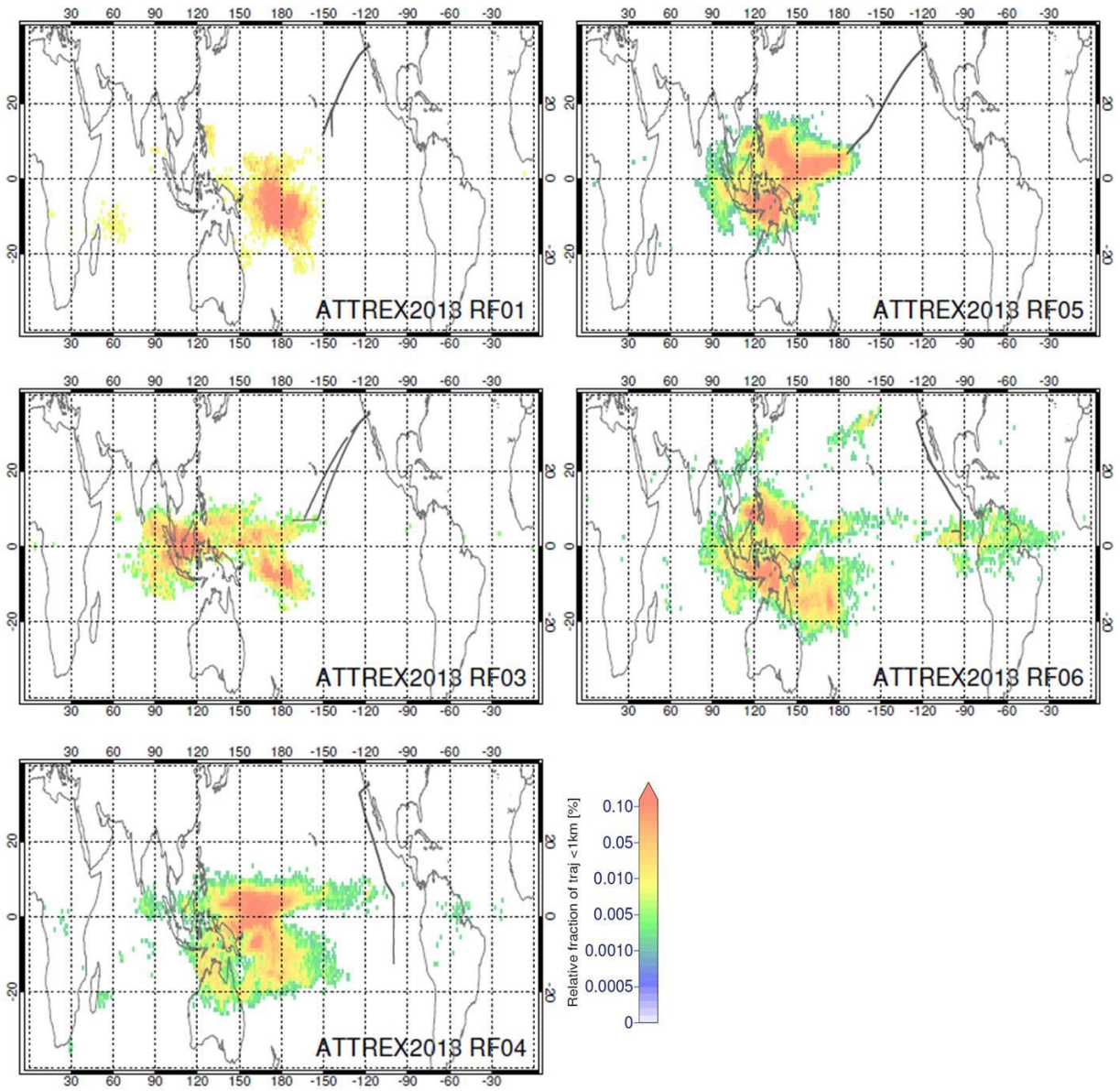

Figure 4.7 Distribution of regions contributing boundary layer air (regions where released particles first crossed below 1 km) to the sampled TTL during the ATTREX 2013 Research Flights (RF paths marked as solid grey lines).

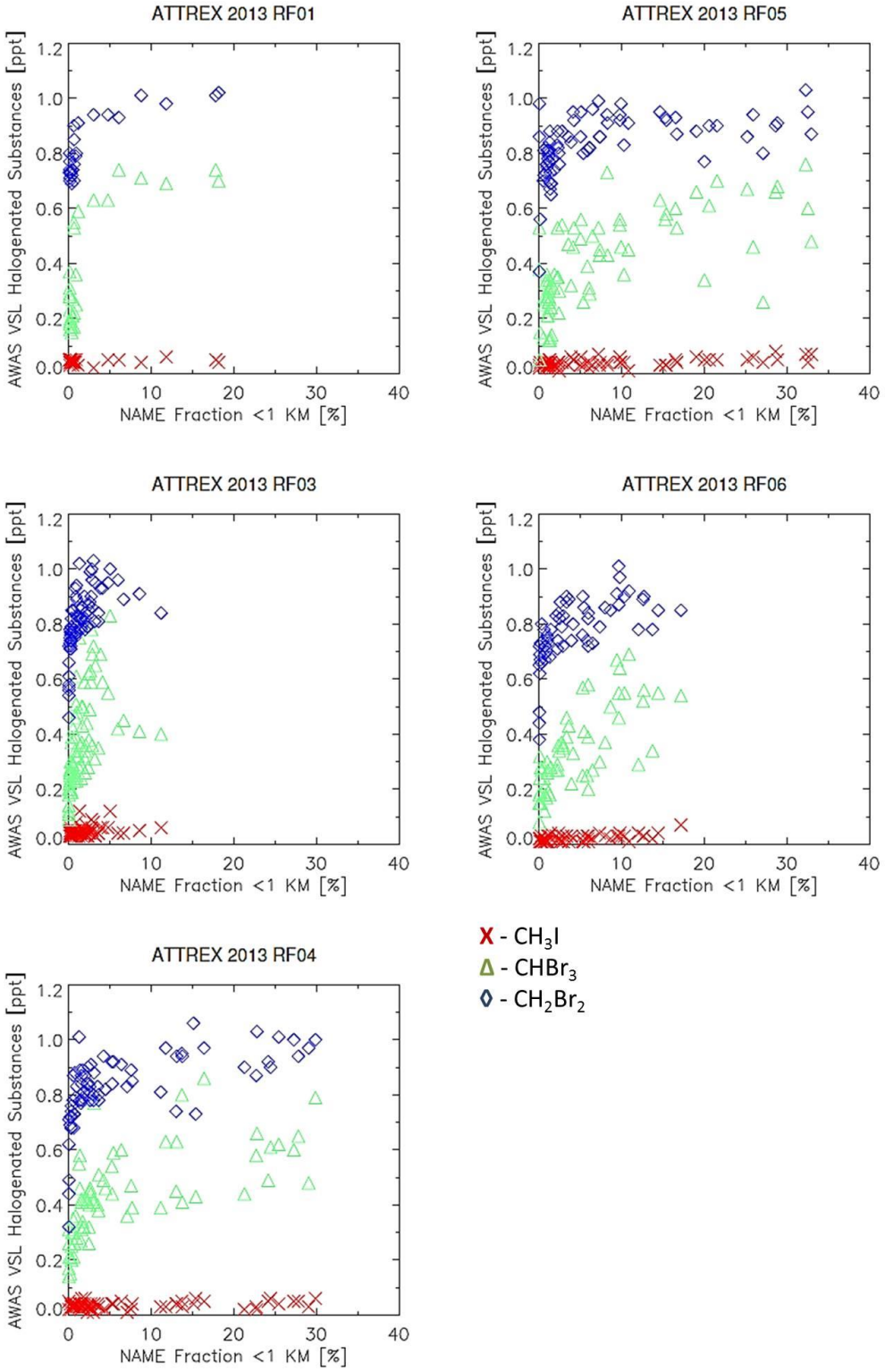

Figure 4.8 Relationship between measured very short lived halogenated substances and modelled NAME fractions of trajectories below 1 km for individual ATTREX 2013 flights.

4.2.2. ATTREX 2014 Research Flights

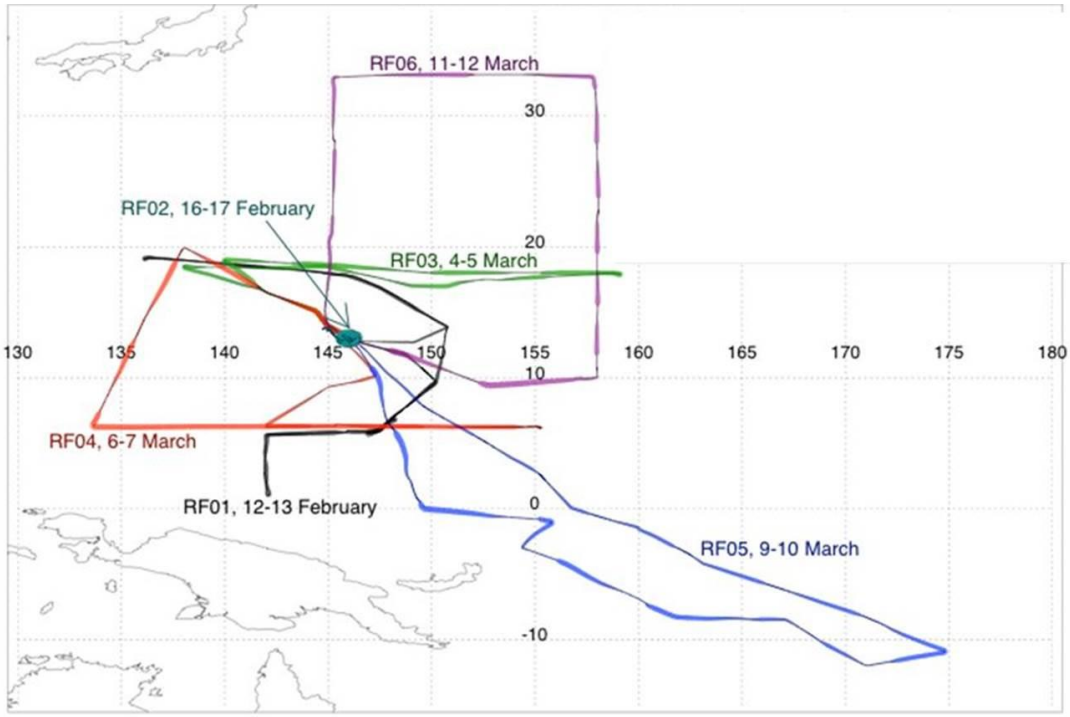

Figure 4.9 ATTREX 2014 Research Flights (Local Flights shown only, Transit Flights to Guam and back are omitted).

2 Transit Flights and 6 Research Flights in the West Pacific were made in January-March, 2014 (Figure 4.9). This period coincides with the active phase of Madden-Julian Oscillation (MJO) and the increased activity of tropical cyclones. RFs noted high frequency of recent convective events, reflected in the elevated CH_3I and $CHBr_3$ mixing ratios and high values of NAME fractions of trajectories from below 1 km.

Transit Flight to Guam 2014-01-16/17

A transit flight was made from Dryden Flight Research Centre to Andersen Air Force Base, (AAFB), Guam. The Global Hawk cruised near the tropical tropopause for most of the flight in a constant latitude band (within 12-16^{o}N). Low CH_3I in the TTL and low NAME fractions of trajectories from below 1 km are observed (Figures 4.10 and 4.13). High $CHBr_3$ and CH_2Br_2 in the TTL are measured, decreasing with altitude (Figures 4.11-12). Most air masses have little boundary layer signature from the West Pacific (Figure 4.14).

Research Flight 01 2014-02-12/13

26 vertical profiles were made. Profile-to-profile variability in $CHBr_3$ and CH_2Br_2 is noted (Figures 4.11-12). One episode showing high CH_3I and $CHBr_3$ mixing ratios in the lower TTL is observed, coincident with the elevated influence from the boundary layer (Figures 4.10-11 and 4.13). The first part of the flight (northwest of Guam) encountered air of the westerly flow residing in the TTL. A high fraction of this air came from the boundary layer around the western Indian Ocean 7 days prior to the flight. This marks the outflow from the emerging tropical cyclone Fobane. The second part of the flight (south of Guam) experienced high boundary layer air influence, originating from the recent convective centres developed south of Guam, and near the Philippines (Figure 4.14). Low percentage of boundary layer air originated from the equatorial Atlantic Ocean region, with taking 10-12 days to reach a GH flight path.

Research Flight 02 2014-02-16/17

The flight was conducted in a confined area east of Guam due to a faulty primary satellite communications system for Global Hawk command and control, Inmarsat. 26 vertical profiles were made. Each profile shows a gradation in CH_3I distribution in the TTL, higher in the lower TTL, decreasing with altitude (Figure 4.10). The largest boundary layer air mass influence is noted for 14-15 km with the minimal influence and dominant horizontal long-range transport of air masses noted for 17-18 km (Figure 4.13). Two major boundary layer air mass origins are distinguished: the localised convective centre southeast of Guam (a band being a part of the ITCZ) and the Indian Ocean, resulting from the tropical cyclone Fobane activity (Figure 4.14).

Research Flight 03 2014-03-04/05

20 vertical profiles were completed. The Global Hawk profiled through the TTL in the vicinity of tropical cyclone Faxai, which was active north of the flight path. Low ozone was measured, with high CH_3I and $CHBr_3$ even in the upper TTL, showing the highest CH_3I and short-lived bromocarbon mixing ratios for ATTREX 2014 (Figures 4.10-12). This is coincident with enhanced boundary layer air mass contribution (e.g. the sampled air at 14-15 km being composed of over 80% boundary layer air mass, Figure 4.13). The SPCZ (confined within the 150-190^{o}W, Equator-15^{o}S) emerges as the second major boundary layer source

origin (Figure 4.14). The boundary layer air mass from the ITCZ is also differentiated. RF03 marks the beginning of a shift of convection toward the Southern Hemisphere, and a clear eastern propagation of the MJO [*Jensen, et al., 2017*].

Research Flight 04 2014-03-06/07

The Global Hawk surveyed western Pacific TTL, east of Guam. High CH_3I, $CHBr_3$ and CH_2Br_2 mixing ratios coincide with high NAME 1 km fraction values for 14-16 km (Figures 4.10-13). The convective influence derived from the strong MJO is observed predominantly from the ITCZ, SPCZ and the west of Guam (Figure 4.14). From 17 km up, air masses are mostly transported horizontally within the TTL, with negligible signal of low level air mass influence.

Research Flight 05 2014-03-09/10

Surveying the TTL southeast of Guam, the flight path was modified to avoid active deep convection and to maximise sampling of air detrained from tropical cyclone Lusi. Multiple encounters of air masses with high low troposphere / boundary layer signatures are observed, given high values for the NAME 1 km fractions and high CH_3I and $CHBr_3$ mixing ratios (Figures 4.10-11 and 4.13). The atmospheric transport patterns resemble those seen in RF04, as it is the second most convectively influenced flight, and was similarly subject to the direct outflow of the low troposphere air masses via tropical cyclone activity. The same confined areas of the West Pacific ITCZ and SPCZ are the sources of the boundary layer air masses for the sampled TTL. No remote boundary layer air mass source origins are observed (Figure 4.14).

Research Flight 06 2014-03-11/12

The flight surveyed north of Guam, providing profiles of extra-tropical upper troposphere and lower stratosphere composition. The Global Hawk flew north of the subtropical jet, then east and south into the edge of the anticyclone. A region southwest of Guam and downstream of deep convection was sampled near the end of the flight. A distinction of these two sampling stages (above and below 20^oN) is reflected in CH_3I and $CHBr_3$ measurements and in the corresponding NAME 1 km fractions (Figures 4.10-11 and 4.13). Higher CH_3I and brominated tracers are observed below 20^oN. The boundary layer air influence is stronger

there, originating from the western edges of the ITCZ and SPCZ bands (Figure 4.14).

Transit Flight to the USA 2014-03-14/15

The final flight was a transit back to the DFRC. Two distinct episodes of high CH_3I and bromocarbons are observed (Figure 4.10-12). The first one (near Guam) encounters air masses originating from the confined area within the ITCZ and dispersed SPCZ. The second episode (Central Pacific) was near the major convective centre within the ITCZ, with the second dominant source being the SPCZ. The boundary layer air masses from the remote central Indian Ocean and the Maritime Continent contribute less to the sampled TTL. The final part of the flight surveyed above 20^oN, above 16 km. Minimal low level air mass influence is observed there, originating mostly in the West Pacific and being transported horizontally (Figure 4.14).

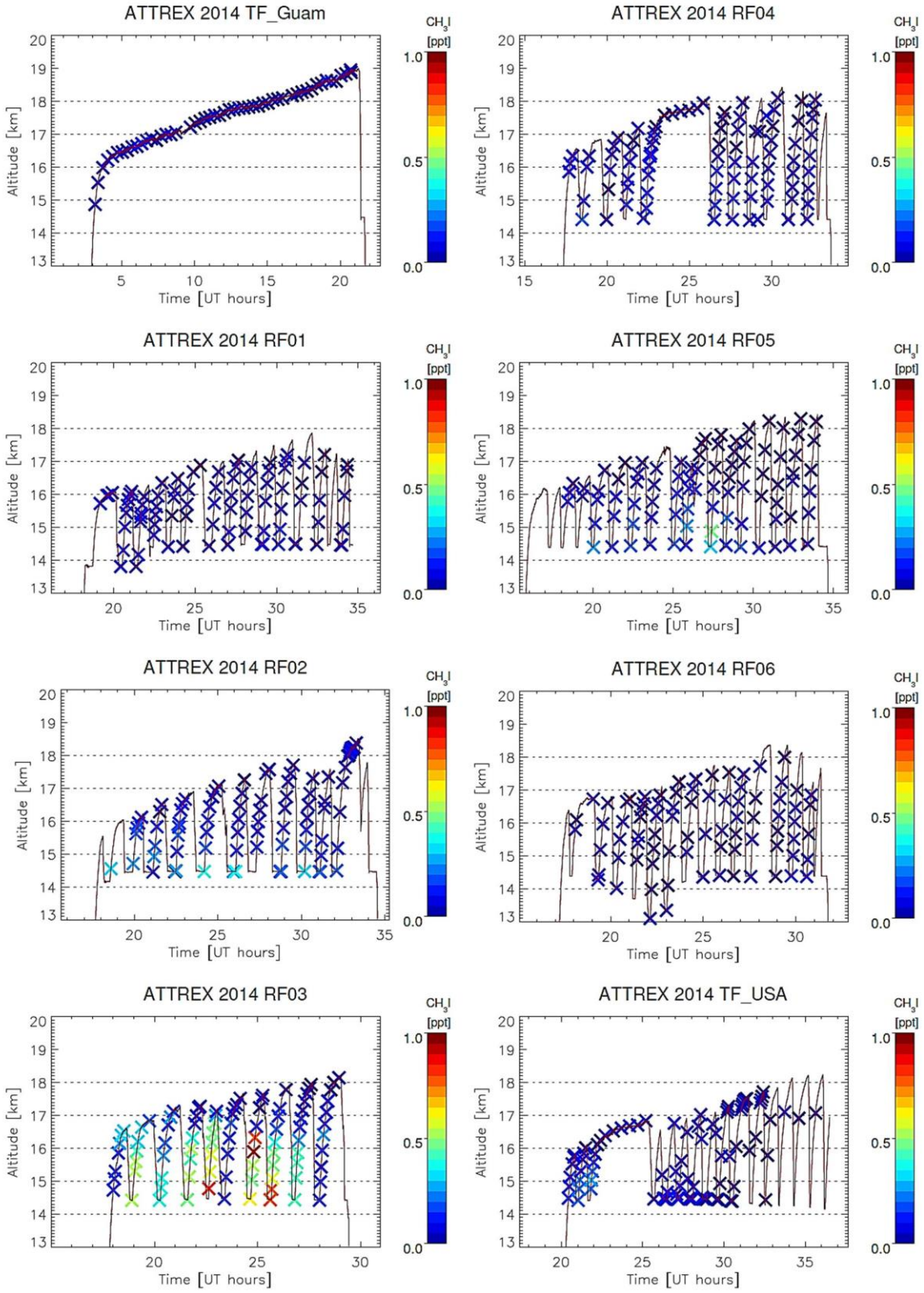

Figure 4.10 Vertical distribution of AWAS CH_3I in the TTL, ATTREX 2014.

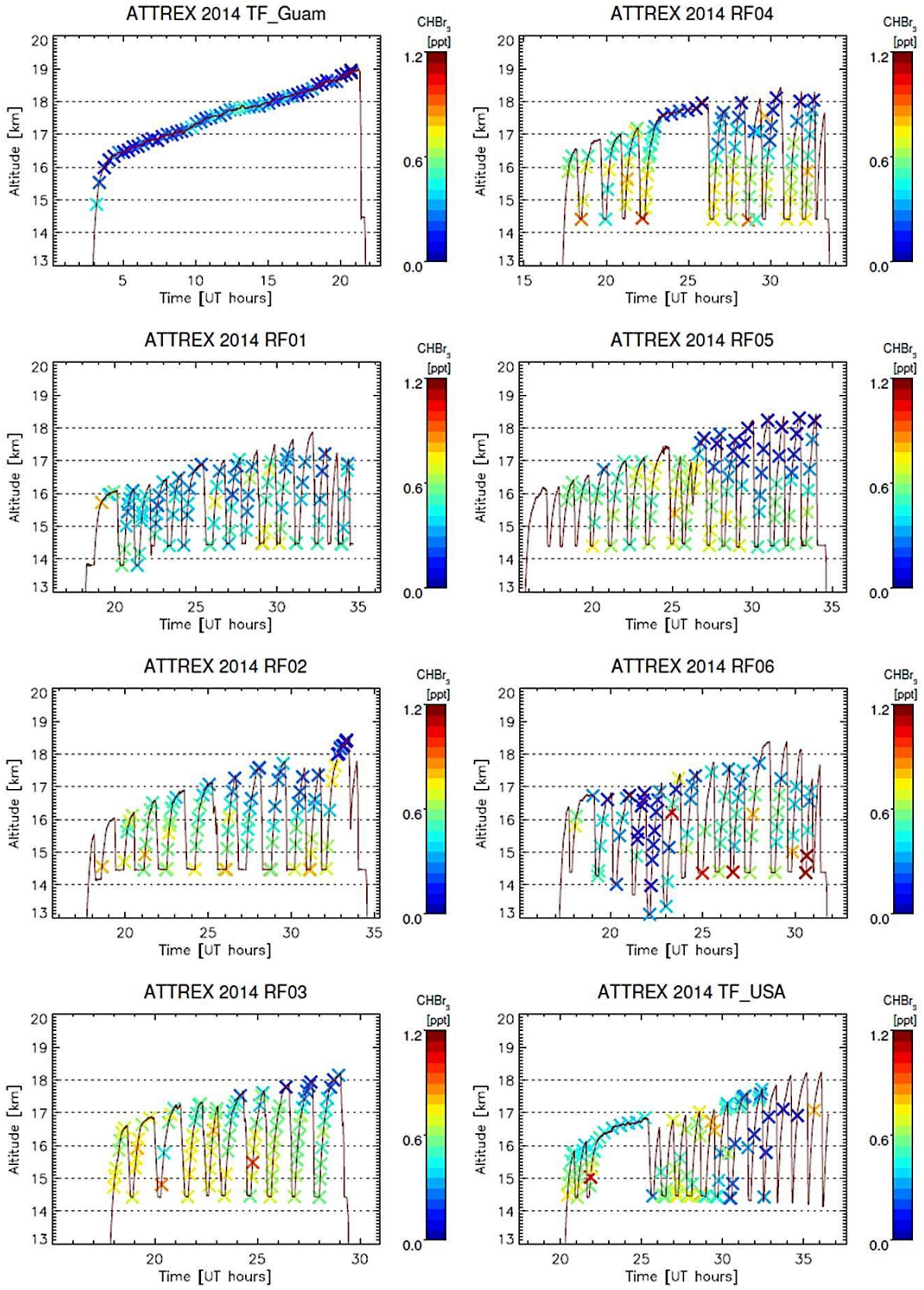

Figure 4.11 Vertical distribution of AWAS $CHBr_3$ in the TTL, ATTREX 2014.

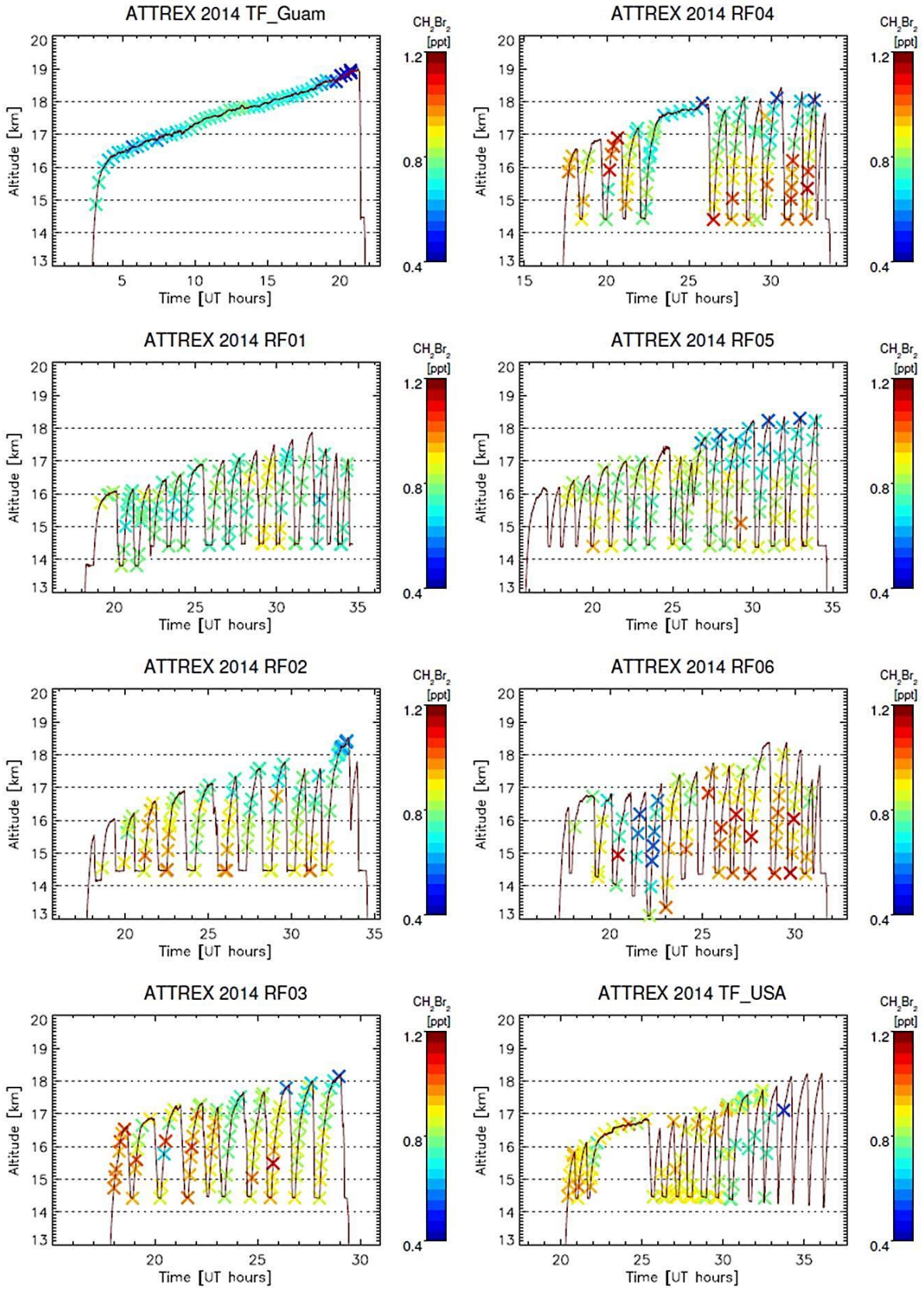

Figure 4.12 Vertical distribution of AWAS CH_2Br_2 in the TTL, ATTREX 2014.

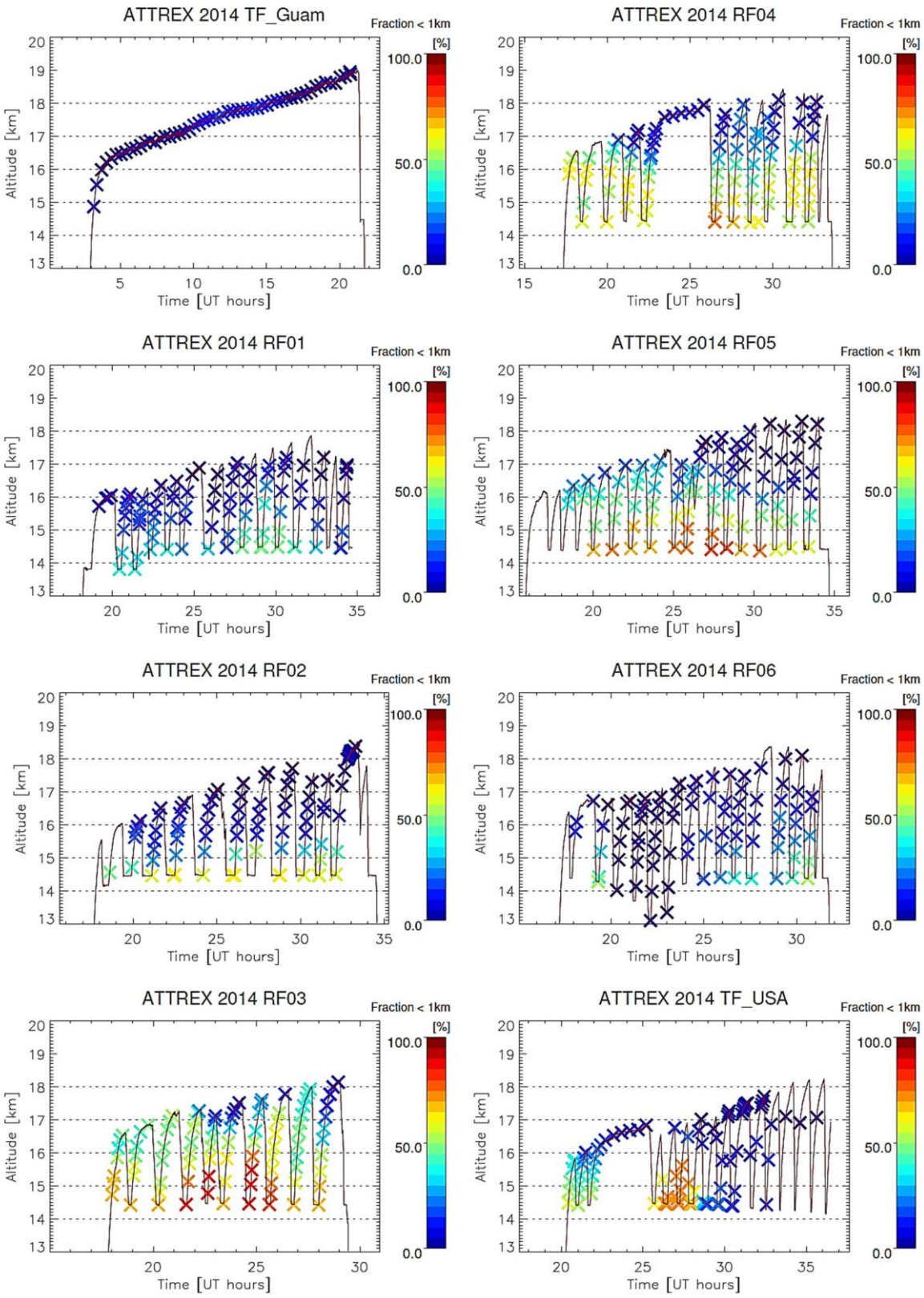

Figure 4.13 Vertical distribution of the NAME fractions of trajectories crossing below 1 km in the TTL, ATTREX 2014.

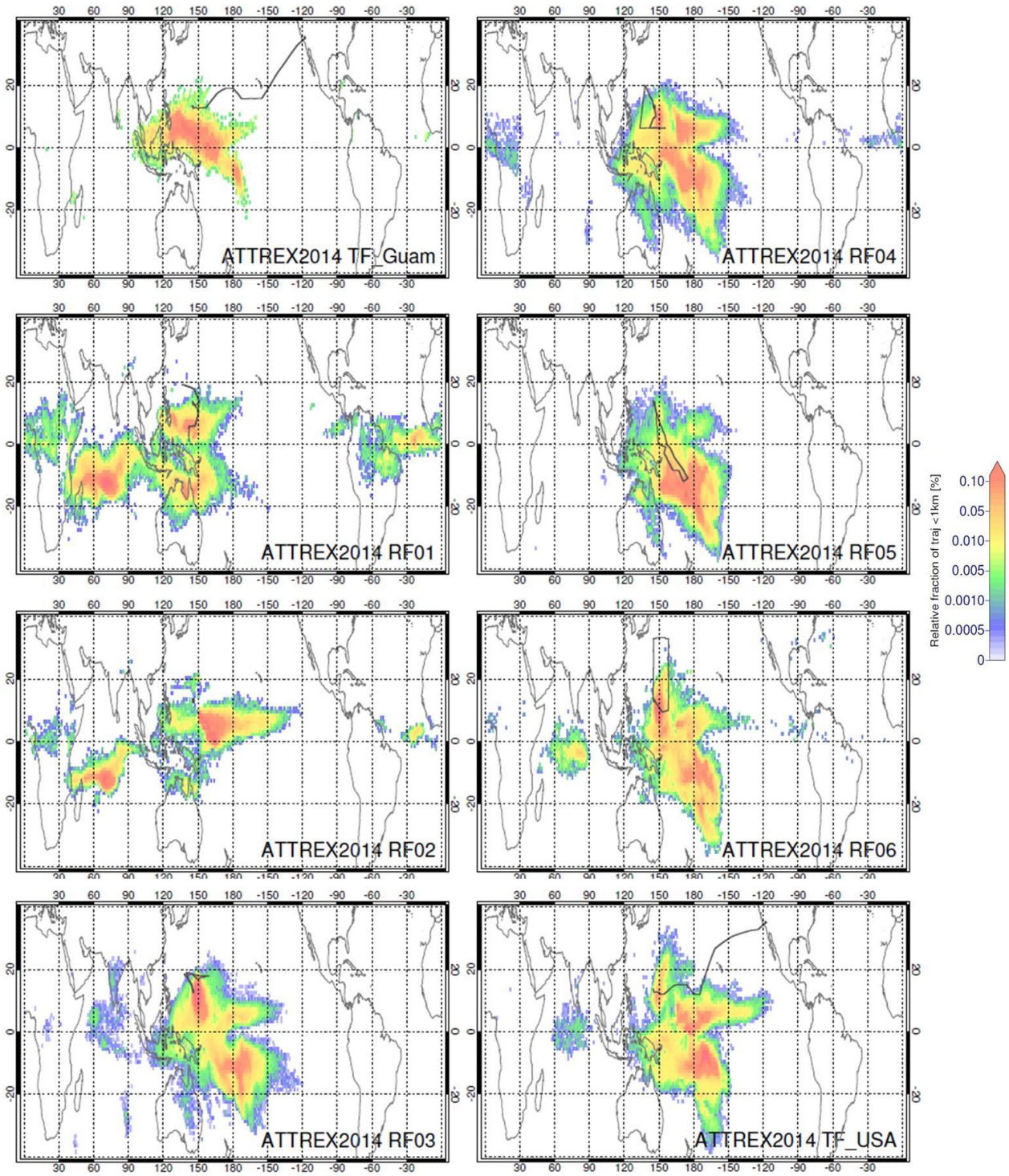

Figure 4.14 Distribution of regions contributing boundary layer air (regions where released particles first crossed below 1 km) to the sampled TTL during the ATTREX 2014 Research Flights (RF paths marked as solid grey lines).

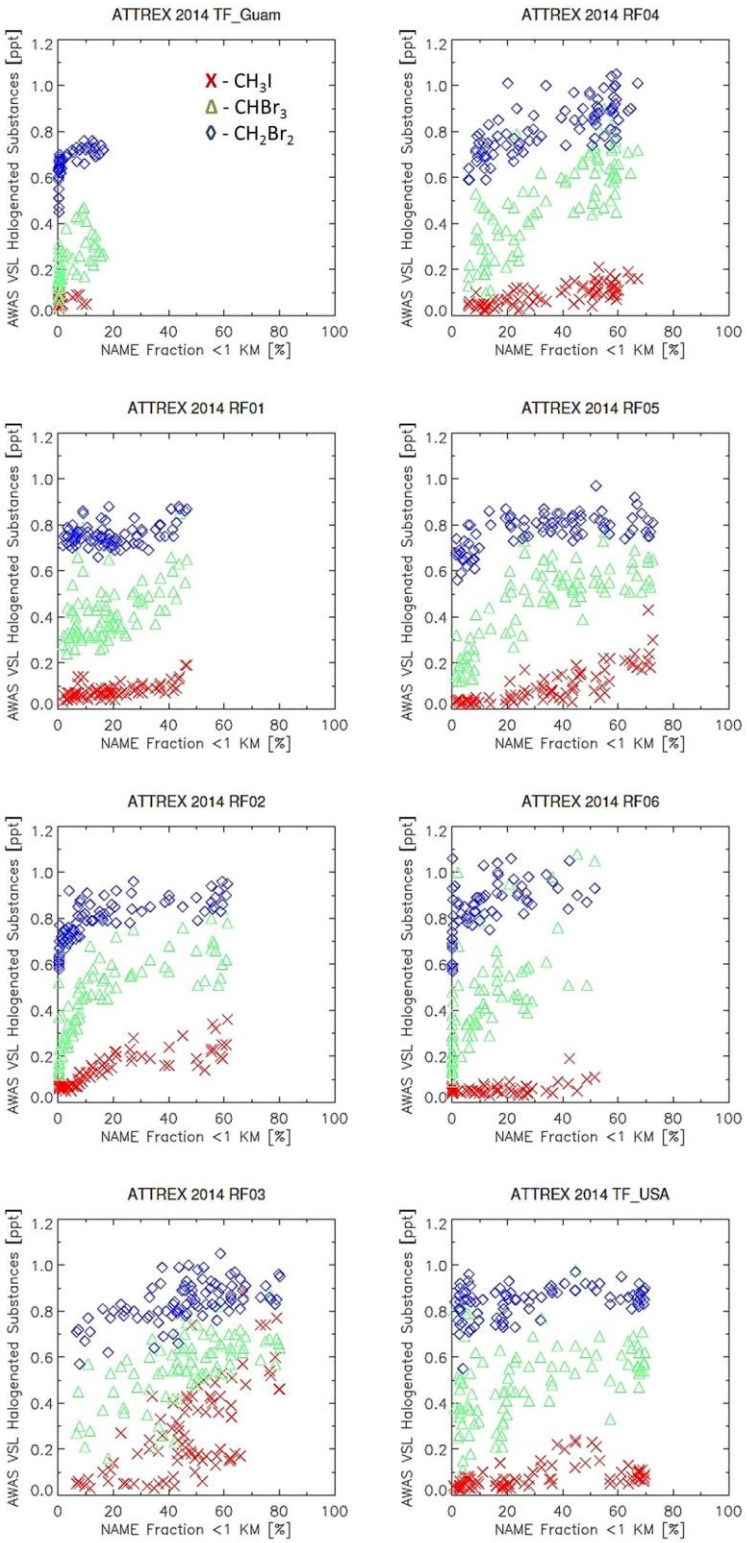

Figure 4.15 Relationship between measured very short lived halogenated substances and modelled NAME fractions of trajectories below 1 km for individual ATTREX 2014 flights.

4.3. Summary

This chapter introduces the NAME procedure compatible with analysing the measurements of CH_3I, $CHBr_3$ and CH_2Br_2 taken during the NASA ATTREX 2013 and 2014 flights. NAME is run for each AWAS sampling location along the ATTREX flight paths to investigate the influence of the boundary layer air in the sampled TTL air.

This chapter examines the vertical distribution of CH_3I, $CHBr_3$ and CH_2Br_2 in the TTL over the West and East Pacific. The episodes of high CH_3I coincide with the episodes of the elevated NAME calculated boundary layer influence to the TTL. The highest CH_3I is found in the lower TTL and drops with altitude to minimum values in the upper TTL. ATTREX 2014 sees much higher CH_3I mixing ratios than ATTREX 2013.

ATTREX 2013 and 2014 see similar vertical distribution of $CHBr_3$ and CH_2Br_2 in the TTL. Higher $CHBr_3$ was observed in ATTREX 2014. As the $CHBr_3$ atmospheric lifetime is shorter (15 days) than CH_2Br_2, its TTL concentrations are more affected by the transport times from the emission sources (boundary layer). The frequency and magnitude of convective activity influences these transport times. In the West Pacific, 2014, Global Hawk encountered the air which had a signature of larger boundary layer air mass influence due to the presence of recent and rapid convective activities, tropical cyclones and the strong MJO phase. ATTREX 2013 experienced minimal influence from the convective activity over the East Pacific. $CHBr_3$ and CH_2Br_2 decrease with altitude, with distinct gradients, dependent on the atmospheric lifetime of these two substances. CH_2Br_2 drops off slower due to its longer atmospheric lifetime of 94 days.

Individual ATTREX 2014 flights saw episodes of high CH_3I and $CHBr_3$ coinciding qualitatively with high fractions of trajectories crossing below 1 km (indicative of the high boundary layer air loading to the TTL; as shown by Figure 4.15). This relationship is attenuated for ATTREX 2013 flights (Figure 4.8). This emerging chemistry-dynamics relationship between the NAME modelled results and CH_3I observations is probed in Chapter 5. Convective Influence on Methyl Iodide in the TTL. The vertical distribution of $CHBr_3$ and CH_2Br_2 in the East and West Pacific TTL, in 2013 and 2014, respectively, is further assessed

in Chapter 7. Transport and distribution of short-lived brominated organic substances in the TTL.

5. Convective Influence on Methyl Iodide in the TTL

In this chapter, the influence of fast convective transport on the atmospheric distribution of methyl iodide (CH_3I) is investigated. CH_3I is relatively short-lived (3-7 days, [*Tegtmeier et al., 2013*]), and is emitted at the Earth's surface. Its presence in the tropical tropopause layer (TTL) implies recent transport from the surface. This study quantifies that transport using the NAME dispersion model including its new convective transport scheme. It uses measurements from two NASA ATTREX stages, which took place in 2013 and 2014, in the East and West Pacific, respectively. In Section 5.1, I show how the NAME approach can be used to estimate the contribution of boundary layer air to the air sampled during one flight of the Global Hawk: ATTREX 2014 Research Flight 02. The NAME procedure to quantify CH_3I in the TTL is assessed then. This analysis is extended to all the 2014 flights in Section 5.2 and all the 2013 flights in Section 5.3. These results are summarised and conclusions on the performance of the NAME procedure in quantifying CH_3I in the TTL are drawn.

5.1 NAME for ATTREX 2014: Individual Flight – Research Flight 02

In this section, the NAME procedure is demonstrated for one of the ATTREX 2014 flights: the Research Flight 02, RF02. After a brief overview of the flight, the vertical distribution of CH_3I in the TTL is analysed. The spatial and temporal variability of the boundary layer air mass influence to the TTL as well as the procedure to quantify its contribution to the TTL are described. Methods developed to estimate the background contribution are assessed and finally the NAME modelled results of the summed CH_3I boundary layer and background contribution estimates are compared with the AWAS observations. The following sections deal with AWAS observations for all the ATTREX 2014 and 2013 flights cumulatively, and the corresponding NAME modelled results.

5.1.1 ATTREX 2014 Research Flight 02: Overview

The ATTREX 2014 RF02 took place on 16-17 February. Inmarsat, the primary satellite communications system, was not operational during the flight, so a full length mission was conducted off the east coast of Guam and within the Ultra High Frequency – Line of Sight (UHF-LOS) range. Consequently, the Global Hawk surveyed a small region to the east of Guam (12-13^{o}N, 146-147^{o}E, Figure 5.1).

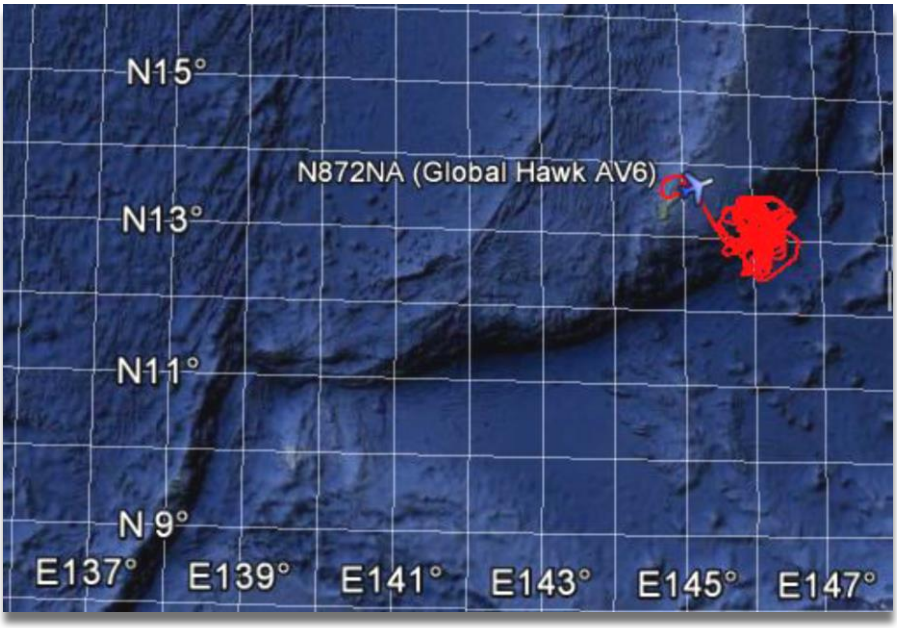

Figure 5.1 ATTREX 2014 RF02 path (marked as a red line).

26 vertical profiles were performed with AWAS measurements taken on each ascent (Figure 5.2).

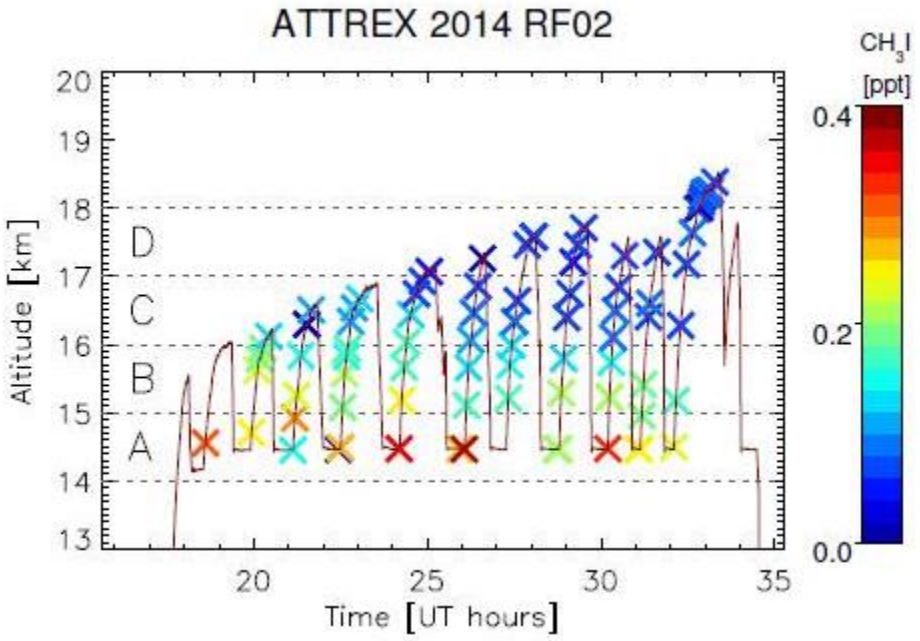

Figure 5.2 ATTREX 2014 RF02 path with AWAS CH_3I measurements. Symbols A-D mark four 1 km TTL segments: 14-15, 15-16, 16-17 and 17-18 km, used in further analysis.

The observations show a high degree of variability of CH_3I in the TTL (from > 0.4 ppt at 14-15 km to near-0 ppt values at 17-18 km, Figure 5.2). In general, higher values are measured in the lower TTL regime up to 16 km, decreasing gradually with altitude.

5.1.2 NAME assessment of the vertical distribution of CH_3I in the TTL

The following NAME procedure is used to (a) investigate the vertical distribution of CH_3I in the TTL, and (b) quantify CH_3I contribution from the boundary layer.

15,000 particles are released from a NAME defined box (0.1 x 0.1 x 0.3 deg^2km) covering each AWAS measurement location along the RF02 path (83 measurements, in total) and followed 12 days back. Particles which first cross below 1 km, marked as the boundary layer altitude, are counted and turned into fractions. These fractions quantitatively illustrate the influence of boundary layer air masses to the TTL (Figure 5.3).

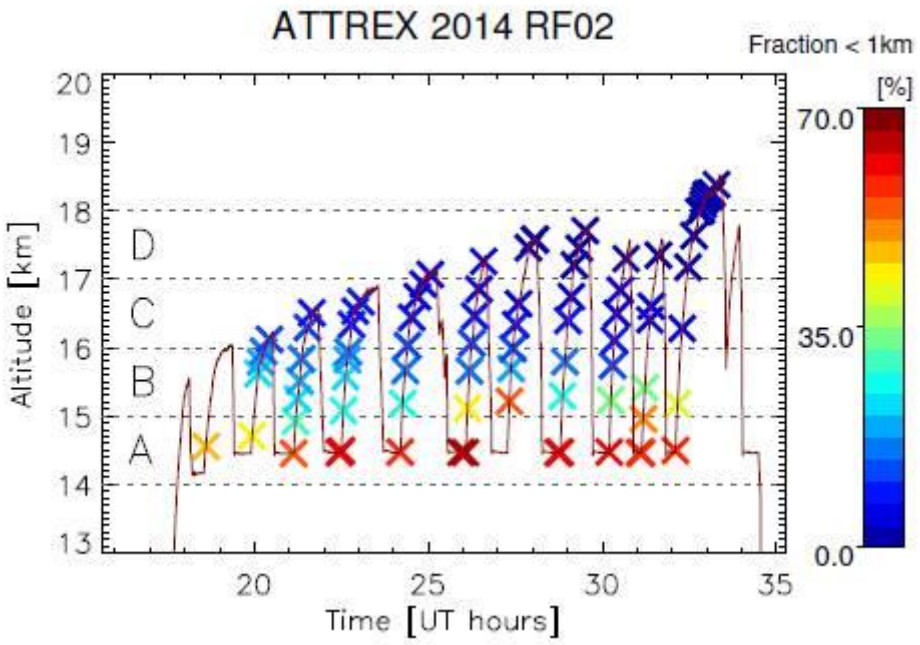

Figure 5.3 ATTREX 2014 RF02 path with NAME fractions of trajectories below 1 km.

AWAS samples with high CH_3I correspond to those with high influence of the boundary layer air mass. The boundary layer influence decreases with altitude, similarly to CH_3I measurements.

The vertical distribution of NAME 1 km fractions in the TTL is attributed to differences in (a) atmospheric transport pathways, (b) boundary layer origin locations, and (c) their transport timescales. The following NAME analysis investigates the above statement.

All NAME runs for the RF02 are grouped into four 1 km TTL segments: 14-15 km – A, 15-16 km – B, 16-17 km - C, and 17-18 km - D. Evolution of the vertical spread of particles for individual NAME runs from each 1 km TTL segment, illustrated by Figure 5.4, shows the dominance of different atmospheric transport pathways.

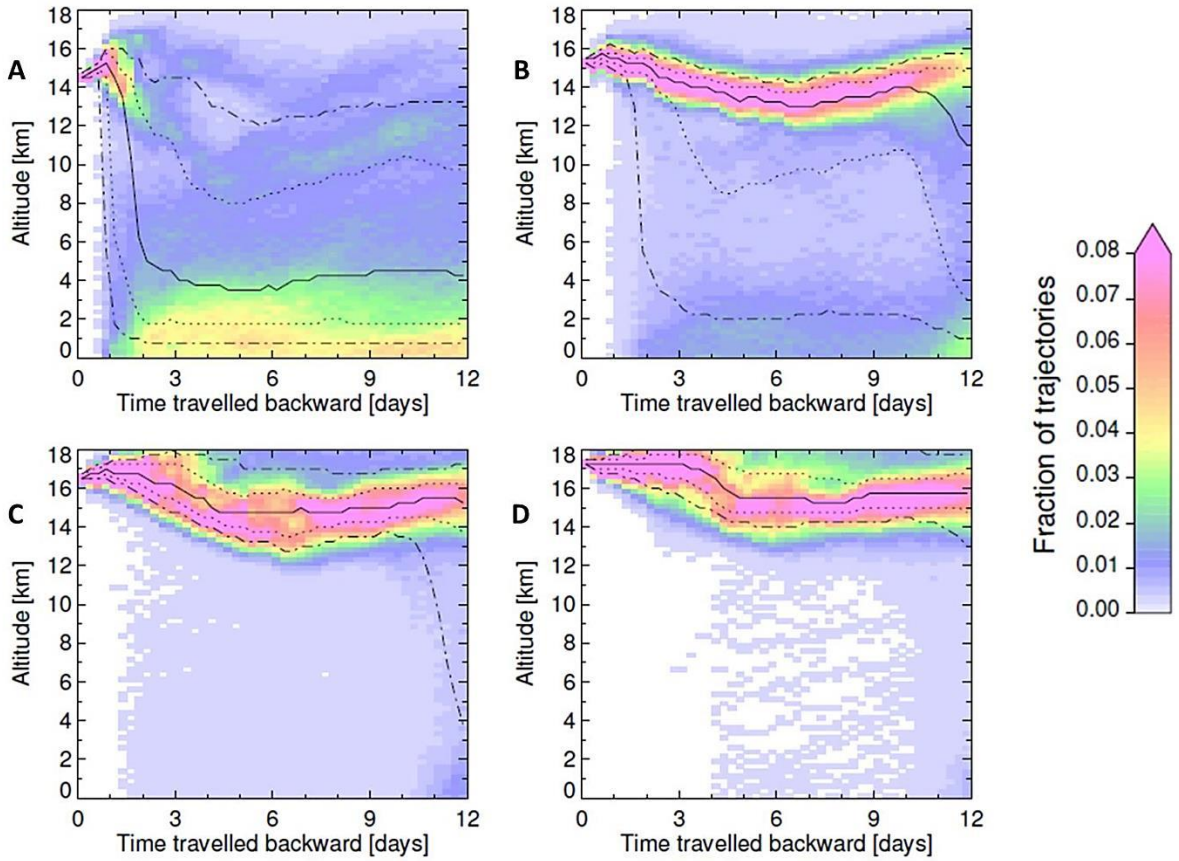

Figure 5.4 Particle density vertical distribution over time for four NAME runs, representative of the 1 km TTL segments (A) 14-15 km [SRC103647, Release Altitude (RA): 14.5 km], (B) 15-16 km [SRC103689, RA: 15.3 km], (C) 16-17 km [SRC104434, RA: 16.4 km], (D) 17-18 km [SRC105133, RA: 17.2 km], ATTREX 2014 RF02. The solid black line (median) indicates 50% of the released particles below given altitude at given time after the release (time=0); 10^{th} and 90^{th} (dashed-dot) and 25^{th} and 75^{th} (dotted) percentiles.

The 14-15 km NAME run shows a distinct particle population, with most particles reaching the low troposphere within 2 days after the release (Figure 5.4A). This represents the fast vertical uplift of the low troposphere air masses to the lower TTL. At 15-16 km, two particle populations are observed (Figure 5.4B). The first stream is marked by the 10^{th} percentile line and represents a signal of the recent vertical uplift. Most particles, though, are contained in the second stream which resides above the upper troposphere for the duration of the 15-16 km run. Towards the end of this run (on 11-12th day) this stream reaches through the upper troposphere. This is indicative of second vertical uplift occurring far from the particle release area. Above 16 km, a stream of particles residing within the TTL dominates, with negligible influence from the low troposphere. This shows the dominance of the horizontal long-range transport for the 16-17 and 17-18 km NAME runs (Figures 5.4C-D).

The information inferred from the crossing location maps (Figure 5.5) gives locations where trajectories, released from the TTL, first cross the 1 km altitude. The West Pacific is a major source of the boundary layer air masses to the lower TTL (14-15 km, Figure 5.5A). At 15-16 km, two regions are equal in magnitude: the West Pacific (first peak corresponding to the recent fast vertical uplift) and the central Indian Ocean (second peak matching a remote source, marking the activity of the Fobane tropical cyclone, Figure 5.5B). Above 16 km, remote sources: the Indian Ocean and the tropical band of the African continent become dominant (Figures 5.5C-D).

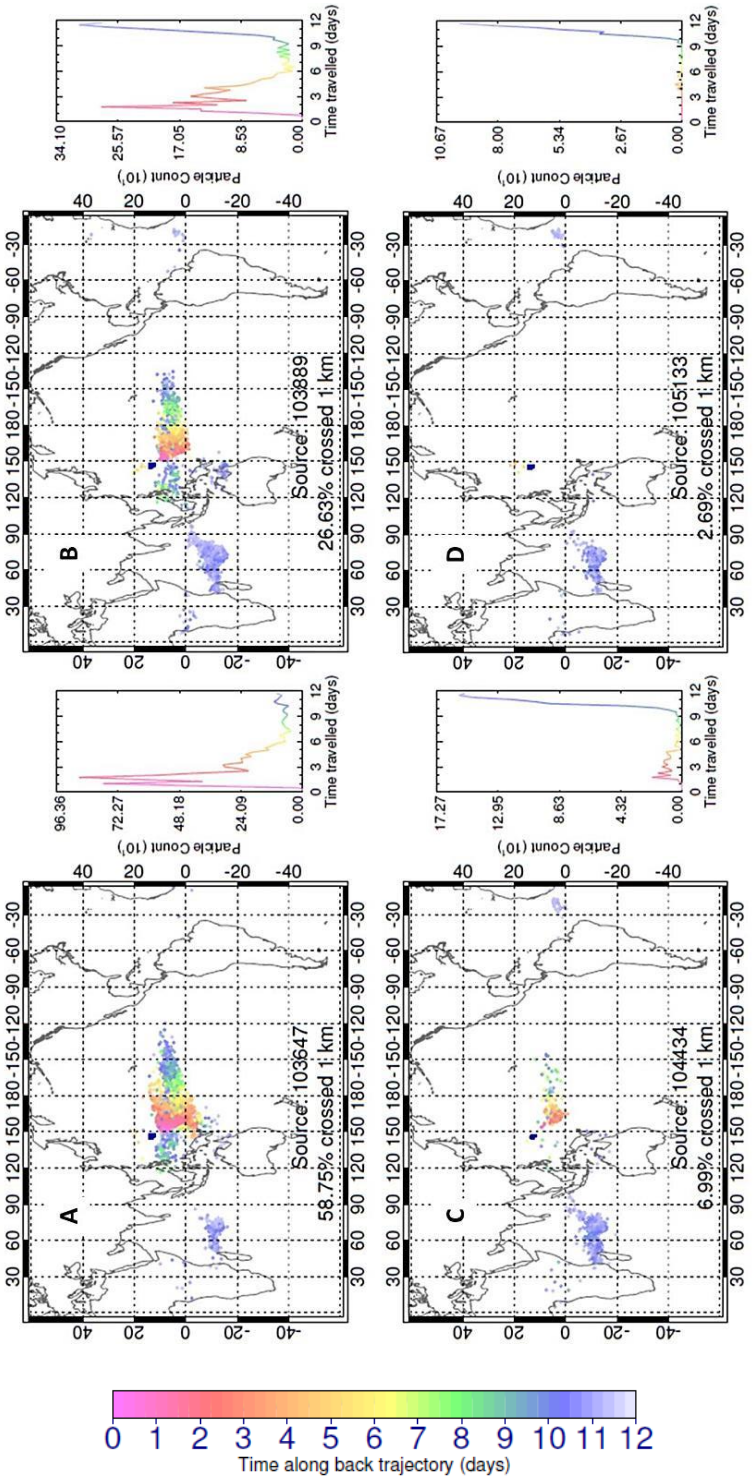

Figure 5.5 The 1 km crossing location maps for four individual NAME runs (as in Fig. 5.4), each from 1 km TTL segments (A-D), ATTREX 2014 RF02. Points, where particles first cross below 1 km, are marked and colour-coded with the time taken for these particles to cross below 1 km. Histograms show the evolution of particle crossing distribution in time.

This analysis is shown for the four individual NAME runs, representative of each 1 km TTL segment. As RF02 sampled on a single-point area for 18 hours, the meteorology conditions stayed virtually the same (Figure 5.6). Each of the ascending profile 1-km segments featured similar characteristics in temperature (T) and wind components (u and v, zonal and meridional velocity, respectively; Figure 5.6). A temperature vertical profile showed two minima in the TTL – first at 16.5 km and second at 18 km (Figure 5.6.B). Thus, all NAME runs for RF02, as grouped in 1 km TTL segments, can be assessed cumulatively (Figure 5.7).

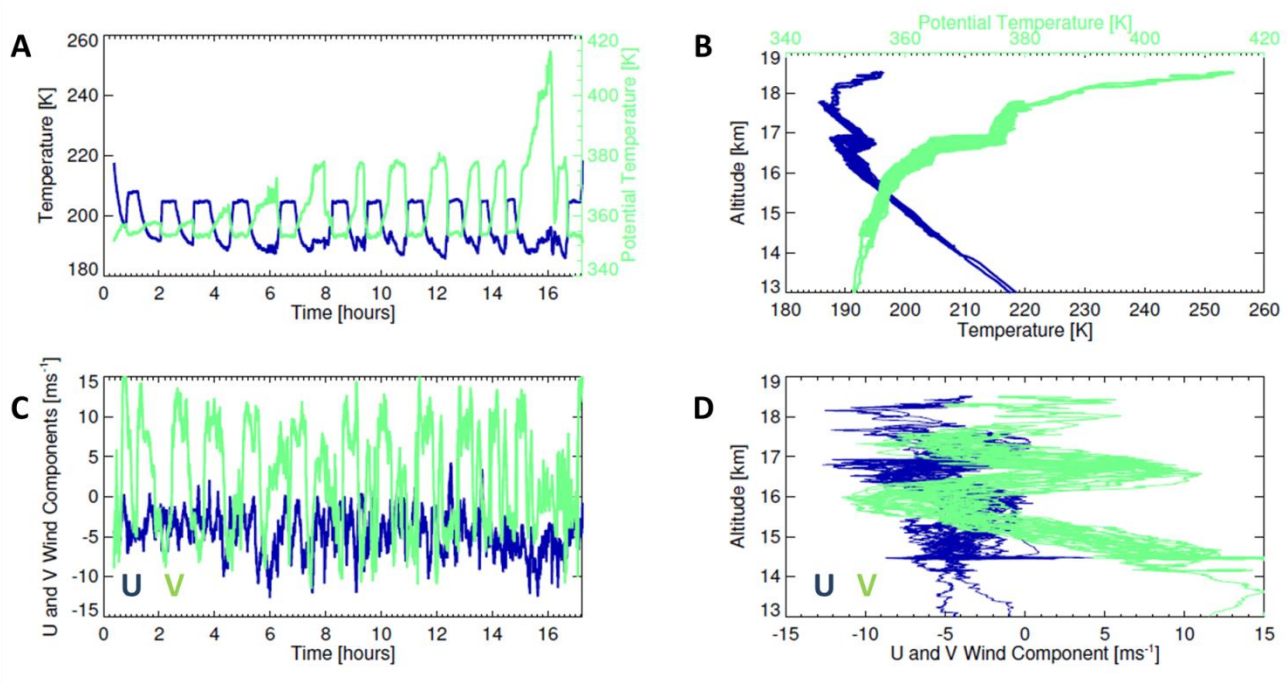

Figure 5.6 Meteorological conditions during the ATTREX RF02 flight: temperature and potential temperature profiles against time (A) and altitude (B), and horizontal wind vector (U and V – zonal and meridional velocities, respectively) against time (C) and altitude (D).

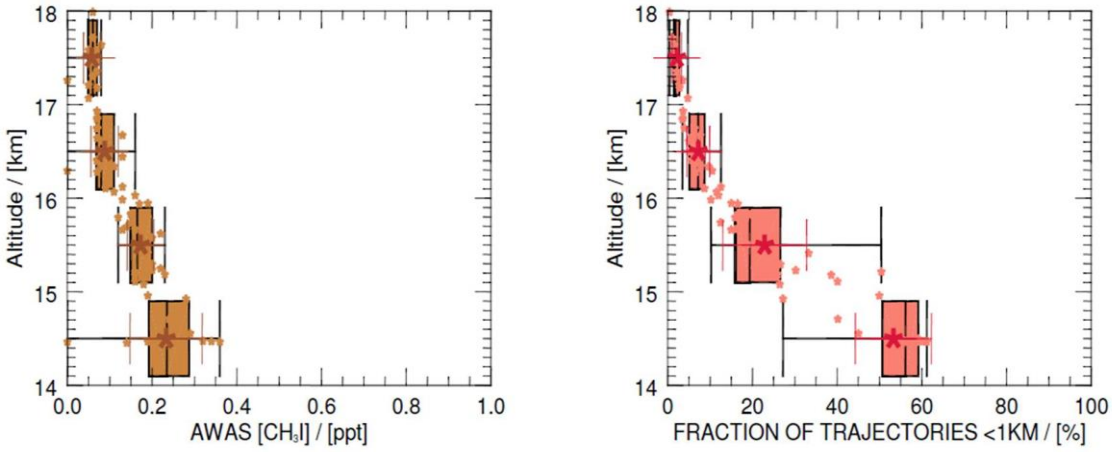

Figure 5.7 Vertical distribution of CH_3I in the TTL (AWAS observations, left) and NAME fractions of trajectories from below 1 km (right). Box and whisker plots show the range: minima and maxima, lower and upper quartiles and medians; means are marked with a star symbol, and standard deviations - with red caps, dots show individual data points.

Cumulatively, the highest fractions below 1 km are observed for the lower TTL (14-15 km). A noticeable transition occurs between the lower and upper TTL (15 to 17 km). From 16 km up, almost no influence of the low-level air masses is seen.

The crossing location distribution map shows locations of all the trajectories from the RF02 NAME runs which first cross below 1 km (binned into 1 x 1 degree longitude x latitude fractions, Figure 5.8). Two regions are dominant: the West Pacific and central Indian Ocean.

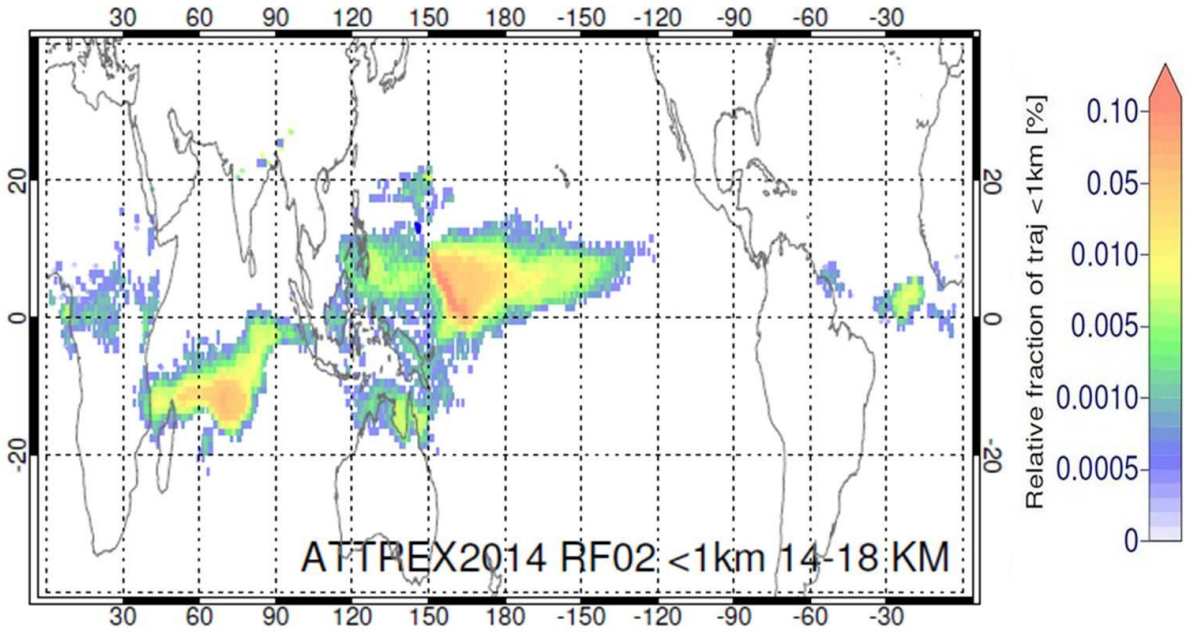

Figure 5.8 Crossing location distribution map of the boundary layer source origins contributing to the TTL, ATTREX 2014 RF02.

Figure 5.9 shows the variability in contribution of different boundary layer air mass origin areas to the TTL. The western and central Pacific Ocean is predominant for the lowest TTL segment (14-15 km, Figure 5.9A). Remote areas: the Maritime Continent, the Northern Australia coast, the Indian Ocean and the equatorial band of the African continent dominate as altitude increases (Figures 5.9C-D).

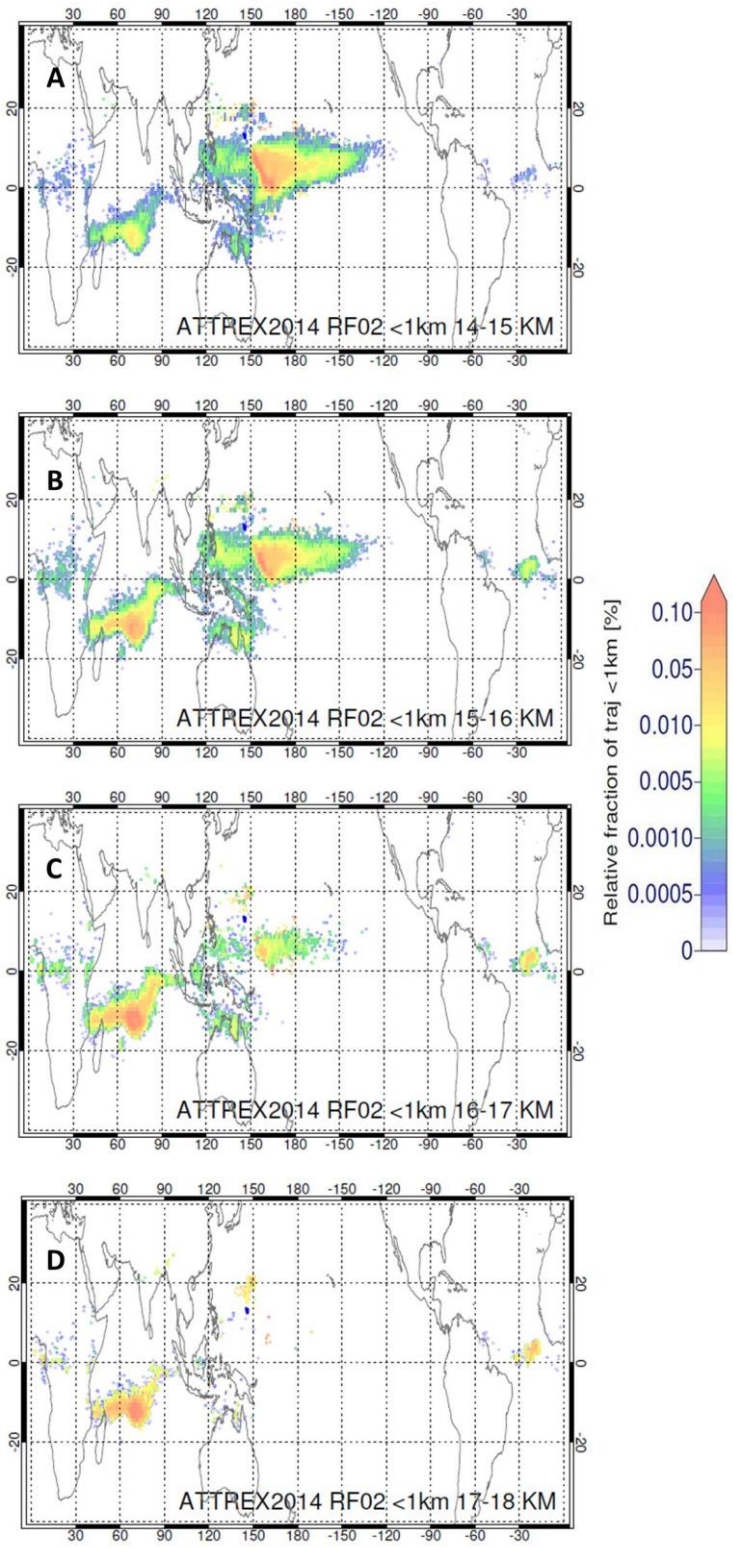

Figure 5.9 Variation in the importance of the boundary layer source regions to the 1 km TTL segments, as shown by the crossing location distribution maps, ATTREX 2014 RF02.

The differences in times taken for the particles to cross below 1 km are shown in Figure 5.10.

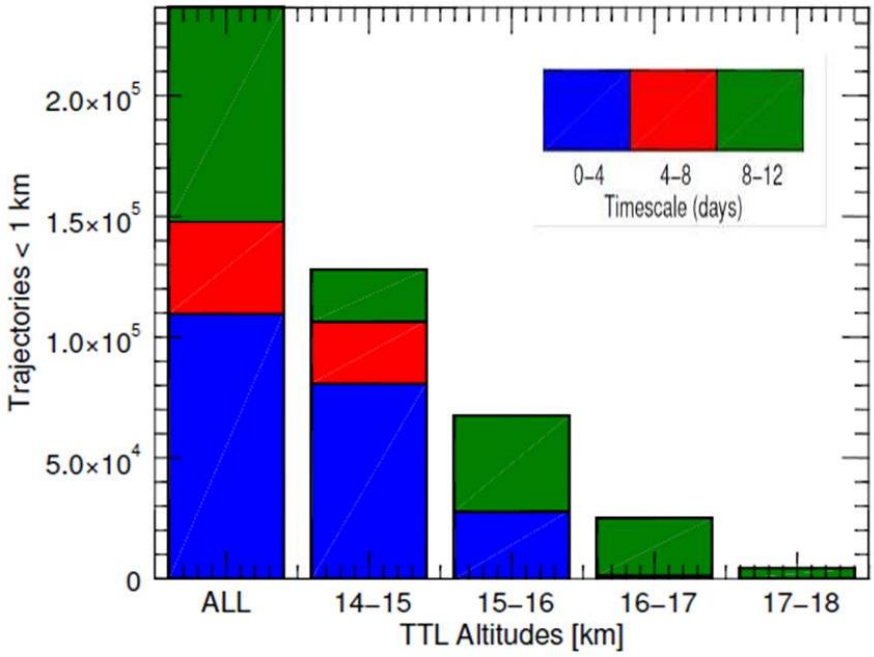

Figure 5.10 Distribution of transport times taken for the trajectories to first cross below 1 km (boundary layer) for all the NAME runs (ALL) and the NAME runs grouped into 1 km TTL segments, ATTREX 2014 RF02.

Particles, taking less than 4 days to reach 1 km, represent 'young' fresh air masses originating from the boundary layer of the western and central Pacific. Rapid vertical uplift is the dominant transport mechanism here. The 'old' air masses, represented by particles taking 8 days and more, are of horizontally transported, long-range origin. All NAME runs in RF02 show significant contribution of fresh air masses to the TTL (Figure 5.10). However, while analysing four 1 km TTL segments individually, the lowest TTL regime (14-15 km) receives the highest fraction of these fresh air masses. From 16 km up, the long-distance 'older' air masses dominate.

NAME trajectory analysis shows that variability in where the boundary layer air masses originate from and the corresponding transport timescales influence its loading and distribution in the TTL. Similarly, the vertical distribution of CH_3I in the TTL is explained as its presence is affected by very short atmospheric lifetime and transport pathways.

Consequently, high fractions of trajectories from the boundary layer in the lower TTL (14-15 km) lead to high CH_3I as it is brought up by convectively driven air masses of local origin and short transport timescales. The upper TTL (17-18 km) sees almost no CH_3I due to dominance of 'old' air masses of long-range horizontal transport CH_3I-reduced signature.

5.1.3 Quantifying the CH_3I boundary layer contribution to the TTL

In order to quantify the CH_3I boundary layer contribution to the TTL, the following are accounted for:

- NAME fractions of trajectories below 1 km
- transport timescales of trajectories crossing below 1 km
- the initial concentration value for CH_3I
- the atmospheric lifetime-induced loss of CH_3I.

15,000 particles are released from each NAME defined box of 0.1 x 0.1 x 0.3 deg^2km (representative of AWAS sampling location) along the RF02 path and followed 12 days backwards. Particles which cross below 1 km are selected and turned into fractions (indicative of the boundary layer air mass influence). The initial concentration of CH_3I from the boundary layer is assigned to each particle which crosses below 1 km. The final concentration of CH_3I is reduced by photochemical loss. Therefore, the final concentration of CH_3I in the TTL is calculated assuming an exponential decay and incorporating two fixed variables: the initial concentration of CH_3I from the boundary layer (at time, t = 0) and the atmospheric lifetime of 4 days [*Carpenter et al., 2014*].

The following equation (Equation 5.1) is constructed, encapsulating the above concept. For each model output time step (t=1 to t=48, corresponding to 0.25 and 12 days, respectively), a contribution of CH_3I from the boundary layer is calculated, $[CH_3I]_{BL\_contribution,t}$.

$$\mathbf{(5.1)} \qquad [CH_3I]_{BL\_contribution,\,t} = [CH_3I]_{0\text{-}1km} \times fraction_t \times \exp^{(-t/\tau)}$$

Where: $[CH_3I]_{0\text{-}1km}$ is the CH_3I initial concentration at 0-1 km (a marine boundary layer mean value taken from the cumulative CAST and CONTRAST WAS observations at 0-1 km), t is the time taken for each particle to reach 1 km, and τ, the atmospheric lifetime (Table 5.1).

A fraction in Equation 5.1 corresponds to a number of particles crossing below 1 km at a given model output time step, t, over a total number of particles crossing below 1 km within 12 days (Equation 5.2). This fraction, $fraction_{BL}$, is to distinguish a total number of particles which crossed below 1 km from those which did not over 12 days – fraction background, $fraction_{BG}$ (Equation 5.3). A value of 1 in Equation 5.3 represents a number of particles released: 15,000.

(5.2) $$\mathbf{fraction_{BL} = \sum(fraction_t)}$$

(5.3) $$\mathbf{fraction_{BL} + fraction_{BG} = 1}$$

Equation 5.4 calculates the contribution of methyl iodide from the boundary layer over 12 days of a NAME run. It essentially sums up the contribution from all output time steps. It has to be noted that a $[CH_3I]_{BL\_contribution}$ term includes a $fraction_{BL}$.

(5.4) $$\mathbf{[CH_3I]_{BL\_contribution} = \sum[CH_3I]_{BL\_contribution,\ t}}$$

Table 5.1 CH_3I initial concentration mixing ratios and the atmospheric lifetime used in the NAME boundary layer contribution calculations.

Marine Boundary Layer [CH_3I] / [ppt]		**Atmospheric Lifetime / [days]**
CAST-CONTRAST Mean (Standard Deviation)	***Carpenter et al., 2014*** Median (Range)	
0.696 (0.334)	0.800 (0.3-2.1)	4

A fixed value of 0.696 ppt is assigned to the initial concentration of CH_3I below 1 km, assuming a well-mixed boundary layer. The open ocean and coastal areas are not distinguished due to limited data availability. This value is chosen as it is derived from the CAST and CONTRAST measurements taken in the West Pacific in the same period of January-March 2014 as for the ATTREX measurements in the TTL.

Equation 5.1 calculates a decay of CH_3I after it leaves the boundary layer (0-1 km). Since 15,000 particles are released for each AWAS sample, contributions from each particle have to be summed. For those taking less than 12 days, a decay time of 4 days (i.e. constant chemical loss rate) is assumed. *Bell et al., 2002* shows a mean model lifetime of CH_3I in the 0- to 12-km column to be ~4 days, thus this value stays fixed. Thus a particle getting to the TTL in one day contributes more CH_3I to that air mass than a particle taking 10 days. Once this chemical loss term is taken into account, the NAME trajectories can be used to calculate the contribution of convection of air masses from the boundary layer within the preceding 12 days.

Calculations based on this analysis in this and following chapters (Chapters 6 and 7) use means and standard deviations. Using medians and percentiles, shown on the following figures and in the appendix, are necessary to provide a better, more accurate assessment of this study. In some instances (Appendix 1. Table 1.5.1-3), the mean is very much biased by occasional high values. The skewness of [CH_3I] boundary layer mixing ratio is obvious from the *Carpenter et al., 2014* median being much closer to the lower bound than the upper bound.

5.1.4 Estimation of the CH_3I background

To make these study results truly comparable against the AWAS observations, the background contribution, $[CH_3I]_{BG\_Contribution}$ (meaning the contribution from the fraction of trajectories which do not cross below 1 km) needs to be accounted for. This $[CH_3I]_{BG\_Contribution}$ constitutes of two terms: fraction of particles which do not cross below 1 km and background concentration of CH_3I which is assumed to be assigned to these particles, $[CH_3I]_{Background}$ (Equation 5.5).

$$\mathbf{(5.5)} \qquad \mathbf{[CH_3I]_{BG\_Contribution} = fraction_{BG} \times [CH_3I]_{Background}}$$

The $[CH_3I]_{Background}$ background is estimated in two ways, both using NAME calculations to identify AWAS samples in all the 2014 and 2013 flights with low or none convective influence by filtering for air masses with:

- Boundary layer fraction, $fraction_{BL}$, values less than 1%, 5% or 10%

- Lowest 10% of boundary layer fractions, $fraction_{BL}$.

Then, the CH_3I AWAS observations, corresponding to the boundary layer fraction values less than 1%, 5% or 10%, or the lowest 10% of boundary layer fractions, are averaged to make the CH_3I background mixing ratios (Figure 5.11).

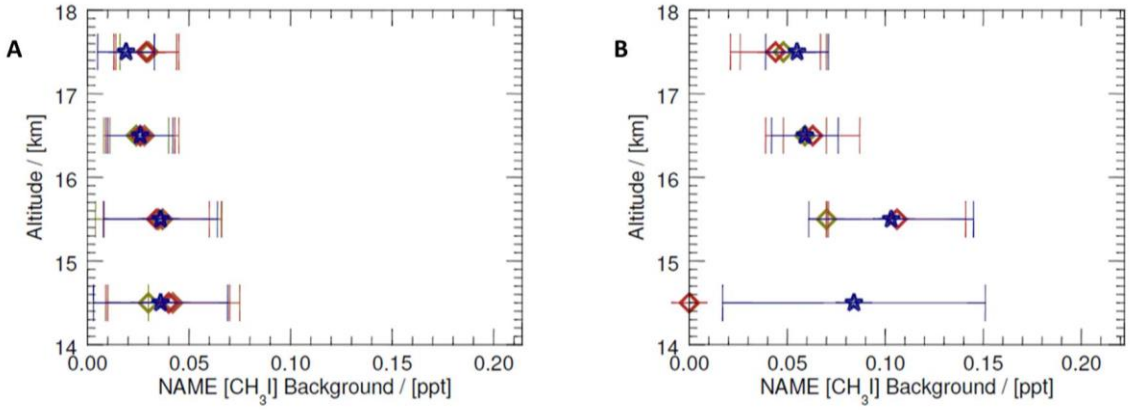

Figure 5.11 NAME calculated CH_3I background based on the NAME boundary layer fractions which are less than 1, 5, and 10% values (green, brown and red diamonds) and the lowest 10% of the boundary layer fractions (blue stars) for ATTREX 2013 (A), and 2014 (B).

ATTREX 2013 shows low CH_3I background mixing ratios most likely due to sampling the air not affected by convective influence. All approaches show similar background mixing ratios (Figure 5.11A). ATTREX 2014 sees higher CH_3I background mixing ratios due to encountering air of the recent rapid vertical uplift signature. No boundary layer fractions less than 1% are found for the 14-17 km bins, and less than 5% for the 14-15 km (Figure 5.11B).

ATTREX 2013 and 2014 need to be treated separately due to the large difference in CH_3I background estimates. The lowest 10% of the boundary layer fractions approach is used to estimate the background contribution for the 2014 flights as not enough data meet the former condition. The background values, inferred from the 1 km fractions for all the ATTREX 2014 flights, are used in the individual flight calculations as again there are not enough data from each individual flight to make background calculations for each individual flight only. ATTREX 2013 uses the boundary layer fractions less than 5% approach for the CH_3I background estimation. As a result, the ATTREX 2014 background estimates are probably

the upper limits. The effect of using longer trajectories (30 days) is discussed in Chapter 7 (Transport and distribution of short-lived brominated organic substances in the TTL).

Given the fact that there is not enough data points per 1-km altitude segment per flight, a background fraction, $fraction_{BG}$, is calculated as a mean value using all the ATTREX 2013 and 2014 flights (separately for each year, Equation 5.6).

(5.6) $$\mathbf{fraction_{BG} = 1 - mean(fraction_{BL})}$$

5.1.5 Comparison of the modelled and observed CH_3I in the TTL

The sums of the NAME boundary layer and background estimates can be compared against the AWAS observations. The complete formula (Equation 5.7) for the NAME modelled CH_3I estimates in the TTL, $[CH_3I]_{NAME\_TTL}$ (i.e. the sum of the boundary layer and background contribution) is given below:

(5.7) $$\mathbf{[CH_3I]_{NAME\_TTL} = [CH_3I]_{BL\_Contribution} + [CH_3I]_{BG\_Contribution}}$$

Figure 5.12 shows the vertical distribution of CH_3I in the TTL from AWAS observations (A), the NAME 1 km fractions of trajectories (B), the NAME calculated CH_3I boundary layer contribution (C), and the sums of the NAME modelled CH_3I boundary layer and background contribution estimates (D).

CH_3I is highest in the lower TTL (14-15 and 15-16 km, Figure 5.12A), followed by a decrease at 16 km, with minimal values noted for the upper TTL 17-18 km segment. A significant contribution (of over 50%) of the boundary layer air mass to the 14-15 km segment is noted, with negligible influence at 16-17 and 17-18 km (Figure 5.12B). The calculated boundary layer contribution for CH_3I from the 1 km fractions shows highest values for 14-15 km, dropping off with altitude. Almost no boundary layer contribution is calculated for 17-18 km (Figure 5.12C). The background contribution component is generally bigger for the upper TTL and the lowest for 14-15 km. The sums of the NAME CH_3I boundary layer and background contribution estimates are in good agreement with the AWAS observations, for all the 1 km TTL segments (Figure 5.12D).

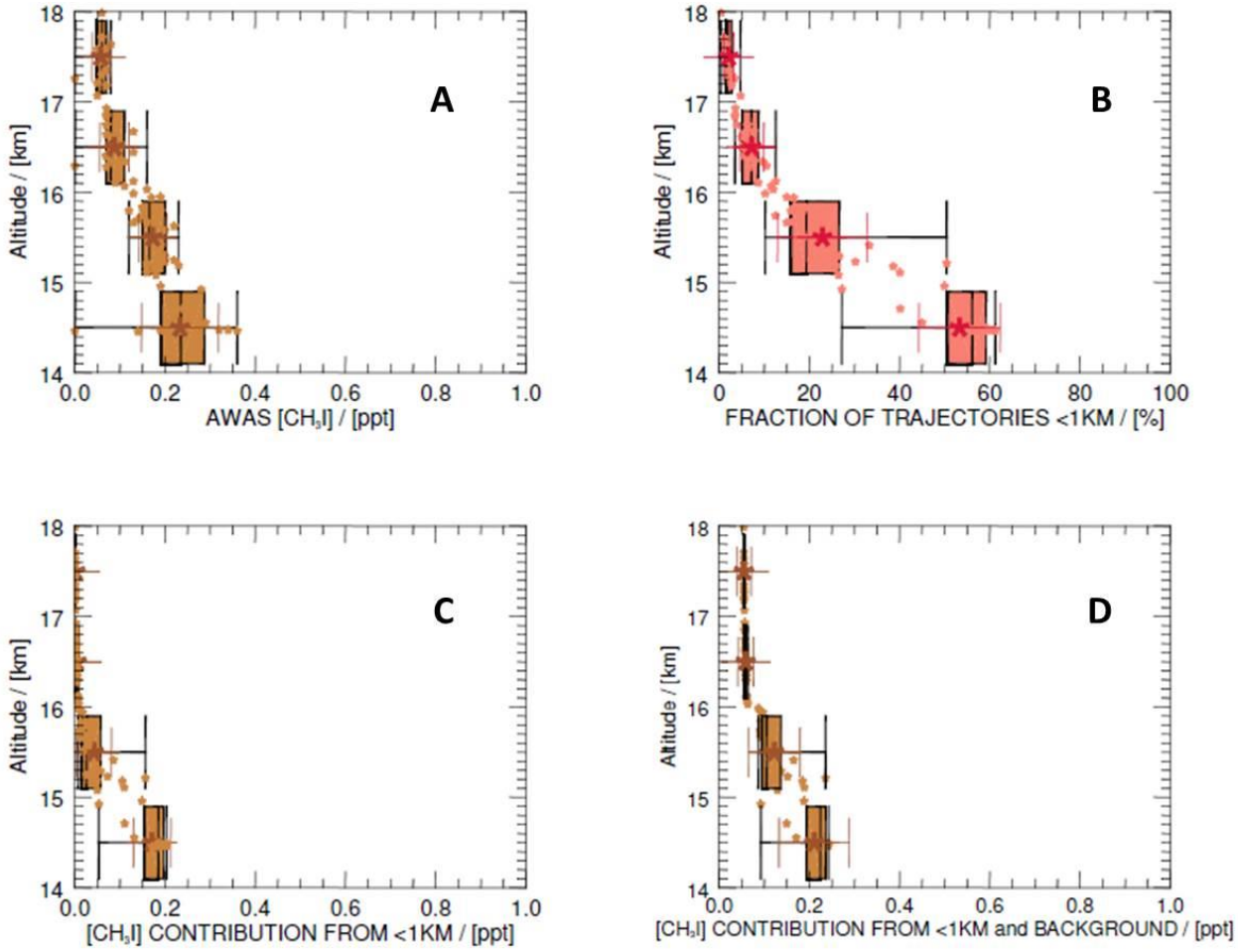

Figure 5.12 Vertical distribution of (A) CH_3I AWAS observations, (B) NAME 1 km fractions of trajectories, (C) NAME modelled CH_3I boundary layer contribution to the TTL, and (D) NAME modelled sum of the boundary layer and background contribution estimates in the TTL, ATTREX 2014 RF02.

At 14-15 km, the modelled contribution of boundary layer CH_3I accounts for most of the AWAS observations (i.e. very close to the AWAS observations). This implies that the higher CH_3I concentrations are brought by higher values of the 1 km fractions. This reflects that whenever the signal of recent rapid convective uplift arises, CH_3I values are expected to be high. There is a good agreement, particularly for the 14-15 km level, which gives evidence that the new convection scheme provides a realistic representation of deep convection.

At higher altitudes, NAME underestimates the CH_3I boundary layer concentration contribution in relation to AWAS observations. Low boundary layer contribution is noted, and the background contribution takes on more significance. This may reflect an issue within the model that the new convection scheme does not work for these altitudes above which the rapid deep convection ceases. More in-depth analysis on the performance of the improved convective scheme in NAME, using the CH_3I AWAS observations from the ATTREX 2014 flights, is provided in Chapter 6. Representation of Deep Convection in NAME.

The background contribution is probably overestimated since the process of identifying samples with no convective influence for the ATTREX 2014 flights proved hard. This is particularly true for the lower TTL altitudes since the ATTREX 2014 flights were close to the region of strong convection.

5.2 Quantifying the CH_3I in the ATTREX 2014 flights

The procedure for quantitative assessment of the CH_3I boundary layer contribution to the TTL is probed for all the ATTREX 2014 flights. Figure 5.13 illustrates the CH_3I AWAS observations, the corresponding NAME 1 km fractions of trajectories, the calculated CH_3I boundary layer contribution, and the modelled sums of CH_3I boundary layer and background contribution estimates in the TTL.

AWAS observations from ATTREX 2014 flights show the highest CH_3I in the lower TTL (14-15 km), dropping off with altitude in a less steep gradient than for individual RF02 (Figure 5.13A). Large flight-to-flight variability in CH_3I measurements is noted (reflected by the high values for the standard deviation and a wider range of measurements). Subsequently, the NAME 1 km fractions are highest at 14-15 km and decrease with altitude in a similar fashion (Figure 5.13B). Again, the CH_3I boundary layer contribution can explain most of the observations for the 14-15 and 15-16 km (Figure 5.13C). Disparities arise from 16 km up. Background estimate values are minimal, oscillating between zero and the limit of detection of the AWAS instrument for the iodinated short-lived organic substances, 0.01 ppt. The sums of the CH_3I boundary layer and background contribution estimates show good agreement with AWAS observations for all the TTL 1 km segments (Figure 5.13D).

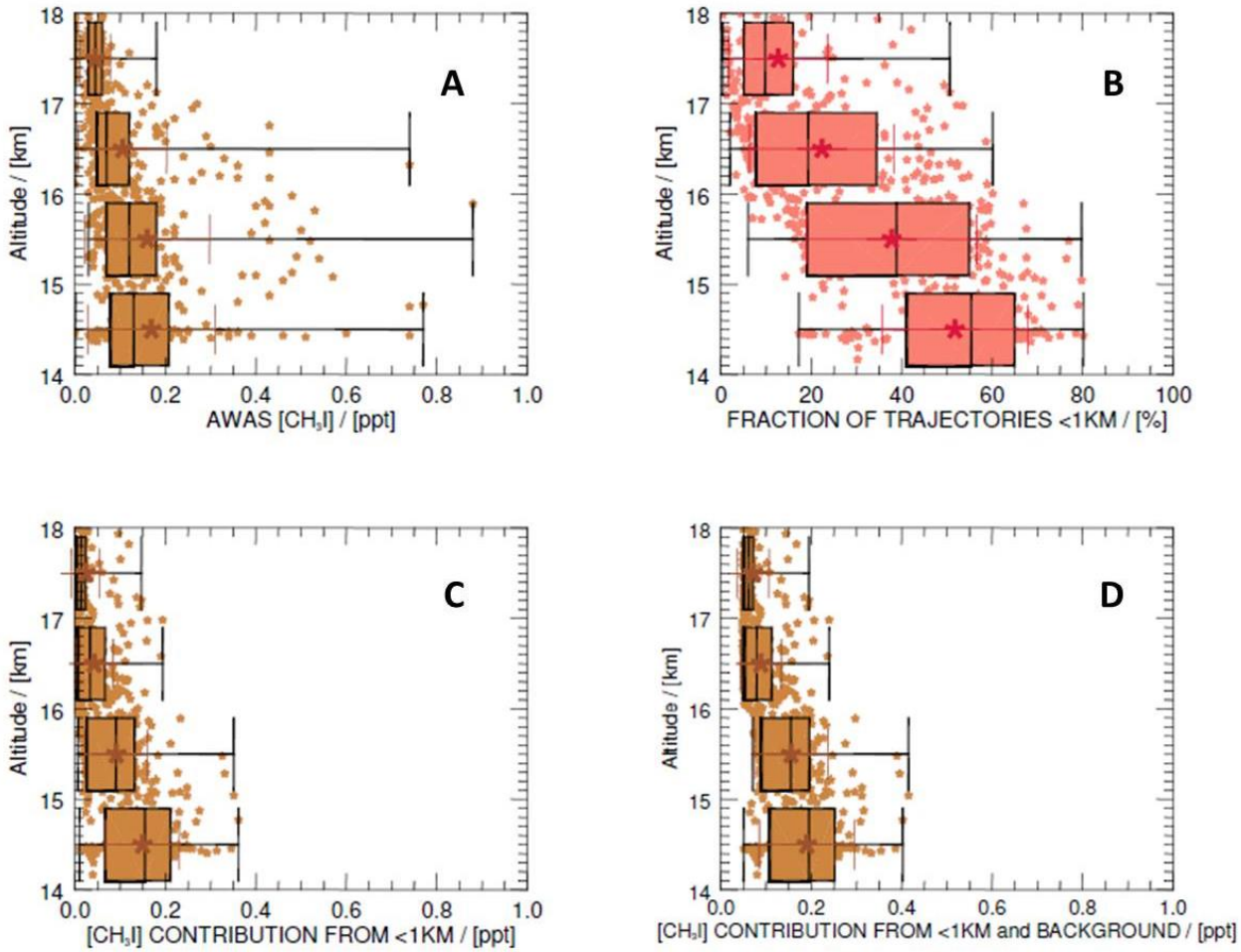

Figure 5.13 Vertical distribution of (A) CH_3I AWAS observations, (B) NAME 1 km fractions of trajectories, (C) NAME modelled CH_3I boundary layer contribution to the TTL, and (D) NAME modelled sums of the boundary layer and background contribution estimates in the TTL, all ATTREX 2014 flights.

Good agreement for the 14-15 and 15-16 km segments may be attributed to the improved representation of deep convection in NAME, provided by the new convection scheme. However, the underestimation of the boundary layer contribution for the upper TTL levels (16-17 and 17-18 km) may result from the new convection scheme not working well at these altitudes (as these are mostly where the convection ceases).

Both AWAS observations and the modelled sums are higher than reported previously in the literature [*Carpenter et al., 2014*] for all the TTL segments. This may be explained by sampling the TTL in a region of high convective activity.

5.3 Quantifying the CH_3I in the ATTREX 2013 flights

The NAME procedure to quantify CH_3I in the TTL, including the estimations of the boundary layer and background contribution to the TTL, is expanded to the ATTREX 2013 flights. Figure 5.14, analogously to Figure 5.13, shows the results for the ATTREX 2013 flights.

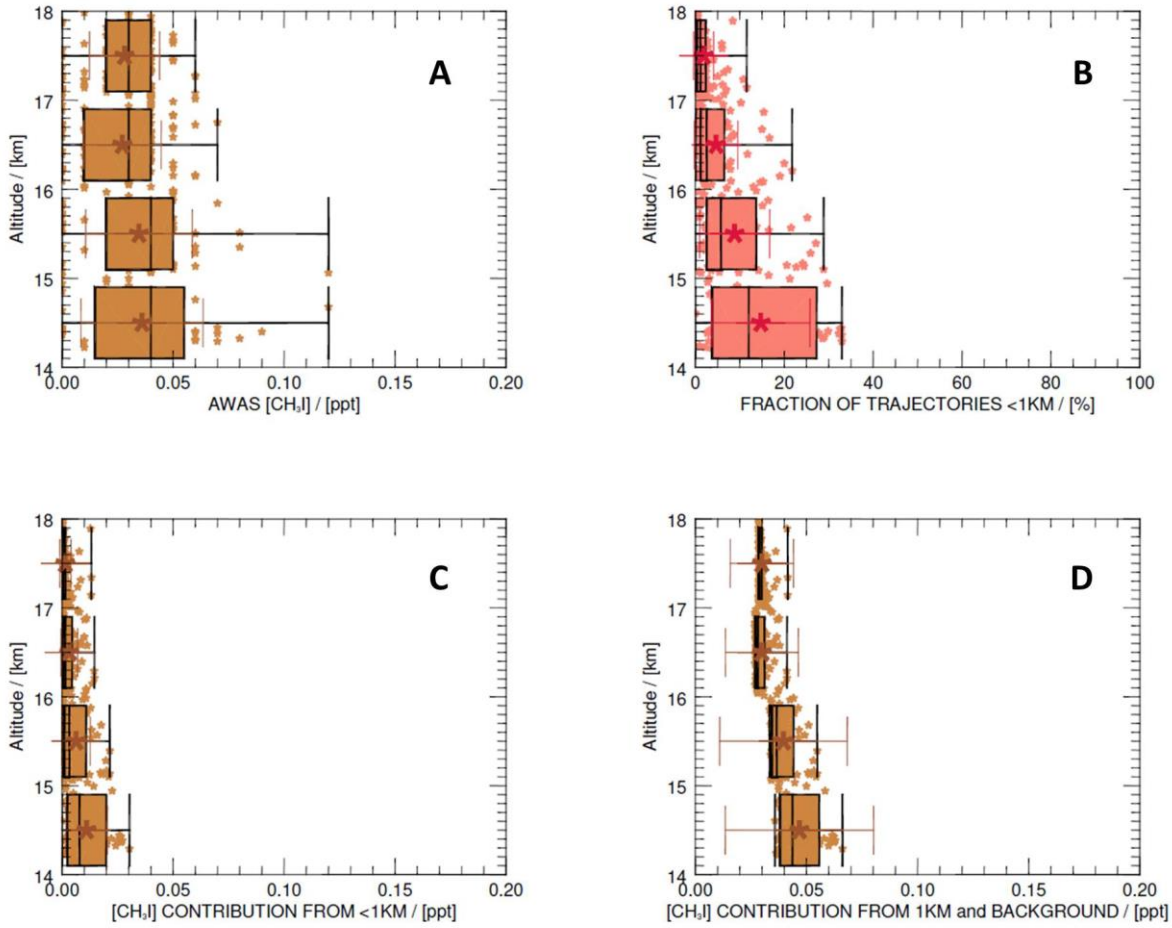

Figure 5.14 Vertical distribution of (A) CH_3I AWAS observations, (B) NAME 1 km fractions of trajectories, (C) NAME modelled CH_3I boundary layer contribution to the TTL, and (D) NAME modelled sums of the boundary layer and background contribution estimates in the TTL, all ATTREX 2013 flights.

ATTREX 2013 shows much lower CH_3I observations than in 2014 (Figure 5.14A). The NAME 1 km fractions are considerably low, and the corresponding boundary layer

contribution show values close to the limit of detection of the AWAS instrument for CH_3I (Figures 5.14B-C). The background contribution comprises over 85-90% of the sums of the modelled CH_3I estimate in the TTL (Figure 5.14D). Good agreement is provided between the sums of the boundary layer and background contribution estimates, against the AWAS observations. Both the observed and modelled values are in the low end of the CH_3I concentrations reported by the WMO2014 Ozone Assessment [*Carpenter et al., 2014*].

5.4 CH_3I in ATTREX 2013 and 2014: Inter-campaign comparison

ATTREX 2013 and 2014 display clear differences in the vertical distribution of CH_3I in the TTL. High CH_3I values, corresponding to high values in the NAME modelled 1 km fractions, are reported in 2014, whereas 2013 sees almost no CH_3I in the TTL, with minimal contribution of the boundary layer air masses. The following assessment of spatial and temporal variability seeks to explain why the vertical distributions of CH_3I and the NAME 1 km fractions in the TTL differ for these two campaigns.

5.4.1 Spatial variability in ATTREX 2013 and 2014

Most trajectories released from the ATTREX 2013 flight paths first crossed below 1 km at the West Pacific Tropical Warm Pool area and the South Pacific Convergence Zone (SPCZ, Figure 5.15). A strong contribution of the low troposphere is also observed from the Maritime Continent (around the Arafura and Timor Seas). The new convection scheme runs reveal the local sources of the boundary layer air masses to the East Pacific TTL (particularly for Research Flights 04 and 06, performed along the western coast of the Central and South America). However remote sources of boundary layer air masses dominate.

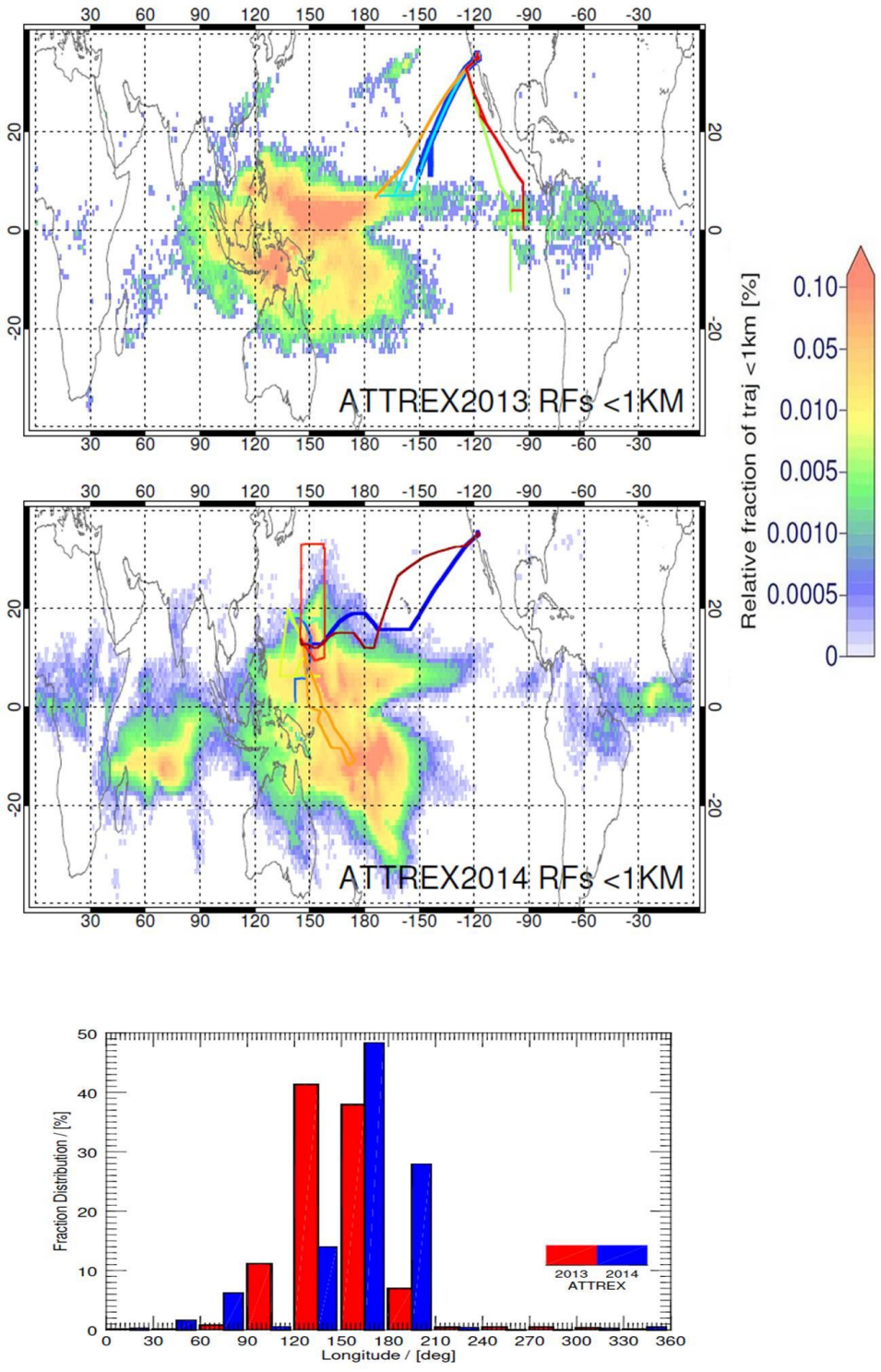

Figure 5.15 Crossing location distribution maps showing locations where trajectories first cross below 1 km, all ATTREX 2013 (top) and 2014 (bottom) Research Flights. The longitudinal distribution of where trajectories cross below 1 km is shown in the bottom panel (grouped in 30^{o} bins of fixed latitude range of 20^{o}N-20^{o}S).

Regarding the ATTREX 2014 flights, the western and central Pacific remains a dominant source origin of the boundary layer air masses to the TTL. Increased tropical cyclone activity in this area (particularly Faxai and Lusi) and the strong signal from the MJO contribute to more frequent episodes of strong and rapid vertical uplifts of the low-level air masses to the TTL. The significant contribution is also seen from the central Indian Ocean, marking the activity of the Fobane tropical cyclone. Minimal contribution from the other remote sources is found (Figure 5.15).

5.4.2 Transport timescales variability in ATTREX 2013 and 2014

Both ATTREX 2013 and 2014 show trajectories crossing below 1 km in similar regions, with the dominance of the West Pacific and SPCZ. The times taken for these trajectories to reach the 1 km (boundary layer) and 5 km (low troposphere) vary significantly (Figure 5.16).

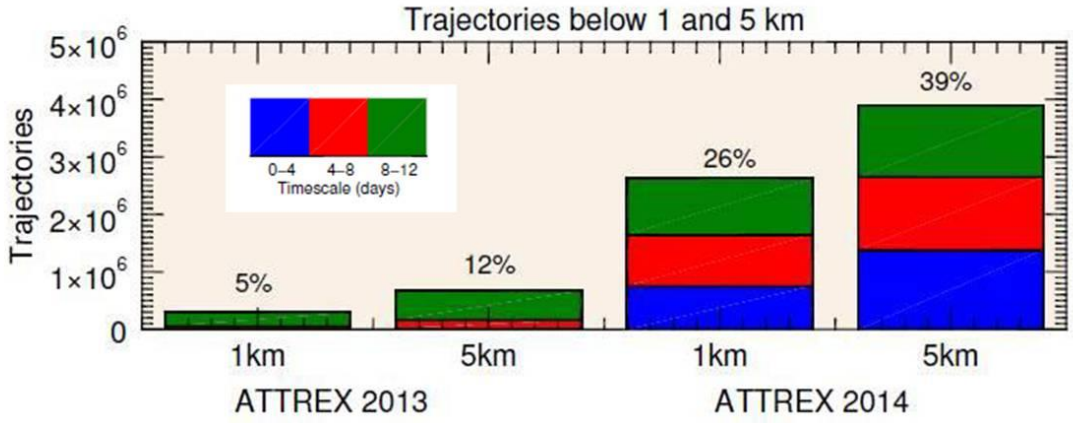

Figure 5.16 Transport timescales distribution for trajectories which cross below 1 and 5 km, ATTREX 2013 (left) and 2014 (right). Fractions of particles [in %] which cross below 1 / 5 km for all NAME runs for ATTREX 2013 and 2014 are given.

The ATTREX 2013 measurements show almost no episodes of recent rapid vertical uplift, with most particles taking 8 days and more to cross the 1 / 5 km. This is indicative of the dominant role of long-range horizontal transport. In ATTREX 2014, unlike 2013, there is a significant increase in trajectories which cross the 1 / 5 km in time less than 4 days. This fraction represents the 'young' air masses being brought from the low troposphere via recent

and rapid vertical uplift. This is a signal of the ATTREX 2014 experiencing more frequent and stronger convective activity in the West Pacific TTL.

5.4.3 Summary

Spatial variability in the boundary layer air mass source origins, as well as the variation in atmospheric transport pathways and transport timescales can explain the differences in the distribution of the NAME 1 km fractions in the TTL. These 1 km fractions are indicative of the boundary layer air mass influence. In 2014 (2013), higher (lower) boundary layer fractions correspond well with higher (lower) CH_3I values in the TTL (Figure 5.17). This is especially true for the flights with the most convective influence which have the highest fractions of particles arriving within the 4 days (Figure 5.18).

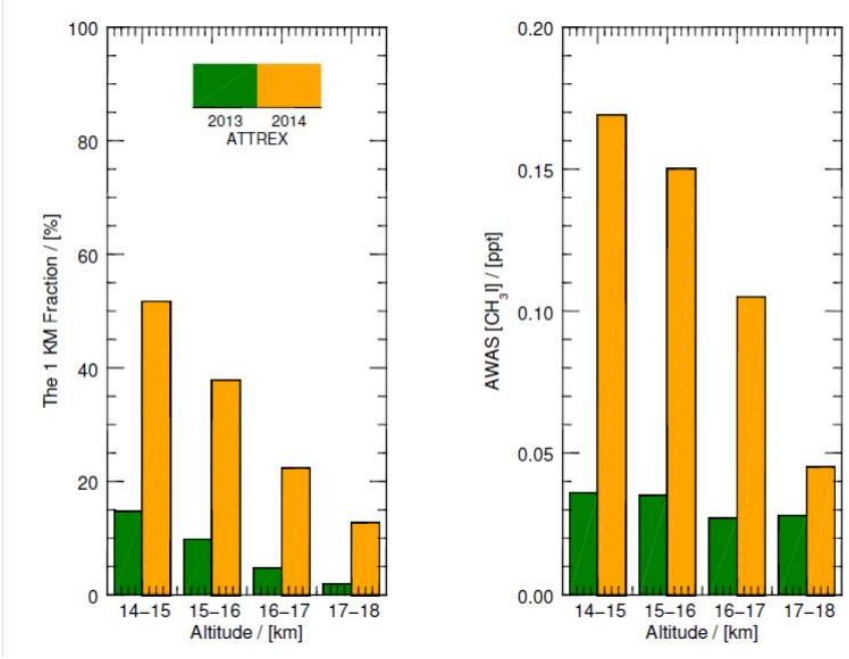

Figure 5.17 Vertical distribution of NAME 1 km fractions, and CH_3I (AWAS measurements) in the TTL, ATTREX 2013 and 2014 flights.

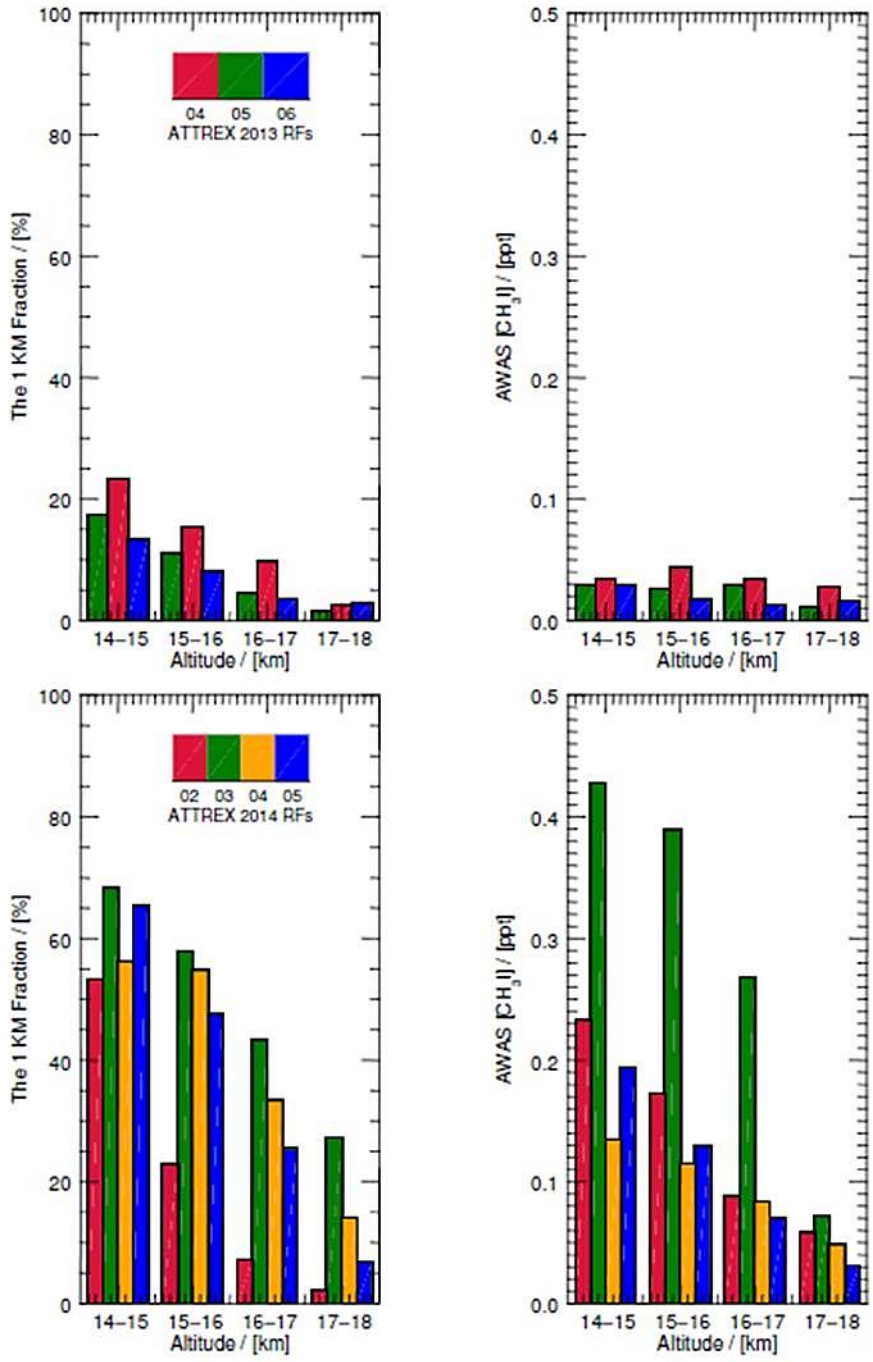

Figure 5.18 Vertical distribution of NAME 1 km fractions and CH_3I (AWAS measurements) in the TTL, ATTREX 2013 (top) and 2014 (bottom) flights with the most convective influence.

5.5 Summary

This chapter presents the NAME procedure to assess quantitatively the vertical distribution of CH_3I in the TTL. NAME modelled results of CH_3I boundary layer and background contribution estimates are compared against the AWAS observations from the two NASA ATTREX campaigns in 2013 and 2014.

NAME can explain the vertical distribution of CH_3I in the TTL. The study of the individual ATTREX 2014 RF02 unveils similar characteristics for the four 1 km TTL segments in the boundary layer air mass influence and the boundary layer source origins. The elevated flow of low-level air masses is observed for the lower TTL (14-15 km), coincident with high CH_3I measured. The West Pacific is the major boundary layer air source for this TTL altitude range. The transition phase occurs between 15 and 16 km, where no clear dominance of localised convective uplift or the horizontal transport of the air masses within the TTL is present. The upper TTL (16-18 km) experiences the dominance of the long-range horizontal transport and almost no influence of the low-level air masses. This reflects on the drop in CH_3I observations in the upper TTL. The remote source origins of the low-level air masses dominate: Indian Ocean, the African continental equatorial band.

NAME can quantify CH_3I in the TTL by estimating the boundary layer and the background contribution. Good agreement is shown between the modelled NAME sums of these estimates and the CH_3I observations for the individual ATTREX 2014 RF02, all the ATTREX 2014 and 2013 flights.

The NAME CH_3I boundary layer contribution estimates can explain the AWAS measurements in the lower TTL (14-15 km) for the ATTREX 2014 flights. High CH_3I is brought up to the TTL via a strong and recent convective activity, and this is reflected by the NAME analysis. The high fractions of trajectories which originate in the boundary layer are transported to 14-15 km within the short transport times (within 4 days). The composition of the 14-15 km segment is thus strongly dominated by the CH_3I-rich fresh air masses recently lofted from the boundary layer.

The implementation of the background contribution estimate improves the agreement against the CH_3I AWAS observations in the upper TTL. The possible explanation might be that the convective cloud tops (one of the input variables required in the new convection scheme) are located below the upper TTL and so there is no effect of the particle displacement via convection in there. The reason for this mismatch is then the particles, once they detrain from the convective cloud tops, may be subject to different transport mechanisms not currently represented in the NAME model.

Differences in the CH_3I AWAS measurements between the East and West Pacific TTL, in the ATTREX 2013 and 2014 flights, respectively, are explained by NAME. ATTREX 2013 flights were in the East Pacific away from the main region of strong convection. Longer transport timescales were seen as horizontal transport is more important in ATTREX 2013, with much less recent convective influence than in ATTREX 2014. Thus, more chemical removal of CH_3I is allowed, leading to lower CH_3I concentrations in the East Pacific TTL.

For this study, a number of uncertainties need to be accounted for, both related to the nature of sampling and modelling approaches. Sampling errors include: instrument calibrations, sampling procedures and limit of detection values (of 0.01 ppt for CH_3I). Modelling errors cover the insufficient parameterization of sub-grid processes and dependence of the meteorological data, with the horizontal resolution not high enough to pick up all the small-scale convective motions. The effect of these uncertainties is difficult to estimate and is typical to any study which compares modelled to measured data [*Meneguz et al., 2016*].

6. Representation of Deep Convection in NAME

In this chapter, the representation of deep convection in the NAME model is investigated. There are three ways in which deep convection can be represented in NAME (see Chapter 2. Methodology). The first two provide crude and unrealistic representation of particle transport via convection, which underestimate the strength of the vertical uplift. The improved convection scheme was developed and implemented in the latest version of NAME (NAME 6v5, *Meneguz et al., 2016*). The performance of this new scheme is validated here using CH_3I AWAS observations from ATTREX 2014 campaign. Section 6.1 provides the reasoning behind selecting CH_3I as a convection tracer for this study. In Section 6.2, the individual ATTREX 2014 flights which saw most convective activity are described. This is followed by comparison of the results from NAME runs with no and improved convection scheme. Differences in the boundary layer air mass influence in the TTL, the CH_3I boundary layer contribution to the TTL, and the modelled sums of CH_3I boundary layer and background contribution estimates in the TTL are assessed. The results are summarised and conclusions on the performance of the improved convection scheme in NAME are drawn.

6.1 Use of CH_3I in testing the performance of NAME new convection scheme

The performance of the new convection parameterisation is tested using CH_3I AWAS observations taken during the ATTREX 2014 campaign. CH_3I is regarded as an oceanic convection tracer as it is relatively short-lived (3-7 days, [*Tegtmeier, et al., 2013*]). Its presence in the TTL implies recent transport from the surface.

CH_3I AWAS observations provide a suitable dataset to be used to quantify whether NAME is reproducing the convectively-induced displacement of particles with reasonable approximation. CH_3I has spatial and temporal patterns which are sensitive to sub-grid scale processes such as tropospheric convection. Its atmospheric lifetime is comparable to the half-life of radon−222 (^{222}Rn) another convection tracer, making its upper troposphere concentrations similarly sensitive to convective mixing [*Donner L. et al., 2007*; *Meneguz, et al., 2016*]. The CH_3I AWAS dataset comes from the West Pacific which is one of the regions of the globe where the spatial and temporal frequency of moist atmospheric convection is high. Combining these with the NCAR CONTRAST and NERC CAST measurements made mainly in the mid- and upper troposphere, and in the low troposphere, respectively, a unique dataset of CH_3I measurements throughout the whole troposphere and the lower stratosphere has been obtained.

6.2 NAME Convection Scheme for CH_3I in ATTREX 2014: Individual Flights

ATTREX 2014 flights took place in the West Pacific in January-March 2014. The most convectively influenced flights are: Research Flights 02, 03, 04 and 05 (see Chapter 4. Assessment of the NASA ATTREX 2013 and 2014 Research Flights using NAME). The influx of the convective outflow originated either from the presence of the localised convective centres (RF02), the active phase of the Madden-Julian Oscillation, MJO, (RF04), or the activity of the West Pacific tropical cyclones (RF03 – Faxai, RF05 – Lusi).

The vertical distribution of CH_3I in the TTL, inferred from the AWAS observations, for ATTREX 2014 RF02, RF03, RF04 and RF05 is illustrated in Figure 6.1A-D. This is followed by the vertical distribution of NAME modelled fraction of trajectories which cross

below 1 km (Figures 6.2-5, Panel A), NAME calculated CH_3I boundary layer contribution to the TTL (Figures 6.2-5.B), and the modelled sums of CH_3I boundary layer and background contribution estimates in the TTL (Figures 6.2-5.C) for ATTREX 2014 RF02, RF03, RF04 and RF05. The data are inferred from 12 day NAME runs with convection scheme switched off (NOCONV) and with the improved convection scheme activated (NEWCONV).

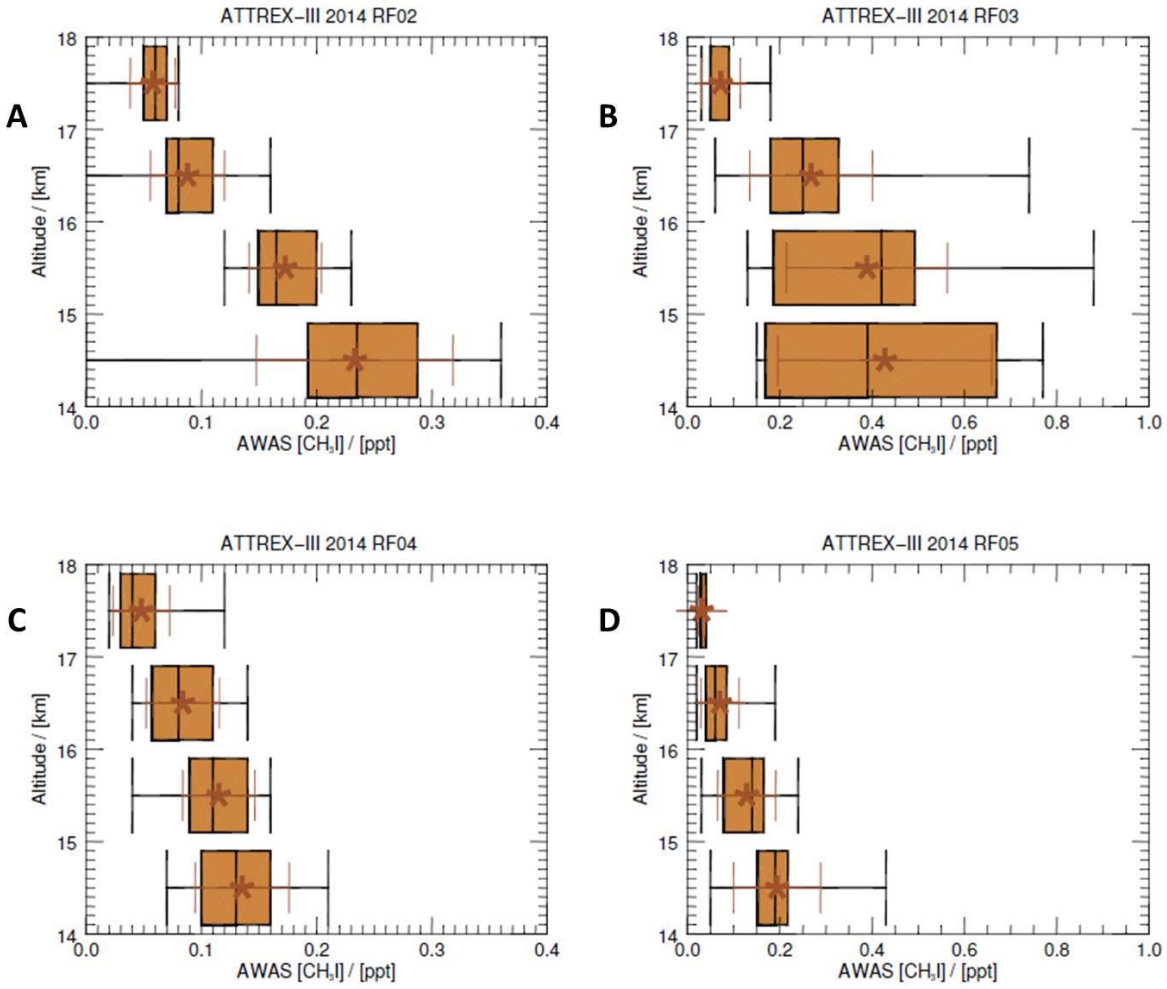

Figure 6.1 Vertical distribution of CH_3I in the TTL, AWAS observations, ATTREX 2014 RF02, RF03, RF04, RF05 (A-D). Means are represented by star symbols and standard deviations by red capped lines.

ATTREX 2014 Research Flight 02, 16-17/02/2014

The Global Hawk surveyed the TTL east of Guam. The sampled air had a signature of the convective systems developed over Guam.

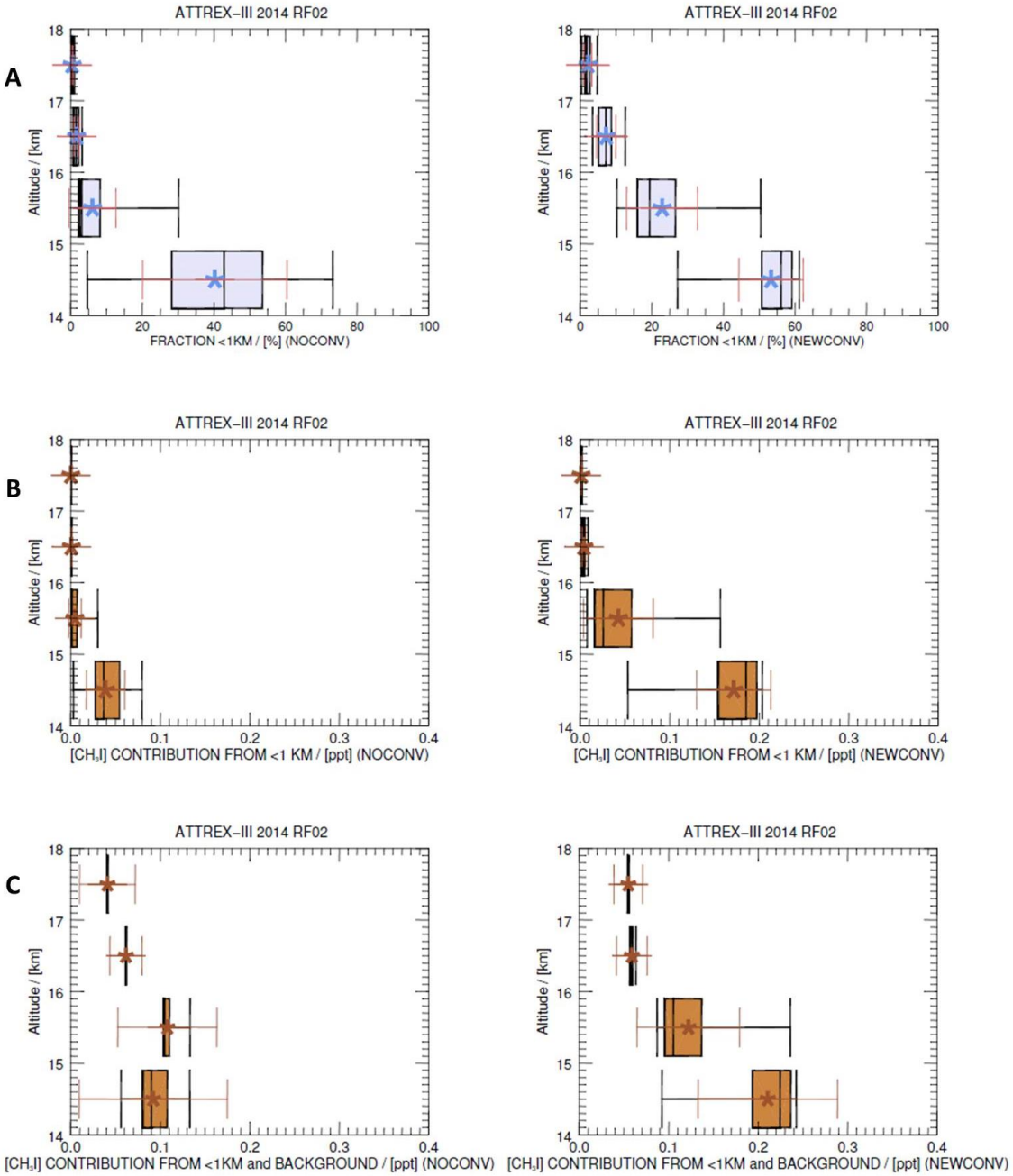

Figure 6.2 ATTREX 2014 RF02: (A) NAME Fractions of trajectories below 1 km, (B) NAME CH_3I boundary layer contribution, (C) NAME Sums of CH_3I boundary layer and background contribution estimates in the TTL. NAME runs with NOCONV (left) and NEWCONV (right). Means marked with stars, standard deviations as red capped lines.

ATTREX 2014 Research Flight 03, 04-05/03/2014

The Global Hawk surveyed the TTL north of Guam, following the path of the tropical cyclone Faxai. The detrained air from the fresh convective outflow was sampled.

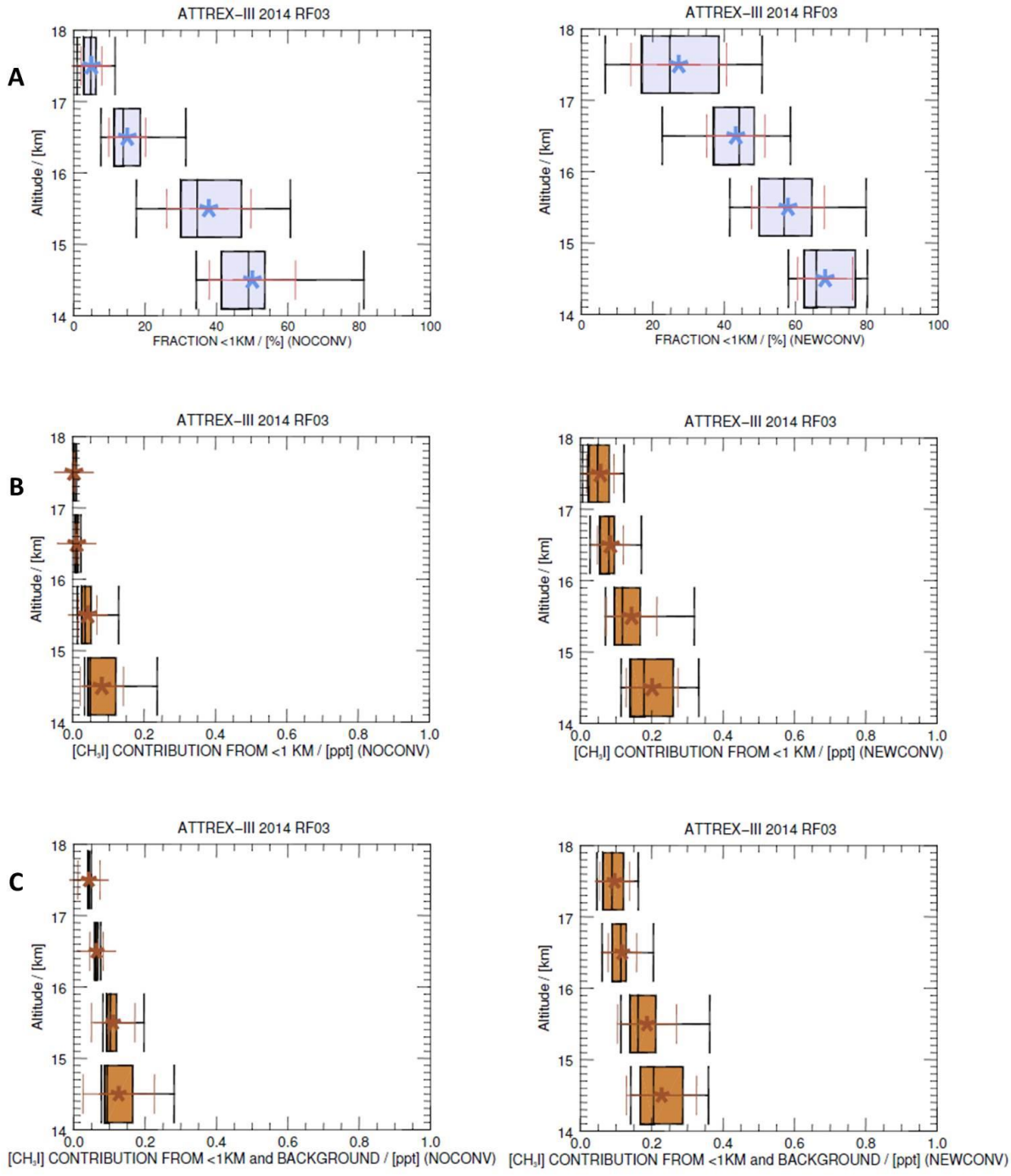

Figure 6.3 ATTREX 2014 RF03. Panels A-C as in Figure 6.2.

ATTREX 2014 Research Flight 04, 06-07/03/2014

The Global Hawk surveyed the West Pacific TTL, experiencing the signal of the MJO active phase. The air with the strong convective influence was sampled.

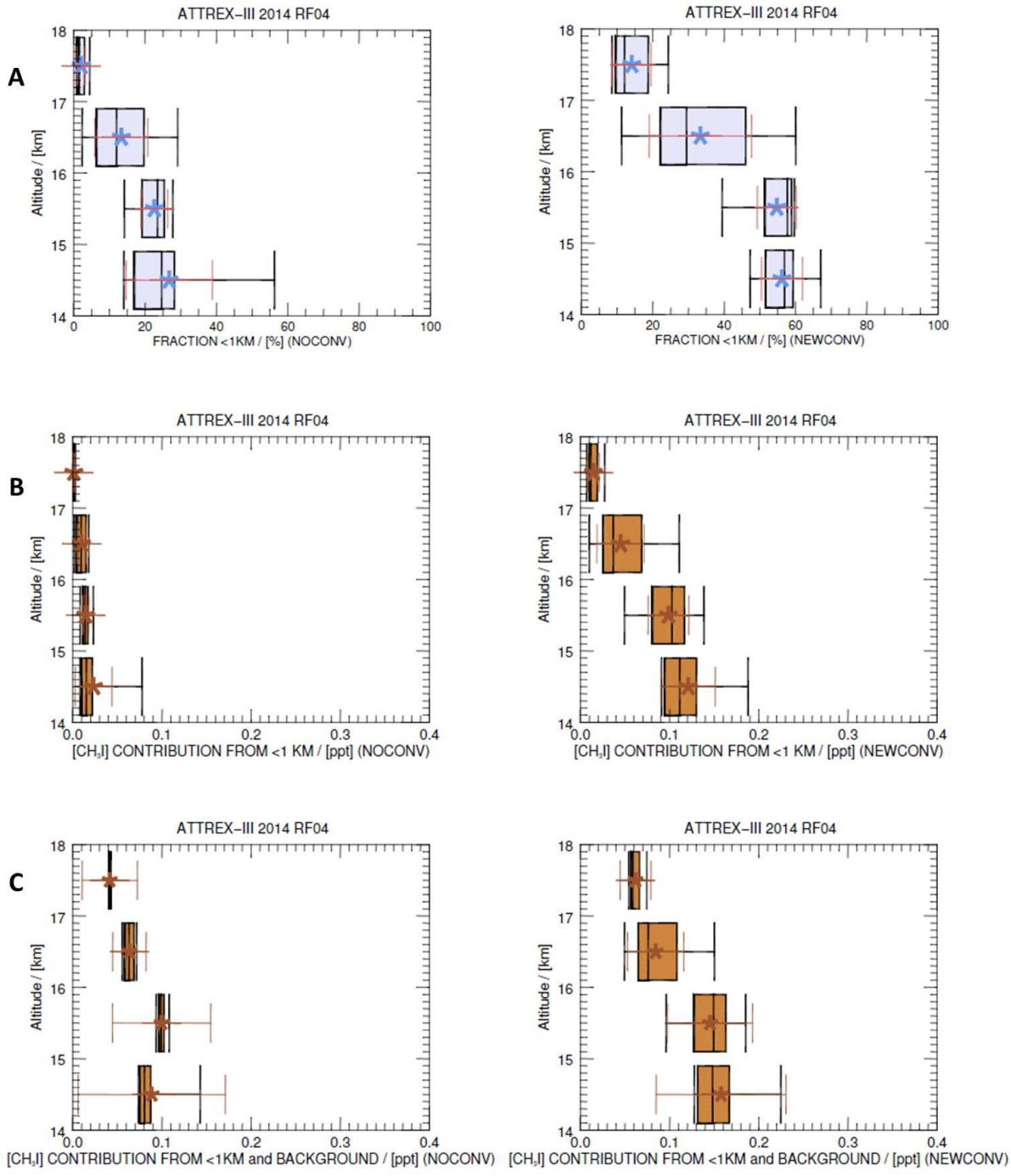

Figure 6.4 ATTREX 2014 RF04. Panels A-C as in Figure 6.2.

ATTREX 2014 Research Flight 05, 09-10/03/2014

The Global Hawk surveyed the South Pacific TTL. The sampled air had a signature of the strong recent convective activity from the tropical cyclone Lusi.

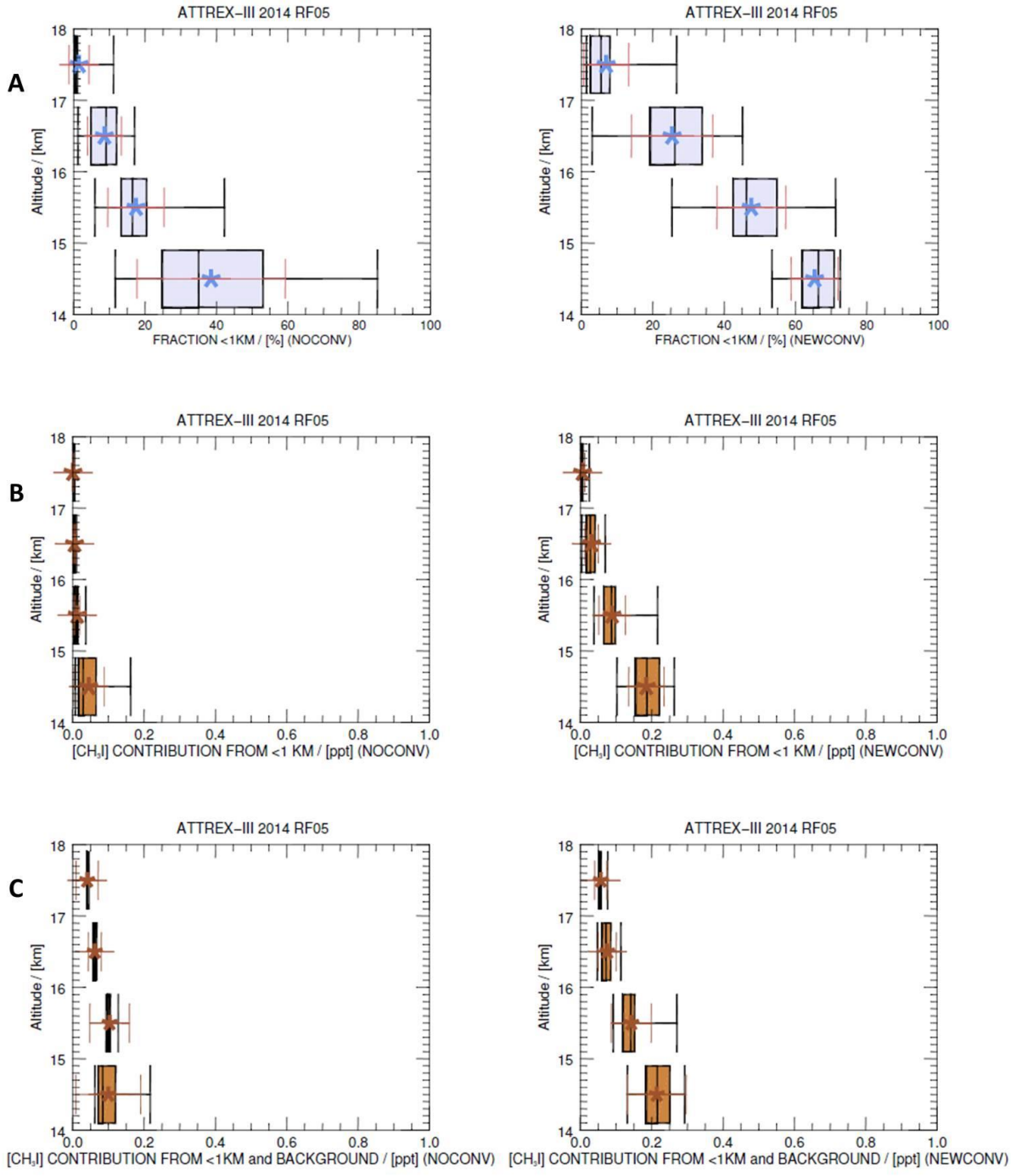

Figure 6.5 ATTREX 2014 RF05. Panels as in Figure 6.2.

High CH_3I is observed at 14-16 km in these flights. This is coincident with high NAME 1 km fractions, indicative of elevated influence of the low-level air masses at these 1 km TTL segments. CH_3I and NAME 1 km fractions decrease with altitude.

Table 6.1 ATTREX 2014 RF02, RF03, RF04 and RF05 averaged NAME fractions of trajectories below 1 km for NOCONV and NEWCONV NAME runs.

TTL altitude bins / [km]	NAME 1 km fractions Means (Standard Deviation) / [%]	
	NOCONV	NEWCONV
17-18	2.6 (1.7)	12.6 (7.9)
16-17	9.6 (5.1)	27.3 (10.1)
15-16	21.0 (8.0)	45.8 (9.1)
14-15	38.9 (16.8)	60.8 (7.4)

The biggest difference in the NAME 1 km fractions, inferred from the NOCONV and NEWCONV runs, occurs at 14-15 and 15-16 km (Table 6.1). This is where the convective uplift mostly reaches. The least difference is observed at 17-18 km where the convective influence is minimal.

The NEWCONV NAME runs yield higher fractions of trajectories reaching the TTL from the boundary layer (Table 6.1). This implies an increased amount of recent uplift resulting from the convective activity. Figure 6.6 illustrates the evolution of transport timescales for the particles reaching the TTL from below 1 km, for the NOCONV and NEWCONV NAME runs. Most particles take less than 3 days to move from boundary layer to 14-15 km for the NEWCONV runs. This is represented by large peaks present at the early stages of these runs, indicative of the displacement of particles via rapid vertical uplift. The NEWCONV RF03 highest peak matches the age of the sampled air of 0.5-2 days old, being convectively driven and detrained from Faxai [*Jensen et al., 2017*]. The NEWCONV RF04 sees highest peaks in number of particles reaching 14-15 km slightly later at 3-5 days. This marks the significant convective influence about 3-5 days old from the strong MJO that dominated the last two

weeks of February [*Jensen et al., 2017*]. These peaks are absent for the NOCONV NAME 14-15 km runs.

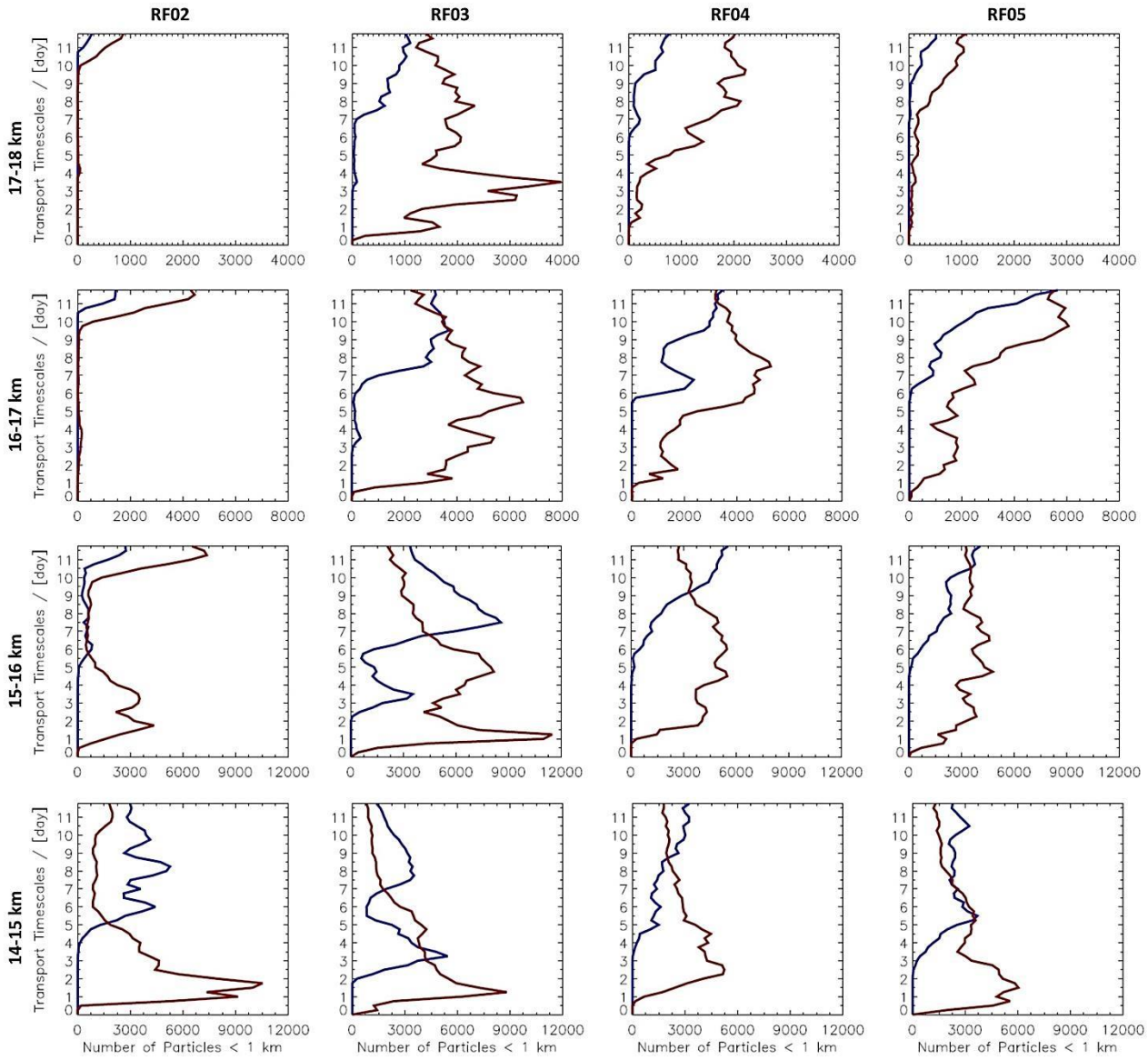

Figure 6.6 Distribution of transport timescales (how long it has taken for particles to cross below 1 km, from being released from the AWAS sample location TTL altitudes (14−18 km) for 4 individual ATTREX 2014 Research Flights RF02, RF03, RF04 and RF05. These show a summed number of particles for each 0.25 day (NAME output time step) for all AWAS samples within 1 km TTL segments. Flights (in columns), 1 km TTL segments 14-15, 15-16, 16-17 and 17-18 km (rows), 12 day NAME runs: NOCONV and NEWCONV (blue and red solid lines, respectively).

A similar evolution in transport timescales and distribution of particles reaching 17-18 km is observed for RF02, RF04 and RF05. Below the upper TTL is usually where the transport of convectively driven air masses stops. However, the NEWCONV RF03 sees a peak indicative of a high fraction of particles reaching 17-18 km via rapid vertical motions. This is coincident with the reported high TTL cirrus cloud tops of 17.3 km and the coldest measured temperatures during the ATTREX 2014 flights, showing the presence and impact of deep, organised convection with the low-level air masses reaching the upper TTL in short transport timescales [*Jensen et al., 2017*].

Larger fractions of boundary layer particles reaching the TTL more recently are reflected in higher CH_3I boundary layer contribution estimates (Table 5.2) for the NEWCONV runs. As CH_3I boundary layer contribution calculations are determined by the fractions of trajectories below 1 km and the component expressing the CH_3I loss due to transport times, the highest addition to CH_3I boundary layer contribution is noted for the lower TTL, 14-16 km (Figure 6.7, Table 6.2).

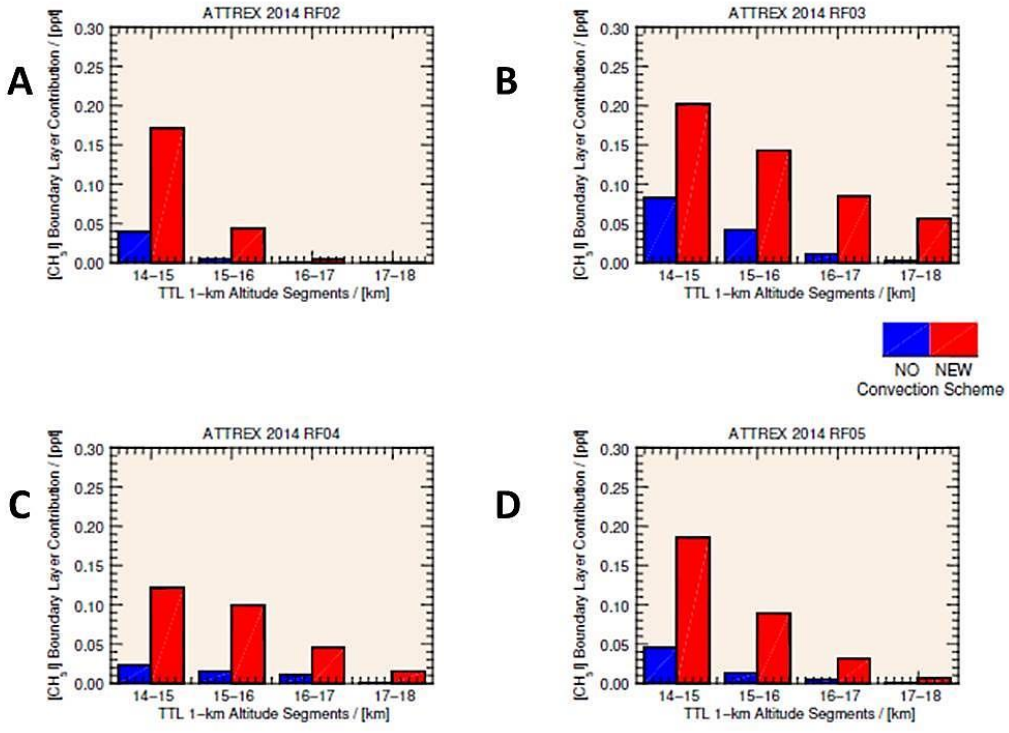

Figure 6.7 Vertical distribution of NAME calculated CH_3I boundary layer contribution in the 1 km TTL segments, ATTREX 2014 RF02, RF03, RF04 and RF05 (A-D), NAME NOCONV (blue) and NEWCONV (red) runs.

Except for RF03, these can explain the CH_3I AWAS observations at 14-15 km. The RFs 02-05 averaged modelled sums of CH_3I boundary layer and background contribution estimates are in satisfactory agreement with CH_3I AWAS observations for all the 1 km TTL segments (Table 6.2). A very good agreement is achieved though for the individual RF02, RF04 and RF05.

Table 6.2 ATTREX 2014 RFs 02-05 averaged CH_3I AWAS observations compared against the NAME estimates for CH_3I boundary layer contribution and sums of CH_3I boundary layer and background contribution estimates; means (standard deviations) medians.

TTL altitude bins / [km]	[CH_3I] AWAS observations / [ppt]	[CH_3I] Boundary Layer Contribution / [ppt]		[CH_3I] Boundary Layer and Background Contribution / [ppt]	
		NOCONV	NEWCONV	NOCONV	NEWCONV
17-18	0.05 (0.03) 0.05	0.00 (0.00) 0.00	0.02 (0.02) 0.01	0.04 (0.03) 0.04	0.06 (0.03) 0.07
16-17	0.13 (0.07) 0.09	0.01 (0.00) 0.01	0.04 (0.03) 0.03	0.06 (0.02) 0.06	0.08 (0.03) 0.09
15-16	0.20 (0.09) 0.16	0.02 (0.02) 0.01	0.09 (0.04) 0.09	0.10 (0.06) 0.10	0.13 (0.06) 0.16
14-15	0.25 (0.13) 0.19	0.05 (0.04) 0.04	0.17 (0.06) 0.17	0.10 (0.09) 0.09	0.20 (0.09) 0.22

In case of the NOCONV runs, the calculated averaged CH_3I boundary layer contribution for RFs 02-05 is lower than in NEWCONV runs (Table 6.2). The modelled sums of CH_3I boundary layer and background contribution estimates are in poor agreement with CH_3I AWAS observations (Table 6.2*)*. The background contribution estimates constitute more in these sums, which makes them unrealistic as CH_3I is very short-lived in the TTL.

6.3. Summary

The NAME runs with the new convection parameterisation provide a better and more realistic representation of the particle transport and displacement via convection. The NEWCONV runs produce higher fractions of trajectories below 1 km, indicative of the larger

influence of the boundary layer air to the TTL. These trajectories reach the TTL at shorter timescales, accounting for the more recent uplift.

These higher fractions of trajectories being transported at shorter transport times lead to the higher NAME calculated CH_3I boundary layer contribution estimates to the TTL. A better statistical match between the averaged NEWCONV NAME modelled sums of CH_3I boundary layer and background contribution estimates, and the CH_3I AWAS observations is achieved for all the 1 km TTL altitude segments for the ATTREX 2014 RFs 02-05.

The NAME runs with the improved convection scheme are consistent in indicating that the composition of air at 14-16 km is strongly dominated by fresh air masses recently lofted from the boundary layer within short timescales. For ATTREX RF02, RF04 and RF05, the higher estimates of CH_3I boundary layer contribution are obtained. These can explain CH_3I AWAS observations at 14-15 km. Addition of the background contribution estimates improves the agreement with the CH_3I AWAS observations at all the 1 km TTL altitudes.

RF03 sees poor agreement between the NAME modelled sums of CH_3I boundary layer and background contribution estimates, and AWAS observations. Exceptionally high CH_3I was recorded, even in the upper TTL, as the fresh masses, detrained from the convective outflow of the tropical cyclone Faxai, were sampled [*Jensen et al. 2017*]. This poses a limitation of NAME not being capable to pick up enough signal subject to direct deep convective uplift at very short timescales.

Even though the agreement between the modelled sums of the CH_3I boundary layer and background contribution estimates is good for most of the investigated ATTREX 2014 flights, the CH_3I boundary layer contribution itself cannot explain the AWAS observations at higher TTL altitudes. The performance of the improved convection scheme decreases with height. Possible explanations are that (i) convective tops in the UK Met Office Unified Model (which are a required input to the convection parameterisation) may not reach high enough, (ii) smaller scale turbulence, perhaps associated with jets, plays a role, and/or (iii) the NAME mass fluxes are not large enough near the cloud tops [*Meneguz et al., 2016*].

7. Transport and Distribution of Short-Lived Brominated Organic Substances in the TTL

This chapter investigates the influence of convective transport on the atmospheric distribution of the short-lived brominated organic substances: bromoform ($CHBr_3$) and dibromomethane (CH_2Br_2) in the tropical tropopause layer (TTL). $CHBr_3$ and CH_2Br_2 are longer-lived than CH_3I (atmospheric lifetime of 15 and 94 days, respectively [*Carpenter et al., 2014*]*)*, and so their presence in the TTL is influenced by atmospheric transport at longer timescales. This transport is again quantified using the NAME dispersion model. This study is analogous with the CH_3I study presented in Chapter 5 (Convective Influence on Methyl Iodide in the TTL) and uses the $CHBr_3$ and CH_2Br_2 AWAS measurements from the NASA ATTREX campaign. Section 7.1 shows how the NAME approach can be used to estimate the contribution of boundary layer bromocarbons to the air sampled by the Global Hawk. It also outlines the importance of the background contribution in the NAME calculations. Section 7.2 shows the analysis for one flight of the Global Hawk before extending to all the 2014 and 2013 flights. Section 7.3 compares the NAME analysis results inferred from the 12 day and 30 day NAME runs. The contribution of the short-lived brominated organic substances to the stratospheric bromine budget is assessed in Section 7.4. These results are summarised and conclusions on the NAME performance in quantifying $CHBr_3$ and CH_2Br_2 in the TTL are drawn.

7.1 Quantifying $CHBr_3$ and CH_2Br_2 in the TTL using NAME

The quantification of the contribution of $CHBr_3$ and CH_2Br_2 from the boundary layer to the TTL is first presented. Subsequently, the procedure for adding the background is put forward. Summing the modelled estimates of the boundary layer and background contributions leads to a total concentration estimate, which can be compared against the AWAS observations. This procedure is analogous to quantifying CH_3I boundary layer contribution to the TTL (See: Chapter 5. Convective Influence on Methyl Iodide in the TTL). Calculation of the background estimate is more important for bromocarbons than CH_3I due to their longer lifetimes.

7.1.1 Quantifying the $CHBr_3$ and CH_2Br_2 boundary layer contribution to the TTL

15,000 particles are released from each AWAS sampling location along the ATTREX flights, and followed 12 days backwards. Particles which cross below 1 km are summed and converted into fractions, indicative of the boundary layer air mass influence. An initial concentration of $CHBr_3$ and CH_2Br_2 is assigned to each particle which crosses below 1 km. The final concentration of $CHBr_3$ and CH_2Br_2 in the TTL is affected by chemical loss. The final concentration can be calculated assuming an exponential decay and incorporating two fixed variables: initial concentrations of $CHBr_3$ and CH_2Br_2 from the boundary layer (at time, *t=0*) and the atmospheric lifetimes of 15 and 94 days, respectively [*Carpenter et al., 2014*].

The following set of equations is constructed, encapsulating the above concept.

(7.1) $$[X]_{BL\_contribution,\ t} = [X]_{0\text{-}1km} \times fraction_t \times \exp^{(-t/\tau)}$$

(7.2) $$[X]_{BL\_contribution} = \sum [X]_{BL\_contribution,\ t}$$

(7.3) $$fraction_{BL} = \sum fraction_t$$

Where: X is $CHBr_3$ / CH_2Br_2, $[X]_{0\text{-}1km}$ - the initial concentrations from the boundary layer (boundary layer mean mixing ratios taken from the cumulative CAST and CONTRAST WAS observations at 0-1 km), t is the time taken for each particle to reach 1 km, and τ, the atmospheric lifetime (Table 7.1).

Table 7.1 Initial concentrations and atmospheric lifetimes for $CHBr_3$ and CH_2Br_2 used in the boundary layer contribution calculations.

Tracer	Boundary Layer (0-1 km) Mixing Ratio / [ppt]		Atmospheric Lifetime / [days]
	CAST, CONTRAST *Mean (Range)*	[*Carpenter et al., 2014*] *Median (Range)*	
$CHBr_3$	0.828 (0.41-2,56)	1.6 (0.5-2.4)	15
CH_2Br_2	0.899 (0.61-1.38)	1.1 (0.7-1.5)	94

A mixing ratio of 0.828 (0.899) is chosen as the $CHBr_3$ (CH_2Br_2) boundary layer initial concentration, given the condition of the uniform mixing within the boundary layer. The CAST and CONTRAST means are used as they represent the boundary layer values measured in the West Pacific at the same time as the ATTREX measurements took place. The WMO2014 Ozone Assessment [*Carpenter et al., 2014*] boundary layer medians are taken from the range of the measurement campaigns which took place within the past decade in different geographical locations, thus are less compatible for this study.

7.1.2 Estimation of the $CHBr_3$ and CH_2Br_2 backgrounds

To make these study results comparable with the AWAS observations, the background contribution, $[X]_{BG\_Contribution}$ (meaning the contribution from the fraction of trajectories which do not cross below 1 km, $fraction_{BG}$) needs to be accounted for (Equations 7.4-5). The background, [X], is estimated in two ways, both using NAME calculations to identify AWAS samples in all the 2014 and 2013 flights with low convective influence by filtering for (i) air masses with boundary layer fraction values less than 1, 5 and 10%, or (ii) the lowest 10% of boundary layer fractions. The means of tracer mixing ratios, corresponding to the fractions which meet the above conditions, are taken as final background estimates.

(7.4) $$fraction_{BL}+fraction_{BG} = 1$$

(7.5) $$[X]_{BG\_Contribution}=fraction_{BG} \times [X]_{Background}$$

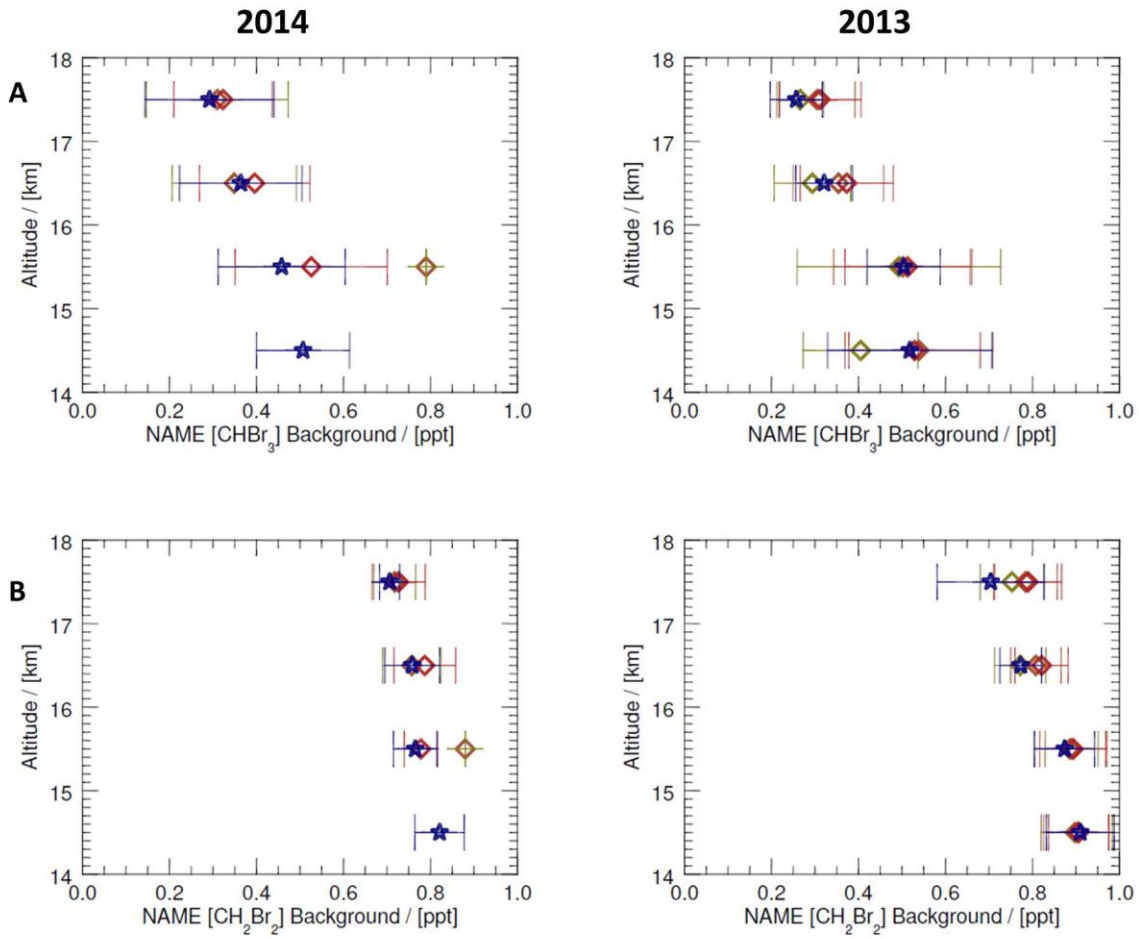

Figure 7.1 Assessment of NAME modelled background $CHBr_3$ (A) and CH_2Br_2 (B) mixing ratios in ATTREX 2014 (left) and 2013 (right). Mean values, inferred from fractions of trajectories from below 1 km of less than 1%, 5% and 10%, are marked as diamonds (green, brown, red, respectively) whereas stars represent the AWAS observations corresponding to the lowest 10% of NAME 1 km fractions.

Two approaches for estimating the $CHBr_3$ and CH_2Br_2 background mixing ratios see similar values between the two ATTREX campaigns (Figure 7.1), unlike in CH_3I case (see Chapter 5.). Higher consistency and less variation is observed for CH_2Br_2 due to its longer atmospheric lifetime.

The approach of the lowest 10% of the NAME 1 km fractions is used to estimate the background contribution for the 2014 flights as not enough data meet the former condition. This makes the background contribution component an overestimate as it is hard to identify samples with no convective influence for the ATTREX 2014 flights. This is especially true

for the lower TTL since ATTREX 2014 flights were close to the region of strong convection. The background values, inferred from the 1 km fractions for all the ATTREX 2014 flights, are applied in the individual flight calculations as again there are not enough data from each individual flight to make background calculations for each individual flight only. The ATTREX 2013 flights use the approach involving the fractions of trajectories from below 1 km of values lower than 5% to estimate the background.

As both $CHBr_3$ and CH_2Br_2 are longer-lived than CH_3I, the boundary layer contribution should constitute a lower fraction of the modelled sums. Thus, the background contribution estimate plays a bigger part, particularly in the upper TTL. The period of 12 days may not be long enough to pick up significant contribution from the boundary layer. Sensitivity tests with 30 day NAME runs are performed and assessed further in Section 7.3.

7.1.3 Estimation of the total estimates of $CHBr_3$ and CH_2Br_2 in the TTL

The sums of the NAME boundary layer and background contribution estimates can be compared against the AWAS observations. The complete formula for the NAME modelled $CHBr_3$ and CH_2Br_2 estimates in the TTL, $[X]_{NAME\_TTL}$ (i.e. the sum of the boundary layer and background contribution) is given below (Equation 7.6):

(7.6) $$[X]_{NAME\_TTL} = [X]_{BL\_Contribution} + [X]_{BG\_Contribution}$$

The above approach is applied firstly for the individual flight, ATTREX 2014 Research Flight 02 (see Chapter 5 for the ATTREX 2014 RF02 overview), before expanding the analysis to cover all the ATTREX 2014 and 2013 flights.

7.2 Modelled $CHBr_3$ and CH_2Br_2 in the TTL

This section applies the procedure in quantifying $CHBr_3$ and CH_2Br_2 in the TTL, presented in Section 7.1, to the individual ATTREX 2014 flight, Research Flight 02. Then, this approach is expanded to all the ATTREX 2014 and 2013 flights.

7.2.1 ATTREX 2014 Research Flight 02

Figures 7.2-3, Panel A, show the vertical distribution of $CHBr_3$ and CH_2Br_2 in the TTL, inferred from the AWAS observations for the ATTREX 2014 RF02. This is followed by the distribution of NAME fractions of trajectories below 1 km in the TTL, the corresponding NAME calculated $CHBr_3$ and CH_2Br_2 boundary layer contribution and the modelled sums of boundary layer and background contribution estimates for $CHBr_3$ and CH_2Br_2 in the TTL (Figures 7.2-3.B.C.D, respectively).

$CHBr_3$ and CH_2Br_2 are highest in concentration in the lower TTL (14-15 and 15-16 km), with a gradual drop-off from 16 km up. A significant contribution (indicative of NAME 1 km fractions over 50%) of the boundary layer air masses to 14-15 km is noted, with negligible influence for 16-17 and 17-18 km. The calculated boundary layer contribution for $CHBr_3$ and CH_2Br_2 from the 1 km fractions is biggest for 14-15 km, dropping off with altitude. Almost no contribution is calculated for 17-18 km. The background contribution estimate is higher for the upper TTL, and the lowest for 14-15 km. The sums of the NAME boundary layer and background contribution estimates are in good agreement with $CHBr_3$ and CH_2Br_2 AWAS observations, for all the 1 km TTL segments.

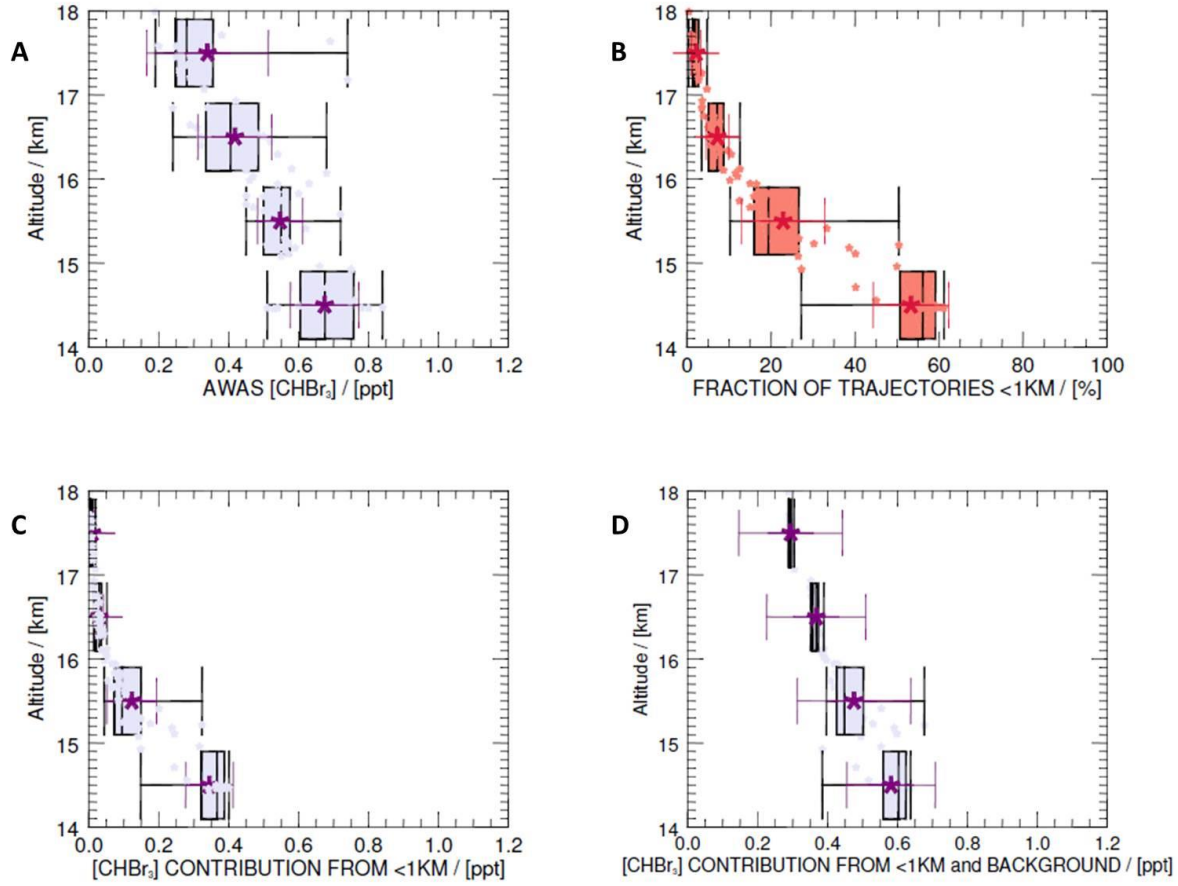

Figure 7.2 $CHBr_3$ AWAS observations and NAME estimates in the TTL, ATTREX 2014 RF02: (A) $CHBr_3$ AWAS observations, (B) NAME 1 km fractions of trajectories, (C) NAME modelled $CHBr_3$ boundary layer contribution to the TTL, (D) NAME modelled sums of the boundary layer and background contribution estimates in the TTL. Box and whiskers show range, lower and upper quartiles; star symbols mark the means, and the capped lines mark the standard deviations.

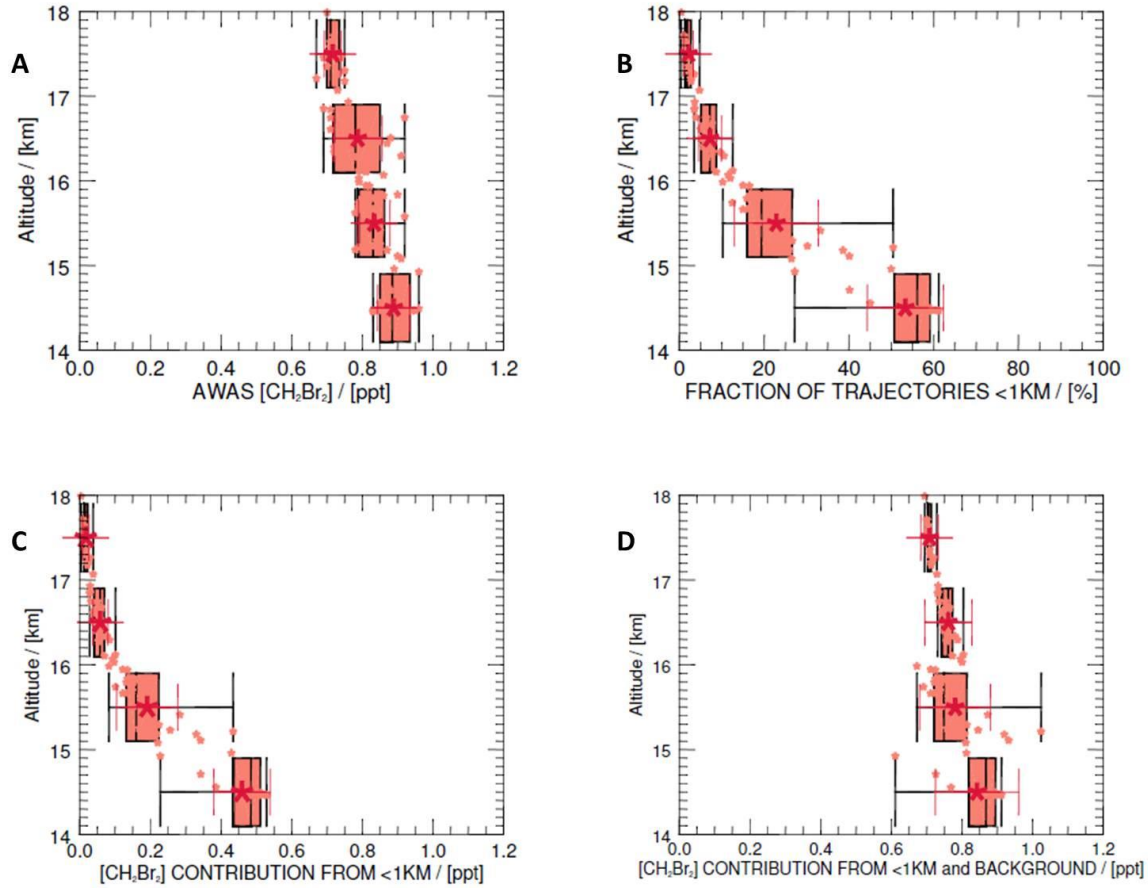

Figure 7.3 CH_2Br_2 AWAS observations and NAME estimates in the TTL, ATTREX 2014 RF02. Panels as in Figure 7.2.

CH_2Br_2 drops off with a lower gradient than $CHBr_3$. The magnitude of a vertical drop-off is lower for CH_2Br_2 as it is longer-lived (atmospheric lifetime of 94 days, compared to 15 days for $CHBr_3$) and reacts slower with OH radicals in the TTL [*Hossaini, et al. 2010*]. At 14-15 km, the boundary layer contribution accounts for ~50% of the modelled sums of $CHBr_3$ and CH_2Br_2 in the TTL. The percentage drops to less than 5% for $CHBr_3$ and CH_2Br_2 at 17-18 km. This implies that the higher NAME 1 km fractions result in greater loading of the investigated tracers from the boundary layer. For the upper TTL, the background contribution estimate constitutes over 85% of the modelled sums, thus taking more significance.

7.2.2 ATTREX 2014 Research Flights

AWAS observations are highest in the lower TTL (14-15 km), dropping off with altitude (Figures 7.4-5.A). The large flight-to-flight variability is observed (indicated by high values for standard deviation, Figures 7.4-5 - red capped lines). The NAME 1 km fractions, highest at 14-15 km (maximum of 80%), decrease with altitude in similar fashion (Figures 7.4-5B). The boundary layer contribution constitutes varied percentages of the NAME modelled sums: from approximately 50% at 14-15 km (unlike for CH_3I where at 14-15 km over 85% of the modelled sum is attributed to the boundary layer contribution) to < 20% at 17-18 km (Figures 7.4-5C). The sums of the boundary layer and background contribution estimates show good agreement with AWAS observations (Figures 7.4-5D). The NAME modelled sums are within the range of the WMO Ozone Assessment 2014 [*Carpenter et al., 2014*].

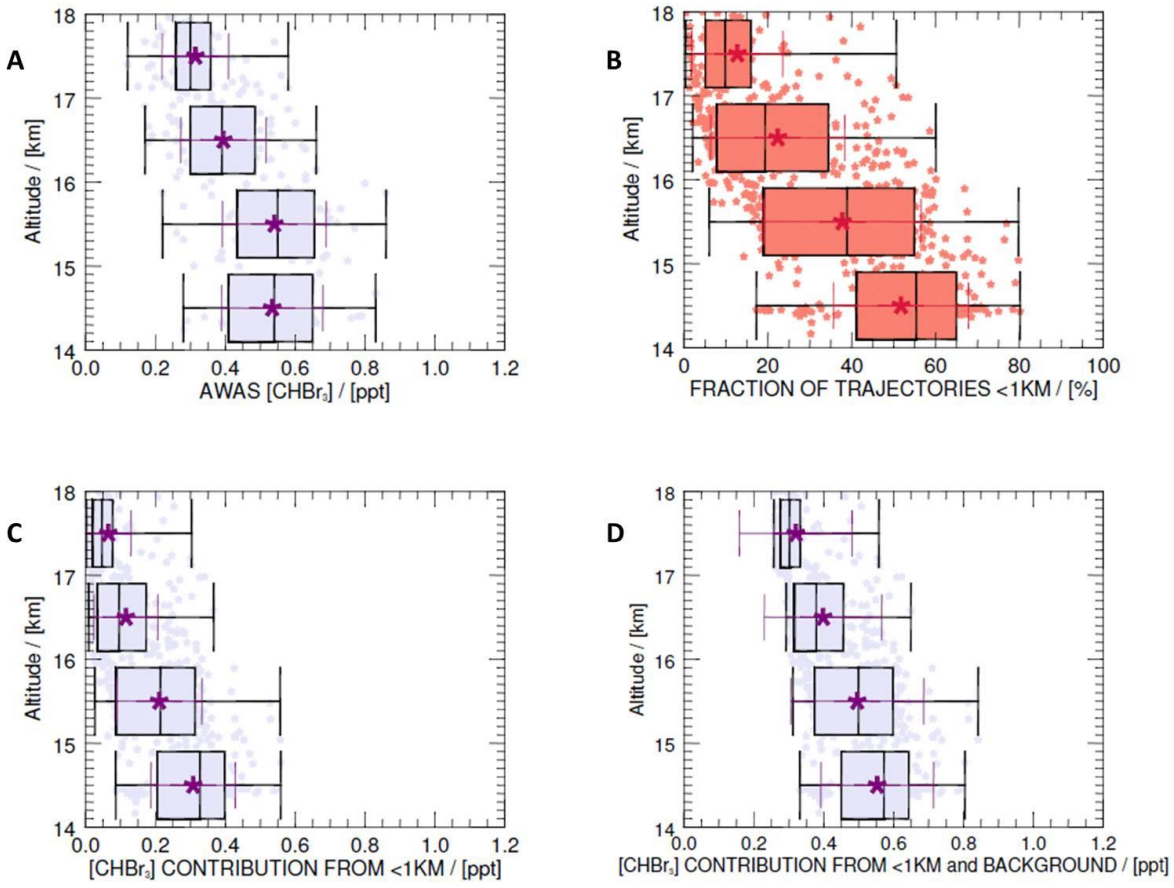

Figure 7.4 $CHBr_3$ AWAS observations and NAME estimates in the TTL, ATTREX 2014 Research Flights. Panels as in Figure 7.2.

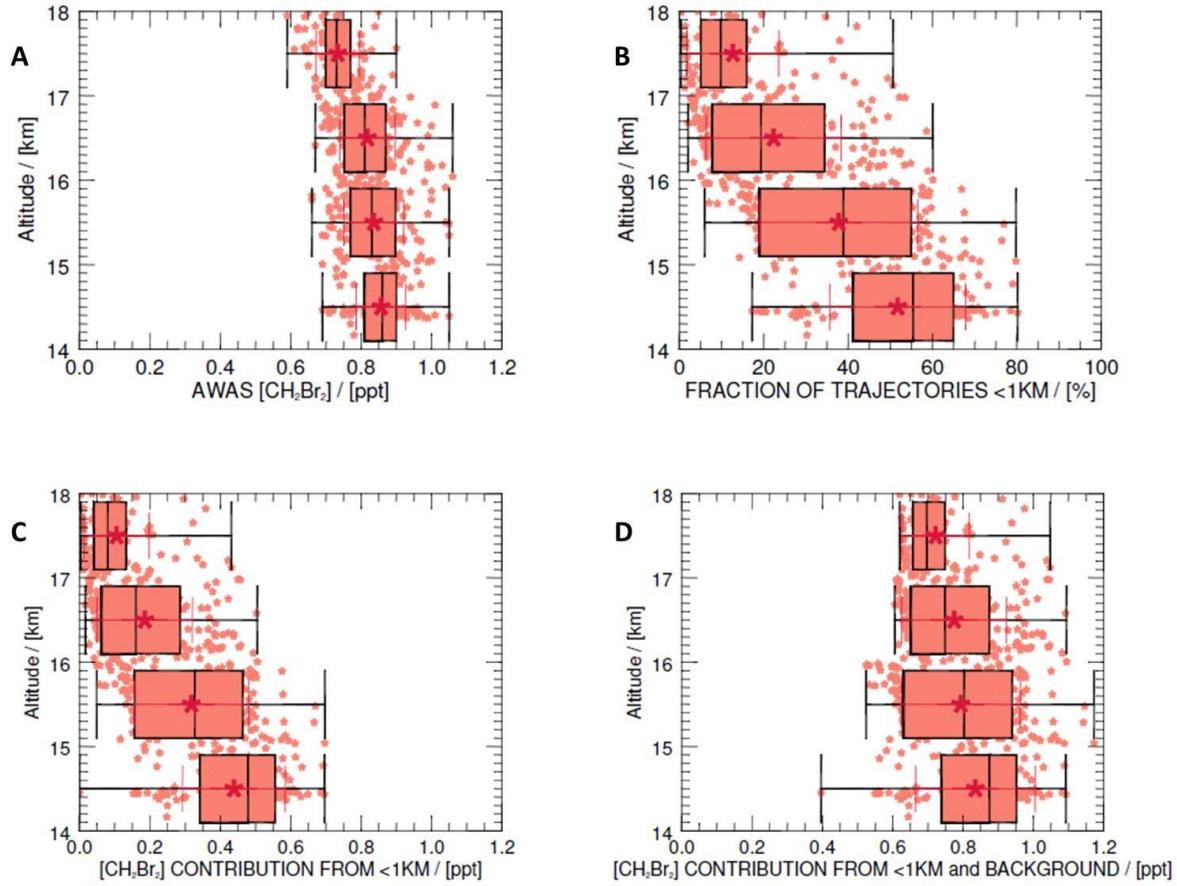

Figure 7.5 CH_2Br_2 AWAS observations and NAME estimates in the TTL, ATTREX 2014 Research Flights. Panels as in Figure 7.2.

7.2.3 ATTREX 2013 Research Flights

ATTREX 2013 shows lower $CHBr_3$ and higher CH_2Br_2 than in 2014 (Figures 7.6-7.A). The NAME modelled 1 km fractions are lower fourfold, and the corresponding NAME calculated $CHBr_3$ and CH_2Br_2 boundary layer contribution is negligible (Figures 7.6-7.B-C). The boundary layer contribution constitutes approximately 10% of the NAME modelled sums for 14-15 km, and less for the upper TTL segments. The background contribution estimates comprise over 85% of the modelled sums. Good agreement is found between the sums of the boundary layer and background contribution estimates and the $CHBr_3$ and CH_2Br_2 AWAS observations.

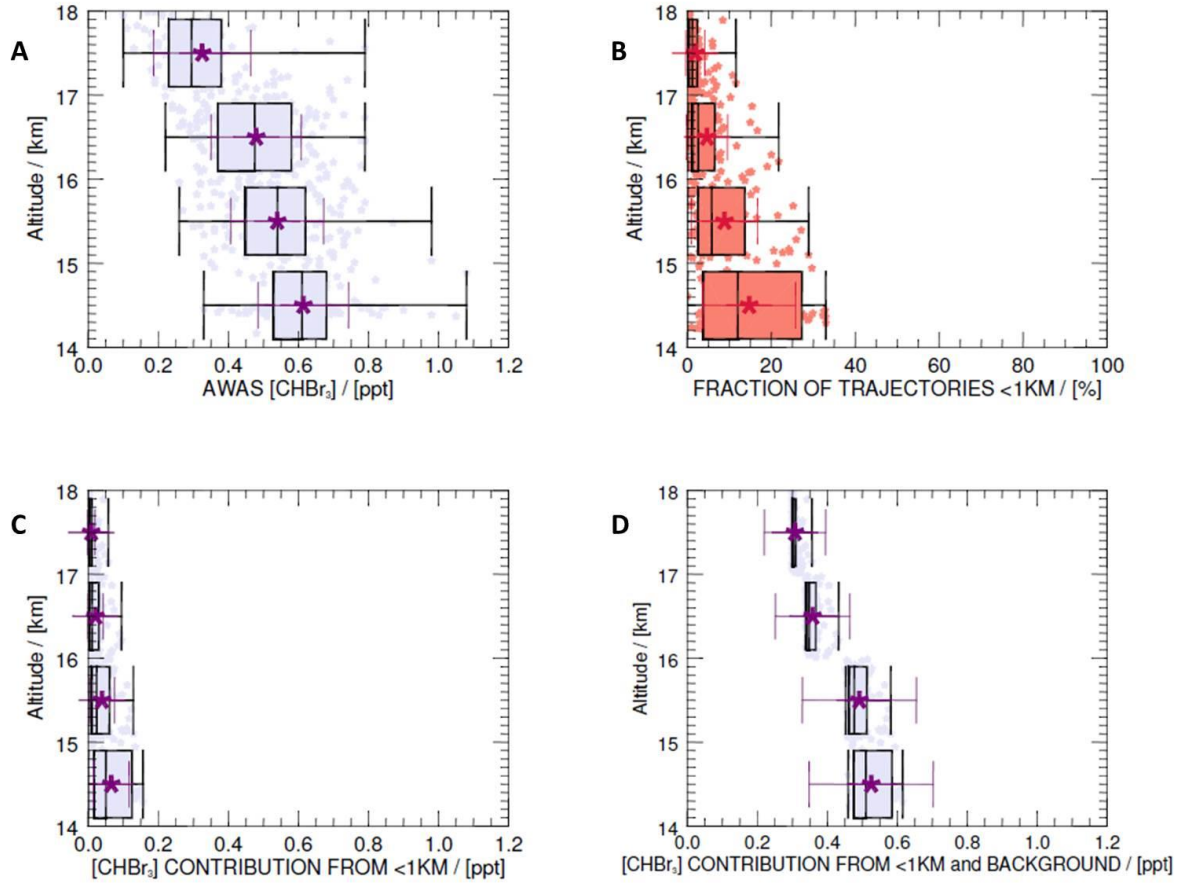

Figure 7.6 $CHBr_3$ AWAS observations and NAME estimates in the TTL, ATTREX 2013 Research Flights. Panels as in Figure 7.2.

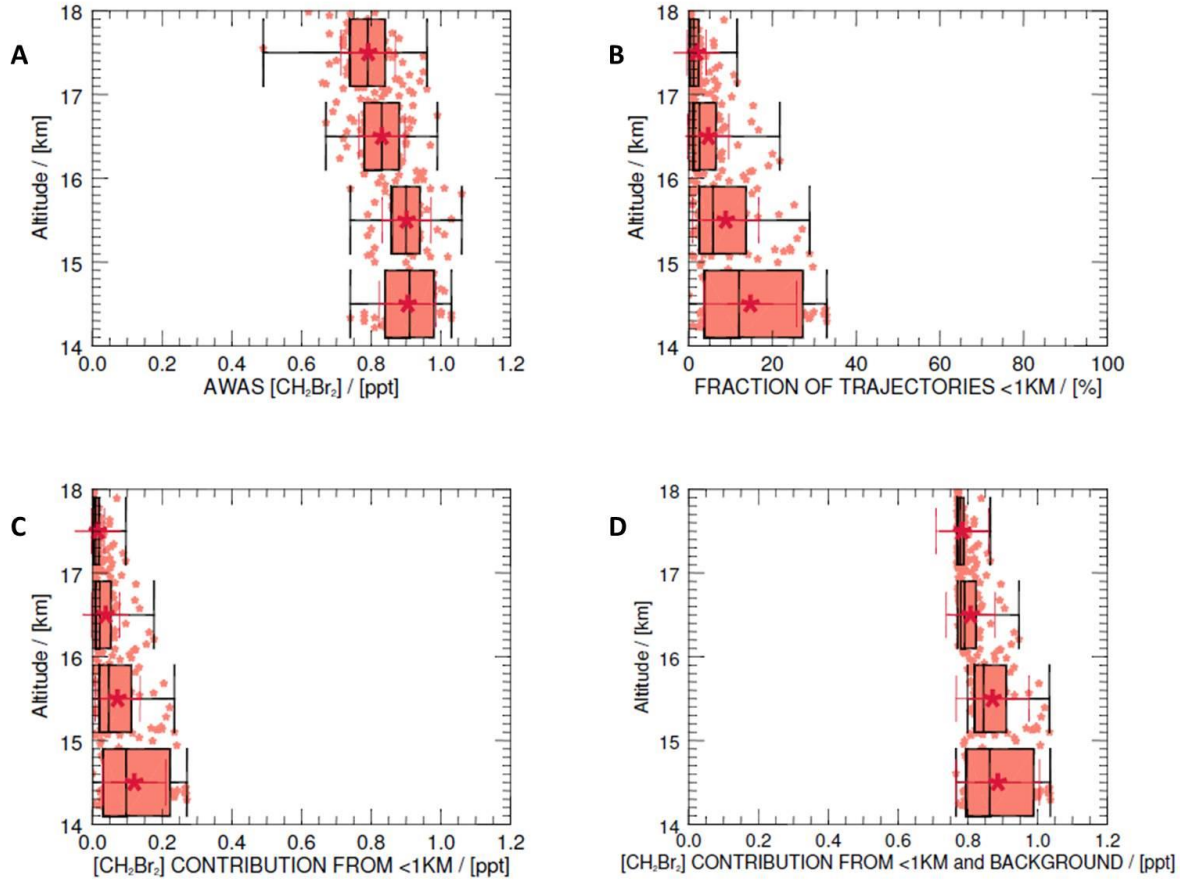

Figure 7.7 CH_2Br_2 AWAS observations and NAME estimates in the TTL, ATTREX 2013 Research Flights. Panels as in Figure 7.2.

ATTREX 2013 was in the East Pacific away from the main region of strong convection. Longer transport timescales are seen as horizontal transport was more important in ATTREX 2013, with much less recent convective influence than in ATTREX 2014. More chemical removal of $CHBr_3$ has thus taken place, leading to lower concentrations in the East Pacific TTL.

These results are based on 12 day NAME runs. As atmospheric lifetimes for $CHBr_3$ and CH_2Br_2 are higher than 12 days, a contribution from the boundary layer for a period over 12 days is omitted. To investigate whether this leads to large errors, NAME simulations are extended to 30 days (double the time for atmospheric lifetime of $CHBr_3$).

7.3 Modelled $CHBr_3$ and CH_2Br_2 in the TTL: Sensitivity tests with 30 day NAME runs

As CH_3I is very short-lived (atmospheric lifetime of 4 days), most of its contribution to the TTL occurs via the recent rapid convective uplift, i.e. within the early stage of the 12 day period of the NAME run. The period of 12 days works well for CH_3I calculations (See: Chapter 5.), but it is shorter than the atmospheric lifetimes for the short-lived brominated organic substances. Thus, there is a risk of omitting the significant contribution from the period over 12 days. Here the 30 day simulations are tested to see if the 12 day runs lack this contribution in calculating $CHBr_3$ and CH_2Br_2 boundary layer loading. Extending the NAME runs to 30 days is also to show that CH_3I is not influenced by a longer NAME run duration.

7.3.1 ATTREX 2014 Research Flight 02, 30 day NAME runs

For the ATTREX 2014 RF02 (see Appendix A4.7.4), 30 day NAME runs produce much higher 1 km fractions, with biggest differences at 15-16 and 16-17 km. For CH_3I, extending the runs to 30 days, and thus having these higher 1 km fractions, does not influence the CH_3I boundary layer contribution (negligible differences in calculated concentrations). Unlike for CH_3I, the boundary layer contribution for $CHBr_3$ and CH_2Br_2 is correspondingly higher: fourfold and fivefold ($CHBr_3$), and fivefold and sevenfold (CH_2Br_2) at 16-17 km and 17-18 km, respectively. At 14-15 km, the boundary layer contribution accounts for the 60% and 75% of $CHBr_3$ and CH_2Br_2 AWAS observations, as opposed to 50% from the 12 day NAME runs. The weight of the background estimate component is lower, and overall a good agreement is found between the modelled sums and the AWAS observations.

7.3.2 ATTREX 2014 Research Flights, 30 day NAME runs

Figure 7.8 shows the vertical distribution of the fractions of trajectories from below 1 km in the TTL for the ATTREX 2014 Research Flights, inferred from the 12 and 30 day NAME runs (Panel A and B, respectively). A comparison of NAME calculated boundary layer contribution values and the modelled sums of boundary layer and background contribution estimates for $CHBr_3$ (Figure 7.9.A-B) and CH_2Br_2 (Figure 7.10.A-B) is provided then. Table 7.2 summarises the above for $CHBr_3$ and CH_2Br_2.

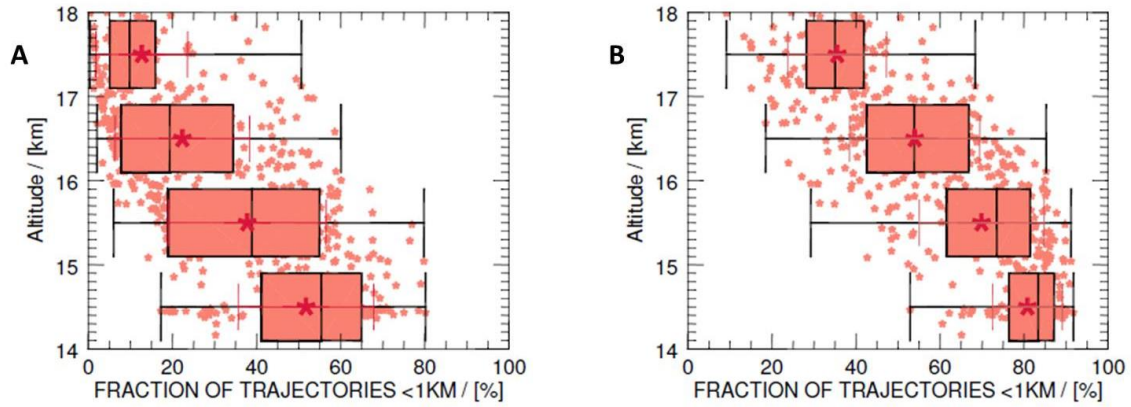

Figure 7.8 Vertical distribution of NAME calculated fractions of trajectories below 1 km, ATTREX 2014 Research Flights, 12 (A) and 30 (B) day NAME runs.

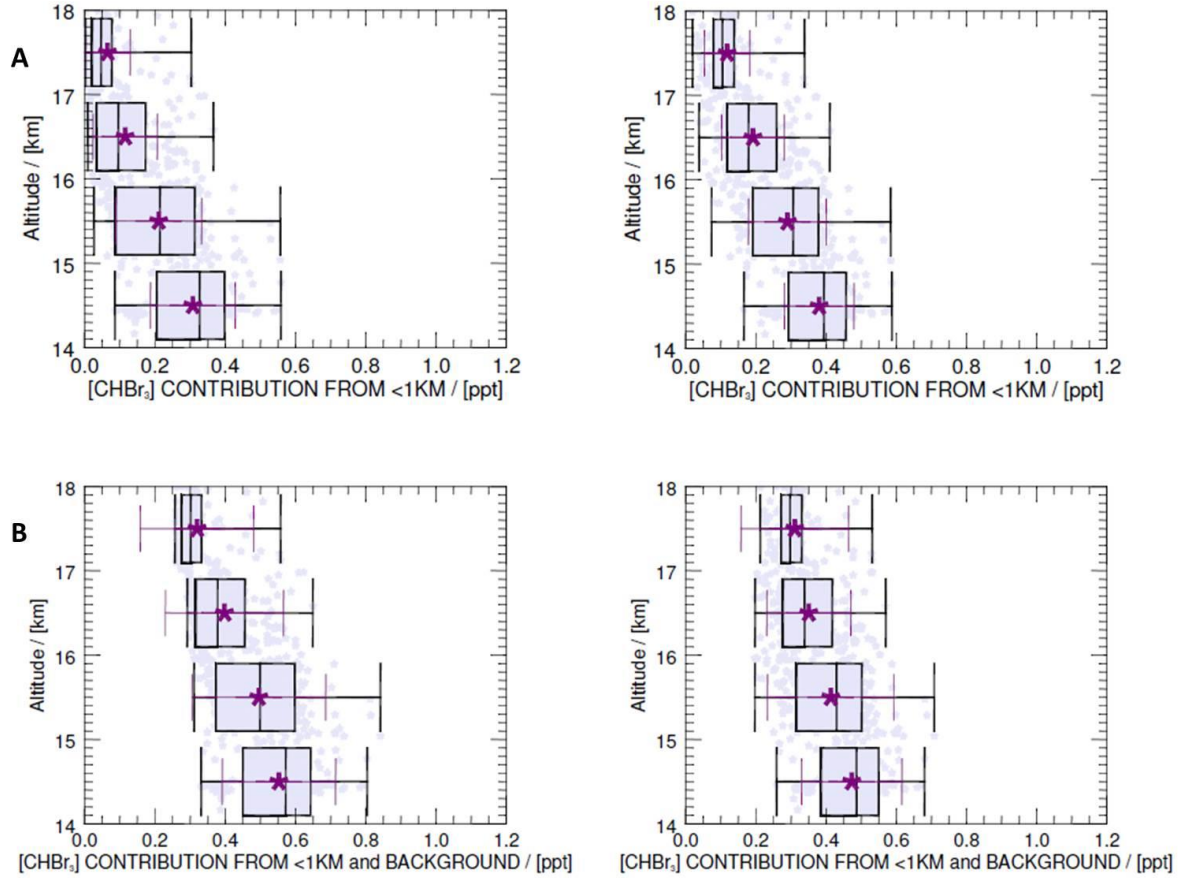

Figure 7.9 $CHBr_3$ NAME estimates in the TTL, ATTREX 2014 Research Flights, 12 (left) and 30 (right) day NAME runs: (A) Boundary layer contribution to the TTL, (B) NAME modelled sums of boundary layer and background contribution estimates.

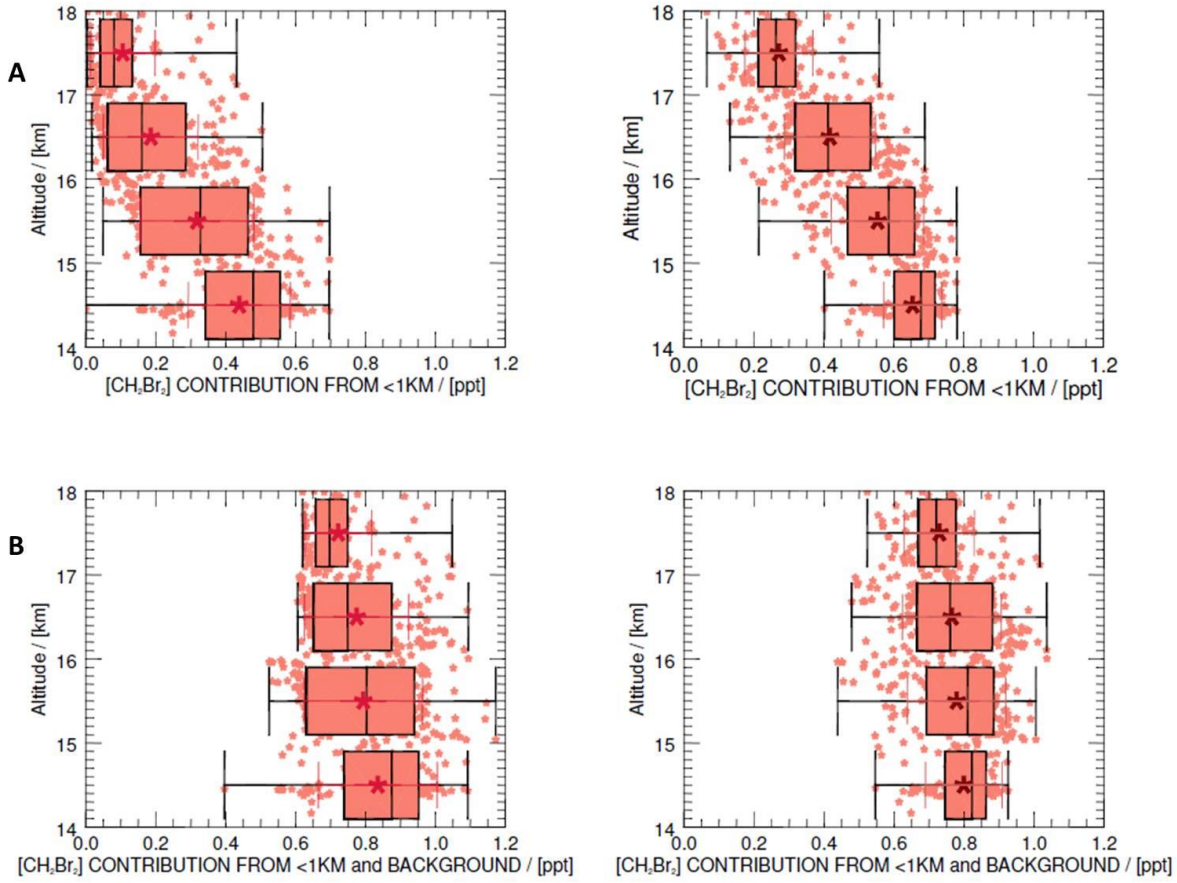

Figure 7.10 CH_2Br_2 NAME estimates in the TTL, ATTREX 2014 Research Flights, 12 (left) and 30 (right) day NAME runs; Panels as in Figure 7.9.

30 day NAME runs produce higher fractions of trajectories below 1 km, which yield higher boundary layer contributions (Table 7.2). The biggest attribution in the NAME 1 km fractions and the corresponding $CHBr_3$ and CH_2Br_2 boundary layer contribution is noted at 15-16 km and 16-17 km. The background estimate constitutes less in the modelled sums of the boundary layer and background contribution estimates in the lower TTL. It still dominates in the upper TTL. The modelled sums, inferred from 30 day NAME runs, are lower and in satisfactory agreement with the AWAS observations.

Table 7.2 NAME modelled $CHBr_3$ and CH_2Br_2 boundary layer contribution and the modelled sums of boundary layer and background contribution estimates for ATTREX 2014 Research Flights, inferred from 12 and 30 day NAME runs.

[$CHBr_3$]	*Boundary Layer Contribution [ppt]*		*Boundary Layer and Background Contribution [ppt]*	
	12 DAY	*30 DAY*	*12 DAY*	*30 DAY*
17-18 km	0.06 (0.06) 0.05	0.12 (0.06) 0.10	0.32 (0.16) 0.30	0.31 (0.15) 0.30
16-17 km	0.12 (0.09) 0.10	0.19 (0.09) 0.18	0.40 (0.17) 0.38	0.35 (0.12) 0.34
15-16 km	0.21 (0.12) 0.21	0.29 (0.11) 0.31	0.50 (0.19) 0.50	0.41 (0.18) 0.43
14-15 km	0.31 (0.12) 0.33	0.38 (0.10) 0.39	0.55 (0.16) 0.57	0.48 (0.14) 0.49

[CH_2Br_2]	*Boundary Layer Contribution [ppt]*		*Boundary Layer and Background Contribution [ppt]*	
	12 DAY	*30 DAY*	*12 DAY*	*30 DAY*
17-18 km	0.11 (0.09) 0.08	0.27 (0.10) 0.26	0.73 (0.09) 0.70	0.73 (0.10) 0.72
16-17 km	0.19 (0.14) 0.16	0.42 (0.13) 0.41	0.78 (0.15) 0.75	0.77 (0.14) 0.81
15-16 km	0.32 (0.16) 0.33	0.55 (0.13) 0.59	0.80 (0.17) 0.81	0.78 (0.14) 0.81
14-15 km	0.44 (0.15) 0.48	0.65 (0.08) 0.68	0.84 (0.17) 0.87	0.80 (0.11) 0.82

7.3.3 ATTREX 2013 Research Flights, 30 day NAME runs

Figure 7.11 shows the vertical distribution of the fractions of trajectories from below 1 km in the TTL for the ATTREX 2013 Research Flights, inferred from the 12 and 30 day NAME runs (Panel A and B, respectively). This is followed by a comparison of NAME calculated boundary layer contribution values and the modelled sums of boundary layer and background contribution estimates for $CHBr_3$ (Figure 7.12A-B) and CH_2Br_2 (Figure 7.13A-B). Table 7.3 summarises the above for $CHBr_3$ and CH_2Br_2.

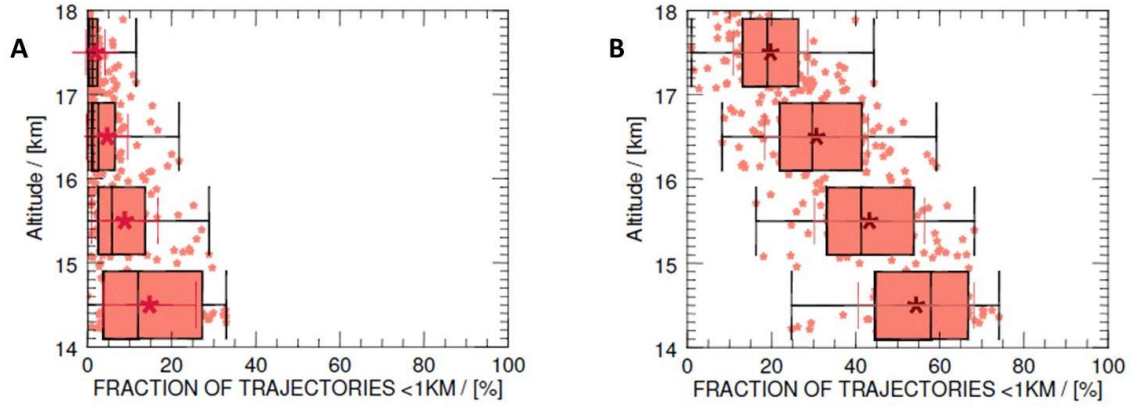

Figure 7.11 Vertical distribution of NAME calculated fractions of trajectories below 1 km, ATTREX 2013 Research Flights, 12 (A) and 30 (B) NAME runs.

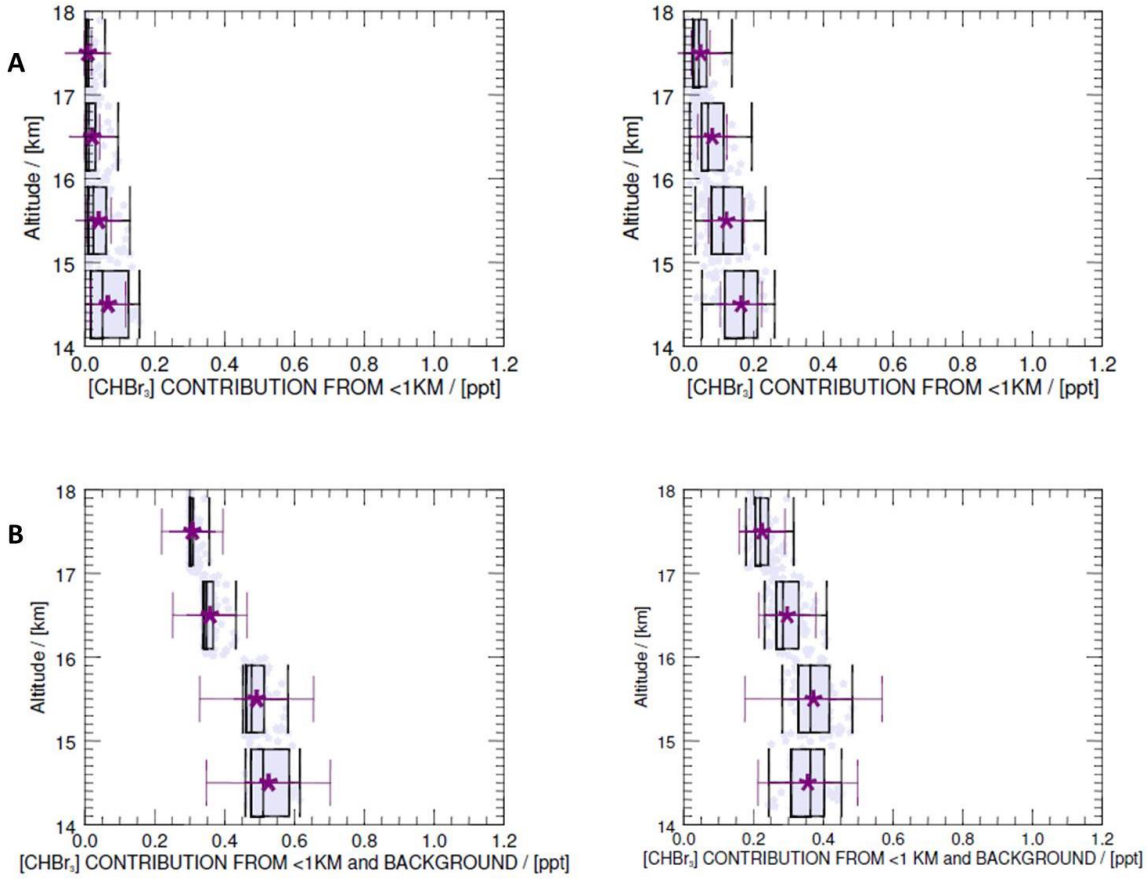

Figure 7.12 $CHBr_3$ NAME estimates in the TTL, ATTREX 2013 Research Flights, 12 (left) and 30 (right) day NAME runs; Panels as in Figure 7.9.

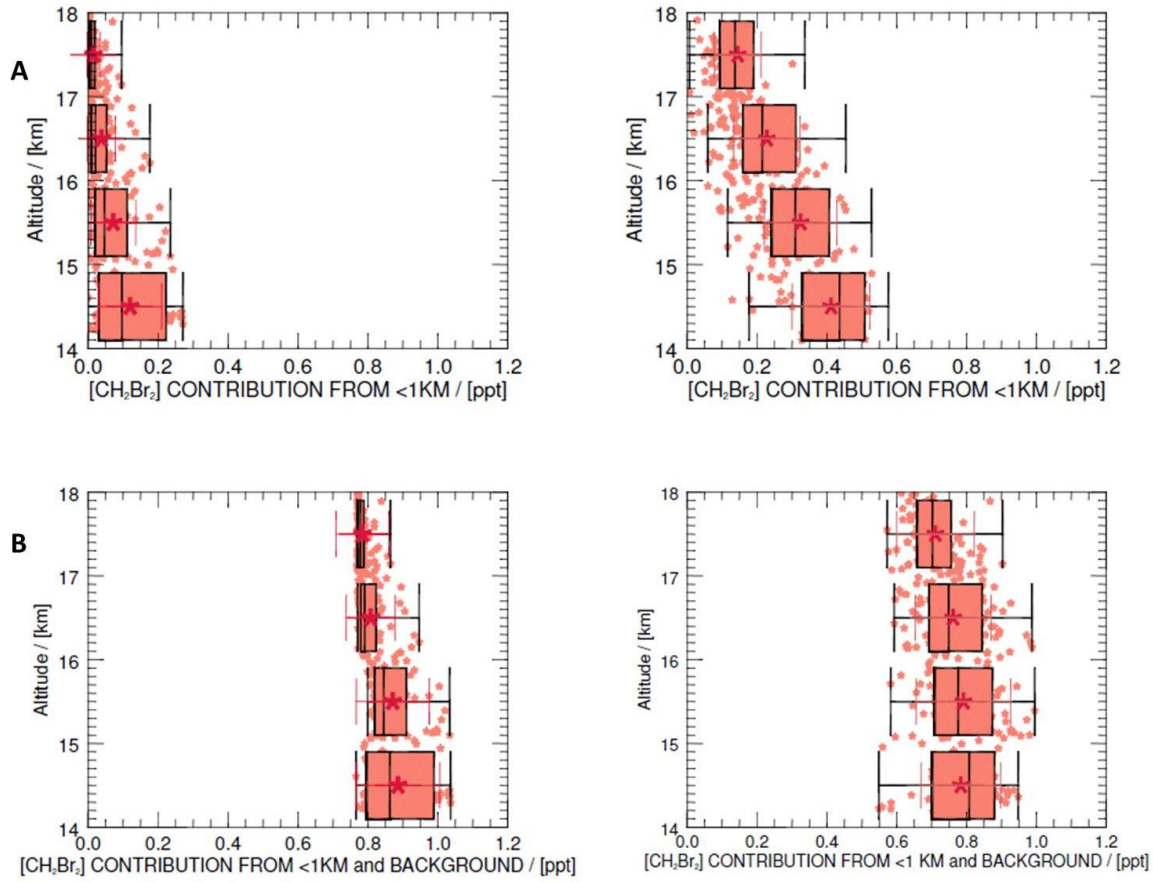

Figure 7.13 CH_2Br_2 NAME estimates in the TTL, ATTREX 2013 Research Flights, 12 (left) and 30 (right) day NAME runs; Panels as in Figure 7.9.

ATTREX 2013 flights show increased fractions of trajectories below 1 km in 30 day runs, predominantly in the lower TTL. The boundary layer contribution estimates are higher, but the modelled sums of the boundary layer and background contribution estimates are lower, compared against the 12 day NAME run results. The modelled $CHBr_3$ and CH_2Br_2 total estimates in the TTL are in satisfactory agreement with AWAS observations.

Table 7.3 NAME modelled $CHBr_3$ and CH_2Br_2 boundary layer contribution and the modelled sums of boundary layer and background contribution estimates for ATTREX 2013 Research Flights, inferred from 12 and 30 day NAME runs.

[$CHBr_3$]	*Boundary Layer Contribution [ppt]*		*Boundary Layer and Background Contribution [ppt]*	
	12 DAY	*30 DAY*	*12 DAY*	*30 DAY*
17-18 km	0.01 (0.01) 0.01	0.05 (0.03) 0.04	0.31 (0.09) 0.30	0.23 (0.06) 0.22
16-17 km	0.02 (0.02) 0.01	0.08 (0.04) 0.07	0.35 (0.11) 0.35	0.30 (0.08) 0.29
15-16 km	0.04 (0.04) 0.02	0.12 (0.05) 0.11	0.49 (0.16) 0.47	0.37 (0.20) 0.36
14-15 km	0.07 (0.05) 0.05	0.16 (0.06) 0.17	0.53 (0.18) 0.51	0.35 (0.14) 0.36

[CH_2Br_2]	*Boundary Layer Contribution [ppt]*		*Boundary Layer and Background Contribution [ppt]*	
	12 DAY	*30 DAY*	*12 DAY*	*30 DAY*
17-18 km	0.02 (0.02) 0.01	0.14 (0.07) 0.14	0.78 (0.07) 0.78	0.71 (0.11) 0.70
16-17 km	0.04 (0.04) 0.02	0.23 (0.10) 0.22	0.81 (0.07) 0.79	0.76 (0.11) 0.75
15-16 km	0.07 (0.06) 0.05	0.33 (0.10) 0.31	0.87 (0.10) 0.85	0.79 (0.14) 0.77
14-15 km	0.12 (0.09) 0.10	0.41 (0.11) 0.44	0.89 (0.12) 0.86	0.79 (0.11) 0.81

7.3.4 Modelled $CHBr_3$ and CH_2Br_2 in the TTL: Sensitivity tests with 30 day NAME runs - Summary

Extending the NAME runs to 30 days sees the increased influence of boundary layer air masses to the TTL, indicated by higher fractions of trajectories from below 1 km. This results in a higher boundary layer contribution estimate, which is partly offset by greater chemical removal. The highest attribution in fractions of trajectories below 1 km and the $CHBr_3$ and CH_2Br_2 boundary layer contribution is noted for the 15-16 and 16-17 km. These boundary layer contribution estimates are the dominant fractions in the modelled sums of the boundary layer and background contribution estimates in the lower TTL. The background contribution dominates in the upper TTL, and is more important for CH_2Br_2 due to its longer atmospheric lifetime. The modelled $CHBr_3$ and CH_2Br_2 total estimates are lower due to the lower background contribution component (lower fractions of trajectories which do not cross below 1 km). These are in satisfactory agreement with the AWAS observations. Both are near the upper range values of the WMO2014 Ozone Assessment [*Carpenter et al., 2004*].

The elevated fractions of trajectories below 1 km for the ATTREX 2014 and 2013 make it harder to quantify the background. No values of NAME 1 km fractions less than 10% are present for most of the TTL 1 km segments in ATTREX 2014 and 2013. The only approach to estimate the background is to use the lowest 10% of the NAME 1 km fractions, which in case of 14-15 km applies to the NAME 1 km fraction values of 50-60% and 15-25% for ATTREX 2014 and 2013, respectively. This leads to overestimation of the background component.

It is important to realise that imposing a background value means that there is a minimum value below which the model cannot go: i.e. when a boundary layer air fraction equals or is close to zero than the tracer equals the background value. Using the mean or median background value means that the model will never reproduce measured values below the measured mean or median chosen as background. This biases statistics strongly when a boundary layer air fraction is close to zero. Using standard deviations in e.g. Fig 7.2D gives a false impression that the model can reproduce values below the background. However, these standard deviations for modelled sums of tracers are combined from two contributions:

boundary layer air and background. As the background is calculated from measurements with, effectively, a NAME-modelled filter, there is no a priori reason why the ages from different tracers should be consistent.

Overall however, the total $CHBr_3$ and CH_2Br_2 estimates are similar for the 12- and 30-day trajectories, consistent with the picture that air which undergoes convective uplift between 12 and 30 days is attributed to the background fraction in the 12 day trajectories with reasonable accuracy.

7.4 Contribution of $CHBr_3$ and CH_2Br_2 to the active bromine loading in the TTL

The NAME modelled $CHBr_3$ and CH_2Br_2 total estimates in the TTL are used to calculate how much bromine from the short-lived bromocarbons enters the lower stratosphere via the TTL. The spatial difference between the West and East Pacific, and temporal difference between January-March 2014 and 2013, are investigated.

$CHBr_3$ and CH_2Br_2 are the dominant short-lived organic bromine substances, and the minor ones: CH_2BrCl, $CHBr_2Cl$, etc. are excluded in this study. The NAME modelled $CHBr_3$ and CH_2Br_2 total estimates are multiplied by the number of bromine atoms (bromine atomicity), and then summed to yield the total of bromine from the short-lived bromocarbons, VSL_{org}.

Figure 7.14 shows the vertical distribution of NAME modelled $CHBr_3$ and CH_2Br_2 atomicity mixing ratios, and their sums, VSL_{org}.

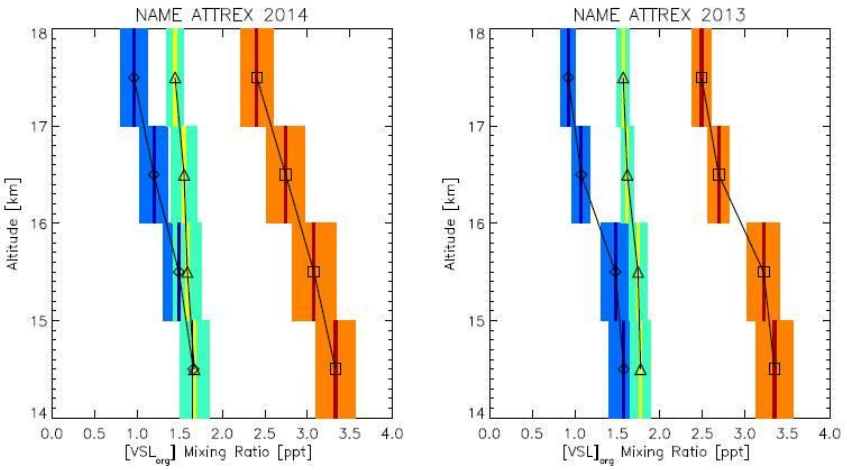

Figure 7.14 NAME modelled bromine loading from the short-lived organic bromine substances, VSL_{org}, for ATTREX 2014 (left) and 2013 (right). $CHBr_3$ (means – diamonds, navy blue lines, standard deviation – shaded blue area), and CH_2Br_2 (means – triangles, light green lines, standard deviations – shaded green area), $CHBr_3$ and CH_2Br_2 sums (means – squares, red lines, standard deviations – orange area).

For ATTREX 2014 and 2013, similar contributions of $CHBr_3$ and CH_2Br_2 to VSL_{org} are observed in the lower TTL (Table 7.4). In 2014, $CHBr_3$ in the lower TTL is abundant enough to contribute as much as CH_2Br_2. A combination of larger boundary layer air mass influence in the TTL and shorter mean times that these air masses take to reach the TTL results in the observed higher $CHBr_3$ contribution to the VSL_{org} in the lower TTL in 2014, than in 2013 (*Navarro et al., 2015*). The CH_2Br_2 contribution dominates in the upper TTL due to its longer atmospheric lifetime.

Table 7.4 Bromine loading in the TTL, attributed from the NAME modelled $CHBr_3$ and CH_2Br_2 contribution (VSL_{org}).

Campaign	Altitude [km]	NAME modelled [$CHBr_3$] [ppt]	NAME modelled [CH_2Br_2] [ppt]	Br from $CHBr_3$ [ppt]	Br from CH_2Br_2 [ppt]	Total VSL_{org} [ppt]
ATTREX 2014	17-18	0.32	0.73	0.96	1.46	**2.42**
	16-17	0.40	0.78	1.20	1.56	**2.76**
	15-16	0.50	0.80	1.50	1.60	**3.10**
	14-15	0.55	0.84	1.65	1.68	**3.33**
ATTREX 2013	17-18	0.31	0.79	0.93	1.58	**2.51**
	16-17	0.35	0.81	1.05	1.62	**2.67**
	15-16	0.49	0.87	1.47	1.74	**3.21**
	14-15	0.53	0.89	1.59	1.78	**3.37**

The NAME modelled VSL_{org} in the TTL is contrasted against the VSL_{org} inferred from the AWAS observations (Figure 7.15, Table 7.5). A good agreement is found between the datasets, with higher bromine loading around the cold point tropopause (16-17 km) in ATTREX 2014.

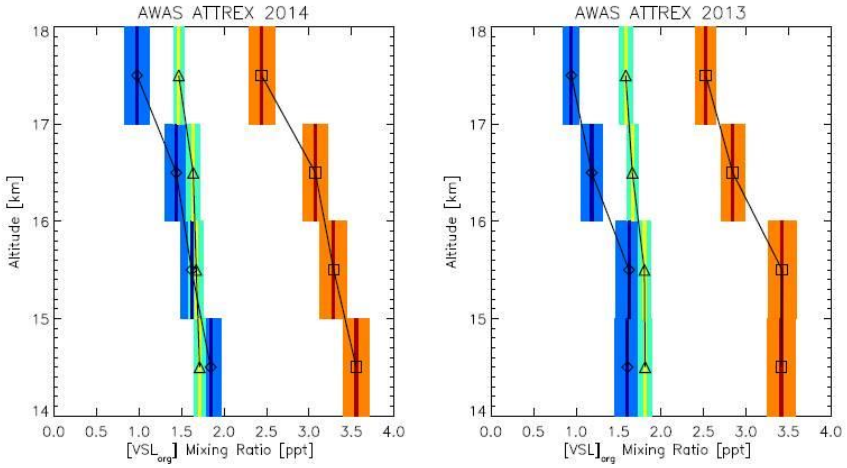

Figure 7.15 Bromine loading from the short-lived organic bromine substances, VSL_{org}, for ATTREX 2014 (left) and 2013 (right), AWAS observations. $CHBr_3$ (means – diamonds, navy blue lines, standard deviation – shaded blue area), and CH_2Br_2 (means – triangles, light green lines, standard deviations – shaded green area), $CHBr_3$ and CH_2Br_2 sums (means – squares, red lines, standard deviations – orange area).

Table 7.5 Bromine loading in the TTL, attributed from the $CHBr_3$ and CH_2Br_2 contribution (VSL_{org}), AWAS observations.

Campaign	Altitude [km]	AWAS [$CHBr_3$] [ppt]	AWAS [CH_2Br_2] [ppt]	Br from $CHBr_3$ [ppt]	Br from CH_2Br_2 [ppt]	Total VSL_{org} [ppt]
ATTREX 2014	17-18	0.33	0.73	0.99	1.46	**2.45**
	16-17	0.48	0.81	1.44	1.62	**3.06**
	15-16	0.54	0.84	1.62	1.68	**3.30**
	14-15	0.61	0.86	1.83	1.72	**3.55**
ATTREX 2013	17-18	0.31	0.79	0.93	1.58	**2.51**
	16-17	0.39	0.83	1.17	1.66	**2.83**
	15-16	0.54	0.90	1.62	1.80	**3.42**
	14-15	0.53	0.91	1.59	1.82	**3.41**

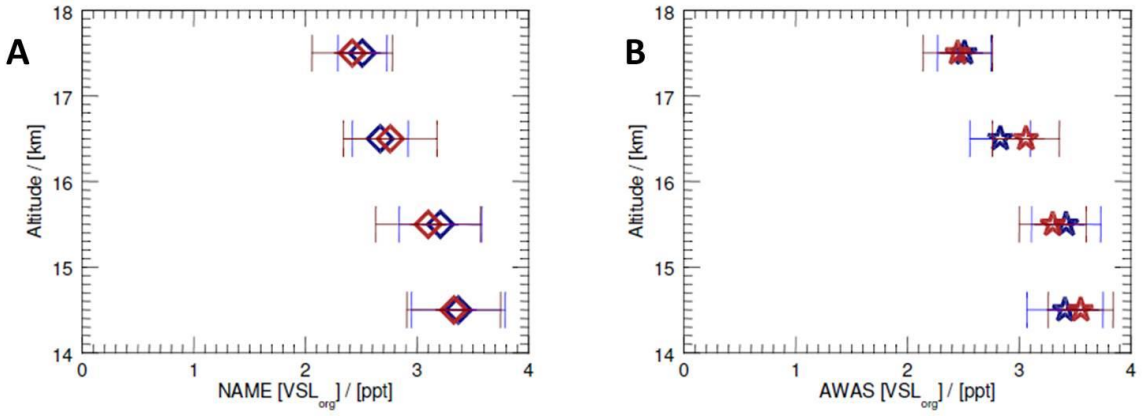

Figure 7.16 NAME (A) and AWAS (B) $CHBr_3$ and CH_2Br_2 (short-lived brominated organic substances, VSL_{org}) contribution to the active bromine in the East and West Pacific TTL, in ATTREX 2013 (blue) and 2014 (red), respectively; stars (diamonds) represent AWAS (NAME) total VSL_{org} estimates from Tables 7.4 and 7.5.

Navarro et al., 2015 reports slightly higher bromine loading from the VSL_{org} at the tropopause level (17 km) in the West Pacific, 2014 than in the East Pacific, 2013 (the VSL_{org} values of 3.27 (+/-0.47) and 2.96 (+/-0.42) ppt, respectively, AWAS observations). The minor short-lived organic bromine substances are used in *Navarro et al., 2015*, which account for the higher VSL_{org} (compared to Table 7.5).

Butler et al., 2017 infers a mean mole fraction and range of 0.46 (0.13-0.72) ppt and 0.88 (0.71-1.01) ppt of $CHBr_3$ and CH_2Br_2 being transported to the TTL during January and February, 2014. This is consistent with a contribution of 3.14 (1.81-4.18) ppt of bromine to the TTL Br_y budget over the region of the campaign. The NAME modelled results presented here (Figure 7.16) are in good agreement with the values reported by *Navarro et al., 2015* and *Butler et al., 2017*.

7.5 Summary

This chapter examines the vertical distribution of $CHBr_3$ and CH_2Br_2 in the TTL over the West and East Pacific. The ATTREX 2014 and 2013 $CHBr_3$ and CH_2Br_2 AWAS observations are contrasted with the NAME modelled sums of the boundary layer and background contribution estimates. The inter-campaign differences are assessed. The NAME procedure is tested using the run period of 30 days to investigate the role of boundary layer contribution for short-lived bromocarbons. Finally, the contribution of $CHBr_3$ and CH_2Br_2 to the bromine budget in the TTL is investigated.

The NAME procedure using the fractions of trajectories below 1 km as a metric of the boundary layer air mass influence, can explain the vertical distribution of $CHBr_3$ and CH_2Br_2 in the TTL. This procedure (a) identifies and differentiates which atmospheric transport pathways are dominant, (b) assesses the transport timescales, particularly indicating the signals of the recent rapid convection episodes, and (c) quantifies the contribution from the low troposphere boundary layer and from the TTL. The NAME procedure to quantify $CHBr_3$ and CH_2Br_2 in TTL works well, providing a good agreement of the total estimates against the AWAS observations. In 2014, the boundary layer contribution component dominates in the lower TTL, while the background contribution component is dominant in the upper TTL (constituting a higher fraction of the modelled sums of the total estimates).

Extending the NAME runs to 30 days unveils the significant attribution to the $CHBr_3$ and CH_2Br_2 boundary layer contribution estimates. It also consolidates the dominant weight of the boundary layer (background contribution) component in the lower (upper) TTL in ATTREX 2014. ATTREX 2013 shows the dominance of background contribution in all TTL 1 km altitude bins, due to negligible convective influence and dominant horizontal transport mechanism. The total $CHBr_3$ and CH_2Br_2 estimates are similar for the 12- and 30-day trajectories; and consistent with the picture that the air which undergoes convective uplift between 12 and 30 days is attributed to the background fraction in the 12 day trajectories with reasonable accuracy.

Extending NAME runs to 30 days does not affect the concentrations of CH_3I in the TTL. The

early stage of the NAME runs is when the critical CH_3I boundary layer contribution to the TTL occurs. This strengthens the role of the rapid and recent convection in transporting CH_3I to the TTL, and the correlation between the high CH_3I and the high percentage of the low-level air masses of the short transport times, present in the TTL.

NAME modelled $CHBr_3$ and CH_2Br_2 total estimates contribute a similar fraction (as the contribution from the short-lived bromocarbons, VSL_{org}) to the active bromine loading in the TTL. $CHBr_3$ contributes more in the lower TTL in the West Pacific 2014, due to the increased convective activity in this region. CH_2Br_2 takes dominance in the East and West Pacific upper TTL, in 2013 and 2014, respectively. The findings correlate well with the AWAS observations, and match the results from the recent literature [*Navarro et al., 2015; Butler et al., 2017*].

8. Concluding Discussion and Further Work

The major results from this thesis are summarised in this chapter. Section 8.1 gives an overview of each chapter highlighting the main scientific findings. The potential further work is put forward in Section 8.2. The ways to develop the techniques are proposed, and to use them to address the science questions instilled in this thesis. This lays the foundation for expanding the study on the scientific findings from this thesis.

8.1 Concluding Discussion

This thesis is divided into two parts. The first investigates the use of NAME, a Lagrangian particle dispersion model, in supporting the flight planning activities for the CAST, CONTRAST and ATTREX 2014 joint research campaign. A novel procedure is established making the NAME model a viable tool in the flight planning and achieving the multi aircraft coordination. The second part of the thesis investigates the transport and distribution of the very short-lived halogenated organic substances in the troposphere and the tropical tropopause layer (TTL) in the Pacific region. NAME is used to quantify the vertical distribution of the very short-lived halogenated organic substances in the TTL, and explain its differences in the East and West Pacific TTL, with reference to the AWAS measurements obtained from the NASA ATTREX 2013 and 2014 campaigns. The spatial and temporal variability in the transport and the influence of the low level air masses to the TTL is assessed. The role of convection in this transport is studied in depth with the new convection parameterisation developed for NAME [*Meneguz, et al., 2016*].

The first chapter gives an introduction to the atmospheric dynamics of the Pacific region, including the tropospheric Walker and Hadley circulations. The intraseasonal Madden-Julian Oscillation and interannual El Nino Southern Oscillation phenomena affecting the circulation in the Pacific are explained then. A structure of the TTL is described later, including its tropospheric and stratospheric like features, and the transport of air masses to and through the TTL into the stratosphere. The composition, distribution and transport of the very short-lived halogenated organic substances: methyl iodide, CH_3I, bromoform, $CHBr_3$, and dibromomethane, CH_2Br_2, within the tropical troposphere and the TTL is put forward next. A review of the recent findings on the short-lived bromocarbons attributing to the bromine loading in the TTL is provided. Chapter 1 concludes with the thesis overview, listing its objectives and the proposed scientific questions.

These objectives included the development of the NAME procedure used to support the flight planning activities and to achieve the multi aircraft coordination in the CAST, CONTRAST and ATTREX 2014 campaigns. The vertical distribution of CH_3I, $CHBr_3$ and CH_2Br_2 in the East and West Pacific TTL is examined. The NAME approach is used to quantify these compounds in the TTL, differentiating between the boundary layer and the background contribution estimates. The role of convective transport in the distribution of short-lived tracers: CH_3I and $CHBr_3$ is assessed using the improved convection scheme embedded in NAME. Having tested the convective influence on the CH_3I distribution in the TTL and on the performance of the new convection scheme, the investigation is made on how good is the quantification of bromocarbons and its contribution to the active bromine loading in the TTL.

Chapter 2 discusses in detail the modelling methods used throughout this project. The UK Meteorological Office NAME model is introduced and an assessment of how NAME represents the transport of particles, the turbulence and the deep convection is provided. The performance of NAME with different convection scheme setups is investigated and the results are compared. The new convection scheme improves the representation of the particle transport via convection as more particles move upwards within shorter timescales. A description of how the very short-lived halogenated organic substances are measured by the Whole Air Sampler (WAS) instrumentation during the CAST, CONTRAST and ATTREX 2014 joint research campaign comes last.

Chapter 3 is the first of the five results chapters. It describes the use of NAME in supporting the flight planning activities for the CAST, CONTRAST and ATTREX 2014 campaigns. Firstly, an overview of these campaigns is given. Then, the NAME procedure is developed and tailored to meet the scientific objectives of the CAST BAe-146 flights. A novel approach is also taken to achieve the multi aircraft coordination with CONTRAST Gulfstream V and ATTREX Global Hawk. This coordination relies on the sampling of the same or similar air mass streams at different altitudes. This NAME procedure is tested for the ATTREX 2013 campaign, further modified and applied in the CAST, CONTRAST and ATTREX 2014 joint campaign. The data output and the operational NAME running times for the proposed sets of NAME flight planning runs produced routinely pose a potential limitation to the efficiency of the procedure. The compromise between the robustness of the statistical analysis and operating NAME in a timely and efficient manner is reached. The NAME flight planning products are available in near real-time, in advance of the CAST, CONTRAST and ATTREX flight planning meetings. The meteorological data forecasts, provided by the UK Meteorological Office, are a pivotal part of this NAME flight planning procedure. Its consistency and quality is high, so that the NAME flight planning products are reliable and accurate. The developed NAME flight planning procedure can be applied to any future research campaigns utilising the airborne measurement platforms as it is relatively straightforward and easy to be (i) tailored to meet different scientific objectives, and (ii) executed.

Chapter 4 gives a detailed analysis of the AWAS measured CH_3I, $CHBr_3$ and CH_2Br_2 in the ATTREX 2013 and 2014 flights. The inter-campaign variability in the distribution of shorter-lived CH_3I and $CHBr_3$ is observed. CH_3I and $CHBr_3$ are high in the West Pacific TTL, due to the enhanced convective activity in this region. The method used to investigate the low level air mass influence in these AWAS samples is described next, followed by an assessment of the boundary layer air mass contribution to the TTL. This contribution is indicated by the metric of the NAME calculated fractions of trajectories which first cross below 1 km. This is complemented with a summary of the regions from which these boundary layer air masses originate. The correlation between the high CH_3I, $CHBr_3$ and high fractions of trajectories below 1 km is observed, and investigated further in the following chapters.

Chapter 5 focuses on the convective influence on CH_3I in the TTL. Its vertical distribution is assessed first for ATTREX 2014 Research Flight 02. High CH_3I in the lower TTL is due to the stronger and more recent boundary layer air mass influence. The approach by which NAME quantifies CH_3I in the TTL is presented, including the calculations for the boundary layer and the background contribution estimates. This approach is used for the RF02 and expanded to all ATTREX 2014 and 2013 flights. The NAME modelled total CH_3I estimates are in good agreement with the AWAS observations. In 2014 the boundary layer contribution constitutes the larger part of these total estimates giving evidence for most of CH_3I found in the TTL as a result of the strong and recent convection. The NAME approach underestimates the boundary layer contribution to the upper TTL as these estimates do not explain the AWAS observations made there. It also overestimates the background contribution to the lower TTL as it is hard to filter the AWAS samples which have little or no convective influence in the West Pacific. Large differences in CH_3I in the West and East Pacific TTL are found. The negligible convective activity, indicative of the minimal boundary layer air mass influence, results in low CH_3I observed in the East Pacific TTL. This chapter concludes that the presence of high CH_3I in the TTL predominantly depends on the atmospheric transport via rapid vertical uplift (convective activity).

Chapter 6 validates the new convection scheme embed in NAME. The performance of this scheme is tested using the NAME approach quantifying CH_3I in the TTL. The results are compared against the AWAS CH_3I measurements from the four individual ATTREX 2014 research flights which experienced the most convective influence. The new convection scheme represents the particle displacement due to convection in a more realistic manner, showing better agreement between the modelled and measured CH_3I in the TTL. This chapter also strengthens the confidence in estimating the boundary layer contribution in the developed NAME approach of quantifying the CH_3I in the TTL, and hence that using NAME in this way provides a reasonable estimate of how much air is transported in the convection.

Chapter 7 investigates the transport and distribution of the short-lived bromocarbons in the TTL. $CHBr_3$ and CH_2Br_2 in the TTL are quantified using NAME. As these are longer lived than CH_3I, the focus is on assessing the background contribution. This study, along with extending the NAME runs to 30 days, gives confidence in estimating the background

component in the NAME approach. A satisfactory agreement is achieved between the modelled and measured $CHBr_3$ and CH_2Br_2 in the TTL. NAME provides a good estimate of the short-lived brominated organic substances contribution to the active bromine loading in the TTL. These estimate values of 3.37 +/-0.42 ppt (3.33 +/-0.42 ppt) in the lower East (West) Pacific TTL (14-15 km) and 2.51 (+/-0.22) ppt (2.42 +/-0.36 ppt) in the upper East (West) Pacific TTL lie within the range of the recent literature findings [2.96 +/-0.42 ppt (3.27 +/-0.47 ppt) from AWAS observations at the tropopause level of 17 km for the East (West) Pacific ATTREX 2013 (2014) *Navarro, et al., 2015;* 3.14 (1.81-4.18) ppt for the TTL (above 13 km and below the local tropopause) for the West Pacific ATTREX 2014 *Butler et al., 2017*].

8.2 Further Work

This section offers the potential ways in which this study could be extended. It covers the technical model aspects of the project, and the development or improvement of the scientific themes, emerging from the analysis of this work.

8.2.1 Future directions for the NAME model

A novel procedure involving the use of NAME in supporting the flight planning activities is developed. This procedure can be streamlined by reducing the operational NAME running times, the size of the model output, and the use of meteorological data forecasts (given its high quality and consistency). The NAME flight planning procedure offers flexibility so that it can be applied to any future research campaigns (i) utilising the airborne measurement platforms (aircraft, balloons, sondes), (ii) aiming to achieve the multi platform coordination, and (iii) linking measurements from these platforms.

This study also tests the performance of the new convection scheme in NAME. This new scheme provides a more realistic representation of the particle transport via convective clouds. This is less evident for the upper TTL. The focus should be on further studying what happens to the modelled particles once they detrain from the tops of the convective clouds.

Even though there is a good agreement between the modelled and measured CH_3I in the TTL for the individual, and all ATTREX 2014 and 2013 Research Flights, the model poorly estimates the total CH_3I for ATTREX 2014 Research Flight 03. This flight sampled the direct convective outflow detrained from the Faxai tropical cyclone. Exceptionally high CH_3I was recorded, even in the upper TTL. This poses a potential limitation of the convection scheme and the model itself in not picking up the high particle load in very fine temporal resolution. This also offers an opportunity to invert the modelling procedure and ask whether marine boundary layer values used in the calculations were too low under these extreme conditions.

The global meteorological data with a horizontal resolution of 25 km limits the ability of the NAME model to represent the recent and strong small-scale convection events. Introducing the higher resolution in the global meteorological data (12 km from 2017, the UK Meteorological Office) would enhance NAME's capability of representing these convective events. The drawback is as the size of the meteorological data increases, the operational NAME running times and the data storage requirements would increase accordingly.

8.2.2 Expansion of the scientific investigation

The NAME approach is developed to quantify the short-lived halogenated organic substances and explain their vertical distribution in the TTL. This approach works well compared against the ATTREX AWAS CH_3I, $CHBr_3$ and CH_2Br_2 measurement datasets. The further study would involve the analogous NAME analysis compared against the CONTRAST AWAS CH_3I, $CHBr_3$ and CH_2Br_2 observations, made in the upper troposphere. This is the region where the main convective outflow occurs. This study would strengthen the validity of the developed NAME approach in quantifying the vertical distribution of CH_3I, $CHBr_3$ and CH_2Br_2 in the upper troposphere. It would also provide more tests for validating the performance of the new convection scheme in NAME.

The NAME approach to quantify the CH_3I, $CHBr_3$ and CH_2Br_2 in the TTL can be expanded to cover the other short-lived halogenated organic substances, measured by the WAS in the ATTREX, CONTRAST and CAST campaigns. These would have to be characterised by the short atmospheric lifetimes, similar chemistry, the signature of the convectively driven

distribution in the upper troposphere and the TTL, and the well documented, uniform emission sources.

This NAME approach can also be used against the similar datasets from the past campaigns which measured the composition of the short-lived halogenated organic compounds in the TTL. The scarcity of these datasets relevant to this scientific investigation poses the main limitation here.

The NAME procedure to identify the source origins of the different tracers being measured in the upper troposphere and the TTL can be applied to other chemical substances: boundary layer tracers: methyl ethyl ketone (MEK) and dimethylsulfide (DMS), and ozone (O_3). DMS has a short atmospheric lifetime and is emitted by the oceans. Several studies suggested that the presence of high DMS in the upper troposphere can be attributed to the fast convective transport directly from the emission sources [*Marandino et al., 2013]*. This suggestion would be worth probing using the NAME procedure.

Ozone is an important pollutant in the troposphere; its high levels in the upper troposphere and the TTL come either from the inflow of the polluted air (caused by the biomass burning and the industrial man-made emissions sources) or the stratospheric intrusions. Most of this polluted air outflow from the Southeast Asia and the Maritime Continent can reach the West Pacific region and enter the stratosphere via the TTL there. The ATTREX and CONTRAST flights saw the episodes of the high O_3 (greater than 100 ppb), originated from the Southeast Asia [*Anderson et al., 2016*]. The NAME procedure would be applied to test this source-receptor relationship.

Furthermore, the ATTREX 2014 RF03 recorded very low O_3 in the sampled air (less than 20 ppb), detrained from the fresh convective outflow of the tropical cyclone Faxai. This low O_3 is a signature of the clean oceanic boundary layer air environment [*Pan et al., 2015*]. Thus, NAME can investigate if the low O_3 found in the TTL comes from the oceanic environment. One of the CAST branches of measurements included the daily ground based and sonde measurements of O_3 in the Manus island (2.1°S, 146.9°E). Low O_3 prevailed on the ground, typical of the oceanic clean air environment. The high episodes of the O_3 occurred

sporadically and these were attributed to the island forest fires [*Newton et al., 2014*]. The NAME model identified the sources of the low and high O_3 in the upper troposphere and on the ground. Therefore, the procedure developed in this thesis to use NAME to track the air masses backwards can be used to identify the sources of the low and high O_3 in the upper troposphere and the TTL.

Finally, the NAME procedure can be used to investigate the intraseasonal variability of the MJO influence on the upper troposphere and the TTL. The MJO is redistributing the large-scale convective systems along the Equator in the Maritime Continent and the West Pacific. The fractions of trajectories from below 1 and 5 km can be used as a proxy for the low-level air mass influence to the upper troposphere. The routine NAME runs can be designed to investigate the periods of the varied MJO activity via identifying the loading of the low-level air to the upper troposphere. This analysis would have to be supported with the meteorological analysis of the variables typical of the MJO signature: convective precipitation, outgoing longwave radiation. This analysis can be expanded further to investigate the ENSO driven interannual variability in the boundary layer air influence to the upper troposphere and the TTL.

Bibliography

Ahrens D., (2012), Meteorology Today (10th Edition): An Introduction to Weather, Climate and the Environment, *Brooks Cole*.

Anderson D., Nicely J., Salawitch R., Canty T., Dickerson R., et al., (2016), A pervasive role for biomass burning in tropical high ozone/low water structures., *Nat.Comms*, 7, 10267 [10.1038/ncomms10267].

Andrews S., Jones C., Carpenter L., (2013), Aircraft measurements of very-short-lived halocarbons over the tropical Atlantic Ocean., *Geophys.Res.Lett.*, 40, 1005-1010 [10.1002/GRL.50141].

Andrews S., Carpenter L., Apel E., Atlas E., Donets V., et al., (2016), A comparison of very-short-lived halocarbon (VSLS) and DMS aircraft measurements in the Tropical West Pacific from CAST, ATTREX and CONTRAST., *Atmos.Meas.Tech.*, 9, 5213-5225 [10.5194/amt-9-5213-2016].

Aschmann J., Sinnhuber B-M., (2013), Contribution of very short-lived substances to stratospheric bromine loading: Uncertainties and constraints. *Atmos.Chem.Phys.*, 13, 1203–1219 [10.5194/acp-13-1203-2013].

Ashfold M., Harris N., Pyle J., Robinson A., et al., (2012), Transport of short-lived species into the Tropical Tropopause Layer, *Atmos.Chem.Phys.*, 12, 6309-6322 [10.5194/acp-12-6309-2012].

Athanassiadou M., Flocas H., Harrison M.A.J., Hort M.C., Witham C.S. and Watkin

S., (2006), The dust event of 17 April 2005 over Athens, Greece, *Weather*, 61(5), 125-131.

Atlas E., Blake D.R., et al., (2014), HAIS Advanced Whole Air Sampler (AWAS), www.acom.ucar.edu/start/HAISAdvancedWholeAirSampler.pdf.

Bell N., Hsu L., Jacob D., Schultz M., Blake D., et al., (2002), Methyl iodide: Atmospheric budget and use as a tracer of marine convection in global models., *J.Geophys.Res.*, 107, D17, 4340 [10.1029/2001JD001151].

Bergman J., Jensen E., Pfister L., Yang Q., (2012), Seasonal differences of the vertical transport efficiency in the tropical tropopause layer: on the interplay between tropical deep convection, large scale vertical ascent, and the horizontal circulations. *J.Geophys.Res.*, 117, D05302 [10.1029/2011JD016992].

Brewer A., (1949), Evidence for a world circulation provided by the measurements of helium and water vapour distribution in the stratosphere., *Q.J.R.Meteorol.Soc.*, 75, 351-363 [10.1002/qj.49707532603].

Brinckmann, S., Engel A., Bönisch H., Quack B., Atlas E., (2012), Short-lived brominated hydrocarbons – observations in the source regions and the tropical tropopause layer, *Atmos. Chem. Phys.*, 12 (3), 1213-1228, [10.5194/acp-12-1213-2012].

Bunzel F., Schmidt H., (2013), The Brewer Dobson Circulation in a Changing Climate: Impact of the Model Configuration, *Amer.Meteorol.Soc.*, 1437-1455 [10.1775/JAS-D-12-0215.1].

Butler J., King D., Lobert B., Montzka S., Yvon-Lewis S., et al., (2007), Oceanic distributions and emissions of short-lived halocarbons., *Glob.Biogeochem.Cy.*, 21, GB1023 [10.1029/2006GB002732].

Butler R., Palmer P., Feng L., Andrews S., Atlas E., et al., (2017), Quantifying the vertical transport of $CHBr_3$ and CH_2Br_2 over the Western Pacific. *Atmos.Chem.Phys.Discuss* [10.5194/acp-2016-936].

Camargo S., Wheeler M., Sobel A., (2009), Diagnosis of the MJO Modulation of Tropical Cyclogenesis Using an Empirical Index., *JAS*, 66, 3061-3074 [10.1175/2009JAS3101.1].

Carpenter L., (2003), Iodine in the Marine Boundary Layer, *Chem.Rev.*, 2003, 103, 4953-4962 [10.1021/cr0206465].

Carpenter L., Jones C., Dunk R., Hornsby K., Woeltjen J., (2009), Air-sea fluxes of biogenic bromine from the tropical and North Atlantic Ocean, *Atmos.Chem.Phys.*, 9, 1805-

1816 [10.5194/acp-9-1805-2009].

Carpenter L., Archer J., Beale R., (2012), Ocean-atmosphere trace gas exchange., *Chem.Soc.Rev*., 41, 6473-6506 [10.1039/C2CS35121H].

Carpenter L., Reimann S., Coauthors and Contributors, (2014), Ozone-Depleting Substances (ODSs) and Other Gases of Interest to the Montreal Protocol, Chapter 1 in Scientific Assessment of Ozone Depletion., Global Ozone Research and Monitoring Project, Report No. 55, World Meteorological Organisation, Geneva, Switzerland.

Chameides W., Davis D., (1980), Iodine: its possible role in tropospheric photochemistry., *J.Geophys.Res.*, 85, 7383 [10.1029/JC085iC12p07383].

Chatfield R., Crutzen P., (1984), Sulfur dioxide in remote ocean air: cloud transport of reactive precursors, *J. Geophys. Res.*, 89, 7111-7132 [10.1029/JD089iD05p07111].

Cohan D., Schultz M., Jacob D., Heikes B., Blake D., (1999), Convective Injection and Photochemical Decay of Peroxides in the Tropical Upper Troposphere: Methyl Iodide as a Tracer of Marine Convection., *J.Geophys.Res.*, 104, D5: 5717-5724 [10.1029/98JD01963].

Collins W., Derwent R., Johnson C., Stevenson D., (2002), A comparison of two schemes for the convective transport of chemical species in a Lagrangian global chemistry model. *Q.J.R.Meteorol.Soc.*, 128, 991-1009 [10.1256/0035900021643629].

Convective Clouds, Atmospheric Dynamics Lecture, Wageningen University, http://www.met.wur.nl/education/atmospract/unit13/convective%20clouds.pdf.

Cullen, M.J.P., (1993), The unified forecast/climate model., *Meteorol. Mag.*, 1449: 81-94.

Danielsen E., (1982), A dehydration mechanism for the stratosphere, *Geophys.Res.Lett.*, 9, 605-608 [10.1029/GL009i006p00605].

Danielsen E., (1993), In situ evidence of rapid, vertical, irreversible transport of lower tropospheric air into the lower tropical stratosphere., *J.Geophys.Res.*, 98, 8665-8681 [10.1029/92JD02954].

Davis L.S., Dacre H.F., (2009), Can dispersion model predictions be improved by increasing the temporal and spatial resolution of the meteorological input data?, Weather, 64, 9.

DeMott, C., Klingaman, N., Woolnough S., (2015), Atmosphere-ocean coupled processes in the Madden Julian Oscillation, *Rev. Geophys.*, 53,1-54 [10.1002/2014RG000478].

Dessens O., Zeng G.., Warwick N., Pyle J., (2009), Short-lived bromine compounds in the lower stratosphere; impact of climate change on ozone., *Atmos.Sci.Let.*, 10, 201-206 [10.1002/asl.236].

Donner L., Horowitz L., Fiore A., Seman C., Blake D., Blake N., (2007), Transport of radon-222 and methyl iodide by deep convection in the GFDL Global Atmospheric Model AM2., *J.Geophys.Res.*, 112, D17303 [10.1029/2006JD007548].

Dragani R., Redaelli G., Visconti G., Mariotti A., Rudakov V., MacKenzie A.R., Stefanutti L., (2002), High resolution stratospheric tracer fields reconstructed with Lagrangian techniques: a comparative analysis of predictive skill, *J.Atmos.Sci*., 59, 1943-1958 [10.1175/1520-0469(2002)059].

El Niño Southern Oscillation (ENSO) Diagnostic Discussion, December 2010, Climate Prediction Centre / NCEP / NWS and the International Research Institute for Climate and Society.

Emanuel K., Neelin J., Bretherton C., (1994), On large-scale circulations in convecting atmospheres., *Q.J.R.Meteorol.Soc.*, 120, 1111-1143.

Emanuel K., (1994), Atmospheric Convection, Oxford University Press, New York, USA.

ENSO Information Website, http://www.bom.gov.au/climate/enso/history/ln-2010-12/three-phases-of-ENSO.shtml, Bureau of Meteorolofenggy, Australian Government.

Feng J., Liu P., Chen W., Wang X., (2015), Contrasting Madden-Julian Oscillation activity during various stages of EP and CP El Niños, *Atmos.Sci.Let.*, 16, 32-37 [10.1002/asl2.516].

Fernandez R., Salawitch R., Kinnison D., Lamarque J-F., Saiz-Lopez A., (2014), Bromine partitioning in the tropical tropopause layer: Implications for stratospheric injection. *Atmos. Chem. Phys.*, 14, 13391–13410 [10.5194/acp-14-13391-2014].

Fueglistaler S., Dessler A., Dunkerton T., Folkins I., Fu Q., et al., (2009), Tropical Tropopause Layer. *Reviews of Geophysics*, 47 [10.1029/2008RG000267].

Ganesan A., Manning A., Grant A., Young D., Oram D., Sturges W., (2015), Quantifying methane and nitrous oxide emissions from the UK and Ireland using a national-scale monitoring network., *Atmos. Chem. Phys.*, 15, 6393–6406 [10.5194/acp-15-6393-2015].

Gettelman A., Forster P., Fujiwara M., Fu Q., Vomel H., et al., (2004), Radiation balance of the tropical tropopause layer. *J.Geophys.Res*: *Atmospheres*, 109

[10.1029/2003JD004190].

Gloster J., Champion H.J., Sorensen J.H. et al., (2003), Airborne transmission of foot-and-mouth disease virus from Burnside Farm., Heddon-on-the-Wall, Northumberland during the 2001 epidemic in the United Kingdom., *Vet.Rec.*, 152, 525-533.

Gloster J., Sellers R., Webster H. and Valarcher J-F., (2006), Assessing the risk of airborne spread of foot-and-mouth disease - a case study, Weather, 61, 137-142 [10.1256/wea.164.05].

Gloster, J., Burgin, L., Jones, A. and Sanson, R., (2011), Atmospheric dispersion models and their use in animal and plant disease transmission, *Rev.Sci.Tech.*, 30, 457-465.

Gottschalck J., Kousky V., Higgins W., L'Heureux M., (2005), Madden-Julian Oscillation Impacts. NOAA/NWS/NCEP Climate Prediction Center.

Gregory D., Rowntree P., (1990), A mass flux convection scheme with representation of cloud ensemble characteristics and stability dependent closure., Mon.Weather Rev., 118, 1483-1506.

Hamer, P.D., Marécal V., Hossaini R., Pirre M., Warwick N., Chipperfield M., et al., (2013), Modelling the chemistry and transport of bromoform within a sea breeze driven convective system during the SHIVA Campaign, *Atmos.Chem.Phys.Discuss.*, 13, 20611-20676 [10.5194/acpd-13-20611-2013].

Harris N., NERC CAST team, (2010), Co-ordinated Airborne Studies in the Tropics - CAST, Case for Support.

Harris N., Carpenter L., Lee J., Vaughan G., Filus M. et al.,(2017), Co-ordinated Airborne Studies in the Tropics (CAST), *Bull. Amer. Meteor. Soc.*, [10.1175/BAMS-D-14-00290.1].

Helber R.W., Weisberg R.H., (2001), Equatorial upwelling in the Western Pacific Warm Pool, *Marine Science Faculty Publications*, 128 [10.1029/2000JC000401].

Highwood E., Hoskins B., (1998), The tropical tropopause., *Q.J.R.Meteorol.Soc.*, 124, 1579-1604 [10.1002/qj.49712454911].

Holton J., (1989), Global transport processes in the atmosphere. *Handbook of Environmental Chemistry* (O.Hutzinger, Ed.), 1, Pt.E, Springer-Verlag, 98-145.

Holton J., Haynes P., McIntyre M., Douglass A., Rood R., et al., (1995), Stratosphere-troposphere exchange., *Reviews of Geophysics*, 33, 403-439.

Holton J., (2012), An Introduction to Dynamic Meteorology, Volume 88, Fifth

Edition, Academic Press.

Hosking S., Russo M., Braesicke P., Pyle J., (2012), Tropical convective transport and the Walker circulation., *Atmos.Chem.Phys.*, 12, 9791-9797 [10.5194/acp-12-9791-2012].

Hossaini R., Chipperfield M., Monge-Sanz B., Richards A., Atlas E., Blake D., (2010), Bromoform and dibromomethane in the tropics: a 3-D model study of chemistry and transport. *Atmos.Chem.Phys*., 10, 719-735 [10.5194/acp-10-719-2010].

Hossaini R., Mantle H., Chipperfield M., Montzka S., Hamer P., et al., (2013), Evaluating the global emission inventories of biogenic bromocarbons., *Atmos.Chem.Phys.*, 13, 11819-11838 [10.5194/acp-13-11869-2013].

Hossaini R., Chipperfield M., Montzka S., Rap A., Dhomse S., et al., (2015), Efficiency of short-lived halogens at influencing climate through depletion of stratospheric ozone., *Nature Geoscience*, [10.1038/NGE02363].

IPCC, (2001), Climate Change 2001: The Scientific Basis., Cambridge University Press, Cambridge, United Kingdom.

Ivanova A., (2013), The tropopause: Variety of definitions and modern approaches to identification., *Russ. Meteorol. Hydrol.*, 38, 808 [10.3103/S1068373913120029].

Jacob, D.J. (1999), Introduction to Atmospheric Chemistry, Princeton University Press, Princeton.

Jensen E., (2009), Airborne Tropical Tropopause Experiment – ATTREX. A Venture Class Mission to Understand the Role of the Tropical Tropopause Layer in Earth's Climate. An Earth Venture-1 Proposal, NASA.

Jensen E., Pfister L., Jordan D., Bui T., Ueyama R., et al.,(2017), The NASA Airborne Tropical Tropopause Experiment (ATTREX): High Altitude Aircraft Measurements in the Tropical Western Pacific., *BAMS*, [10.1175/BAMS-D-14-00263.1].

Jones A., Thomson D., Hort M., Devenish B., (2004), The U.K. Met Office's Next Generation Atmospheric Dispersion Model, NAME III., British Crown Copyright, Met Office.

Jones A.R., Thomson D.J., Hort M. and Devenish B., (2007), The U.K. Met Office s next-generation atmospheric dispersion model, NAME III, in Borrego C. and Norman A.-L. (Eds) Air Pollution Modelling and its Application XVII (*Proceedings of the 27th NATO/CCMS International Technical Meeting on Air Pollution Modelling and its Application*), *Springer*, pp. 580-589.

Jones C., Andrews S., Carpenter L., Hogan C., Hopkins F., et al., (2011), Results from the first national UK inter-laboratory calibration for very short-lived halocarbons., *Atmos.Meas.Tech.*, 4, 865-874 [10.5194/amt-4-865-2011].

Kollmann W., Barry T., Spurlock F., (2009), Methyl Iodide, Risk Characterisation Document for Inhalation Exposure, Volume III, Environmental Fate., Environment Monitoring Branch, Department of Pesticide Regulation, California Environmental Protection Agency.

Laing A., Evans J-L., (2011), Introduction to Tropical Meteorology (2nd edition), *University Corporation for the Atmospheric Research*.

Lau W., Waliser D., (2012), Intraseasonal Variability in the Atmosphere-Ocean Climate System.*Springer*.

Laube, J.C., Engel A., Bönisch H., Möbius T., Worton D.R., Sturges W., et al., (2008), Contribution of very short-lived organic substances to stratospheric chlorine and bromine in the tropics - a case study, *Atmos. Chem. Phys.*, 8 (23), 7325-7334 [10.5194/acp-8-7325-2008].

Leadbetter S., Burgin L., Hort M., Cooke M., (2014), Smethwick recycling plant fire – a Met Office perspective, *Chemical Hazards and Poisons Report*, September 2014, Issue 24, 4-6.

Levine J., Braesicke P., Harris N., Savage N., Pyle J., (2007), Pathways and timescales for troposphere-to-stratosphere transport via the tropical tropopause layer and their relevance for very short-lived substances. *J.Geophys.Res.*, 112, D04308 [10.1029/2005JD006940].

Levine J., Braesicke P., Harris N., Savage N., Pyle J., (2008), Seasonal and interannual variations in the troposphere-to-stratosphere transport from the tropical tropopause layer. *Atmos.Chem.Phys.*, 8, 813-823 [10.5194/acp-8-3689-2008].

Liang Q., Stolarski R., Kawa S., Nielsen J., Douglass A., et al., (2010), Finding the missing stratospheric Bry: a global modelling study of $CHBr_3$ and CH_2Br_2., *Atmos.Chem.Phys.*, 10, 2269-2286 [acp-10-2269-2010].

Liang Q., Atlas E., Blake D., Dorf M., Pfeilsticker K., et al., (2014), Convective transport of very short-lived bromocarbons to the stratosphere., *Atmos.Chem.Phys.*, 14, 5781-5792 [10.5194/acp-14-5781-2014].

Lin J., Gerbig C., Wofsy S., Chow V., Gottlieb E., et al., (2007), Designing Lagrangian experiments to measure regional-scale trace gas fluxes., *J.Geophys.Res.*, 112,

D13312 [10.1029/2006JD008077].

Lin J., Brunner D., Gerbig C., Stohl A., Luhar A., Webley P., (2012), Lagrangian modelling of the atmosphere., *American Geophysical Union, AGU* [10.1029/GM200].

Ling J., Li C., Li T., Jia X., Khouider B., Maloney E., et al., (2016), Challenges and opportunities in MJO studies., *BAMS*, [BAMS-D-16-0283.1].

Liu P., (2014), MJO structure associated with the higher-order CEOF modes, *Clim. Dyn.*, 43, 1939-1950 [10.1007/s00382-013-2017-0].

Lovelock J., (1975), Natural halocarbons in the air and in the sea., *Nature*, 256, 193-194.

MacKenzie A.R., Schiller C., et al., (2006), Tropopause and hygropause variability over the equatorial Indian Ocean during February and March 1999., *J.Geophys.Res.*, 111, D18112, [10.1029/2005JD006639].

Madden R., Julian P., (1972), Description of global-scale circulation cells in the tropics with a 40-50 day period, *J.Atmos.Sci.*, 28, 702-708.

Mahlman J.D., (1997), Dynamics of Transport Processes in the Upper Troposphere., *Science*, 276, 1079-1082 [10.1126/science.276.5315.1079].

Marandino C., Tegtmeier S., Kruger K., Zindler C., Atlas E., et al., (2013) Dimethylsulphide (DMS) emissions from the western Pacific Ocean: a potential marine source for stratospheric sulphur?, *Atmos.Chem.Phys.*, 13, 8427-8437 [10.5194/acp-13-8427-2013].

Maryon R.H., Best M.J., (1995), Estimating the emissions from a nuclear accident using observations of radioactivity with dispersion model products. *Atmo.Environ.*, 29, 1853-1869.

Maryon R.H., Ryall D.B., Malcolm A.L., (1999), NAME 4 dispersion model: Science documentation, turbulence and diffusion, note 262, Met Office.

MEI information website: https://www.esrl.noaa.gov/psd/enso/mei/, Earth System Research Laboratory, National Oceanic and Atmospheric Administration.

Meneguz E., Thomson D., (2014), Towards a new scheme for parameterisation of deep convection in NAME III., *International Journal of Environment and Pollution*, 54, 128-136.

Meneguz E., Thomson D., (2016), Parameterisation of deep convection in NAME III., NAME III Document, MD1/3, the UK Met Office.

Meneguz E., Thomson D., Witham C., Filus M., Harris N., Navarro M., Atlas E., (2016-2017), Improved parametrisation scheme to represent tropospheric moist convection in NAME., NAME documentation.

Montzka S., Reimann S., et al., (2011), Ozone depleting substances and related chemicals, in Scientific Assessment of Ozone Depletion 2010; Global Ozone Research and Modelling Project – Report No 52., Geneva, Switzerland.

Nassar R., Logan J., Megretskaia I., Murray L., Zhang L., (2009), Analysis of tropical tropospheric ozone, carbon monoxide, and water vapour during the El Nino using TES observations and the GEOS-Chem model., *J.Geophys.Res.*, 114, D17304 [10.1029/2009JD011760].

National Oceanic and Atmosphere Administration, (1976), The US Standard Atmosphere, http://www.srh.noaa.gov/jetstream/global/jet.html.

Navarro M., Atlas E., Saiz-Lopez A., Rodriguez-Lloveras X., Kinnison D., Filus M., Harris N., et.al., (2015), Airborne measurements of organic bromine compounds in the Pacific tropical tropopause layer., *PNAS*, 112, 13789–13793 [10.1073/pnas.1522889113].

Newell R., (1961), The transport of trace substances in the atmosphere and their implications for the general circulation of the stratosphere, *Geof.Pura.et.Appl.*, 49 ,137-158 [10.1007/BF01992149].

Newton R., Vaughan G., Ricketts H., Pan L., Weinheimer A., et al., (2016), Ozonesonde profiles from the West Pacific Warm Pool: measurements and validation., *Atmos.Chem.Phys.*, 16, 619-634 [10.5194/acp-16-619-2016].

O'Brien L., Harris N., Robinson A., Gostlow B., Warwick N., et al., (2009), Bromocarbons in the tropical marine boundary layer at the Cape Verde observatory – measurements and modelling., *Atmos.Chem.Phys.*, 9, 9083-9099 [10.5194/acp-9-9082-2009].

Oram D., Penkett S., (1994), Observations in eastern England of elevated methyl iodide concentrations in air of Atlantic origin., *Atmos.Environ.*, 28,1159-1174 [10.1016/1352-2310(94)90293-3].

Ordonez C., Lamarque J-F., Tilmes S., Kinnison D., Atlas E., et al., (2012), Bromine and iodine chemistry in a global chemistry-climate model: description and evaluation of very short-lived oceanic sources., *Atmos.Chem.Phys.*, 12, 1423-1447 [10.5194/acp-12-1423-2012].

Pan L., Bowman K., Shapiro M., Randel W., Gao R., et al., (2007), Chemical behaviour of the tropopause observed during the Stratosphere-Troposphere Analyses of

Regional Transport Experiment., *J.Geophys.Res.Atmospheres*, 112, [10.1029/2007JD008645].

Pan L., Honomichl S., Randel W., Apel E., Atlas E., et al., (2015), Bimodal distribution of free tropospheric ozone over the tropical western Pacific revealed by airborne observation., Geophys.Res.Letters., [10.1002/2015GL065562].

Pan L., Atlas E., Salawitch R., Honomichl S., Bresch J. et al.,(2017), The Convective Transport of Active Species in the Tropics, CONTRAST, Experiment. *BAMS*, [10.1175/BAMS-D-14-00272.1].

Papanastasiou D., McKeen S., Burkholder J., (2014), The very short-lived ozone depleting substance $CHBr_3$ (bromoform): revised UV absorption spectrum, atmospheric lifetime and ozone depletion potential. *Atmos.Chem.Phys.*, 14, 3017-3025 [10.5194/acp-14-3017-2014].

Park, S., Atlas, E. L., Jiménez, R., Daube, B. C., Gottlieb, E. W., Nan, J., Jones, D. B. A.,Pfister, L., Conway, T. J., Bui, T. P., Gao, R.-S., and Wofsy, S. C., (2010), Vertical transport rates and concentrations of OH and Cl radicals in the Tropical Tropopause Layer from observations of CO2 and halocarbons: implications for distributions of long- and shortlived chemical species, *Atmos.Chem.Phys.*, 10, 6669-6684, [10.5194/acp-10-6669-2010].

Personal Communication with Xin Yang, Centre for Atmospheric Science, Cambridge, 2013.

Personal Communication with the UK Meteorological Office, Exeter, 2014 and 2015.

Pfeilsticker K., Sturges W., Bosch W., Camy-Peyret C., Chipperfield M., Engel P., et al., (2000), Lower stratospheric organic and inorganic bromine budget for the arctic winter 1998/1999., *Geophys.Res.Lett.*, 27,3305-3308 [10.1029/2000GL011650].

Pickering K., Thompson A., Scala J., Tao W., Simpson J., (1992), Ozone production potential following convective redistribution of biomass burning emissions., *J.Atmos.Chem*., 14, 297-313.

Pommereau J.-P., (2010), Troposphere-to-stratosphere transport in the Tropics., *Compt.Rend.Geos., Elsevier Masson*, 342, 331-338 [10.1016/j.crte.2009.10.015-hal-00448401].

Pyle J., Ashfold M., Harris N., Robinson A., Warwick N., Carver G., et al., (2011), Bromoform in the tropical boundary layer of the Maritime Continent during the OP3., *Atmos.Chem.Phys.*, 11, 529-542 [10.5194/acp-11-529-2011].

Quack B., Wallace D., (2003), Air-sea flux of bromoform: Controls, rates and

implications., *Global Biogeochem. Cy.*, 17, 1023 [10.1029/2002GB001890].

Randel W., Jensen E., (2013), Physical processes in the tropical tropopause layer and their roles in a changing climate., *Nature Geoscience*, [10.1038/NGE01733].

Rui H., Wang B., (1990), Development characteristics and dynamic structure of tropical intraseasonal convection anomalies, *J.Atmos.Sci.*, 47, 357-379.

Roscoe H-K., (2006), The Brewer-Dobson circulation in the stratosphere and mesosphere – is there a trend?, *Advan.Space.Res.*, 38, 2446-2451 [10.1016/j.asr.2006.02.078].

Russo M., Marecal V., Hoyle C., Arteta J., Chemel C., et al., (2011), Representation of deep convection in atmospheric models – Part 1: Meteorology and comparison with satellite observations., *Atmos.Chem.Phys.*, 11, 2765-2786 [10.5194/acp-11-2765-2011].

Russo M., Ashfold M., Harris N., Pyle J., (2015), On the emissions and transport of bromoform sensitivity to model resolution and emission location., *Atmos.Chem.Phys.*, 15, 14031-14040 [10.5194/acp-15-14031-2015].

Ryall D.B., Maryon R.H., (1998), Validation of the UK Met Office's NAME model against the ETEX dataset, *Atmospheric Environment*, 32, 4265-4276 [10.1016/S1352-2310(98)00177-0].

Saiz-Lopez A., Plane J., Baker A., Carpenter L., von Glasow R., et al., (2012), Atmospheric chemistry of iodine., *Chem. Rev.*, 112, 1773-1804 [10.1021/cr200029u].

Saiz-Lopez A., Fernandez R., Ordonez C., Kinnison D., Gomez-Martin J., et al., (2014), Iodine chemistry in the troposphere and its effects on ozone., *Atmos.Chem.Phys.*, 14, 13119-13143 [10.5194/acp-14-13119-2014].

Saiz-Lopez A., Baidar S., Cuevas C., Volkamer R., (2015), Injection of iodine to the stratosphere., *Geophys.Res.Lett.*, 42, 6852-6859 [10.1002/2015GL064796] .

Salawitch R., (2006), Atmospheric chemistry: biogenic bromine., *Nature*, 439, 275-277.

Salby M.L., (2012), Physics of the Atmosphere and Climate, *Cambridge University Press*, New York, USA.

Schauffler, S.M., Atlas E., Flocke F., Lueb R., Stroud V., Travnicek W., (1998), Measurements of bromine containing organic compounds at the tropical tropopause. *Geophys. Res. Let.*, 25, 317-310, [10.1029/98GL00040].

Schauffler, S. M., Atlas E.L., Blake D., Flocke F.M., Lueb R.A., Lee-Taylor J.M., Stroud V.F., Travnicek W., (1999): Distributions of brominated organic compounds in the

troposphere and lower stratosphere. *J.Geophys.Res.-Atmosphere*, 104, 21513-21535, [10.1029/1999JD900197].

Schofield R., Fueglistaler S., Wohltmann I., Rex M., (2011), Sensitivity of stratospheric Bry to uncertainties in very short lived substance emissions and atmospheric transport. *Atmos.Chem.Phys.*, 11, 1379-1392 [10.5194/acp-11-1379-2011].

Schwing F., Mendelssohn R., Bograd S., Overland J., Wang M., et al., (2010), Climate change, teleconnection patterns, and regional processes forcing marine populations in the Pacific., *J.Mar.Systems*, 79, 245-257 [10.1016/jmarsys.2008.11.027].

Seinfeld J., Pandis S., (2016), Atmospheric Chemistry and Physics: From Air Pollution to Climate Change, 3nd edition, Ch.17; Wiley-Interscience.

Sherwen T., Schmidt J., Evans M., Carpenter L., Grossman K., et al., (2016), Global impacts of tropospheric halogens (Cl, Br, I) on oxidants and composition in GEOS-Chem., *Atmos.Chem.Phys.*, [10.5194/acp-2016-12239-2016].

Sinnhuber B-M., Folkins I., (2006), Estimating the contribution of bromoform to stratospheric bromine and its relation to dehydration in the tropical tropopause layer., *Atmos. Chem. Phys.*, 6, 4755–4761 [10.5194/acp-6-4755-2006].

Solomon S., Garcia R., Ravinshankara A. (1994), On the role of iodine in ozone depletion., *J.Geophys.Res.*, 99, 20941 [10.1029/94JD02028].

Stemmler I., Hense I., Quack B., Maier-Reimer E., (2014), Methyl iodide production in the open ocean. *Biogeosciences*, 11, 4459-4476 [10.5194/bg-11-4459-2014].

Stohl A., (1998), Computation, Accuracy and Applications of Trajectories: A review and bibliography. *Atmospheric Environment*, 32, 947-966.

Stohl A., Cooper O., Damoah R., Fehsenfeld F., Forster C., Hsie E-Y., et al., (2004), Forecasting for a Lagrangian aircraft campaign., *Atmos.Chem.Phys*., 4, 1113-1124 [10.5194/acp-4-1113-2004].

Su H., Jiang J., (2013), Tropical Clouds and Circulation Changes during the 2006/07 and 2009/10 El Ninos, *Journal of Climate, American Meteorological Society*, 26, 399-413 [10.1175/JCLI-D-12-00152.1].

Tegtmeier S., Kruger K., Quack B., Atlas E., Pisso I., et al., (2012), Emission and transport of bromocarbons: from the West Pacific ocean into the stratosphere., *Atmos.Chem.Phys.*, 12, 10633-10648 [10.5194/acp-12-10633-2012].

Tegtmeier S., Kruger K., Quack B., Atlas E., Blake D., Boenish H., Engel A., Hepach

H., Hossaini R., Navarro M., Raimund S., Sala S., Shi Q., Ziska F., (2013), The contribution of oceanic methyl iodide to stratospheric iodine., *Atmos.Chem.Phys.*, 13, 11869-11886 [10.5194/acp-13-11869-2013].

Tegtmeier S., Ziska F., Pisso I., Quack B., Velders G., et al., (2015), Oceanic bromoform emissions weighted by their ozone depletion potential., *Atmos.Chem.Phys.*, 15, 13647-13663 [10.5194/acp-15-13647-2015].

UK Meteorological Office, Radioactive Dispersion modelling, leaflet; www.metoffice.gov.uk/media/pdf/m/n/DispersionLeaflet_Nuclear.pdf.

Vogt R., Sander R., von Glasow R., Crutzen P., (1999), Iodine chemistry and its role in halogen activation and ozone loss in the marine boundary layer?: a model study., *J.Atmos.Chem.*, 32,375-395 [10.1023/A:1006179901037].

Verner J-P., Pommereau J-P., Thomason L., Pelon J., Garnier A., et al., 2011), Overshooting of Clean Tropospheric Air in the Tropical Lower Stratosphere as Seen by the CALIPSO lidar., *Atmos.Chem.Phys.*, 11, 9683-9696 [10.5194/acp-11-9683-2011].

Voulgarakis A., Hadjinicolaou P., Pyle J.A., (2011), Increases in global tropospheric ozone following an El Niño event: examining stratospheric ozone variability as a potential driver. *Atmos.Sci.Let.*, 12, 228-232 [10.1002/asl.318].

Waliser D., Sperber K., Hendon H., Kim D., Maloney E., et al., (2009), MJO Simulation Diagnostics., *Journal of Climate*, *American Meteorological Society*, 22, 3006-3030.

Wallace J., Hobbs P., (2006), Atmospheric Science, Second Edition: An Introductory Survey., Academic Press.

Wang B., Liu F., Chen G., (2016), A trio-interaction theory for Madden-Julian oscillation., *Geos.Lett.*, [10.1186/s40562-016-0066-z].

Wang C., Deser C., Yu J-Y., DiNezio P., Clement A., (2012), El Niño and Southern Oscillation (ENSO): A Review., NOAA [10.1007/978-94-017-7499-4_4].

Wang S., Schmidt J., Baidar S., Coburn S., Dix B., et al., (2015), Active and widespread halogen chemistry in the tropical and subtropical free troposphere., *PNAS*, [10.1073/pnas.1505142112].

Webster, H.N., Thomson, D.J., Johnson, B.T., Heard, I.P.C., Turnbull, K., Marenco, F., Kristiansen, N.I., Dorsey, J., Minikin, A., Weinzierl, B., Schumann, U., Sparks, R.S.J., Loughlin, S.C., Hort, M.C., Leadbetter, S.J., Devenish, B.J., Manning, A.J., Witham, C.S.,

Haywood, J.M. and Golding, B.W., (2012), Operational prediction of ash concentrations in the distal volcanic cloud from the 2010 Eyjafjallajokull eruption, *Journal of Geophysical Resesarch*, [10.1029/2011JD016790, 117, D00U08] .

Wisher, A., Oram D.E., Laube J.C., Mills G.P., van Velthoven P., Zahn A., Brenninkmeijer C.A.M., (2014), Very short-lived bromomethanes measured by the CARIBIC observatory over the North Atlantic, Africa and Southeast Asia during 2009-2013., *Atmos.Chem.Phys.*, 14, 3557-3570 [10.5194/acp-14-3557-2014].

Witham C., Webster H., Hort M., Jones A., Thomson D.J., (2011), Modelling concentrations of volcanic ash encountered by aircraft in past eruptions, *Atmospheric Environment*, [10.1016/j.atmosenv.2011.06.073].

Wohltmann I., Rex M., (2009), The Lagrangian chemistry and transport model ATLAS: validation of advective transport and mixing., *Geoscientific Model Development*, 2, 153-173 [10.5194/gmd-2-153-2009].

Yeh S-W., Kug J-S., Dewitte B., Kwon M-H., Kirtman B., et al., (2009), El Niño in a changing climate., *Nature*, 461, 511-515 [10.1038/nature08316].

Zeng G., Pyle J., (2005), Influence of El Niño Southern Oscillation on stratosphere/troposphere exchange and the global tropospheric ozone budget., *Geophysical Research Letters*, 32, L01814 [10.1029/2004GL021353].

Zhang C., (2005), Madden-Julian Oscillation, *Rev.Geophys.*, 43, 1-36 [10.1029/2004RG000158].

Zhang C., (1993), Large-Scale Variability of Atmospheric Deep Convection in Relation to Sea Surface Temperature in the Tropics, Journal of Climate, *Amer.Meteorol.Soc.*, 6, 1898-1913 [10.1175/1520-0442(1993)006<1898].

Zhang C., (2013), Madden-Julian Oscillation. Bridging Weather and Climate., *BAMS*, 1849-1870 [10.1175/BAMS-D-12-00026.1].

Ziemke J., Douglass A., Oman L., Strahan S., Duncan B., (2015), Tropospheric ozone variability in the tropics from ENSO and MJO and shorter timescales. *Atmos.Chem.Phys.*, 15, 8037-8049 [10.5194/acp-15-8037-2015].

Ziska F., Quack B., Abrahamsson K., Archer S., Atlas E., et al., (2013), Global sea-to-air flux climatology for bromoform, dibromomethane and methyl iodide., *Atmos.Chem.Phys.*, 13, 8915-8934 [10.5194/acp-13-8915-2013].

Appendix

APPENDIX 1. Chapter 5: Convective Influence on the Methyl Iodide in the TTL

The AWAS CH_3I observations and the NAME quantified CH_3I, including the boundary layer and background contribution estimates, are collated in the tables below. These apply to the individual ATTREX 2014 Research Flight 02 (A1.5.1, Chapter 5. Figure 5.11), all ATTREX 2014 (A1.5.2, Chapter 5. Figure 5.12) and 2013 (A1.5.3 Chapter 5. Figure 5.13) flights.

A1.5.1 Research Flight 02, ATTREX 2014 (Figure 5.11)

[CH_3I]	***AWAS [ppt]***	***NAME Boundary Layer Contribution [ppt]***	***NAME Background [ppt]***	***NAME Background Contribution [ppt]***	***NAME Boundary Layer and Background Contribution [ppt]***
17-18 km	**0.06** **(0.02)** **0.06**	0.00 (0.00) 0.00	0.06 (0.02)	0.06	**0.06** **(0.02)** **0.06**
16-17 km	**0.09** **(0.03)** **0.08**	0.00 (0.00) 0.00	0.06 (0.02)	0.06	**0.06** **(0.02)** **0.06**
15-16 km	**0.17** **(0.03)** **0.17**	0.04 (0.04) 0.03	0.10 (0.04)	0.08	**0.12** **(0.06)** **0.11**
14-15 km	**0.23** **(0.09)** **0.24**	0.17 (0.04) 0.19	0.08 (0.07)	0.04	**0.21** **(0.08)** **0.23**

TTL altitude	**NAME 1 KM fraction [%]**	**NAME Background fraction [%]**
17-18 km	2.1 (1.1) 1.8	97.9
16-17 km	7.2 (2.7) 7.2	92.8
15-16 km	22.9 (10.0) 19.4	77.1
14-15 km	53.3 (9.0) 56.0	46.7

A1.5.2 All ATTREX 2014 Research Flights (Figure 5.12)

[CH_3I]	*AWAS [ppt]*	*NAME Boundary Layer Contribution [ppt]*	*NAME Background [ppt]*	*NAME Background Contribution [ppt]*	*NAME Boundary Layer and Background Contribution [ppt]*
17-18 km	**0.04** **(0.03)** **0.05**	0.02 (0.03) 0.01	0.06 (0.02)	0.05	**0.07** **(0.04)** **0.06**
16-17 km	**0.11** **(0.10)** **0.07**	0.04 (0.04) 0.03	0.06 (0.02)	0.05	**0.09** **(0.05)** **0.08**
15-16 km	**0.16** **(0.14)** **0.12**	0.09 (0.07) 0.09	0.10 (0.04)	0.06	**0.15** **(0.08)** **0.15**
14-15 km	**0.17** **(0.14)** **0.13**	0.15 (0.08) 0.15	0.08 (0.07)	0.04	**0.19** **(0.11)** **0.19**

TTL altitude	**NAME 1 KM fraction [%]**	**NAME Background fraction [%]**
17-18 km	12.7 (10.9) 9.8	87.3
16-17 km	22.3 (16.0) 19.3	77.7
15-16 km	37.8 (18.8) 38.9	62.2
14-15 km	51.7 (16.1) 55.4	48.3

A1.5.3 All ATTREX 2013 Research Flights (Figure 5.13)

[CH_3I]	*AWAS [ppt]*	*NAME Boundary Layer Contribution [ppt]*	*NAME Background [ppt]*	*NAME Background Contribution [ppt]*	*NAME Boundary Layer and Background Contribution [ppt]*
17-18 km	**0.03** **(0.02)** **0.03**	0.00 (0.00) 0.00	0.03 (0.01)	0.03	**0.03** **(0.01)** **0.03**

16-17 km	**0.03** **(0.02)** **0.03**	0.00 (0.00) 0.00	0.03 (0.02)	0.03	**0.03** **(0.02)** **0.03**
15-16 km	**0.04** **(0.02)** **0.04**	0.01 (0.01) 0.00	0.03 (0.03)	0.02	**0.03** **(0.03)** **0.04**
14-15 km	**0.04** **(0.03)** **0.04**	0.01 (0.01) 0.01	0.04 (0.03)	0.04	**0.05** **(0.03)** **0.04**

TTL altitude	**NAME 1 KM fraction [%]**	**NAME Background fraction [%]**
17-18 km	1.9 (2.3) 1.2	98.1
16-17 km	4.7 (4.9) 3.6	95.3
15-16 km	9.8 (7.9) 5.8	90.2
14-15 km	14.7 (11.1) 12.0	85.3

APPENDIX 2. Chapter 6: Representation of Deep Convection in NAME

Tables A2.6.1-5 show the CH_3I AWAS observations, and the corresponding NAME calculated CH_3I boundary layer contribution, inferred from the NAME 1 km fractions, and the modelled sums of CH_3I boundary layer and background contribution estimates for ATTREX 2014 individual flights: RF02, RF03, RF04 and RF05. This is to compare the results produced from the NAME runs with convection scheme switched off (NOCONV) and the new convection scheme activated (NEWCONV). Format: Means (Standard Deviations) Medians.

A2.6.1 CH_3I AWAS Observations, ATTREX 2014 RFs 02-05

TTL Altitude	**CH_3I AWAS Observations / [ppt]**			
	RF02	**RF03**	**RF04**	**RF05**
17-18 km	0.06 (0.02) 0.06	0.07 (0.04) 0.05	0.05 (0.02) 0.04	0.03 (0.01) 0.03
16-17 km	0.09 (0.03) 0.08	0.27 (0.13) 0.25	0.08 (0.03) 0.08	0.07 (0.04) 0.06
15-16 km	0.17 (0.03) 0.16	0.39 (0.17) 0.42	0.12 (0.03) 0.11	0.13 (0.06) 0.14
14-15 km	0.23 (0.09) 0.24	0.43 (0.23) 0.39	0.14 (0.04) 0.13	0.19 (0.09) 0.19

A2.6.2 Research Flight 02, ATTREX 2014 (Figure 6.2)

TTL Altitude	**NAME [CH_3I] Boundary Layer Contribution [ppt]**		**NAME [CH_3I] Boundary Layer and Background Contribution [ppt]**	
	NOCONV	**NEWCONV**	**NOCONV**	**NEWCONV**
17-18 km	0.00 (0.00) 0.00	0.00 (0.00) 0.00	0.04 (0.03) 0.04	0.06 (0.02) 0.06
16-17 km	0.00 (0.00) 0.00	0.00 (0.00) 0.00	0.06 (0.02) 0.06	0.06 (0.02) 0.06
15-16 km	0.01 (0.01) 0.00	0.04 (0.03) 0.03	0.11 (0.06) 0.11	0.12 (0.06) 0.12
14-15 km	0.04 (0.02) 0.04	0.17 (0.04) 0.18	0.09 (0.08) 0.09	0.21 (0.08) 0.22

TTL altitude	NAME 1 KM fraction [%]	
	NOCONV	NEWCONV
17-18 km	0.4 (0.3)	2.1 (1.1)
16-17 km	1.6 (0.7)	7.2 (2.7)
15-16 km	6.1 (6.5)	22.9 (10.0)
14-15 km	40.2 (20.1)	53.3(9.0)

A2.6.3 Research Flight 03, ATTREX 2014 (Figure 6.3)

TTL Altitude	NAME [CH_3I] Boundary Layer Contribution [ppt]		NAME [CH_3I] Boundary Layer and Background Contribution [ppt]	
	NOCONV	NEWCONV	NOCONV	NEWCONV
17-18 km	0.00 (0.00) 0.00	0.06 (0.04) 0.05	0.04 (0.03) 0.04	0.10 (0.04) 0.10
16-17 km	0.01 (0.00) 0.01	0.08 (0.04) 0.08	0.06 (0.02) 0.06	0.12 (0.04) 0.12
15-16 km	0.04 (0.03) 0.03	0.14 (0.07) 0.12	0.11 (0.07) 0.10	0.19 (0.08) 0.19
14-15 km	0.08 (0.06) 0.05	0.20 (0.07) 0.18	0.13 (0.10) 0.10	0.23 (0.10) 0.24

TTL altitude	NAME 1 KM fraction [%]	
	NOCONV	NEWCONV
17-18 km	5.0 (2.9)	27.3 (13.4)
16-17 km	15.0 (5.2)	43.3 (8.2)
15-16 km	37.9 (11.8)	57.8 (10.2)
14-15 km	50.1 (12.1)	68.3 (7.7)

A2.6.4 Research Flight 04, ATTREX 2014 (Figure 6.4)

TTL Altitude	NAME [CH_3I] Boundary Layer Contribution [ppt]		NAME [CH_3I] Boundary Layer and Background Contribution [ppt]	
	NOCONV	NEWCONV	NOCONV	NEWCONV
17-18 km	0.00 (0.00) 0.00	0.01 (0.01) 0.01	0.04 (0.03) 0.04	0.06 (0.02) 0.07
16-17 km	0.01 (0.00) 0.01	0.05 (0.03) 0.04	0.06 (0.02) 0.06	0.09 (0.03) 0.09

15-16 km	0.01 (0.00) 0.01	0.10 (0.02) 0.10	0.10 (0.06) 0.10	0.14 (0.05) 0.13
14-15 km	0.02 (0.02) 0.02	0.12 (0.03) 0.11	0.09 (0.08) 0.09	0.16 (0.08) 0.16

TTL altitude	**NAME 1 KM fraction [%]**	
	NOCONV	**NEWCONV**
17-18 km	2.1 (1.1)	14.1 (5.4)
16-17 km	13.3 (7.4)	33.3 (14.4)
15-16 km	22.6 (3.7)	54.7 (5.5)
14-15 km	26.7 (12.1)	56.2 (5.8)

A2.6.5 Research Flight 05, ATTREX 2014 (Figure 6.5)

TTL Altitude	**NAME [CH_3I] Boundary Layer Contribution [ppt]**		**NAME [CH_3I] Boundary Layer and Background Contribution [ppt]**	
	NOCONV	**NEWCONV**	**NOCONV**	**NEWCONV**
17-18 km	0.00 (0.00) 0.00	0.01 (0.01) 0.01	0.04 (0.03) 0.04	0.06 (0.02) 0.06
16-17 km	0.01 (0.00) 0.01	0.03 (0.02) 0.03	0.06 (0.02) 0.06	0.08 (0.03) 0.08
15-16 km	0.01 (0.01) 0.01	0.09 (0.04) 0.09	0.10 (0.06) 0.10	0.14 (0.06) 0.17
14-15 km	0.05 (0.04) 0.03	0.19 (0.09) 0.19	0.10 (0.09) 0.09	0.21 (0.08) 0.24

TTL altitude	**NAME 1 KM fraction [%]**	
	NOCONV	**NEWCONV**
17-18 km	2.8 (1.5)	6.9 (6.3)
16-17 km	8.6 (4.7)	25.4 (11.4)
15-16 km	17.5 (7.9)	47.6 (9.7)
14-15 km	38.5 (20.8)	65.3 (6.6)

APPENDIX 3. Chapter 6. Representation of Deep Convection Scheme in NAME

Convective cloud top heights, being one of the NAME modelled meteorological output from the NAME runs for the ATTREX 2014 Research Flights, are plotted for the Research Flights 02, 03 and 05. These flights featured sampling the air masses directly influenced by deep convective motions. These convective cloud top heights maps are contrasted with maps featuring the outgoing longwave radiation, OLR, obtained from the satellite measurements [Earth System Research Laboratory, National Oceanic and Atmospheric Administration, https://www.esrl.noaa.gov/psd/data/gridded/data.uninterp_OLR.html]. OLR is a measure of the amount of energy emitted to space by the Earth's surface, oceans and atmosphere. As such, it is a critical component of the earth's radiation budget. In a different context, OLR values are often used as a proxy for convection in tropical and subtropical regions since cloud top temperatures (colder is higher) are an indicator of cloud height. The higher (lower), colder (warmer) cloud tops imply more (less) convective activity. The higher (lower) cloud tops emit much less (more) infrared radiation into space. Low (high) outgoing longwave radiation, measured in Wm^{-2}, is indicative of enhanced (suppressed) convection.

A3.6.1 ATTREX 2014 Research Flight 02 16-17/02/2014

RF02 experiences high convective cloud tops below 10^{o}N within the 140-160^{o}E band (Figure A3.6.1). This system does not change significantly over a flight period. Areas of high convective cloud tops correlate with areas of low outgoing longwave radiation (Figure A3.6.2).

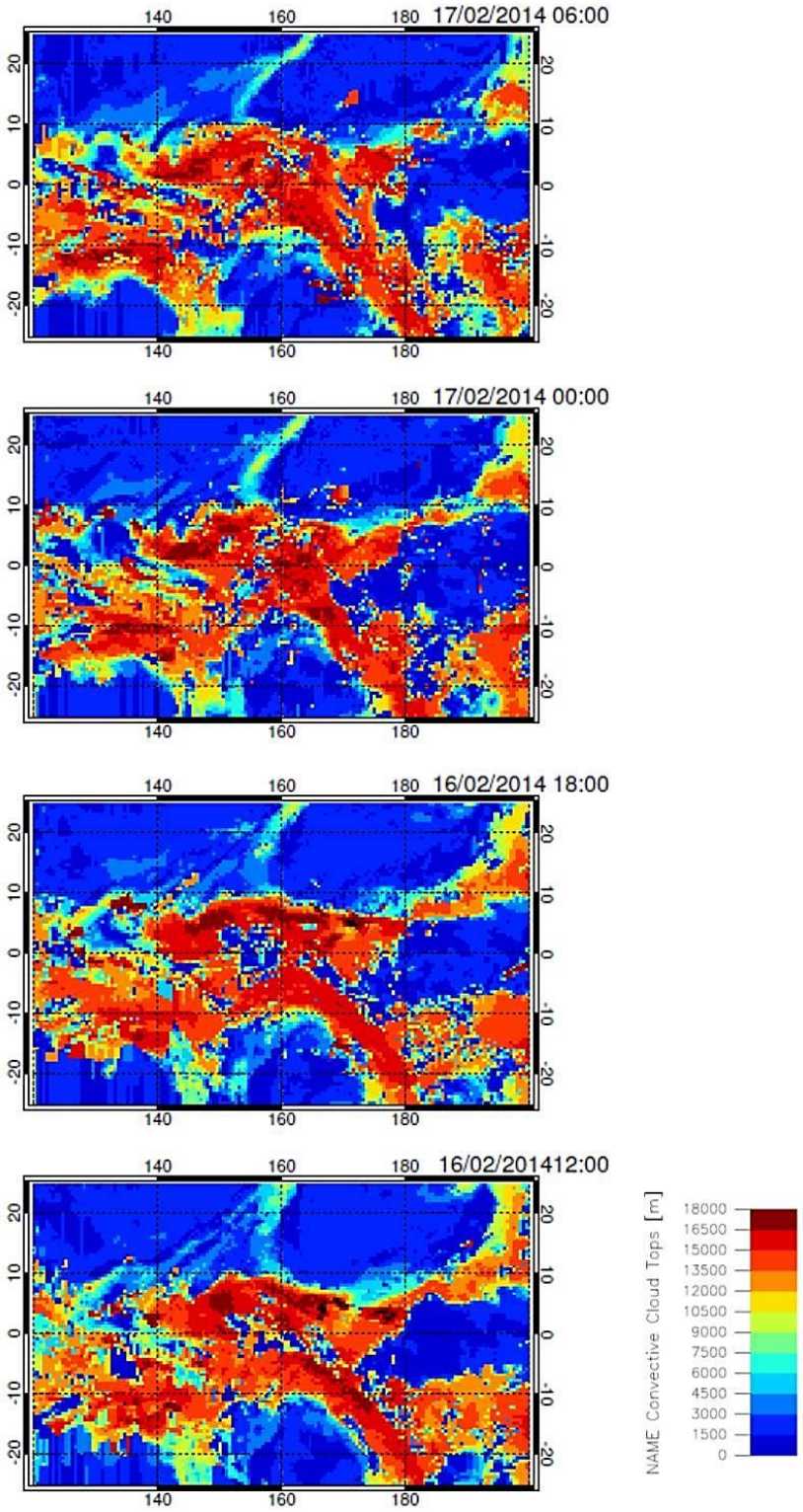

Figure A3.6.1 Convective cloud top heights for the ATTREX Research Flight 02. NAME modelled output (0.5 x 0.5 deg^2 model output, derived from Unified Model analyses of meteorological fields with horizontal resolution of 0.325 x 0.245).

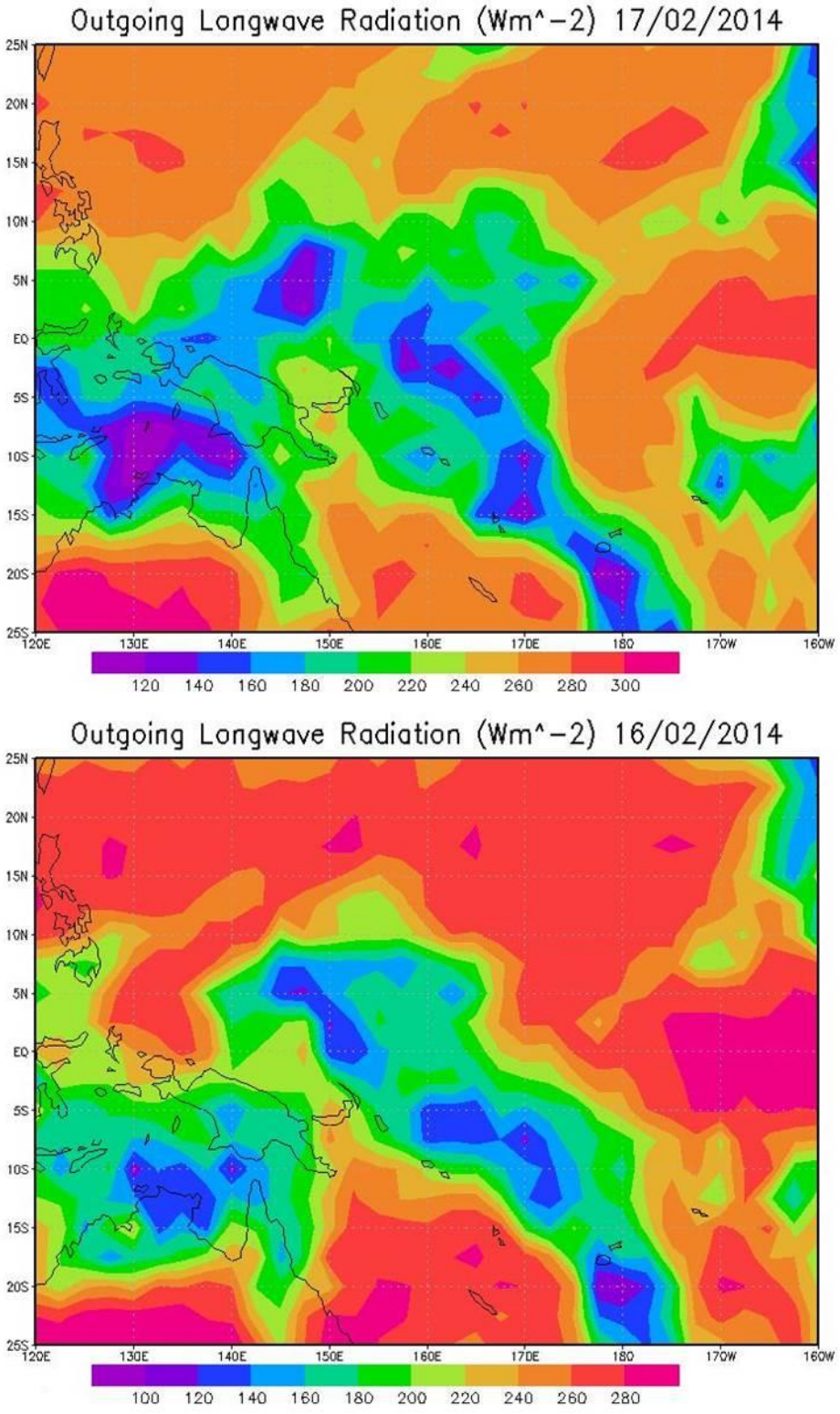

Figure A3.6.2 Outgoing Longwave Radiation daily means for the ATTREX Research Flight 02 (horizontal resolution of 2.5 deg x 2.5 deg).

A3.6.2 ATTREX 2014 Research Flight 03 04-05/03/2014

These convective cloud top images (Figure A3.6.3) feature an evolution of the Faxai tropical cyclone (with a diagonal path confined within 150-155^{o}E and 5-25^{o}N). Another system which shows high convective cloud top heights is marked within 160-165^{o}E, 0-10^{o}N and 150-160^{o}E, 15^{o}S-0. These areas contribute most of the NAME modelled boundary layer air to the air sampled along the RF03 flight path. High convective cloud tops areas are coincident with areas of low outgoing longwave radiation displayed in Figure A3.6.4.

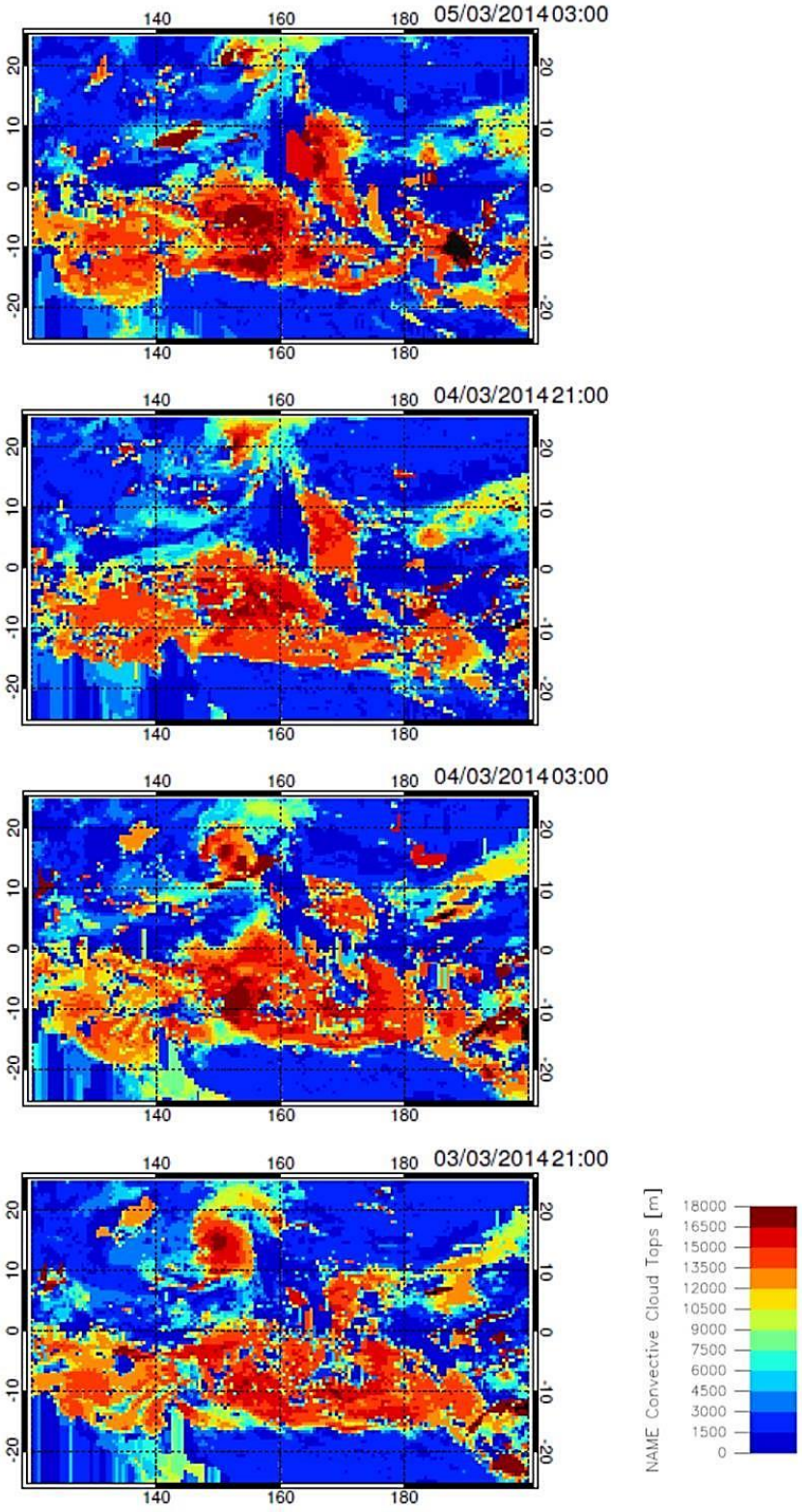

Figure A3.6.3 Convective cloud top heights for the ATTREX Research Flight 03. NAME modelled output (0.5 x 0.5 deg^2 model output, derived from Unified Model analyses of meteorological fields with horizontal resolution of 0.325 x 0.245).

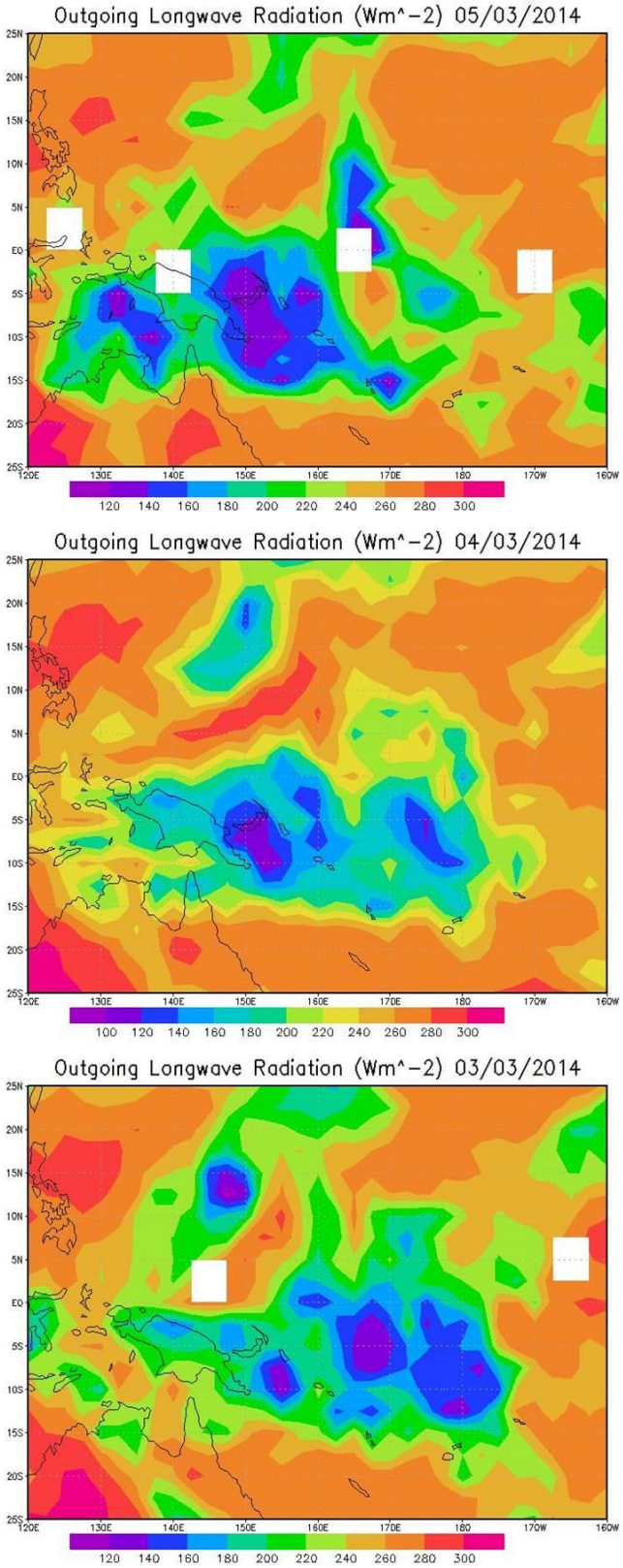

Figure A3.6.4 Outgoing Longwave Radiation daily means for the ATTREX Research Flight 03 (horizontal resolution of 2.5 deg x 2.5 deg).

A3.6.3 ATTREX 2014 Research Flight 05 09-10/03/2014

These images (Figure A3.6.5) show high convective cloud tops predominantly on the Southern Hemisphere within the 155-170^{o}E, 10-20^{o}S. This is coincident with the area where a tropical cyclone Lusi originated from at the time of a research flight. This is coincident with areas of low outgoing longwave radiation presented in Figure A3.6.6.

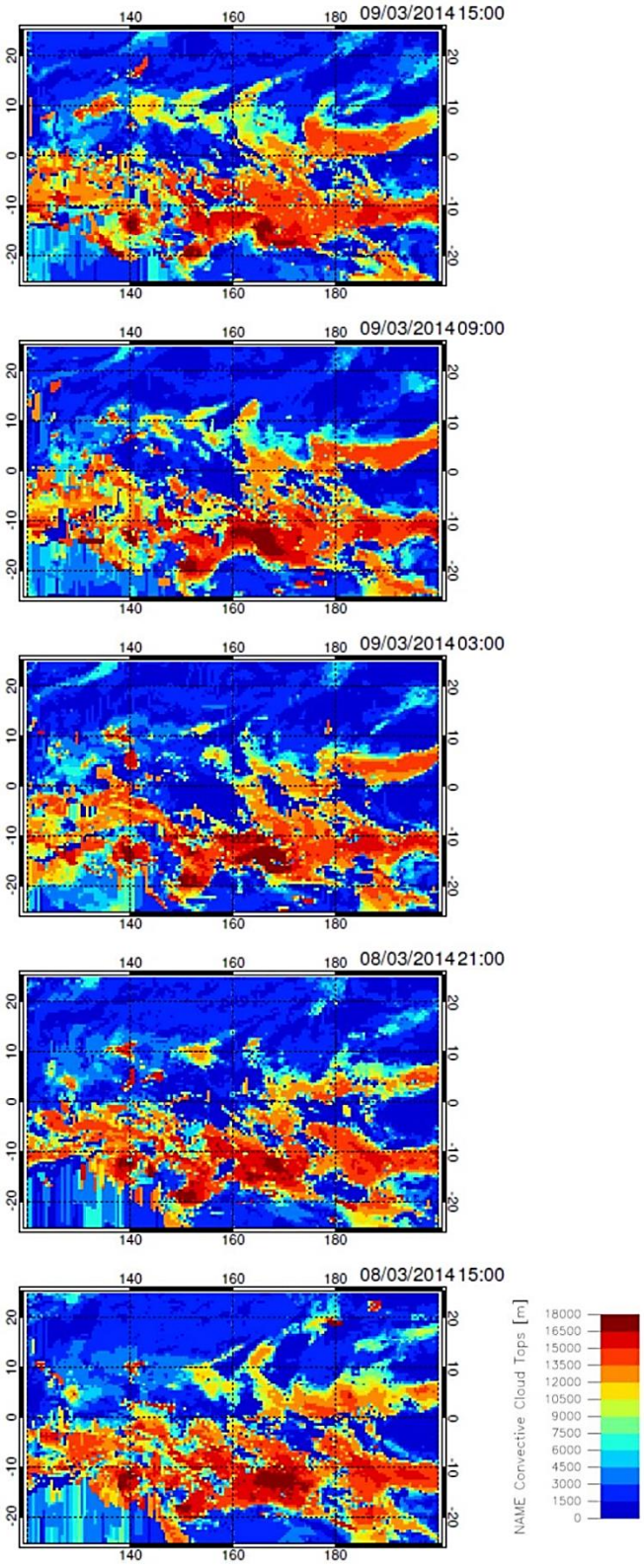

Figure A3.6.5 Convective cloud top heights for the ATTREX Research Flight 05. NAME modelled output (0.5 x 0.5 deg^2 model output, derived from Unified Model analyses of meteorological fields with horizontal resolution of 0.325 x 0.245).

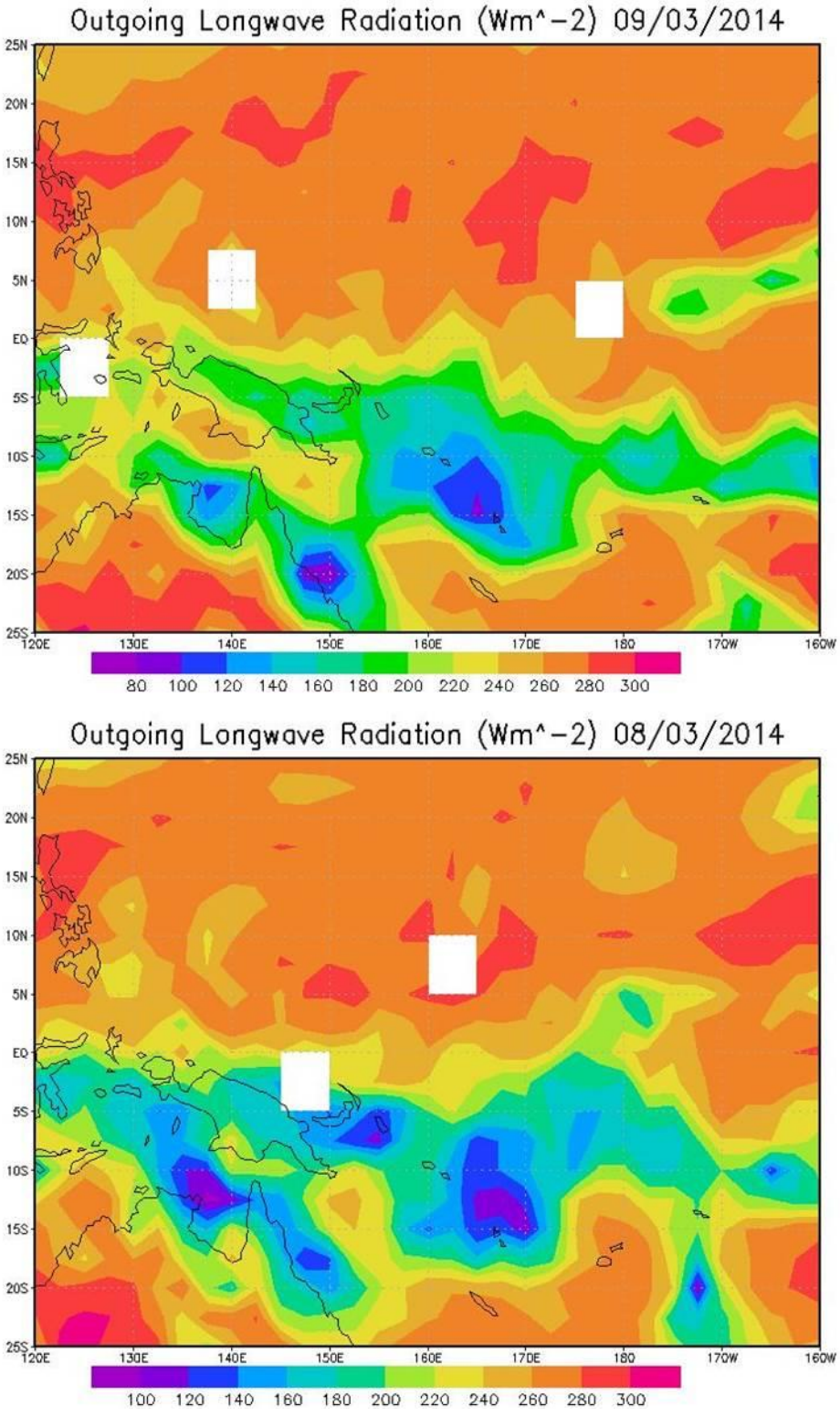

Figure A3.6.6 Outgoing Longwave Radiation daily means for the ATTREX Research Flight 05 (horizontal resolution of 2.5 deg x 2.5 deg).

APPENDIX 4. Chapter 7. Transport and Distribution of Short-Lived Brominated Organic Substances in the TTL

The following tables show the calculations used in this chapter. A4.7.1-3 show the $CHBr_3$ and CH_2Br_2 AWAS observations and NAME calculated estimates of the boundary layer and background contribution to the TTL for the individual ATTREX 2014 Research Flight 02, all the ATTREX 2014 and 2013 flights. A4.7.4-6 show the 12- and 30-day calculations for the boundary layer contribution and the modelled sums of the boundary layer and background contribution estimates for the ATTREX 2014 RF02, ATTREX 2014 and 2013 flights. A4.7.7 shows the calculations for the contribution of short-lived bromocarbons to the active bromine loading in the TTL. Format: Mean (Standard Deviation) Median* (*not in every entry).

A4.7.1 ATTREX 2014 Research Flight 02

[$CHBr_3$]	***AWAS [ppt]***	***NAME Boundary Layer Contribution [ppt]***	***NAME Background [ppt]***	***NAME Background Contribution [ppt]***	***NAME Boundary Layer and Background Contribution [ppt]***
17-18 km	**0.34** **(0.17)** **0.28**	0.01 (0.00) 0.01	0.29 (0.15)	0.28	**0.29** **(0.15)** **0.29**
16-17 km	**0.42** **(0.11)** **0.41**	0.03 (0.01) 0.03	0.36 (0.14)	0.33	**0.36** **(0.14)** **0.36**
15-16 km	**0.55** **(0.06)** **0.55**	0.12 (0.07) 0.10	0.46 (0.15)	0.35	**0.48** **(0.17)** **0.45**
14-15 km	**0.67** **(0.10)** **0.68**	0.35 (0.07) 0.37	0.51 (0.11)	0.24	**0.58** **(0.13)** **0.60**

[CH_2Br_2]	***AWAS [ppt]***	***NAME Boundary Layer Contribution [ppt]***	***NAME Background [ppt]***	***NAME Background Contribution [ppt]***	***NAME Boundary Layer and Background Contribution [ppt]***

17-18 km	**0.72** **(0.02)** **0.71**	0.02 (0.01) 0.01	0.71 (0.02)	0.69	**0.71** **(0.03)** **0.71**
16-17 km	**0.79** **(0.07)** **0.78**	0.06 (0.02) 0.06	0.76 (0.06)	0.70	**0.76** **(0.06)** **0.76**
15-16 km	**0.83** **(0.05)** **0.83**	0.19 (0.09) 0.16	0.77 (0.05)	0.59	**0.78** **(0.10)** **0.75**
14-15 km	**0.89** **(0.05)** **0.89**	0.46 (0.08) 0.49	0.82 (0.09)	0.38	**0.84** **(0.12)** **0.87**

TTL altitude	**NAME 1 KM fraction [%]**	**NAME Background fraction [%]**
17-18 km	2.1 (1.1) 1.8	97.9
16-17 km	7.2 (2.7) 7.2	92.8
15-16 km	22.9 (10.0) 19.4	77.1
14-15 km	53.3 (9.0) 56.0	46.7

A4.7.2 ATTREX 2014 Research Flights

[$CHBr_3$]	***AWAS [ppt]***	***NAME Boundary Layer Contribution [ppt]***	***NAME Background [ppt]***	***NAME Background Contribution [ppt]***	***NAME Boundary Layer and Background Contribution [ppt]***
17-18 km	**0.33** **(0.14)** **0.30**	0.06 (0.06) 0.05	0.29 (0.15)	0.26	**0.32** **(0.16)** **0.30**
16-17 km	**0.48** **(0.13)** **0.47**	0.12 (0.09) 0.10	0.36 (0.14)	0.28	**0.40** **(0.17)** **0.38**
15-16 km	**0.54** **(0.13)** **0.54**	0.21 (0.12) 0.21	0.46 (0.15)	0.29	**0.50** **(0.19)** **0.50**
14-15 km	**0.61** **(0.13)** **0.61**	0.31 (0.12) 0.33	0.51 (0.11)	0.25	**0.55** **(0.16)** **0.57**

[CH_2Br_2]	*AWAS [ppt]*	*NAME Boundary Layer Contribution [ppt]*	*NAME Background [ppt]*	*NAME Background Contribution [ppt]*	*NAME Boundary Layer and Background Contribution [ppt]*
17-18 km	**0.73** **(0.06)** **0.73**	0.11 (0.09) 0.08	0.71 (0.02)	0.62	**0.73** **(0.09)** **0.70**
16-17 km	**0.82** **(0.08)** **0.81**	0.19 (0.14) 0.16	0.76 (0.06)	0.59	**0.78** **(0.15)** **0.75**
15-16 km	**0.84** **(0.09)** **0.83**	0.32 (0.16) 0.33	0.77 (0.05)	0.48	**0.80** **(0.17)** **0.81**
14-15 km	**0.86** **(0.07)** **0.86**	0.44 (0.15) 0.48	0.82 (0.09)	0.40	**0.84** **(0.17)** **0.87**

TTL altitude	**NAME 1 KM fraction [%]**	**NAME Background fraction [%]**
17-18 km	12.7 (10.9) 9.8	87.3
16-17 km	22.3 (16.0) 19.3	77.7
15-16 km	37.8 (18.8) 38.9	62.2
14-15 km	51.7 (16.1) 55.4	48.3

A4.7.3 ATTREX 2013 Research Flights

[$CHBr_3$]	*AWAS [ppt]*	*NAME Boundary Layer Contribution [ppt]*	*NAME Background [ppt]*	*NAME Background Contribution [ppt]*	*NAME Boundary Layer and Background Contribution [ppt]*
17-18 km	**0.31** **(0.10)** **0.30**	0.01 (0.01) 0.01	0.30 (0.09)	0.30	0.31 (0.09) 0.30
16-17 km	**0.39** **(0.12)** **0.39**	0.02 (0.02) 0.01	0.35 (0.10)	0.33	0.35 (0.11) 0.35
15-16 km	**0.54** **(0.15)** **0.55**	0.04 (0.04) 0.02	0.50 (0.16)	0.45	0.49 (0.16) 0.47

14-15 km	**0.53** **(0.15)** **0.54**	0.07 (0.05) 0.05	0.54 (0.17)	0.46	0.53 (0.18) 0.51

[CH_2Br_2]	***AWAS [ppt]***	***NAME Boundary Layer Contribution [ppt]***	***NAME Background [ppt]***	***NAME Background Contribution [ppt]***	***NAME Boundary Layer and Background Contribution [ppt]***
17-18 km	**0.79** **(0.08)** **0.79**	0.02 (0.02) 0.01	0.78 (0.07)	0.77	**0.78** **(0.07)** **0.78**
16-17 km	**0.83** **(0.07)** **0.83**	0.04 (0.04) 0.02	0.81 (0.06)	0.77	**0.81** **(0.07)** **0.79**
15-16 km	**0.90** **(0.07)** **0.90**	0.07 (0.06) 0.05	0.89 (0.08)	0.80	**0.87** **(0.10)** **0.85**
14-15 km	**0.91** **(0.08)** **0.91**	0.12 (0.09) 0.10	0.90 (0.08)	0.77	**0.89** **(0.12)** **0.86**

TTL altitude	**NAME 1 KM fraction [%]**	**NAME Background fraction [%]**
17-18 km	1.9 (2.3) 1.2	98.1
16-17 km	4.7 (4.9) 3.6	95.3
15-16 km	9.8 (7.9) 5.8	90.2
14-15 km	14.7 (11.1) 12.0	85.3

A4.7.4 Research Flight 02,ATTREX 2014) – 12 and 30-Day NAME runs

[CH_3I]	***AWAS [ppt]***	***NAME Boundary Layer Contribution [ppt]***		***NAME Boundary Layer Contribution (Difference from days 12-30) [ppt]***
		12 DAYS	***30 DAYS***	
17-18 km	**0.06** **(0.02)** **0.06**	0.00 (0.00) 0.00	0.00 (0.00) 0.00	0.00

16-17 km	**0.09** **(0.03)** **0.08**	0.00 (0.00) 0.00	0.01 (0.00) 0.01	0.01
15-16 km	**0.17** **(0.03)** **0.17**	0.04 (0.04) 0.03	0.05 (0.04) 0.03	0.01
14-15 km	**0.23** **(0.09)** **0.24**	0.17 (0.04) 0.19	0.17 (0.04) 0.19	0.00

[$CHBr_3$]	***AWAS [ppt]***	***NAME Boundary Layer Contribution [ppt]***		***NAME Boundary Layer Contribution (Difference from days 12-30) [ppt]***
		12 DAYS	***30 DAYS***	
17-18 km	**0.34** **(0.17)** **0.28**	0.01 (0.00) 0.01	0.05 (0.02) 0.04	0.04
16-17 km	**0.42** **(0.11)** **0.41**	0.03 (0.01) 0.03	0.11 (0.03) 0.11	0.08
15-16 km	**0.55** **(0.06)** **0.55**	0.12 (0.07) 0.10	0.23 (0.06) 0.21	0.11
14-15 km	**0.67** **(0.10)** **0.68**	0.35 (0.07) 0.37	0.41 (0.05) 0.43	0.06

[CH_2Br_2]	***AWAS [ppt]***	***NAME Boundary Layer Contribution [ppt]***		***NAME Boundary Layer Contribution (Difference from days 12-30) [ppt]***
		12 DAYS	***30 DAYS***	
17-18 km	**0.72** **(0.02)** **0.71**	0.02 (0.01) 0.01	0.14 (0.04) 0.13	0.12
16-17 km	**0.79** **(0.07)** **0.78**	0.06 (0.02) 0.06	0.30 (0.07) 0.30	0.24
15-16 km	**0.83** **(0.05)** **0.83**	0.19 (0.09) 0.16	0.50 (0.06) 0.49	0.31
14-15 km	**0.89** **(0.05)** **0.89**	0.46 (0.08) 0.49	0.67 (0.04) 0.67	0.21

TTL altitude	NAME 1 KM fraction (12 DAYS) [%]	NAME 1 KM fraction (30 DAYS) [%]	NAME 1 KM fraction (12-30 DAYS, DIFFERENCE) [%]
17-18 km	2.1 (1.1) 1.8	18.6 (5.5) 17.3	16.5
16-17 km	7.2 (2.7) 7.2	40.4 (8.9) 39.6	33.2
15-16 km	22.9 (10.0) 19.4	64.8 (6.2) 64.5	41.9
14-15 km	53.3 (9.0) 56.0	81.4 (4.2) 82.2	28.1

A4.7.5 ATTREX 2014 Research Flights – 30-day NAME simulations

[CH_3I]	*AWAS [ppt]*	*NAME Boundary Layer Contribution [ppt]*	*NAME Background [ppt]*	*NAME Background Contribution [ppt]*	*NAME Boundary Layer and Background Contribution [ppt]*
17-18 km	**0.04 (0.03) 0.05**	0.02 (0.03) 0.03	0.06 (0.01)	0.04	**0.06 (0.03) 0.06**
16-17 km	**0.11 (0.10) 0.07**	0.04 (0.04) 0.05	0.06 (0.01)	0.03	**0.08 (0.04) 0.07**
15-16 km	**0.16 (0.14) 0.12**	0.10 (0.07) 0.09	0.08 (0.03)	0.03	**0.12 (0.07) 0.12**
14-15 km	**0.17 (0.14) 0.13**	0.16 (0.08) 0.16	0.10 (0.06)	0.02	**0.18 (0.10) 0.18**

[$CHBr_3$]	*AWAS [ppt]*	*NAME Boundary Layer Contribution [ppt]*	*NAME Background [ppt]*	*NAME Background Contribution [ppt]*	*NAME Boundary Layer and Background Contribution [ppt]*
17-18 km	**0.33 (0.14) 0.30**	0.12 (0.06) 0.10	0.30 (0.14)	0.19	**0.31 (0.15) 0.30**
16-17 km	**0.48 (0.13) 0.47**	0.19 (0.09) 0.18	0.36 (0.08)	0.16	**0.35 (0.12) 0.34**
15-16 km	**0.54 (0.13) 0.54**	0.29 (0.11) 0.31	0.41 (0.14)	0.12	**0.41 (0.18) 0.43**
14-15 km	**0.61 (0.13)**	0.38 (0.10)	0.48 (0.10)	0.09	**0.48 (0.14)**

	0.61	0.39			**0.49**

[CH_2Br_2]	***AWAS [ppt]***	***NAME Boundary Layer Contribution [ppt]***	***NAME Background [ppt]***	***NAME Background Contribution [ppt]***	***NAME Boundary Layer and Background Contribution [ppt]***
17-18 km	**0.73 (0.06) 0.73**	0.27 (0.10) 0.26	0.71 (0.02)	0.46	**0.73 (0.10) 0.72**
16-17 km	**0.82 (0.08) 0.81**	0.42 (0.13) 0.41	0.75 (0.05)	0.35	**0.77 (0.14) 0.81**
15-16 km	**0.84 (0.09) 0.83**	0.55 (0.13) 0.59	0.76 (0.05)	0.23	**0.78 (0.14) 0.81**
14-15 km	**0.86 (0.07) 0.86**	0.65 (0.08) 0.68	0.77 (0.07)	0.15	**0.80 (0.11) 0.82**

TTL altitude	**NAME 1 KM fraction [%]**	**NAME Background fraction [%]**
17-18 km	35.5 (11.7) 35.0	64.5
16-17 km	54.0 (15.5) 53.9	46.0
15-16 km	69.9 (14.8) 73.5	30.1
14-15 km	80.8 (8.3) 83.4	19.2

A4.7.6 ATTREX 2013 Research Flights – 30-day NAME simulations

[CH_3I]	***AWAS [ppt]***	***NAME Boundary Layer Contribution [ppt]***	***NAME Background [ppt]***	***NAME Background Contribution [ppt]***	***NAME Boundary Layer and Background Contribution [ppt]***
17-18 km	**0.03 (0.02) 0.03**	0.00 (0.00) 0.00	0.03 (0.02)	0.02	**0.02 (0.02) 0.02**
16-17 km	**0.03 (0.02) 0.03**	0.01 (0.01) 0.00	0.03 (0.02)	0.02	**0.03 (0.02) 0.02**
15-16 km	**0.04 (0.02) 0.04**	0.01 (0.01) 0.01	0.02 (0.02)	0.01	**0.02 (0.02) 0.02**

14-15 km	**0.04** **(0.03)** **0.04**	0.02 (0.01) 0.01	0.02 (0.01)	0.01	**0.03** **(0.01)** **0.02**

[$CHBr_3$]	***AWAS [ppt]***	***NAME Boundary Layer Contribution [ppt]***	***NAME Background [ppt]***	***NAME Background Contribution [ppt]***	***NAME Boundary Layer and Background Contribution [ppt]***
17-18 km	**0.31** **(0.10)** **0.30**	0.05 (0.03) 0.04	0.22 (0.06)	0.18	**0.23** **(0.06)** **0.22**
16-17 km	**0.39** **(0.12)** **0.39**	0.08 (0.04) 0.07	0.31 (0.07)	0.22	**0.30** **(0.08)** **0.29**
15-16 km	**0.54** **(0.15)** **0.55**	0.12 (0.05) 0.11	0.44 (0.19)	0.25	**0.37** **(0.20)** **0.36**
14-15 km	**0.53** **(0.15)** **0.54**	0.16 (0.06) 0.17	0.42 (0.13)	0.19	**0.35** **(0.14)** **0.36**

[CH_2Br_2]	***AWAS [ppt]***	***NAME Boundary Layer Contribution [ppt]***	***NAME Background [ppt]***	***NAME Background Contribution [ppt]***	***NAME Boundary Layer and Background Contribution [ppt]***
17-18 km	**0.79** **(0.08)** **0.79**	0.14 (0.07) 0.14	0.70 (0.08)	0.57	**0.71** **(0.11)** **0.70**
16-17 km	**0.83** **(0.07)** **0.83**	0.23 (0.10) 0.22	0.77 (0.05)	0.54	**0.76** **(0.11)** **0.75**
15-16 km	**0.90** **(0.07)** **0.90**	0.33 (0.10) 0.31	0.82 (0.03)	0.48	**0.79** **(0.14)** **0.77**
14-15 km	**0.91** **(0.08)** **0.91**	0.41 (0.11) 0.44	0.82 (0.03)	0.35	**0.79** **(0.11)** **0.81**

TTL altitude	**NAME 1 KM fraction [%]**	**NAME Background fraction [%]**
17-18 km	19.8 (8.9) 19.0	80.2
16-17 km	30.7 (12.3) 29.7	69.3
15-16 km	43.3 (13.1) 41.3	56.7
14-15 km	54.4 (13.7) 57.9	45.6

A4.7.7 ATTREX 2014 and 2013 Contribution of Short-Lived Organic Bromine Substances to the Bromine Budget in the TTL, 12-day NAME simulations

AWAS and NAME brominated VSLS contribution (VSL_{org}) to the bromine in the TTL (TTL altitudes: 14-18 km)

Campaign	**Altitude [km]**	**AWAS [$CHBr_3$] [ppt]**	**AWAS [CH_2Br_2] [ppt]**	**Br from $CHBr_3$ [ppt]**	**Br from CH_2Br_2 [ppt]**	**Total* VSL_{org} [ppt]**
ATTREX 2014	17-18	0.33	0.73	0.99	1.46	2.45
	16-17	0.48	0.81	1.44	1.62	3.06
	15-16	0.54	0.84	1.62	1.68	3.30
	14-15	0.61	0.86	1.83	1.72	3.55
ATTREX 2013	17-18	0.31	0.79	0.93	1.58	2.51
	16-17	0.39	0.83	1.17	1.66	2.83
	15-16	0.54	0.90	1.62	1.80	3.42
	14-15	0.53	0.91	1.59	1.82	3.41

Campaign	**Altitude [km]**	**NAME modelled [$CHBr_3$] [ppt]**	**NAME modelled [CH_2Br_2] [ppt]**	**Br from $CHBr_3$ [ppt]**	**Br from CH_2Br_2 [ppt]**	**Total* VSL_{org} [ppt]**
ATTREX 2014	17-18	0.32	0.73	0.96	1.46	2.42
	16-17	0.40	0.78	1.20	1.56	2.76
	15-16	0.50	0.80	1.50	1.60	3.10
	14-15	0.55	0.84	1.65	1.68	3.33
ATTREX 2013	17-18	0.31	0.79	0.93	1.58	2.51
	16-17	0.35	0.81	1.05	1.62	2.67
	15-16	0.49	0.87	1.47	1.74	3.21
	14-15	0.53	0.89	1.59	1.78	3.37